



HAL
open science

Complexes de métaux électropositifs à travers le prisme du groupe cyclopropyle

Quentin Dufrois

► **To cite this version:**

Quentin Dufrois. Complexes de métaux électropositifs à travers le prisme du groupe cyclopropyle. Chimie de coordination. Université Paul Sabatier - Toulouse III, 2016. Français. NNT : 2016TOU30303 . tel-01688622

HAL Id: tel-01688622

<https://theses.hal.science/tel-01688622>

Submitted on 19 Jan 2018

HAL is a multi-disciplinary open access archive for the deposit and dissemination of scientific research documents, whether they are published or not. The documents may come from teaching and research institutions in France or abroad, or from public or private research centers.

L'archive ouverte pluridisciplinaire **HAL**, est destinée au dépôt et à la diffusion de documents scientifiques de niveau recherche, publiés ou non, émanant des établissements d'enseignement et de recherche français ou étrangers, des laboratoires publics ou privés.



Université
de Toulouse

THÈSE

En vue de l'obtention du

DOCTORAT DE L'UNIVERSITÉ DE TOULOUSE

Délivré par :

Université Toulouse 3 Paul Sabatier (UT3 Paul Sabatier)

Présentée et soutenue par :
Quentin DUFROIS

Le vendredi 25 Novembre 2016

Titre :

Complexes de métaux électropositifs à travers le prisme du groupe
cyclopropyle

Electropositive metal complexes through the prism of the cyclopropyl group

ED SDM : Chimie organométallique de coordination - CO 043

Unité de recherche :

Laboratoire de Chimie de Coordination du CNRS

Directeur(s) de Thèse :

Michel ETIENNE
Chiara DINOI

Rapporteurs :

Florence MONGIN, Professeur, Université de Rennes I
Matthias WESTERHAUSEN, Professeur, Friedrich-Schiller-Universität Jena, Germany

Autre(s) membre(s) du jury :

Yann SARAZIN, Chargé de Recherche, Université de Rennes I (Examinateur)
Didier BOURISSOU, Directeur de Recherche CNRS, Toulouse (Examinateur)
Chiara DINOI, Maître de Conférences, Université Toulouse 3 Paul Sabatier
Michel ETIENNE, Professeur, Université Toulouse 3 Paul Sabatier

“ἔν οἶδα ὅτι οὐδὲν οἶδα”

“I know that I know nothing”

Socrates

Remerciements

Ce travail a été possible grâce à une bourse du Ministère de l'Enseignement Supérieur et de la Recherche.

En premier lieu, je souhaite remercier mon directeur et ma directrice de thèse, le Pr. Michel Etienne et la Dr. Chiara Dinoi. C'est avec une grande implication qu'ils m'ont formé, accompagné et encouragé tout au long de mon travail. J'ai pu pleinement bénéficier de leur grande compétence technique et scientifique. Vous avez changé ma façon de réfléchir et de voir le monde. Un grand merci pour votre gentillesse et votre humanité, cela a été un plaisir de travailler à vos côtés durant ces trois années.

Je tiens ensuite à remercier ceux qui ont travaillé avec moi sur les projets présentés dans ce manuscrit, Nuria, Anthony, Christian et Kane. Nuria, tu m'as donné toute la rigueur et la technique pour manipuler dans un laboratoire de chimie, désolé de t'avoir fait peur avec mes feux de paille et de t'avoir intoxiqué avec mes produits soufrés. Nous nous sommes rencontrés en tant que collègues, et je suis très heureux de te compter désormais parmi mes amis.

I would like to thank the Pr. Westerhausen for both reviewing my work and for welcoming me within its team in Jena. Thank you to all of his students and collaborators: Sven, Kay, Alex, Steff, Stephan, Ralph and all the others. I had a great time in Jena, thanks to all for your kindness and your excellent advises.

Je remercie la Pr. Florence Mongin d'avoir accepté d'être rapporteur de ce travail. Je remercie également le Dr. Yann Sarazin et le Dr. Didier Bourissou d'avoir accepté de figurer dans le jury en tant qu'examineurs.

Un grand merci à tout le personnel technique du service RDX : Laure Vendier, Jean-Claude Daran, Carine Duhayon et Sonia Mallet-Ladeira, du service RMN : Christian Bijani, Francis Lacassin et David Paryl, et du service microanalyse : Isabelle Borget et Alain Moreau.

Je remercie les collègues de l'équipe E : Kyle pour ses relectures attentives, Antoine, Chen et Natalie.

Merci à tous les collègues des autres équipes du laboratoire, en particulier un grand merci à l'équipe O et à tous ses membres, présents et passés, qui se reconnaîtront j'en suis sûr.

Je vais en oublier, mais merci à Pascal, Yohan, Tugce, Damien, Mirko, Chong wei, Amelle, Clève, Yin, Marlène, Sylvain et Armelle.

A toute la bande de Limoges : Delou, Yohan, Lucas, Poe, Nils, Maymay, Jerem, Clem, Louisa, Philou, Clémence, Clément, Carole, Jo, Marie, Marion, Brian, Nanou, Vincent, Buff, Zabou, Doud, Francky, Milena et Thotho (je ne vous ai pas cité par ordre de préférence) je dis merci. Pour des personnes liées par une telle amitié, les mots sont inutiles.

Enfin, merci à toute ma famille, mes parents, Nathan, Micheline, Domi et Philou, Raph et Martine, Laurie et JM, et tous les cousins. Merci à toi Marion pour avoir été là à chaque instant.

Table of contents

List of abbreviations.....	9
Complexes presented.....	10
General introduction.....	13
The cyclopropyl ring.....	15
A. The bonding in cyclopropane.....	15
B. Cyclopropyl complexes.....	19
Chapter 1. Cyclopropyllithium complexes.....	25
A. Introduction.....	25
I.1. The organolithium complexes.....	25
I.2. Secondary interactions.....	33
I.3. The cycloalkyllithium compounds.....	40
B. Results and discussion.....	47
I.1. 1-(trimethylsilyl)cyclopropyllithium.....	47
I.2. 1-phenylcyclopropyllithium.....	54
I.3. 1-(phenylthio)cyclopropyllithium.....	69
C. Conclusion and perspectives.....	72
D. Experimental part.....	73
Chapter 2. Cyclopropylcalcium complexes.....	79
A. Introduction.....	79
I.1. The organocalcium complexes.....	79
I.2. Synthesis of organocalcium complexes.....	80
B. Results and discussion.....	90
I.1. Salt metathesis reaction.....	90
I.2. Oxidative addition on Ca*.....	95

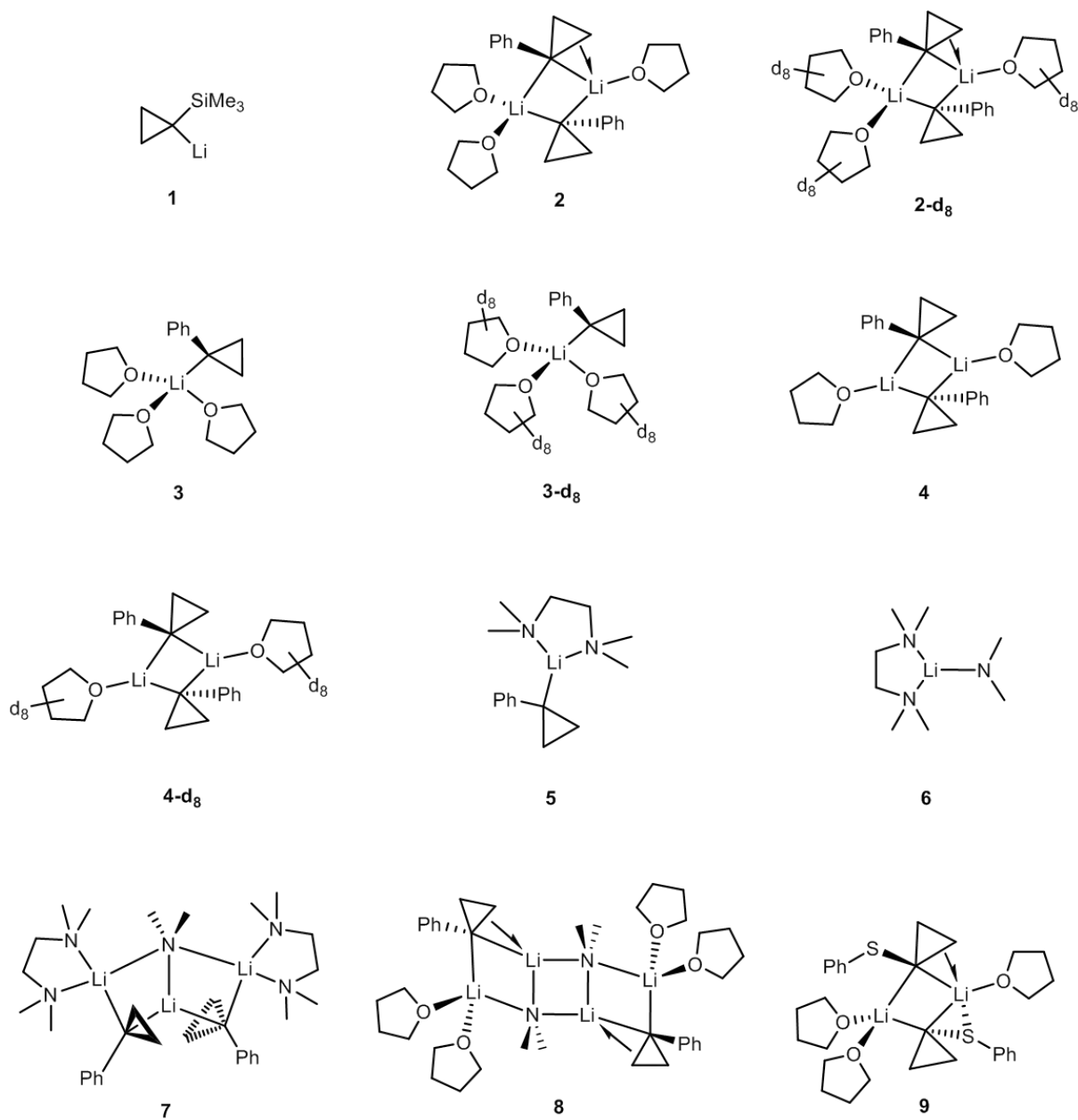
C. Conclusion and perspectives	101
D. Experimental part	102
Chapter 3. Group 4 dicyclopropyl metallocenes.....	107
A. Introduction	107
I.1. Reactive early transition metals complexes.....	107
I.2. C–F activation by early transition metals complexes	113
B. Results and discussion.....	119
I.1. Reaction with pyridine	119
I.2. C–F activation of fluorinated pyridines	133
C. Conclusion and perspectives	158
D. Experimental part	159
General Conclusion	171
References	173
Crystallographic Data.....	187
Résumé en français.....	223
A. Chapitre 1	223
I.1. Introduction.....	223
I.2. Résultats et discussion	226
B. Chapitre 2	231
I.1. Introduction.....	231
I.2. Résultats et discussion	232
C. Chapitre 3	236
I.1. Introduction.....	236
I.2. Résultats et discussion	238

List of abbreviations

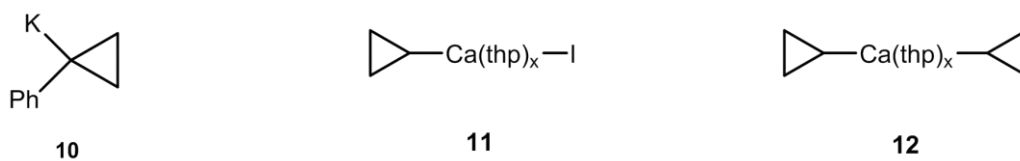
BDE	Bond-Dissociation Energy
Cp	Cyclopentadienyl
Cp*	1,2,3,4,5-pentamethylcyclopentadienyl
ESR	Electron Spin Resonance
ETM	Early Transition Metals
FW	Formula Weight
DFT	Density Functional Theory
DME	1,2-Dimethoxyethane
DOSY	Diffusion-Ordered NMR spectroscopy
eq.	equivalent
HMBC	Heteronuclear Multiple-Bond Correlation
HMQC	Heteronuclear Multiple Quantum Coherence
HOESY	Heteronuclear Overhauser Effect Spectroscopy
HSAB	Hard and Soft Acids and Bases
IR	Infrared
NMR	Nuclear Magnetic Resonance
NOESY	Nuclear Overhauser Effect Spectroscopy
pmdta	N,N,N',N'',N'''-pentamethyldiethylenetriamine.
RT	Room Temperature
teeda	N,N,N',N'-tetraethylethane-1,2-diamine
thf	Tetrahydrofuran
thp	Tetrahydropyran
tmeda	N,N,N',N'-tetramethylethane-1,2-diamine
TON	Turnover Number
triglyme	2,5,8,11-tetraoxadodecane
XRD	X-Ray Diffraction
1D, 2D	One-dimensional, two-dimensional
18-crown-6	1,4,7,10,13,16-hexaoxacyclooctadecane
δ	Chemical shift

Complexes presented

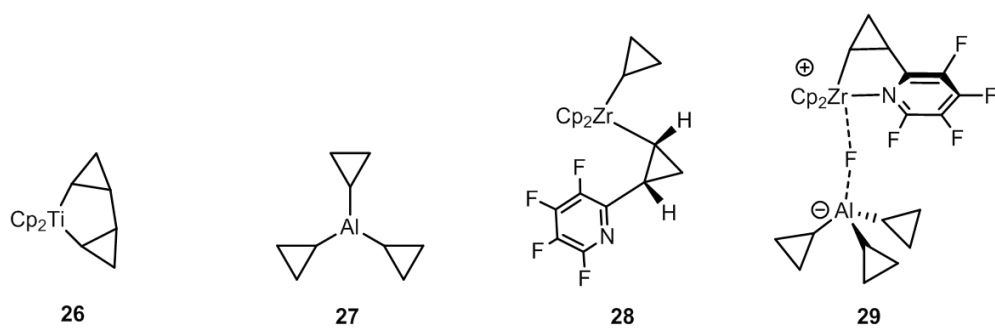
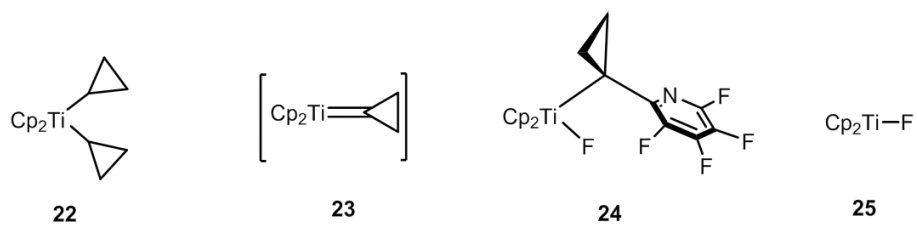
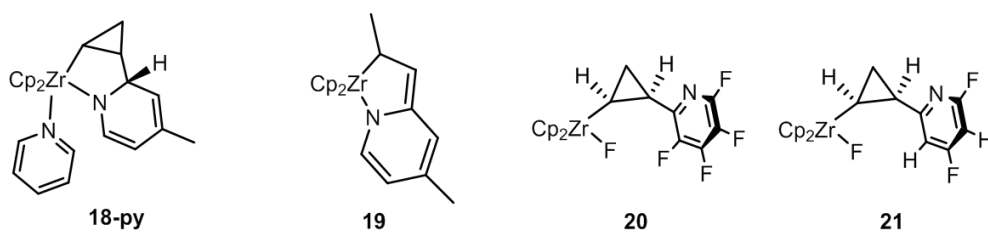
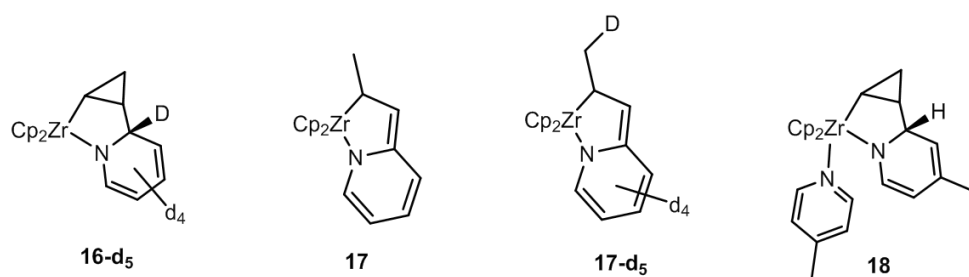
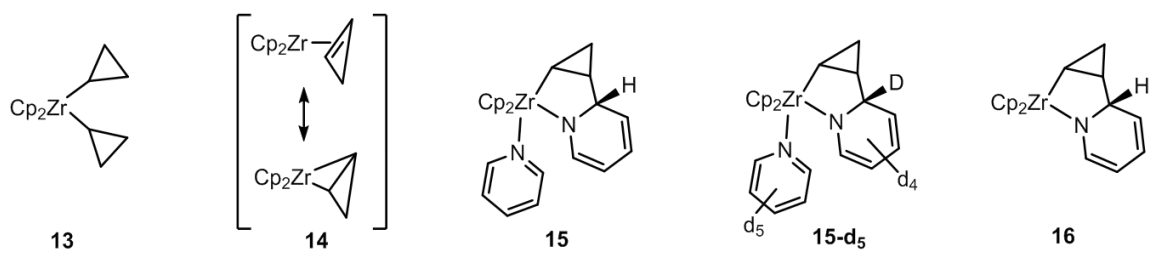
Chapter 1



Chapter 2



Chapter 3



General introduction

Our group “Early Transition Metals” at the Laboratoire de Chimie de Coordination (LCC) has a deep knowledge in the field of organometallic chemistry of the electropositive metals on the left of the periodic table, with an emphasis on structural and mechanistic studies related to the activation of strong and inert bonds like C–H, C–C, C–F, etc., and including C–H and C–C agostic interactions. Following these topics, the main objectives for our project were the following:

- the synthesis and characterisation of new α -cyclopropyl complexes of lithium and calcium, followed by the study of the potential C–C agostic interactions in these complexes. No cyclopropyl complexes of Ca have been reported yet. No C–C agostic interactions are known for Li.

- to go deeper in the work started by Nuria Romero during her PhD (2011-2014) on the reactivity of group 4 cyclopropyl metallocene complexes toward small molecule activation *via* C–H and C–F bond cleavages.

This thesis is divided in three Chapters. As the addressed subjects are quite different from each other, each chapter contain its own bibliographic introduction. Yet, as the unifying link is the cyclopropyl group, this manuscript starts by a short Introduction presenting the essential properties of cyclopropane.

In Chapter 1, we present the synthesis and characterisation of cyclopropyllithium derivatives. We discuss the existence and the strength of C–C agostic interactions on the basis of XRD structures, NMR data and computational chemistry.

Chapter 2 deals with our still ongoing work on the synthesis and characterisation of the first cyclopropylcalcium compounds.

In Chapter 3, we first detail the reaction between dicyclopropylzirconocene and pyridine through a mechanistic study. The stoichiometric C–F activations of fluorinated pyridines by dicyclopropyl- titanocene and zirconocene are investigated next. Eventually, an attempt to reach a genuine catalytic C–C coupling reaction between pentafluoropyridine and a cyclopropyl group involving a C–F activation step by dicyclopropylzirconocene is presented.

Most of the experimental work took place in the Laboratoire de Chimie de Coordination (LCC, CNRS, Toulouse). A one month exchange was conducted in the team of Professor Matthias Westerhausen at the Institut für Anorganische und Analytische Chemie (Friedrich-Schiller-Universität Jena, Germany), related to the chemistry of calcium.

The cyclopropyl ring

A. The bonding in cyclopropane

Cyclopropane C_3H_6 and its derivatives are the smallest stable rings containing only C and H, with a strained geometry where the average CCC angle is compressed to 60° . As a consequence, the C–C bonds in cyclopropane are best described as “bent bonds”.¹ Following Wiberg and Bader, the chemical bonding can be defined as the path of maximum charge density between two atoms; it is therefore, in most cases, nearly collinear with a line drawn between atomic centres, as in the Lewis model.^{1,2} Yet, although cyclopropane and derivatives are drawn as triangles, the charge density is instead located outside the triangle. This has been demonstrated experimentally (*via* XRD)^{3,4} or by calculation of the deformation densities (Figure 1).¹ Consequently, the C–C distance is shorter ($1.512(3)$ Å, internuclear distance as measured by Raman spectroscopy *vs.* *ca* 1.54 Å in linear alkanes)⁵ and the C–C bond is weaker ($E(C-C) = 255$ kJ/mol)⁶ than for normal alkanes ($E(C-C) \sim 350-400$ kJ/mol).⁷

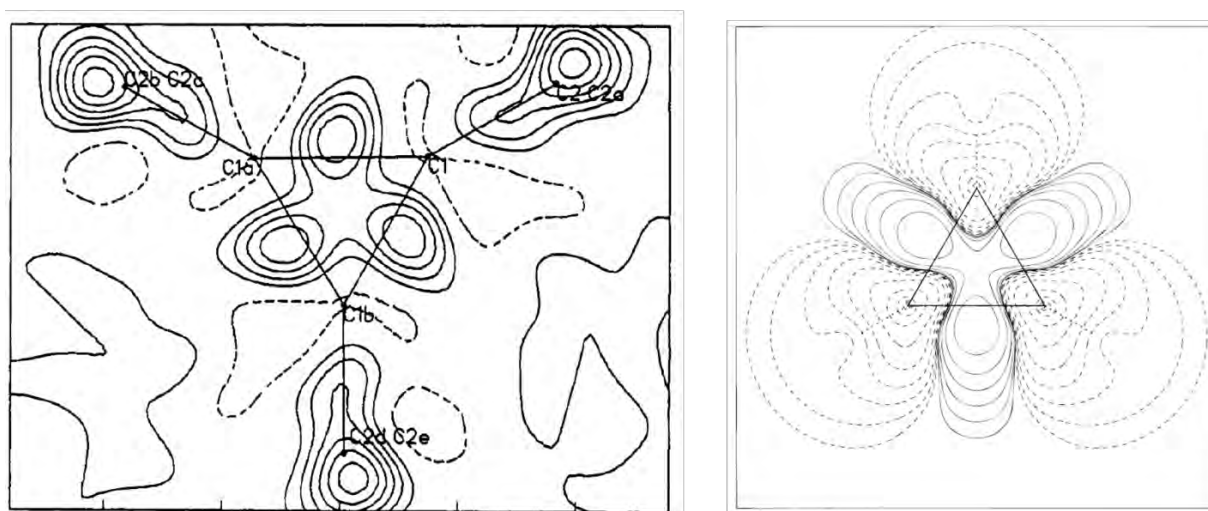


Figure 1 Deformation density plot measured by XRD for 1,2,3-tricyclopropylcyclopropane (left) and calculated for cyclopropane (right - based on MP2/6-31G* wave function). Positive and zero density are depicted in solid contours; negative density is depicted in dashed lines.

Two models are generally used to describe the molecular orbitals of cyclopropane. They are equivalent and can be transformed mathematically into each other.⁸

(i) Walsh proposed that cyclopropane is closer to alkenes than to alkanes and thus the atomic orbitals of the carbons are sp^2 hybridised.^{9,10} As ethylene can be seen as the combination of two methylene carbons ($3 sp^2 + 1 p$ orbitals per carbon), this can be extended to cyclopropane which results from the combination of three methylene carbons arranged with D_{3h} symmetry. Two sp^2 orbitals per carbon are involved in the bonding with two H. The remaining set of sp^2 orbitals combine to form σ -like molecular orbitals and the set of p orbitals generates π -like (sometimes called pseudo- π) molecular orbitals (Figure 2). In this model, the bent bonds come from the overlap of the p orbitals outside of the triangle edges.

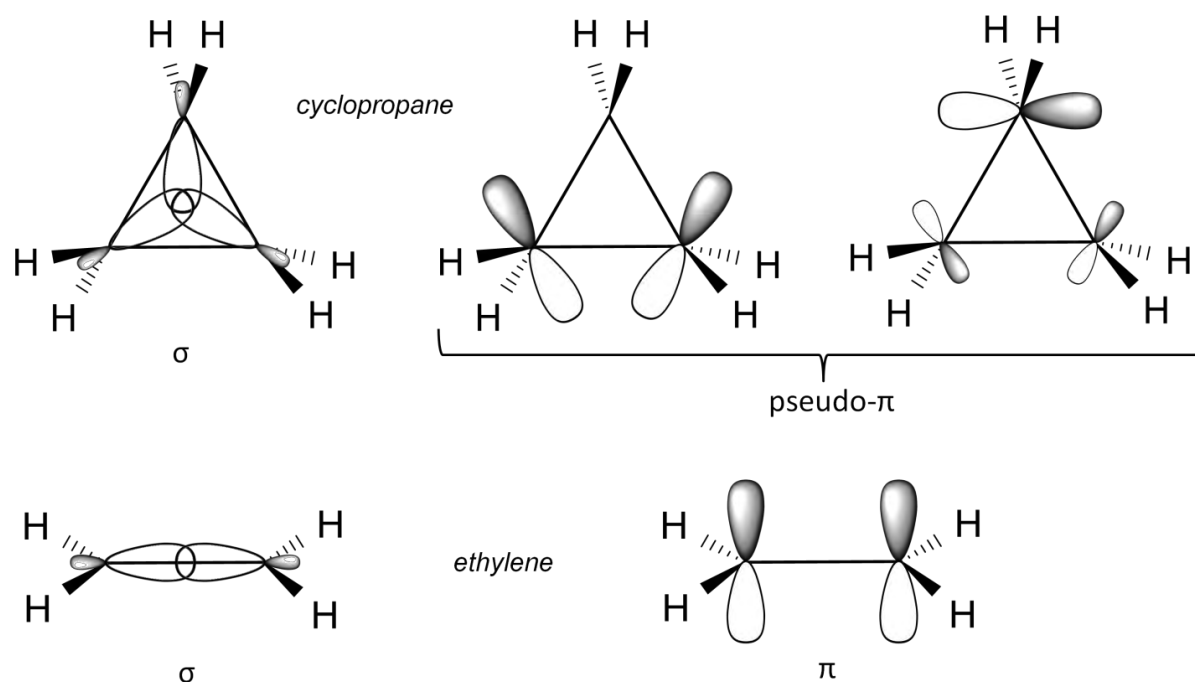


Figure 2 The filled molecular orbitals in cyclopropane (top) and ethylene (bottom). The pseudo- π orbitals of cyclopropane lie in the plane of the ring.

(ii) Coulson and Moffitt proposed that the atomic orbitals of the cyclopropane carbons combine in a sp^5 hybridisation state. Each carbon possesses two sp^2 orbitals that are involved in the bonding with hydrogens and two sp^5 orbitals, directed outside of the C–C lines that overlap to form the molecular orbitals responsible for the bent bonds (Figure 3).

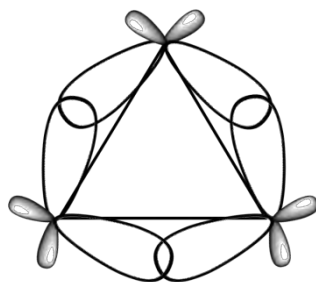


Figure 3 *Overlap of the sp^5 hybrid atomic orbitals in cyclopropane.*

This model can be mathematically summarised as follow:

Assuming that two atomic orbitals per carbon are sp^2 hybridised and involved in the C–H bonds, two equivalent orbitals have to be built to make the two C–C bonds around each carbon. The s and p characters of these orbitals can be calculated:

-There is 1 s orbital per carbon; a is the s character of the new orbital

$$2 \times \left(\frac{1}{3}s\right) + 2 \times as = 1s$$

$$a = \frac{1}{6}$$

-There are 3 p orbitals per carbon; b is the p character of the new orbital

$$2 \times \left(\frac{2}{3}p\right) + 2 \times bp = 1s$$

$$b = \frac{5}{6}$$

We thus obtain two sp^5 orbitals. Coulson proposed a relationship between the coefficient of mixing α in the hybrid orbital sp^α and the angle θ between two sp^α orbitals:¹¹

$$1 + \alpha \cos(\theta) = 0$$

This gives $\theta = 102^\circ$ for sp^5 orbitals explaining why these orbitals overlap outside of the CC lines.

According to the two models, the C–H bonds in cyclopropane involve sp^2 orbitals. This can be assessed by the typical value of $^1J_{CH} = 161$ Hz which is comparable to that of ethylene (157 Hz) or benzene (159 Hz).¹² Based on this coupling constant data, the C–H bond orbitals (s_c) have 32% s character, according to the Muller-Pritchard relationship:¹³

$$^1J_{CH} = 500s_c$$

Another common feature of the two models is the enhanced p character of the C–C orbitals. The measured $^1J_{CC}$ value for cyclopropane is 12.4 Hz, which is much smaller than that for C–C single bonds (*ca* 35 Hz).⁸ This can be rationalised by the theory of Ramsay,¹⁴ which establishes that the coupling constant depends on the sum of four parameters, with the most important being the Fermi-contact. The Fermi-contact reflects the interaction between the spin magnetic moment of the s electrons at the contact surface of the nucleus and the magnetic field inside the nucleus, and is therefore directly linked to the percentage of s electrons in the studied bond. In cyclopropane, the small $^1J_{CC}$ value results mostly from the small Fermi-contact term, which corroborates the high p character of the C–C bond. The exact determination of the s participation in the C–C molecular orbitals of cyclopropane has been proposed by Stöcker¹⁵ using a modified Muller-Pritchard relationship.¹⁶ 16.67% of s character was calculated, which matches with the proposed sp^5 orbitals of the Coulson and Moffitt model. However, a more recent study has shown that the $^1J_{CC}$ in cyclopropane is actually both the result of enhanced p character and of multiple path contributions involving all the C–H and C–C bonds of the molecule, making it difficult to calculate the s and p characters directly from the $^1J_{CC}$.¹⁷

As we study cyclopropyl complexes of electropositive metals, and thus highly ionic bonds, it is essential to discuss the acidity of cyclopropane. Experimental gas-phase acidities of various hydrocarbons are presented in Figure 4 below.^{18–20} The gas-phase acidity is defined as the enthalpy change for the heterolytic R–H bond dissociation, $\Delta H^\circ_{acid}(R-H) = BDE(R-H) - EA(R) + IP(H)$, with BDE = bond dissociation energy, EA = electron affinity and IP = ionisation potential. The smaller the ΔH°_{acid} value, the more acidic the compound.

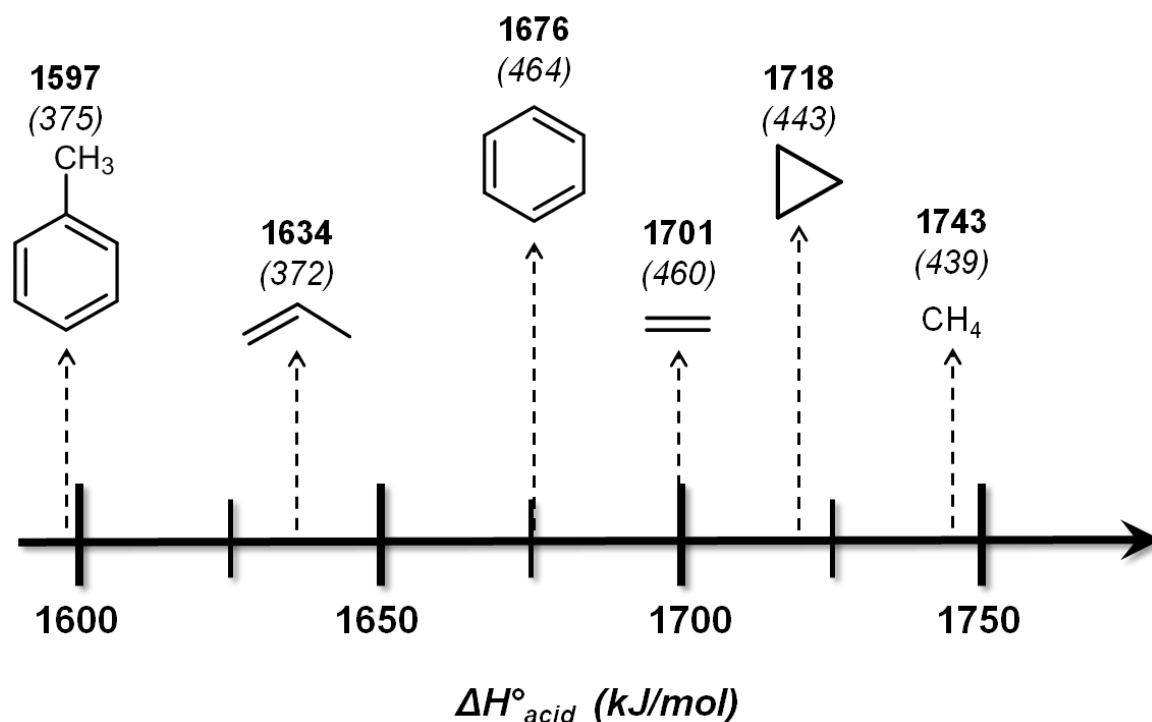


Figure 4 Gas-phase acidities and BDE (in *italic*) of common hydrocarbons. The errors in the acidities and BDE are ± 4 kJ/mol.

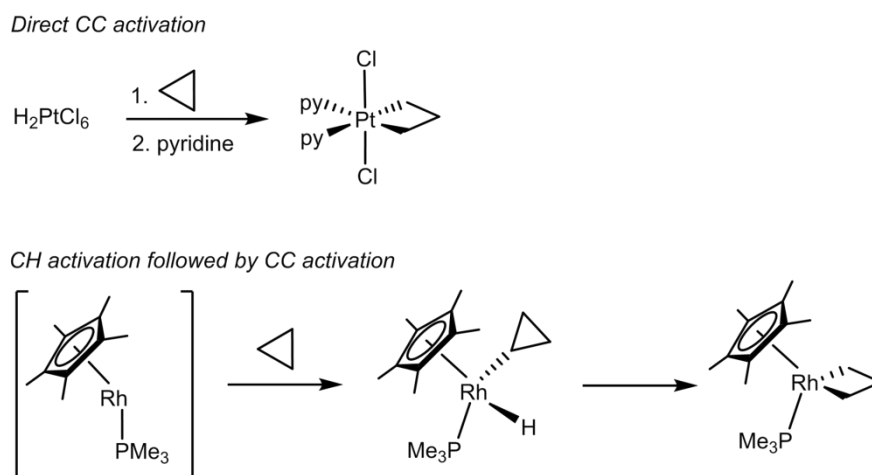
For symmetry reasons and/or due to large energy gaps, negligible back donation into an empty antibonding orbital of the cyclopropyl group is expected for the carbanion. Therefore only its hybridisation state dictates the acidity of cyclopropane ($\Delta H^\circ_{\text{acid}} = 1718$ kJ/mol) which is found between that for alkanes (e.g. for methane: $\Delta H^\circ_{\text{acid}} = 1743$ kJ/mol) and alkenes (e.g. for ethylene: $\Delta H^\circ_{\text{acid}} = 1701$ kJ/mol).

B. Cyclopropyl complexes

Cyclopropyl moieties are found in many natural molecules such as terpenoids, fatty acid metabolites, pheromones, and unusual amino acids.²¹ These products clearly inspired the synthesis of valuable cyclopropyl containing molecules, such as insecticides,²² antifungals,²³ and anti-cancer drugs.²⁴ Besides its biological interest, cyclopropyl is also a versatile functional group that can undergo various reactions such as ring-opening, cycloaddition or ring-enlargement.²⁵

Introduction of a cyclopropyl group into a molecule, or derivatisation reactions of this moiety often involve the use of metal complexes.^{25,26} Hence, there is an interest in the

synthesis of cyclopropyl metal complexes, but also in the study of the interactions between the three-member cycle and the metal centre. For instance, as early as 1955 Tipper observed the C–C cleavage of cyclopropane by a Pt(II) complex (Scheme 1).²⁷ Various examples of such a reaction have been reported later on.²⁸ The C–C cleavage can happen directly or can follow a step of C–H activation of the cyclopropane (Scheme 1).^{29,30}



Scheme 1 C–C bond activation of cyclopropane by $[H_2PtCl_6]$ (top) and $[Cp^*Rh(PMe_3)]$ (bottom).

In electron deficient cyclopropyl complexes, a rare 3c-2e C–C agostic interaction, defined by another name as an intramolecular C–C σ -complex, can sometimes be observed (Figure 5).⁶

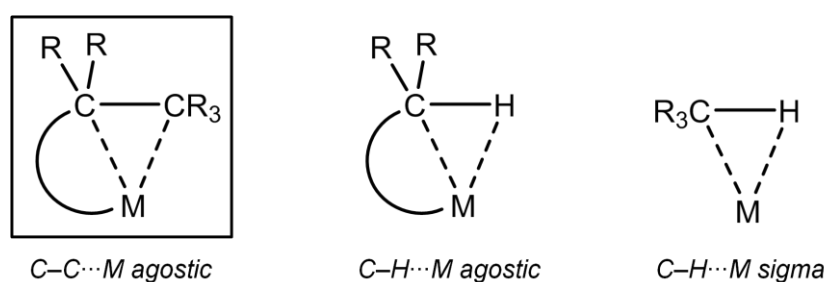


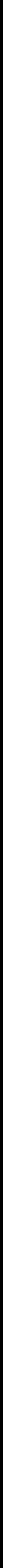
Figure 5 Comparison between C–C agostic interaction, C–H agostic interaction and C–H σ -complex.

This interaction results from the close contact of an electropositive centre with the bent and available bonds of cyclopropane. As for C–H agostic interactions, C–C agostic interactions are believed to be involved in the bond activation pathways. In addition, they can

also stabilise electron deficient highly electropositive metal centres. More details on the characterisation of these C–C agostic interactions are given in Chapter I. Yet, studies of these secondary interactions generally start with the observation of distortions of the cyclopropyl group in the solid state. A search in the Cambridge Structural Database reveals that several XRD structures of cyclopropyl complexes are known for late and third row transition metals but that early metals remain relatively unexplored (Figure 6). Their strong electrophilic character suggests that these interactions should be more common with these metals.

hydrogen 1 H 1.0079																	helium 2 He 4.0026						
lithium 3 Li 6.941	beryllium 4 Be 9.0122																	boron 5 B 10.811	carbon 6 C 12.011	nitrogen 7 N 14.007	oxygen 8 O 15.999	fluorine 9 F 18.998	neon 10 Ne 20.180
sodium 11 Na 22.990	magnesium 12 Mg 24.305																	aluminum 13 Al 26.982	silicon 14 Si 28.086	phosphorus 15 P 30.974	sulfur 16 S 32.065	chlorine 17 Cl 35.453	argon 18 Ar 39.948
potassium 19 K 39.098	calcium 20 Ca 40.078	scandium 21 Sc 44.956	titanium 22 Ti 47.867	vanadium 23 V 50.942	chromium 24 Cr 51.996	manganese 25 Mn 54.938	iron 26 Fe 55.845	cobalt 27 Co 58.933	nickel 28 Ni 58.693	copper 29 Cu 63.546	zinc 30 Zn 65.39	gallium 31 Ga 69.723	germanium 32 Ge 72.61	arsenic 33 As 74.922	selenium 34 Se 78.96	bronine 35 Br 79.904	krypton 36 Kr 83.80						
rubidium 37 Rb 85.468	strontium 38 Sr 87.62	yttrium 39 Y 88.906	zirconium 40 Zr 91.224	niobium 41 Nb 92.906	molybdenum 42 Mo 95.94	technetium 43 Tc [98]	ruthenium 44 Ru 101.07	rhodium 45 Rh 102.91	palladium 46 Pd 106.42	silver 47 Ag 107.87	cadmium 48 Cd 112.41	indium 49 In 114.82	tin 50 Sn 118.71	antimony 51 Sb 121.76	tellurium 52 Te 127.60	iodine 53 I 126.90	xenon 54 Xe 131.29						
caesium 55 Cs 132.91	barium 56 Ba 137.33	57-70 *	lutetium 71 Lu 174.97	hafnium 72 Hf 178.49	tantalum 73 Ta 180.95	tungsten 74 W 183.84	rhenium 75 Re 186.21	osmium 76 Os 192.22	iridium 77 Ir 192.22	platinum 78 Pt 195.08	gold 79 Au 196.87	mercury 80 Hg 200.59	thallium 81 Tl 204.38	lead 82 Pb 207.2	bismuth 83 Bi 208.98	polonium 84 Po [209]	astatine 85 At [210]	radon 86 Rn [222]					
francium 87 Fr [223]	radium 88 Ra [226]	89-102 **	lawrencium 103 Lr [262]	rutherfordium 104 Rf [261]	dundium 105 Db [262]	seaborgium 106 Sg [266]	bohrium 107 Bh [264]	hassium 108 Hs [269]	meitnerium 109 Mt [268]	unnilium 110 Uun [271]	ununium 111 Uuu [272]	unbibium 112 Uub [277]											
* Lanthanide series			lanthanum 57 La 138.91	cerium 58 Ce 140.12	praseodymium 59 Pr 140.91	neodymium 60 Nd 144.24	promethium 61 Pm [145]	samarium 62 Sm 150.36	europium 63 Eu 151.96	gadolinium 64 Gd 157.25	terbium 65 Tb 158.93	dysprosium 66 Dy 162.50	holmium 67 Ho 164.93	erbium 68 Er 167.26	thulium 69 Tm 168.93	ytterbium 70 Yb 173.04							
** Actinide series			actinium 89 Ac [227]	thorium 90 Th 232.04	protactinium 91 Pa 231.04	uranium 92 U 238.03	neptunium 93 Np [237]	plutonium 94 Pu [244]	americium 95 Am [243]	curium 96 Cm [247]	berkelium 97 Bk [247]	californium 98 Cf [251]	einsteinium 99 Es [252]	fermium 100 Fm [257]	mendeleevium 101 Md [258]	nobelium 102 No [259]							

Figure 6 Reported XRD structures of cyclopropyl (and close derivatives) complexes in blue. Zr,³¹ Nb,³² Ta,³³ W,³⁴ Re,³⁵ Fe,³⁶ Os,³⁷ Rh,²⁹ Ir,³⁸ Ni,³⁹ Pt,⁴⁰ Au,⁴¹ Hg,⁴² Al,⁴³ Tl,⁴⁴ Sn.⁴⁵



CHAPTER 1

Chapter 1. Cyclopropyllithium complexes

A. Introduction

The objective of this chapter was to study a new class of organolithium compounds: the cyclopropyllithiums. Indeed, we were particularly interested in studying this unknown class of complexes, since they represent ideal candidates for probing the influence of C–C agostic interactions in the structure of organolithium complexes. Although short contacts have sometimes been noticed between a Li^+ centre and C–C σ -bonds, they have never been the topic of extensive studies.

The organometallic chemistry of lithium has been widely developed for many years and has given rise to a plethora of compounds. For instance, a quick search in the Cambridge Structural Database revealed 1145 structures bearing a Li–C bond. These complexes can include fragments in which electronegative donor atoms such as N, O, S, P, etc. are present and could compete with, or even prevent relatively weak C–H or C–C agostic interactions. In this study, we have therefore decided to restrict the term organolithium to complexes bearing only C, H and Si atoms (with the exception of S in one case).

Also, even though we present some benchmark compounds to exemplify the general properties of organolithium chemistry, the introduction does not aim to list all organolithium compounds (they have been recently reviewed).^{46,47} Furthermore, we limit this study to those that resemble the complexes studied in part B, *i.e.* alkyl, aryl and benzyl moieties (with nonetheless a complete study of cycloalkyllithium complexes, I.3.).

I.1. The organolithium complexes

Since the development of inert-gas techniques by Schlenk and Holtz at the beginning of the 20th century,⁴⁸ organolithium compounds have been revealed to be amongst the most versatile reagents in synthesis. Their easy access, either by well-defined preparation procedures or by their commercial availability, makes them widespread chemicals, used in every laboratory of synthetic chemistry. Because of their strongly polarised Li–C bond, they are reagents of choice for C–C bond formation and deprotonation reactions. Also, they are excellent transmetallating agents, due to the formation of highly stable and often insoluble halogen-lithium salts.

An understanding of these reactions is deeply linked to the structural elucidation of the organolithium compounds involved (in the solid state and in solution). As organolithiums tend to aggregate, the clarification of the reaction mechanisms in which they are involved often relies upon the control of the aggregation processes. Besides, it is sometimes necessary to force highly aggregated organolithium complexes to deaggregate in order to enhance their reactivity (e.g.: nucleophilic substitution reactions, can be prevented by the steric hindrance of the cluster). Thus, it is fundamental to understand the nature of the Li–C bond, but also to evaluate what are the most influential parameters that favour aggregation. XRD, NMR spectroscopy and computational chemistry are now routinely combined techniques for the characterisation of organolithium complexes, and are therefore extensively used in this study.

a. The Li–C bond

Lithium is the third element of the periodic table, and the first of the alkali-metals. Some of its properties are summarised in Table 1.1.

Table 1.1 Selected properties of the Li atom.

Li	Electron configuration	First ionisation energy	Van Der Waals radius ⁴⁹	Ionic radius ⁵⁰
	$1s^2 2s^1$	520.2 kJ/mol	1.82 \AA	0.90 \AA

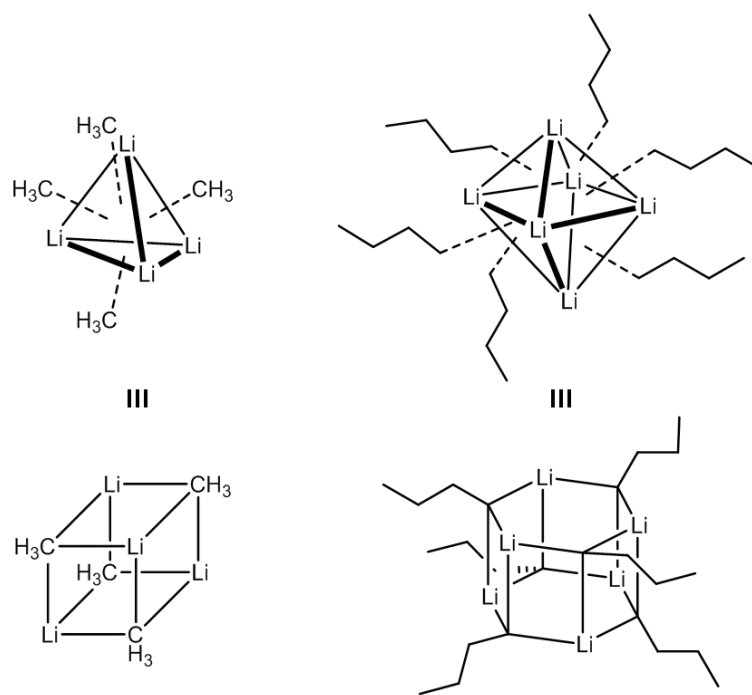
Lithium is easily oxidized to Li(I) as a result of its low first ionisation energy. It is a small electropositive ($\chi(\text{Li}) = 0.97$) non-polarisable metal (hard acid in the HSAB theory), and hence is prone to bond to hard bases such as oxygen, nitrogen or chlorine. Interactions with carbon are less favoured, which explains why organolithiums must be handled under rigorous exclusion of oxygen or moisture.

Until the benchmark works of Schleyer *et al.*,^{51–56} the nature of the Li–C bond was subject to debate between covalent⁵⁷ or ionic bond models.^{58,59} It is now admitted that Li to C bonding is essentially ionic with small, but non negligible, covalent contribution (C–Li is calculated to be *ca* 80–88% ionic).^{52,53,56} More recent experimental charge density studies have definitively validated this model.^{60,61}

Organolithiums are often schematically depicted as monomeric compounds formed by a negatively charged carbanion (R^-) and a lithium cation (Li^+). In fact, they are mainly

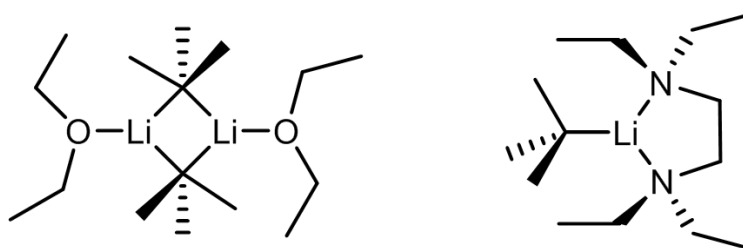
organised as clusters (or aggregates) whose size (*i.e.* aggregation degree) depends on several parameters, such as the bulkiness of the R group, the nature of the solvent used for solubilisation or crystallisation, and secondary interactions (*vide infra*). Lithium cations are generally four-coordinated, but species bearing a coordination number of three are also common, although in these complexes extra stabilisation comes from electronic density of σ - or π -bonds present in the coordination sphere of the metal.

The most frequently encountered aggregates are hexamers and tetramers, consisting of Li_3 faces μ_3 -capped by the carbanionic carbons of the organic groups ($\text{C}\alpha$). This is exemplified by the solid state structure of the tetrameric $[\mu_3\text{-MeLi}]_4$ (Scheme 1.1, up left).^{62,63} The bonding on each face of the tetrahedron, formed by the lithium atoms, can also be described as 4c-2e bond, even though as previously stated, the interactions are mainly electrostatic. A similar pattern is observed in hexameric structures, except that R groups are arranged around lithium octahedrons, with two faces that remain uncapped (see for example the structure of *n*-Buli,⁶⁴ Scheme 1.1, up right). The Li–Li bonds drawn in this scheme are not representative of metal-to-metal interactions; they highlight the coordination polyhedrons. Nonetheless, such a bonding remains an open question.^{63,65} Another representation is often used where the Li–Li bonds are removed and full bonds between C and Li atoms are drawn (Scheme 1.1, bottom). Both representations are used in this work, but the nature of the Li–Li interaction is not discussed further.



Scheme 1.1 Solid state structures of $[\mu_3\text{-MeLi}]_4$ (left) and $[\mu_3\text{-n-BuLi}]_6$ (right).

Upon deaggregation or when organolithiums carry bulkier R groups, dimers and sometimes monomers can be isolated. Dimers are generally organised around Li_2C_2 rings, also described as two Li^+ bridged by the two $\text{C}\alpha$ (the Li-C-Li pattern can be considered as a $3\text{c-}2\text{e}$ bond). Monomers are obtained under certain conditions (detailed in part b) and are very reactive species. They resemble the typical picture of R-Li , even if they are always stabilised with help of a chelating donor ligand and/or extremely bulky groups. Examples of dimer⁶⁵ and monomer⁶⁶ structures are depicted in Scheme 1.2 for the well-known *t*-BuLi.



Scheme 1.2 Solid state structures of $[\mu\text{-}t\text{-BuLi}(\text{Et}_2\text{O})]_2$ (left) and $[t\text{-BuLi}(\kappa^2\text{-teeda})]$ (right) *teeda* = *N,N,N',N'*-tetraethylethane-1,2-diamine.

b. Principles of aggregation

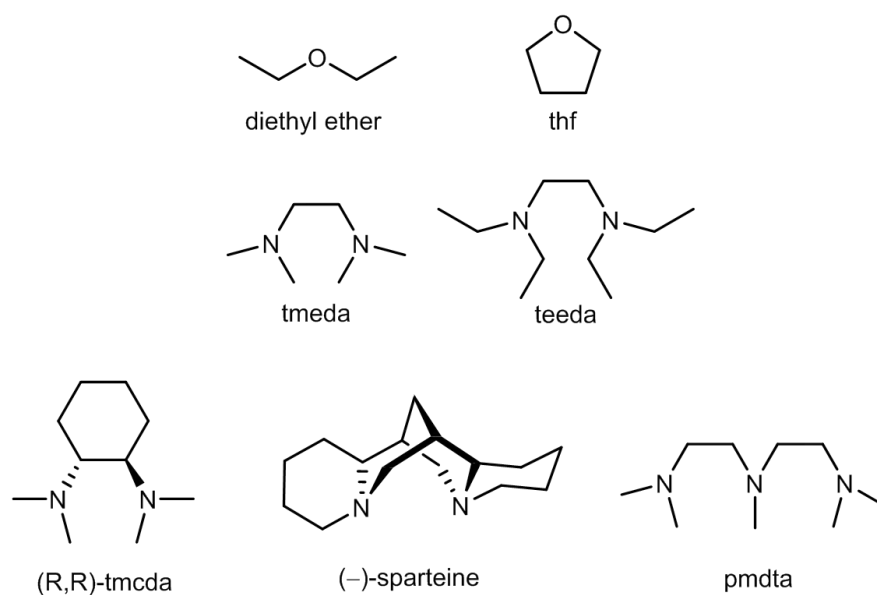
The discovery of the oligomeric nature and the understanding of the strong structure-reactivity relationship in organolithium compounds have led scientists to focus on rules that could describe the deaggregation process. We give herein a brief summary of these empirical rules.^{67,47}

i. Size of the R group

The first factor that rules the degree of aggregation of organolithium is the nature of the R group. Generally, the cluster size is inversely proportional to the bulkiness of the carbanion. This tendency is illustrated by the aggregation states of the different BuLi isomers in non-coordinating media: linear *n*-BuLi is a mixture of nonamer, octamer and hexamer, branched *i*-BuLi is hexameric, secondary alkyl *s*-BuLi is a mixture of hexamer and tetramer and sterically hindered *t*-BuLi is tetrameric.⁶⁸⁻⁷⁰ Nonetheless, one should be cautious when considering this tendency, as many counter-examples can be found, usually because secondary interactions cannot be precluded (for instance tertiary *t*-BuLi is monomeric in thf⁷¹ just like the primary and therefore less bulky benzyl lithium⁷²).

ii. Addition of a Lewis base

A technique commonly used to better control deaggregation is to add Lewis bases to the reaction medium. It can be the solvent itself, such as thf or diethyl ether, or ligands, above all tertiary polyamines such as the ones depicted in Scheme 1.3.



Scheme 1.3 Common Lewis bases used for the coordination of organolithium complexes. *Tmeda* = *N,N,N',N'*-tetramethylethane-1,2-diamine; *(R,R)-tmcda* = *(R,R)-N,N,N',N'*-tetramethylcyclohexane-1,2-diamine; *pmdta* = *N,N,N',N'',N'''*-pentamethyldiethylenetriamine.

As donors they help to stabilise the Lewis acidic Li^+ centres. They can also break the secondary interactions and hence reduce the size of the aggregates. Again, we can illustrate this tendency by considering *n*-Buli (mixture of nonamer, octamer and hexamer in cyclopentane^{68,69} / tetramer in diethyl ether⁷³) and *t*-Buli (tetramer in cyclopentane^{68,69} / monomer in thf⁷²), among a plethora of other studies. The control induced by addition of donor species is much more reliable than that resulting from the bulkiness of the R group. Besides, tuning the bulkiness or the denticity of the Lewis base itself allows a more precise control of the aggregation degree as exemplified by the different solid-state structures of PhLi (Figure 1.1).

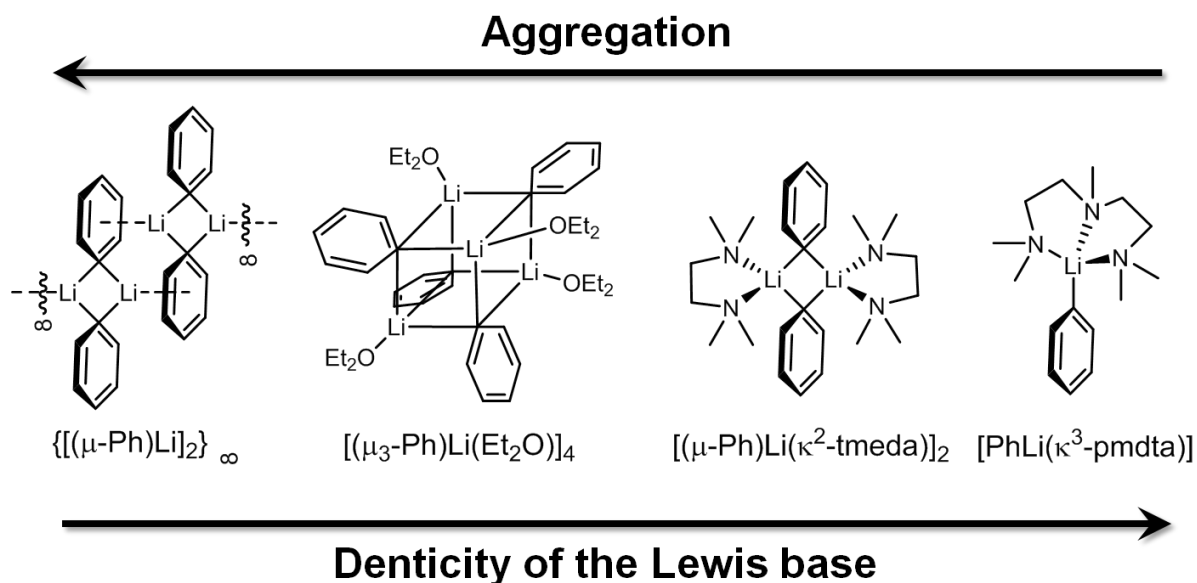
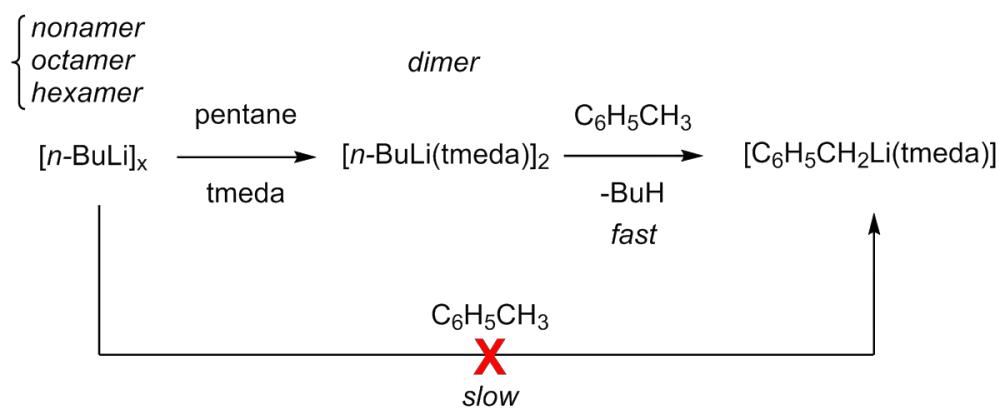


Figure 1.1 Solid state structures of $\{[(\mu\text{-Ph})\text{Li}]_2\}_\infty$, $[(\mu_3\text{-Ph})\text{Li}(\text{Et}_2\text{O})]_4$, $[(\mu\text{-Ph})\text{Li}(\kappa^2\text{-tmeda})]_2$, and $[\text{PhLi}(\kappa^3\text{-pmdta})]$.

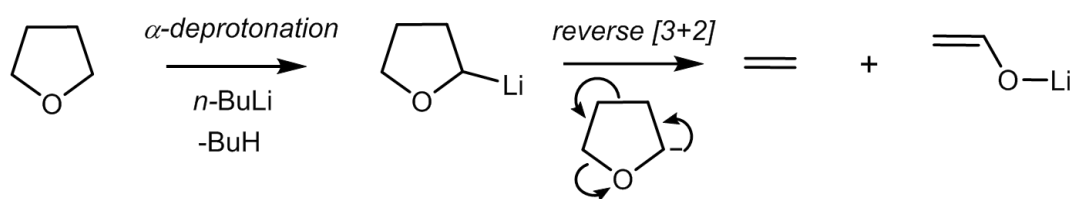
Solvent-free PhLi has a polymeric structure as the result of secondary π -interactions between Li^+ and the aromatic rings.⁷⁴ Introduction of Et_2O prevents these interactions (the donor–acceptor O–Li bond being favoured), leading to a tetrameric structure.⁷⁵ PhLi was then found to deaggregate to form a dimer in the presence of the bidentate tmeda⁷⁶ down to a monomer with the help of the tridentate pmdda.⁷⁷

Deaggregation of organolithiums in the presence of Lewis base is a useful tool when it comes to synthesis. Indeed, small – sometimes monomeric – species enhance the rate of otherwise slow reactions. For instance, the deprotonation reaction of toluene by *n*-BuLi is thermodynamically possible [$\text{pK}_a(\text{butane}) = 50 (\text{H}_2\text{O}) \gg \text{pK}_a(\text{toluene}) = 40 (\text{H}_2\text{O})$],⁷⁸ but immeasurably slow. However, in the presence of 1 eq. of tmeda, the reaction occurs smoothly albeit with a $t_{1/2}$ of approximately one day (Scheme 1.4).⁷⁹



Scheme 1.4 Deprotonation reaction of toluene by *n*-BuLi in presence or absence of tmeda. $x = 6, 8$ or 9 .

A major drawback of the use of Lewis bases is that enhancement of the organolithium reactivity is sometimes directed toward the donor molecules themselves. Ether cleavage reactions occur when a very reactive and basic organolithium compound metallates an ether molecule. The α -deprotonation of thf by *n*-BuLi is followed by a reverse [3+2] cycloaddition that yields ethylene and the lithium enolate of acetaldehyde (Scheme 1.5).^{80,81} Polyamines can also be deprotonated in a methyl or ethyl position with formation of α - or β -lithiated amines (tmeda gives $[\text{Me}_2\text{NCH}_2\text{CH}_2\text{N}(\text{Me})\text{CH}_2\text{Li}]$ and teeda gives $[\text{Et}_2\text{NCH}_2\text{CH}_2\text{N}(\text{Et})\text{CH}_2\text{CH}_2\text{Li}]$).^{66,67,82-85}



Scheme 1.5 Thf cleavage reaction in the presence of *n*-BuLi.

A direct consequence of ether cleavage reactions is the difficulty with storing organolithiums in ethereal media. Hence, they are usually kept and sold as hydrocarbon solutions, and activated by Lewis bases only when necessary.

iii. Concentration and temperature

Two other factors that influence the aggregation state are concentration and temperature, albeit to a lesser extent than addition of donor molecules. The influence of concentration follows Le Chatelier's principle: the size of the aggregate increases when the concentration in organolithium compounds increases. Representative results are compiled in Table 1.2. The influence of temperature is less clear. For alkyllithiums in hydrocarbon solution, an increase of temperature leads to a decrease in aggregation (Table 1.2, entry 1, 2, 3, 5 and 7) however the opposite behaviour was reported for *n*-BuLi in thf (Table 1.2, entry 4). Temperature change had no effect in the case of PhLi (Table 1.2, entry 8 and 9).

Table 1.2 Aggregation degree dependence in concentration (*C*) and temperature (*T*) for several organolithium complexes in solution.

Entry	RLi	Solvent	Aggregation degree when concentration increases	Aggregation degree when temperature increases	References
1	EtLi	Cyclopentane	- ^a	(6+8+9) → 6	68,69,86
2	<i>n</i> -PrLi	Cyclopentane	-	(6+8+9) → 6	87
3	<i>n</i> -BuLi	Cyclopentane	-	(6+8+9) → 6	68,69,86
4		Thf	2 → 4	2 → 4	88
5	<i>i</i> -PrLi	Cyclopentane	-	6 → 4	68,69
6		Benzene/cyclohexane	4 → 6	-	86
7	<i>s</i> -BuLi	Toluene	-	6 → 4	70
8	PhLi	Et ₂ O	(2+4) → 4	No change	89,90
9		Thf	(1+2) → 2	No change	90

^aNo data reported.

1.2. Secondary interactions

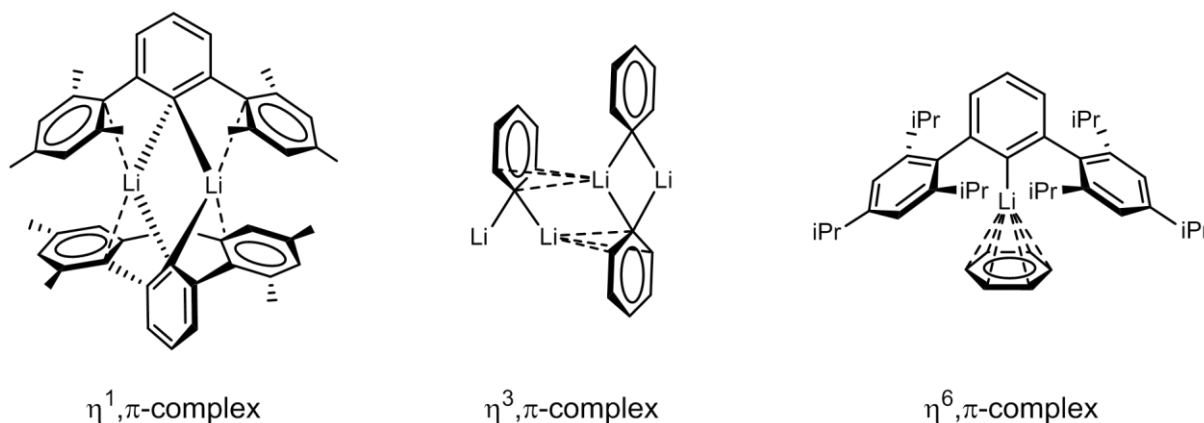
The importance of secondary interactions on the aggregation and properties of organolithiums was acknowledged as early as the elucidation of the structure of MeLi in the

1960s.^{62,63} The methyl groups of the $[\mu_3\text{-MeLi}]_4$ clusters were found to interact with the Li atoms of the neighbouring Li_4 tetrahedrons [$\text{Li}\cdots\text{C}$ 2.36 Å to compare with Li-C 2.31 Å], generating a three dimensional polymeric network. These short contacts were later attributed to $\sigma(\text{C-H})\cdots\text{Li}$ interactions (*vide infra*) by Schleyer.⁵³ These secondary interactions are responsible for low volatility of solid MeLi and its poor solubility in hydrocarbon solvents. Although the structure of *t*-BuLi is similar to that of MeLi, intra- instead of inter-molecular $\text{Li}\cdots\text{Me}$ interactions preclude the formation of a polymeric structure. Hence, *t*-BuLi is soluble in hydrocarbons and sublimes at 70°C/1 mbar.

Secondary interactions in organolithiums are best described as electrostatic interactions between electronic density on the R group (different from the negative charge of the carbanion) and a Li^+ centre. They mostly arise when a π -system of an aromatic substituent or $\sigma(\text{C-H})$ or $\sigma(\text{C-C})$ bonds are in the vicinity of low-coordinate Li centres (2,3). These interactions are usually depicted as weak (*ca* 4-40 kJ/mol),⁹¹ however calculations indicate that they may account for as much as 40% of the valence electron density of the Li atom.⁹² As previously stated donor bases, by filling the coordination sphere of Li, compete with those interactions.

a. π -system $\cdots\text{Li}$ interactions

The simplest system for the study of π -system $\cdots\text{Li}$ interactions is obviously PhLi. In the absence of donor ligands, the secondary interactions cause the structure to be polymeric (Scheme 1.6, centre).⁷⁴ As a consequence, PhLi is not soluble in hydrocarbons. The structure is arranged around Li_2C_2 rings, with short contacts [2.401(12), 2.514(14) and 2.534(14) Å] between Li atoms and three carbons of a phenyl ring of another unit ($\text{Li}\cdots\text{C}$ η^3, π -complex). The coordination between an aromatic ring and a Li^+ centre can be η^1 , η^2 and η^6 as well. An example of an η^1, π -complex is $[(\mu\text{-}2,6\text{-Mes}_2\text{C}_6\text{H}_3)\text{Li}]_2$ depicted in Scheme 1.6 (left).⁹³ The bulkiness of the mesityl groups, together with short contacts with the *Cipso* [$\text{Li}\cdots\text{Cipso}$ distances 2.51(1) and 2.56(1) Å] help to stabilise the Li cations. The combined effects of the very bulky 2,6-(2,4,6-*i*-Pr₃C₆H₂)₂C₆H₃ ligand and the stabilisation brought by the π -system of a molecule of benzene allowed isolation of the first monomeric aryllithium derivative without donor solvent (Scheme 1.6, right).⁹⁴ In this structure, the π -system $\cdots\text{Li}$ coordination is η^6 , with benzene being perpendicular to the aromatic ring σ -bonded to Li^+ . The average $\text{Li}\cdots\text{C}(\text{C}_6\text{H}_6)$ distance is 2.35(2) Å, much shorter than in η^1, π - and η^3, π -complexes.



Scheme 1.6 Solid state structure of $[(\mu\text{-}2,6\text{-Mes}_2\text{C}_6\text{H}_3)\text{Li}]_2$ (left), a fragment of the $\{[\mu\text{-PhLi}]_2\}_\infty$ (centre), and $[2,6\text{-}(2,4,6\text{-}i\text{-Pr}_3\text{C}_6\text{H}_2)_2\text{C}_6\text{H}_3\text{Li}(\eta^6\text{-C}_6\text{H}_6)]$ (right). Secondary $\pi \cdots \text{Li}$ interactions are depicted as dashed lines.

As exemplified by these three structures, XRD is perhaps the most useful technique for the characterisation of the π -system \cdots Li coordination. As $\{[\mu\text{-PhLi}]_2\}_\infty$ and $[2,6\text{-}(2,4,6\text{-}i\text{-Pr}_3\text{C}_6\text{H}_2)_2\text{C}_6\text{H}_3\text{Li}(\eta^6\text{-C}_6\text{H}_6)]$ are not soluble in hydrocarbons and because ethers break the secondary interactions, NMR spectroscopy proves to be less useful. However, $[(\mu\text{-}2,6\text{-Mes}_2\text{C}_6\text{H}_3)\text{Li}]_2$ was analysed by ^{13}C NMR in benzene- d_6 , but the chemical shift for *Cipso* (δ 143.01) is similar to that for the precursor $\text{Mes}_2\text{C}_6\text{H}_3\text{I}$ (δ 144.7)⁹⁵ and is therefore non-representative of the $\pi \cdots \text{Li}$ interaction.

b. $\sigma(\text{C-H}) \cdots \text{Li}$ interactions

Prior to discuss the nature of the $\sigma(\text{C-H}) \cdots \text{Li}$ interactions, we would like to clarify some definitions. The term “agostic interaction” was initially defined as an intramolecular covalent interaction between a C–H bond and a transition metal complex.⁹¹ However, we propose to adopt the definition given by Scherer and McGrady: “agostic interactions are characterised by the distortion of an organometallic moiety which brings an appended C–H bond into close proximity with the metal centre”.⁹⁶ Hence, we consider that an interaction can be classified as agostic, even if it is essentially electrostatic. However, in this report we distinguish an agostic distortion (which is only measured thanks to solid-state structural parameters) from an agostic interaction (which is defined when several data are gathered, including agostic distortion, but also spectroscopic measurements and/or computational calculations).

The C–H agostic interactions can be characterised by combination of several techniques:

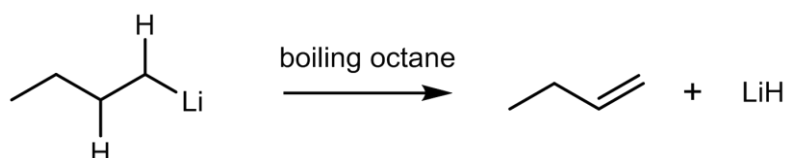
(i) XRD can be used to determine short Li \cdots H distances (short = much smaller than the sum of the van der Waals radii of the two atoms, *ca* 3.02 Å) and sometimes C–H bond lengthening. However, due to its atomic number of 1 and therefore its small electron density, it is difficult to locate the hydrogen atom precisely. Thus, Li \cdots H or C–H distances measured by XRD should be considered with extreme care and establishment of $\sigma(\text{C–H})\cdots\text{Li}$ distortions by this technique alone can be controversial.^{96,97}

(ii) Neutron diffraction is better suited to locate hydrogens, although it cannot be used routinely.

(iii) As C–H agostic interactions can be responsible for a weakening (and a lengthening) of the involved C–H bond, they can be detected by vibrational spectroscopic techniques. For instance, a lowering of the wavenumber is observed in the IR spectra of compounds bearing C–H agostic interactions in the solid state (see below the example of *c*-HexLi).⁹⁸ Solution characterisation of C–H agostic interactions is sometimes possible by NMR (lowering of the J_{CH} coupling constants).⁹¹

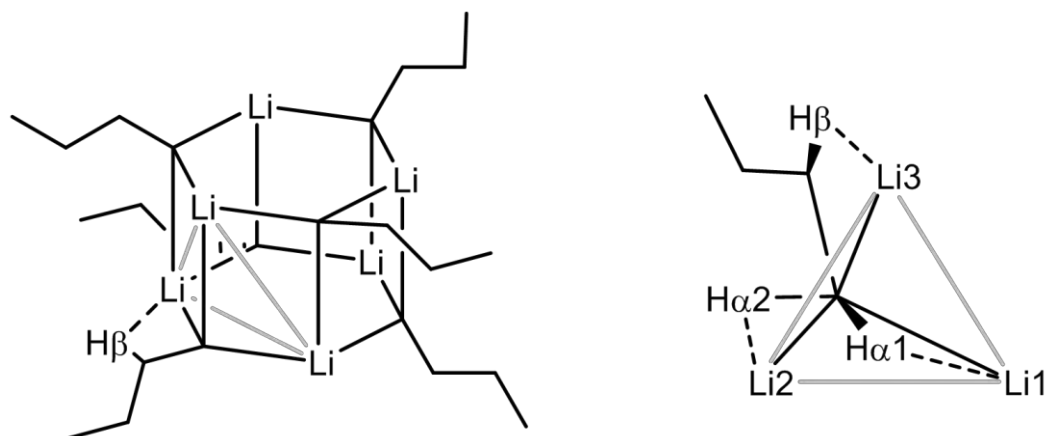
(iv) Theoretical chemistry is also a useful tool to characterise these secondary interactions.⁹⁶ Optimisation of solid-state structures allows one to locate the position of the H atoms, which can be compared with XRD and neutron diffraction measurements. It is possible to calculate J_{CH} coupling constants, which is valuable when the NMR measurements fail due to the high fluxionality of the species.

Early works reported that thermal decomposition of *n*-BuLi in boiling octane occurred *via* α or β -elimination, accompanied by formation of LiH (Scheme 1.7).⁹⁹ Similar behaviour was observed for *c*-HexLi when heated to 70°C.^{98,100}



Scheme 1.7 Thermal decomposition of *n*-BuLi.

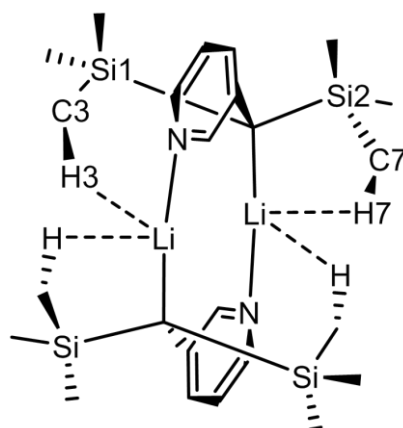
This C–H activation reaction was rationalised as the consequence of C–H agostic interactions in the solid state structure.^{100,101} As depicted in Scheme 1.8, *n*-BuLi features short Li⋯H contacts [Li2⋯H α 2 2.04(2), Li3⋯H β 2.03(2) Å]⁶⁴ that are similar to the Li–H distances [2.043(1) Å] in lithium hydride.¹⁰⁰



Scheme 1.8 Solid state structure of $[\mu_3\text{-}n\text{-BuLi}]_6$ (left) and the projection perpendicular to one of the Li triangles of the distorted octahedron with a coordinated *n*-Bu group. CH⋯Li closest contacts are depicted as dashed lines.

Other works report the existence of C–H agostic interactions in organolithiums, notably for *i*-PrLi¹⁰² and *t*-BuLi.⁶⁴ Furthermore, an extensive study of the CSD by Braga in 1996 established that short Li⋯H contacts (less than 2.20 Å) with C–H bonds were actually quite common.⁹⁷ However, due to the imprecision of XRD, no C–H lengthening could be clearly observed.

A detailed study of $\sigma(\text{C-H})\cdots\text{Li}$ interactions (inter and intramolecular) was performed on the complex $[2\text{-}(\text{Me}_3\text{Si})_2\text{CLiC}_5\text{H}_4\text{N}]_2$, thanks to neutron diffraction.^{60,96} The solid state structure, as depicted in Scheme 1.9, is a dimer generated by an inversion centre. Each fragment possesses an intermolecular $\sigma(\text{C-H})\cdots\text{Li}$ interaction [short Li $_i$ ⋯H3 2.245(5) Å] and a γ -CH agostic interaction [short Li⋯H7 2.320(6) Å and acute Li–C–Si2 88.8(2)°] which compensate for the electron deficiency of the formally two-coordinated Li⁺.



Scheme 1.9 Solid state structure of $[2-(\text{Me}_3\text{Si})_2\text{CLiC}_3\text{H}_4\text{N}]_2$. $(\text{C}-\text{H})\cdots\text{Li}$ short contacts are depicted as dashed lines.

No C–H elongation is measured by neutron diffraction [C7–H 1.089(4), 1.086(4), 1.087(4) Å]. The authors conclude that C–H agostic interactions with Li are not necessarily associated with significant C–H elongation. However, probably due to the presence of an N donor, the interactions are weaker, as indicated by the longer H \cdots Li contacts [Li \cdots H7 2.320(6) vs. Li3 \cdots H β 2.03(2) Å in *n*-BuLi]. Hence, a similar study should be done on hydrocarbyllithium compounds to unambiguously determine the existence of a C–H lengthening.

c. $\sigma(\text{C}-\text{C})\cdots\text{Li}$ interactions

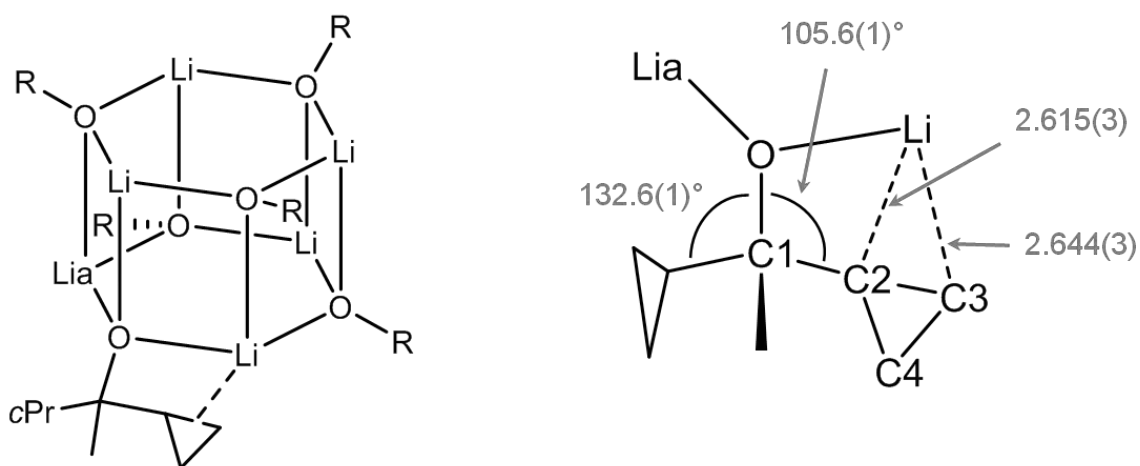
In this report, we extend the definition of agostic interaction given above for $\sigma(\text{C}-\text{H})$ to $\sigma(\text{C}-\text{C})$ bonds, as proposed by Etienne and Weller.⁶ Hence, comparable characterisation techniques can be used, with XRD being this time a powerful technique to measure short Li \cdots C contacts and C–C bond lengthening. Also, a lowering of the J_{CC} coupling constant can be observed by NMR, or calculated as a consequence of a C–C agostic interaction.¹⁰³

Studies of such C–C agostic interactions with Li are scarce and the interactions are generally not very well characterised. Several works report the presence of short Li \cdots C contacts (smaller than *ca* 2.5 Å). In the solid state structures of *n*-BuLi, *i*-PrLi, *c*-HexLi and *t*-BuLi, short Li–C β contacts [ranging from *ca* 2.30 to 2.40 Å] could suggest the existence of C–C agostic interactions.^{64,98,102} However, α - and β -C–H agostic distortions were observed in these structures (*vide supra*) and the C α –C β bonds were not significantly elongated. It is therefore difficult to conclude on the nature of the secondary interactions

Three other studies are worth mentioning.

- The first is an NMR study of ^{13}C enriched 2-(phenyl)cyclopropyllithium, in which a low $\text{C}\alpha\text{-C}\beta$ coupling constant was reported ($J_{\text{CC}} < 0.5$ Hz, $J_{\text{CC}} = 12$ Hz in the non-lithiated precursor).¹⁰⁴ However, the NMR data was accompanied neither by a XRD structure nor by DFT calculations.

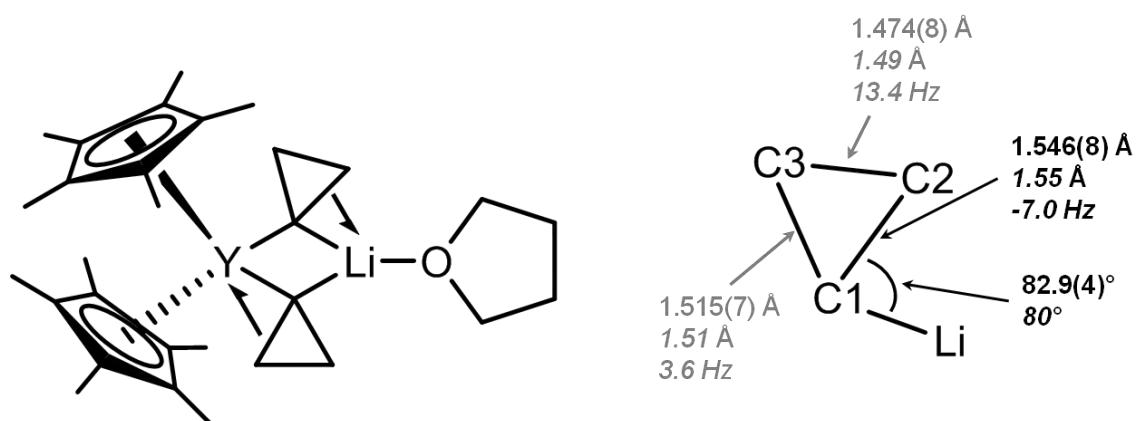
- The second is a complete study of an alkoxy derivative bearing cyclopropyl arms. The solid state structure of $[\mu^3\text{-O-C(CH}_3\text{)-(c-Pr)}_2\text{Li}]_6$ (Scheme 1.10, left) is a hexamer in which one of the cyclopropyl arm of the $\text{O-C(CH}_3\text{)-(c-Pr)}$ is coordinated to the Li^+ via a cyclopropyl edge interaction (as defined by the authors).¹⁰⁵



Scheme 1.10 Solid state structure of $[\mu^3\text{-O-C(CH}_3\text{)-(c-Pr)}_2\text{Li}]_6$ (left) and one of the $[\mu\text{-O-C(CH}_3\text{)-(c-Pr)}_2\text{Li,Lia}]$ unit (right). R stands for $\text{O-C(CH}_3\text{)-(c-Pr)}_2$. $(\text{C-C})\cdots\text{Li}$ short contacts are depicted as dashed lines. Distances are given in Å.

The acute Li-O-C1 [$105.6(1)^\circ$] vs. Lia-O-C1 [$132.6(1)^\circ$] undoubtedly establishes the presence of an interaction (Scheme 1.10, right), although reasonably long $\text{Li}\cdots\text{C}$ distances [C2-Li $2.615(3)$, C3-Li $2.644(3)$ Å] and no significant lengthening of the C2-C3 bond [$1.519(3)$ Å in the coordinated arm vs. $1.499(2)$ in the free arm] are observed.

- The third is a heterobimetallic lithium yttrium cyclopropyl complex.¹⁰⁶ $[(\text{C}_5\text{Me}_5)_2\text{Y}(\mu\text{-c-Pr})_2\text{Li}(\text{thf})]$ (Scheme 1.11, left) exhibits two C-C agostic distortions directed respectively toward the Li and Y centres. They have been characterised by combined XRD analysis and DFT calculations. We describe only the $\text{Li}\cdots\text{C-C}$ agostic interaction and not the $\text{Y}\cdots\text{CC}$ one.



Scheme 1.11 Solid state structure of $[(C_5Me_5)_2Y(\mu\text{-}c\text{-}Pr)_2Li(thf)]$ (left) and the $[Li\text{-}c\text{-}Pr]$ unit (right). C–C agostic interactions are depicted as semi-arrows. Parameters on the cyclopropyl moiety are given as follow: XRD determined bond lengths or angles (top), calculated lengths or angles (middle, italic), calculated J_{CC} (bottom, italic).

The cyclopropyl is tilted toward the three-coordinated Li^+ , with an acute $Li\text{-}C1\text{-}C2$ angle [$82.9(4)^\circ$] vs. $Y\text{-}C1\text{-}C3$ [$127.4(4)^\circ$], which brings Li and C2 in short contact [$2.473(11)^\circ$] (Scheme 1.11, right). A significant lengthening of the $C1\text{-}C2$ bond [$1.546(8) \text{ \AA}$] was observed when compared to $C1\text{-}C3$ [$1.515(7) \text{ \AA}$] and $C2\text{-}C3$ [$1.474(8) \text{ \AA}$]. These parameters were reproduced by DFT calculations and a lowering of the calculated J_{C1C2} coupling constant (-7.0 Hz), compared to J_{C1C3} (3.6 Hz) and J_{C2C3} (13.4 Hz), confirmed the existence of a strong C–C agostic interaction. This example demonstrates the importance of multiple methods of analysis for the characterisation of these secondary interactions.

As seen in the two latter complexes, the ability of the cyclopropyl moiety to exhibit secondary interactions in the presence of O-donors is striking. Indeed, the secondary interactions observed in other organolithium compounds were systematically quenched in presence of Lewis bases (*cf.* structures of the following organolithiums in presence of donors: $MeLi$,¹⁰⁷ $n\text{-}BuLi$,¹⁰⁸ $i\text{-}PrLi$,¹⁰⁹ $t\text{-}BuLi$;⁶⁴ and $PhLi$ ⁷⁵).

1.3. The cycloalkyllithium compounds

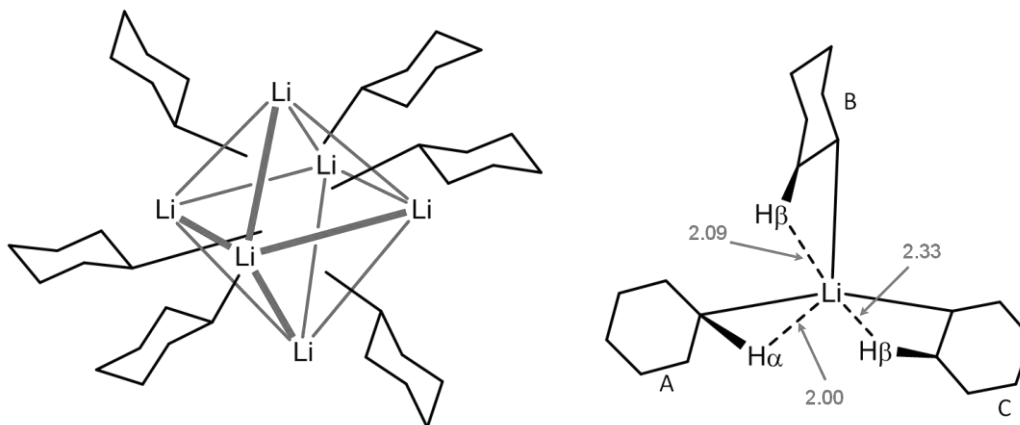
a. Cyclohexyl- and cyclopentyllithium

As stated previously, not only are we interested in the study of secondary C–C agostic interactions with Li, but we also aim at widening the restricted field of fully characterised

cycloalkyllithiums. Only two of them (*c*-HexLi and *c*-PenLi) have been described and are presented herein:

Cyclohexyllithium

c-HexLi was one of the first crystallised alkylolithium.⁹⁸ *c*-HexLi is hexameric in the solid state (Scheme 1.12, left) just like *n*-BuLi⁶⁴ or *i*-PrLi.¹⁰² The cyclohexyl rings are in the chair conformation and are associated equatorially with the faces of the lithium atoms.

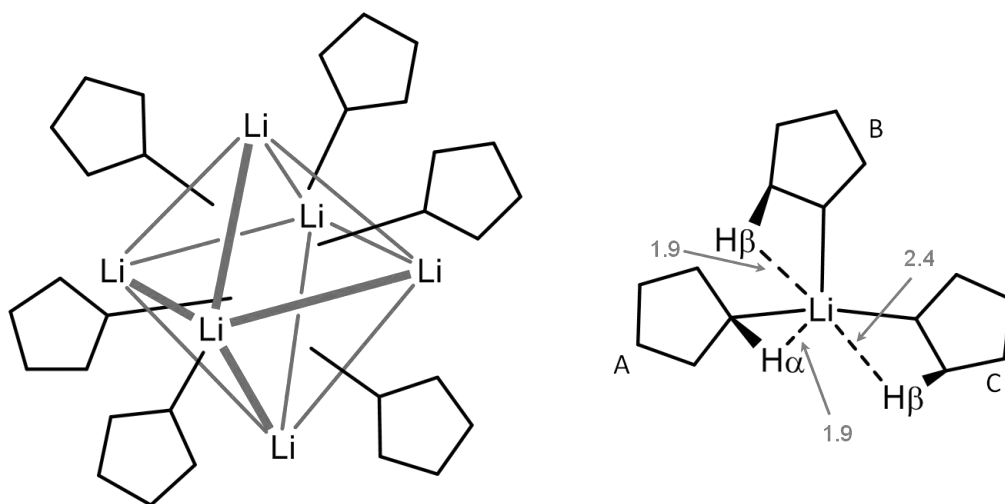


Scheme 1.12 Solid state structure of $[\mu_3\text{-}c\text{-HexLi}]_6$ (left), coordination sphere of lithium atom (right). (C–H)··Li short contacts are depicted as dashed lines. Distances (Å) are averaged from the whole hexamer.

One short Li··H α [av. 2.00 Å] and two Li··H β [av. 2.09 and 2.33 Å] contacts complete the coordination sphere of Li (Scheme 1.12, right). In the infra-red spectrum of *c*-HexLi, in addition, low C–H stretching bands between 2900 cm⁻¹ and 2720 cm⁻¹ have been observed. This constitutes the only proof of a lengthening of this bond (the XRD data being not precise enough). One short Li··C β distance is reported in ring B [2.402(6) Å], but is probably a consequence of the short Li··H β –C β agostic interaction. The solution behaviour was not investigated.

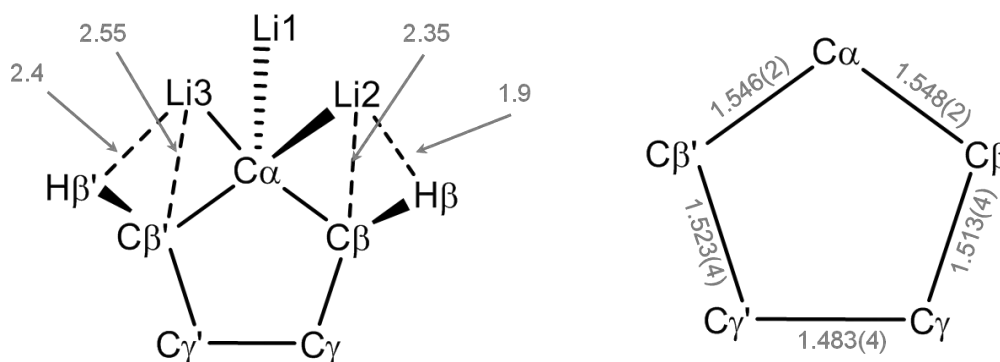
Cyclopentyllithium

The XRD structure of *c*-PenLi was published recently, nearly forty years after that of *c*-HexLi.¹¹⁰ It features the same hexameric pattern, depicted in Scheme 1.13 (left).



Scheme 1.13 Solid state structure of $[\mu_3\text{-}c\text{-PenLi}]_6$ (left), coordination sphere of lithium (right). (C–H)⋯Li short contacts are depicted as dashed lines. Distances (Å) are averaged from the whole hexamer.

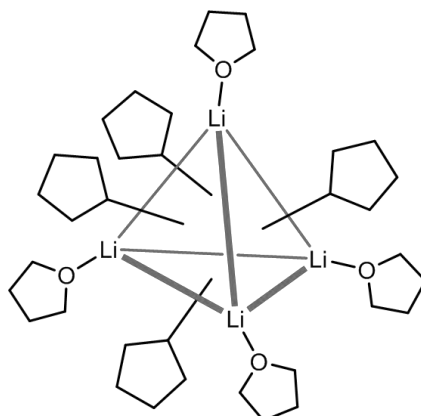
The coordination sphere around Li is similar to that of *c*-HexLi with three C–Li bonds and three CH agostic interactions (Scheme 1.13, right). Yet, the structure presents several short Li⋯C β distances, together with slightly elongated C α –C β / C β ' bonds (Scheme 1.14). No statement was made about the existence of secondary interactions in this study.



Scheme 1.14 Coordination of one cyclopentyl moiety on the Li atoms (left) and bond lengths in the cyclopentyl ring (right). (C–H)⋯Li and (C–C)⋯Li short contacts are depicted as dashed lines. All the cyclopentyl groups are different in the hexamer but the same tendencies are observed for all of them.

The structure of the *c*-PenLi with coordinated thf was also reported in the same study (Scheme 1.15). As expected, the aggregation degree decreases down to a tetramer, and the

secondary interactions are suppressed [$\text{Li}\cdots\text{H} > 2.6 \text{ \AA}$ and $\text{Li}\cdots\text{C}\beta > 2.9 \text{ \AA}$]. No significant elongation of the C–C bonds of the *c*-pentyl ring was observed.



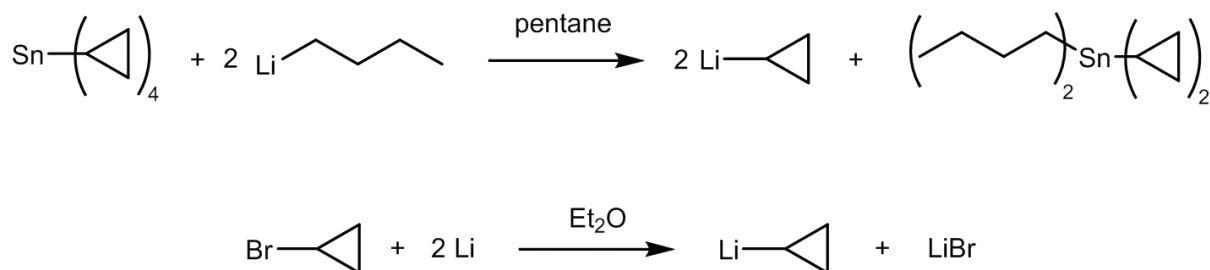
Scheme 1.15 Solid state structure of $[\mu_3\text{-}c\text{-PenLi}(\text{thf})]_4$

The solution behaviour of the two aggregates was studied by mean of 1- and 2-D NMR spectroscopy. *c*-PenLi was revealed to be a mixture of hexamers and tetramers in non-coordinating media and is solely tetrameric in thf.

b. Cyclopropyllithium

Several organolithiums bearing an α -cyclopropyl motif have been reported ($[\mu\text{-bicyclo}[1,1,0]\text{buLi}(\kappa^2\text{-tmeda})]_2$,¹¹¹ $[2,2\text{-Diphenyl-1-(phenylsulfonyl)-}c\text{-PrLi}(\kappa^2\text{-DME})]_2$,¹¹² and tris(trimethylsilyl)tetrahydranyllithium¹¹³). No secondary interaction is present in these examples, likely due to steric constraints, high rigidity and ring strain.

The first synthesis of *c*-PrLi was described by Seyferth and Cohen and consisted in either transmetallation between *n*-BuLi and tetracyclopropyltin in pentane (Scheme 1.16, top) or classical halogen-metal exchange between bromocyclopropane and metallic Li in Et₂O (Scheme 1.16, bottom).^{114,115}



Scheme 1.16 Synthesis of *c*-PrLi by transmetalation (top) and halogen-metal exchange (bottom).

From the second route, a mixed alkyl/halide complex of formula $[(\mu_3\text{-Br})_2(\mu_3\text{-}i\text{-Pr})_2 \text{Li}_4(\text{Et}_2\text{O})_4]$ was crystallised by Schmidbaur.¹¹⁶ Its solid-state structure is depicted in Scheme 1.17, below. The four lithium atoms, each bound to a terminal diethyl ether molecule, are arranged as a distorted tetrahedron. The faces of the tetrahedron are capped by two bromides and two cyclopropyl groups.



Scheme 1.17 Solid state structure of $[(\mu_3\text{-Br})_2(\mu_3\text{-}i\text{-Pr})_2 \text{Li}_4(\text{Et}_2\text{O})_4]$ (left) and magnification on the $[\text{Li}-i\text{-Pr}]$ unit (right). $(\text{C}-\text{H})\cdots\text{Li}$ short contacts are depicted as dashed lines (right). Distances are given in Å.

$\text{Li}\cdots\text{H}\beta$ short contacts [$\text{Li}_2\cdots\text{H}_2$ 2.16 and $\text{Li}_3\cdots\text{H}_3$ 2.26 Å, Scheme 1.17, right] in the crystal structure were attributed to CH agostic distortions by the authors. However, the $\text{Li}_2\cdots\text{C}_2$ distance is in a range [<2.45 Å] where interactions cannot be precluded. No other measurement that could settle the nature of the interaction has been reported. Furthermore, because of the presence of both Br^- and Et_2O in the structure, the secondary interactions are probably restrained.

Our group has attempted to crystallize *c*-PrLi in the absence of donor ligands. *c*-PrLi was synthesised by halogen-metal exchange between bromocyclopropane and Li powder in pentane. LiBr was easily separated as a solid. After filtration, the mother liquor was cooled down and afforded, on several occasions, crops of colourless single crystals. The best attempts to resolve this structure indicates the formation of a cluster of formula [*c*-Pr₁₂Li₂₆O], which contains [*c*-Pr₁₂Li₁₄O] clusters inter mixed with a Li₁₂ structure, as depicted in Figure 1.2 below.

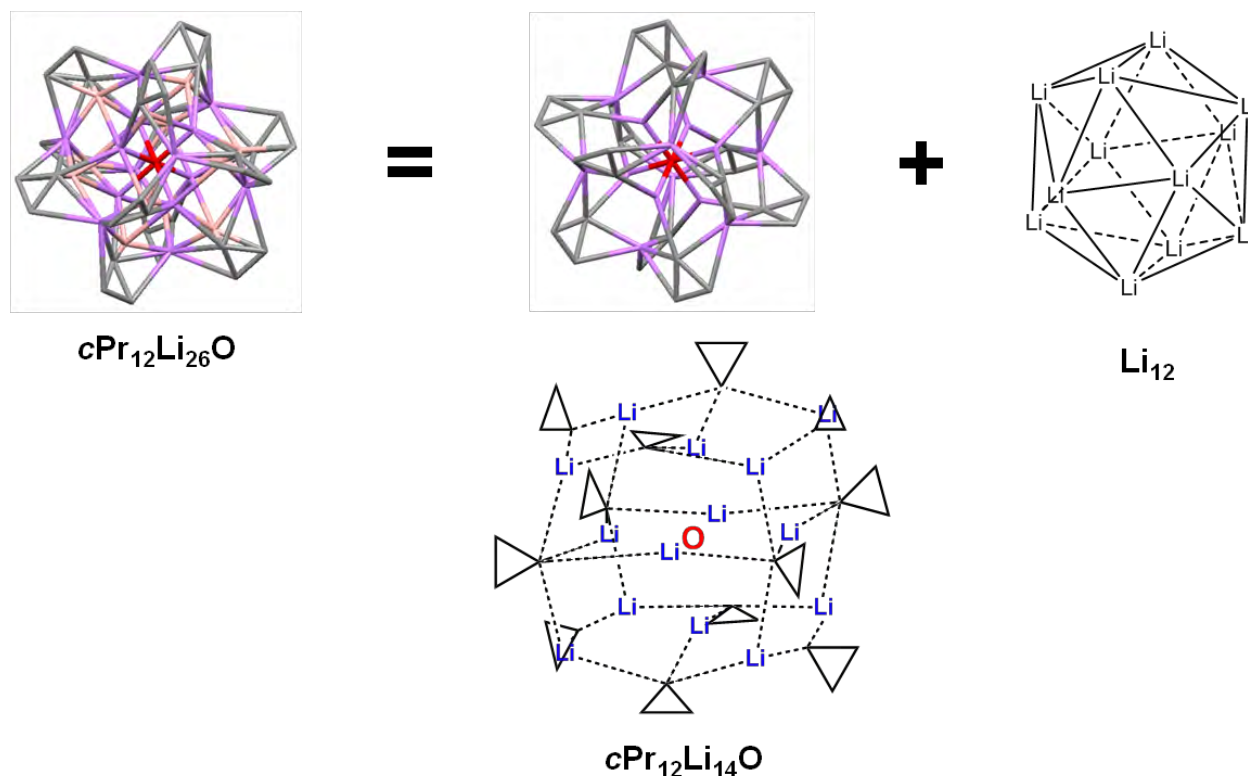


Figure 1.2 Attempt at the resolution of the *c*-PrLi crystal structure.

This intricate structure can perhaps be seen as the result of two superimposed patterns, each occupying half of the crystal cells. One is an O-centred *c*-PrLi compound and the other a Li(0) cluster. Several attempts to crystallise the compound have been carried out, and the O atom is always observed. We propose that this O atom comes from the Li metallic source. Its presence is likely to enhance the formation of these crystals rather than that of purely organolithium compounds. Due to the poor quality of this structure, it is difficult to get any information with respect to bonding and secondary interactions. Changing the Li source does not seem to solve this problem and other synthetic routes should be investigated.

In this work, we focus on the synthesis and characterisation of α -substituted cyclopropyl compounds. We expect, indeed, that the substitution at $C\alpha$ could enhance the stability, change the solubility and decrease the oxophilicity of these very reactive species.

B. Results and discussion

Two cyclopropyl derivatives are studied in details, the 1-(trimethylsilyl)cyclopropyllithium and 1-phenylcyclopropyllithium. In addition, preliminary works on a sulfur substituted cyclopropyl are also presented.

1.1. 1-(trimethylsilyl)cyclopropyllithium

a. The trimethylsilyl moiety

The trimethylsilyl moiety (SiMe_3) is often employed to stabilise a carbanion. Indeed, a phenomenon called hyperconjugation is observed when the carbanion is substituted in the α -position with silyl groups. As shown in Figure 1.3 the anionic charge in the filled orbital of the carbanion is delocalised to the antibonding σ^* orbital of the β -Si-C bonds.

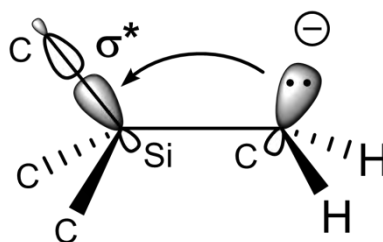
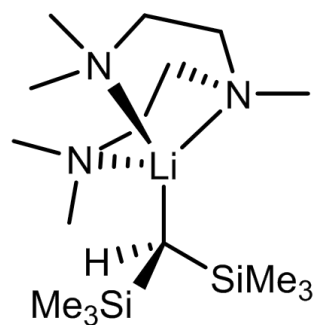


Figure 1.3 Negative hyperconjugation in the $(\text{SiMe}_3)\text{CH}_2^-$ carbanion.

This stabilisation has thermodynamic and kinetic consequences. First, a lowering of the pK_a value between a hydrocarbon and its SiMe_3 (poly)substituted version is observed, as exemplified by methane [$\text{pK}_a = 56$ (DMSO)]¹¹⁷ and tris(trimethylsilyl)methane [$\text{pK}_a = 36.8$ (THF)]¹¹⁸. The electronic delocalisation, together with the steric hindrance of the bulky SiMe_3 group also lead to a decrease of the hydrocarbyl nucleophilicity, therefore limiting side reactions.

The $[\text{CH}_{3-x}(\text{SiMe}_3)_x\text{Li}]$ complexes ($x = 1$,¹¹⁹ 2 ,¹²⁰ 3 ¹²¹) have been characterised. $[\text{CH}(\text{SiMe}_3)_2\text{Li}(\kappa^3\text{-pmdta})]$ was the first alkyl lithium complex isolated as a monomer (Scheme 1.18).¹²⁰



Scheme 1.18 Solid state structure of the $[CH(SiMe_3)_2Li(\kappa_3\text{-pmdta})]$.

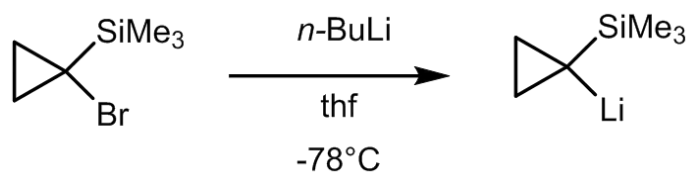
Finally, the $SiMe_3$ moiety enhances the solubility of the carbanion in non-polar media, which should facilitate the synthesis of soluble species without the need of donor bases, aiding our study of any potential agostic interactions.

b. Synthesis

As the cyclopropyl ligand is a secondary alkyl group, only one $SiMe_3$ can be added at α . Although the compound was not isolated, syntheses for 1-(trimethylsilyl)cyclopropyllithium [$\{c\text{-}C(SiMe_3)C_2H_4\}Li$] (**1**) were reported by the teams of Krief¹²² and Paquette.^{123–125} Addition reactions to carbonyl compounds leading to secondary or tertiary alcohols were performed.

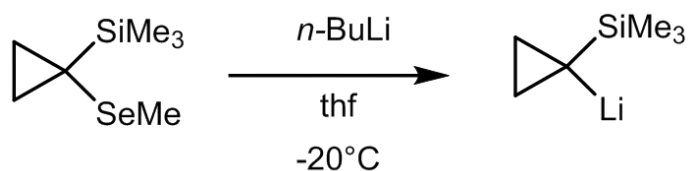
The seemingly easiest route to **1** is the deprotonation reaction of (trimethylsilyl)cyclopropane. As suggested above, the presence of the $SiMe_3$ group should decrease the pK_a of cyclopropane [$pK_a = 48$ (H_2O)],⁷⁸ which is already lower than that of commercially available $n\text{-BuLi}$ [$pK_a = 50$ (H_2O)]⁷⁸ or $t\text{-Buli}$ [$pK_a = 52$ (H_2O)].⁷⁸ Quite surprisingly, the reaction failed even when $s\text{-BuLi}$ was activated by tmda in thf solution.¹²³ Our own attempts were equally unsuccessful. For this reason, other synthetic strategies were investigated by Krief and Paquette (Scheme 1.19,¹²² Scheme 1.20¹²² and Scheme 1.21¹²³).

Route A



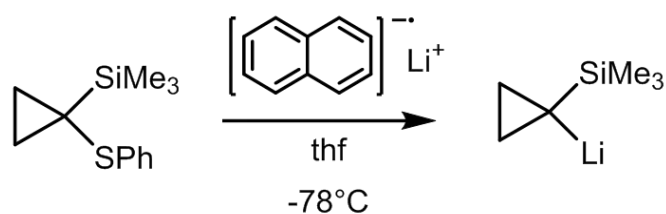
Scheme 1.19 Synthesis of **1** by halogen-metal exchange between 1-bromo-1-(trimethylsilyl)cyclopropane and *n*-BuLi.

Route B



Scheme 1.20 Synthesis of **1** by selenium-lithium exchange between 1-(methylselenide)-1-(trimethylsilyl)cyclopropane and *n*-BuLi.

Route C



Scheme 1.21 Synthesis of **1** by reductive lithiation of the C-S bond of 1-(phenylthio)-1-(trimethylsilyl)cyclopropane by lithium naphthalenide.

Even though route A (Scheme 1.19) seemed attractive, it was not considered, as 1-bromo-1-(trimethylsilyl)cyclopropane is not commercially available and its synthesis, according to the Hunsdiecker reaction, involves the use of highly toxic HgO. For the same reason and also because selenide reagents are expensive chemicals, route B (Scheme 1.20) was rejected as well. Thus, route C (Scheme 1.21) was investigated.

1-(phenylthio)-1-(trimethylsilyl)cyclopropane could be prepared in nearly quantitative yield by deprotonation of (phenylthio)cyclopropane with *n*-BuLi followed by treatment with chlorotrimethylsilane.¹²⁴ Reduction of the C–S bond by lithium naphthalene then led to desired **1**, which was generated *in situ* and reacted directly with carbonyl compounds at -78°C. Isolating this very air and moisture sensitive compound for our own studies proved to be quite challenging.

Following the reported procedure, a solution of lithium naphthalene in thf was added dropwise onto 1-(phenylthio)-1-(trimethylsilyl)cyclopropane at -78°C. Even at this temperature, the dark green lithium naphthalene solution decoloured nearly immediately. To avoid ether cleavage, the solvent was removed at 0°C. The ¹H NMR spectrum of the crude material in benzene-*d*₆ showed new broad cyclopropyl and SiMe₃ signals in the δ 1-0 region. As expected, naphthalene was also present together with an insoluble product which was later identified as lithium thiophenolate. Naphthalene was separated by sublimation at high vacuum (*P* < 10⁻⁴ mbar, RT). This operation removed also most of the coordinated thf. Extraction of the residue with toluene allowed for isolation of **1** in 81% yield. Small amounts of coordinated thf (<0.3 eq.) were still present. **1** was characterised by NMR spectroscopy and XRD. However, it proved impossible to fully remove traces of lithium thiophenolate, even by recrystallisation from mixtures of toluene/pentane.

c. Solid state structure

The solid state structure of **1** (Figure 1.4) consists of a tetramer which is generated (by a screw fourfold axis) from an asymmetric unit containing a single [$\{1-(\text{SiMe}_3)\text{-}c\text{-C}_3\text{H}_4\}\text{Li}$] molecule. The central Li₄C₄ eight-membered ring is puckered along C1...C1ⁱⁱⁱ [59.21(8)°]. Both the four Li⁺ and the four Si atoms form respectively two nearly perfect squares (Li...Li...Li av. 90°, Si...Si...Si av. 90°) perpendicular to the screw axis. Each Li⁺ atom is formally two-coordinate, a rare bonding pattern in organolithium chemistry where common coordination numbers are three and four. This remarkable behaviour has several consequences on the surrounding carbon atoms:

- The Li–μ-Cα bond lengths are remarkably short [Li1–C1 2.033(5), Li1ⁱⁱ–C1 2.025(5) Å]. In organolithium complexes, only a few monomeric^{94,126–128} and one tetrameric⁹³ arrangements present such short Li–C bonds (*i.e.* < 2.05 Å).

- The Li...Cβ distances are also in a range where interactions cannot be precluded [Li1...C12 2.405(6), Li1ⁱⁱ...C11 2.413(6) Å], with acute Li1–C1–C12 [83.7(2)°] and Li1ⁱⁱ–C1–

C11 [84.3(2)°] angles. The cyclopropyl rings look like isoscele triangles, with C α –C β bonds [C1–C12 1.528(4), C1–C11 1.529(4) Å] being longer than C β –C β [C11–C12 1.480(5) Å].

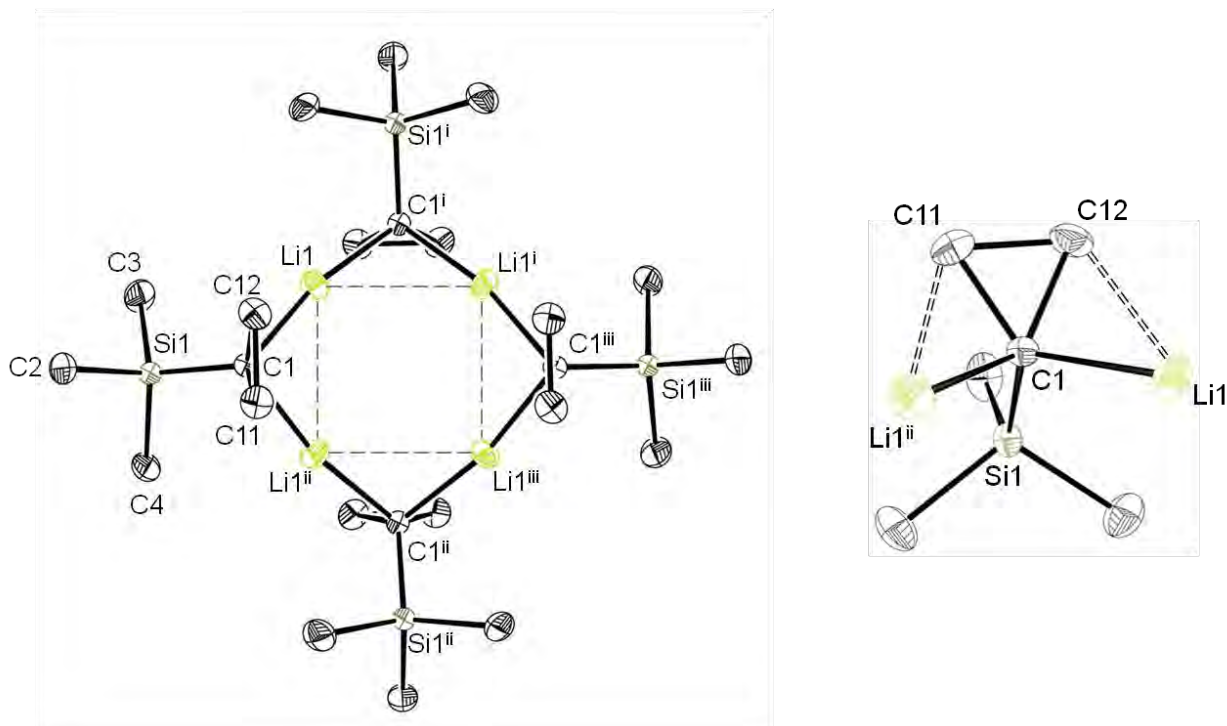


Figure 1.4 ORTEP drawing of $[\{\mu\text{-c-C}(\text{SiMe}_3)\text{C}_2\text{H}_4\}\text{Li}]_4$ (**1**)₄ (left) and $[\{\mu\text{-c-C}(\text{SiMe}_3)\text{C}_2\text{H}_4\}\text{Li}]_2$ unit (right). Ellipsoids at 30% probability level, hydrogen atoms omitted for clarity. Secondary Li...C–C interactions are depicted only on the $[\{\mu\text{-c-C}(\text{SiMe}_3)\text{C}_2\text{H}_4\}\text{Li}]_2$ unit in double dashed bonds. Relevant bond lengths (Å) and angles (°): Li1–C1 2.033(5), Li1ⁱⁱ–C1 2.025(5), Li1...C12 2.405(6), Li1...C11 2.413(6), C1–C11 1.528(4), C1–C12 1.529(4), C11–C12 1.480(5), Si1–C1 1.836(2), Si1–C2 1.874(3), Si1–C3 1.872(3), Si1–C4 1.874(3); Li1–C1–C12 83.7(2)°, Li1ⁱⁱ–C1–C11 84.3(2), Li1–C1–C11 127.5(3), Li1ⁱ–C1–C12 126.3(3), C1–Li1–C1ⁱ 167.5(3), Li1–C1–Li1ⁱⁱ 93.6(3).

The Si–Me bonds [Si1–C2 1.874(3), Si1–C3 1.872(3), Si1–C4 1.874(3) Å] are slightly longer than the Si–C α [Si1–C1 1.836(2) Å] which can be attributed to delocalisation of the negative charge on the carbanion in the $\sigma^*(\text{Si}-\text{C})$ orbitals by hyperconjugation. Due to both the short Li...C β contacts and C α –C β bonds lengthening, we propose the short Li...H distances [min. 2.22 Å] arise from the Li...C–C interactions rather than from Li...C–H interactions.

To date only one comparable crystal structure of an organolithium complex with an eight-membered ring motif of alternating lithium and carbon atoms has been reported.¹²⁹ When extended to other organoalkali metals, two similar examples were crystallised for

mixed Li/Na¹³⁰ and purely Na complexes.¹³¹ Two α -lithiated amine complexes complement the examples of these unusual structure patterns.^{66,132}

Organolithium complexes bearing formally two-coordinate Li⁺ atoms were reported for derivatives of the tris(trimethylsilyl)methylolithiate,^{121,133–135} for SiMe₃ substituted benzylolithiates,¹³⁶ and for a mixed aryl/*n*-BuLi.⁹³ In all these examples, the coordination defect was balanced by extreme steric constraints and/or secondary interactions involving the π -system of aromatic substituents or C–H or C–C bonds. In **1** the bulky SiMe₃ moieties are probably non innocent toward lithium centres, acting as protective cages. However, the SiMe₃ groups alone cannot explain the stability of this structure, and we propose it results from double-sided Li \cdots C α –C β agostic distortions that provide additional electron density on the Li⁺.

d. Solution behaviour

The nature of **1** in solution was also probed. ¹H DOSY NMR spectroscopy in benzene-*d*₆ coupled with a diffusion coefficient-formula weight (D-FW) correlation analysis¹³⁷ yielded an estimated formula weight (FW) of 470 \pm 47 g.mol⁻¹ (Figure 1.5). This result fits nicely with the calculated FW of the tetramer of **1** which is 480.78 g/mol, showing that the structure of **1** remains unchanged upon solubilisation in a non-coordinating non-polar solvent.

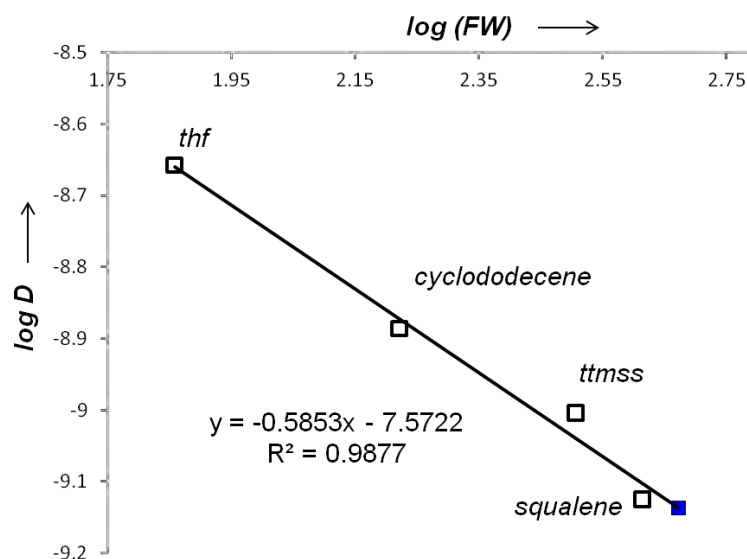


Figure 1.5 Diffusion coefficient-formula weight ¹H DOSY NMR analysis for **1** in benzene-*d*₆ (blue square). Calibrants (empty squares): thf (72.11 g/mol), cyclododecene (166.3 g/mol), tetrakis(trimethylsilylsilane), ttms (320.8 g/mol), squalene (410.7 g/mol).

The ^1H NMR spectrum of **1** in benzene- d_6 at RT is presented in Figure 1.6. It features the expected resonances for the SiMe_3 moiety at $\delta -0.01$, and the β -protons of the cyclopropyl ring at $\delta 0.80$ and 0.59 (one signal for each enantioface, attributed thanks to a NOESY experiment). The H_β atoms are on the same face as the SiMe_3 group. Some coordinated thf is also present (*vide supra*), probably leading to the formation of small quantities of deaggregated products in solution. However, this did not lead to a significant decrease of the formula established by the DOSY experiment (470 ± 47 g/mol) compared to that of the tetramer of **1** (480.78 g/mol).

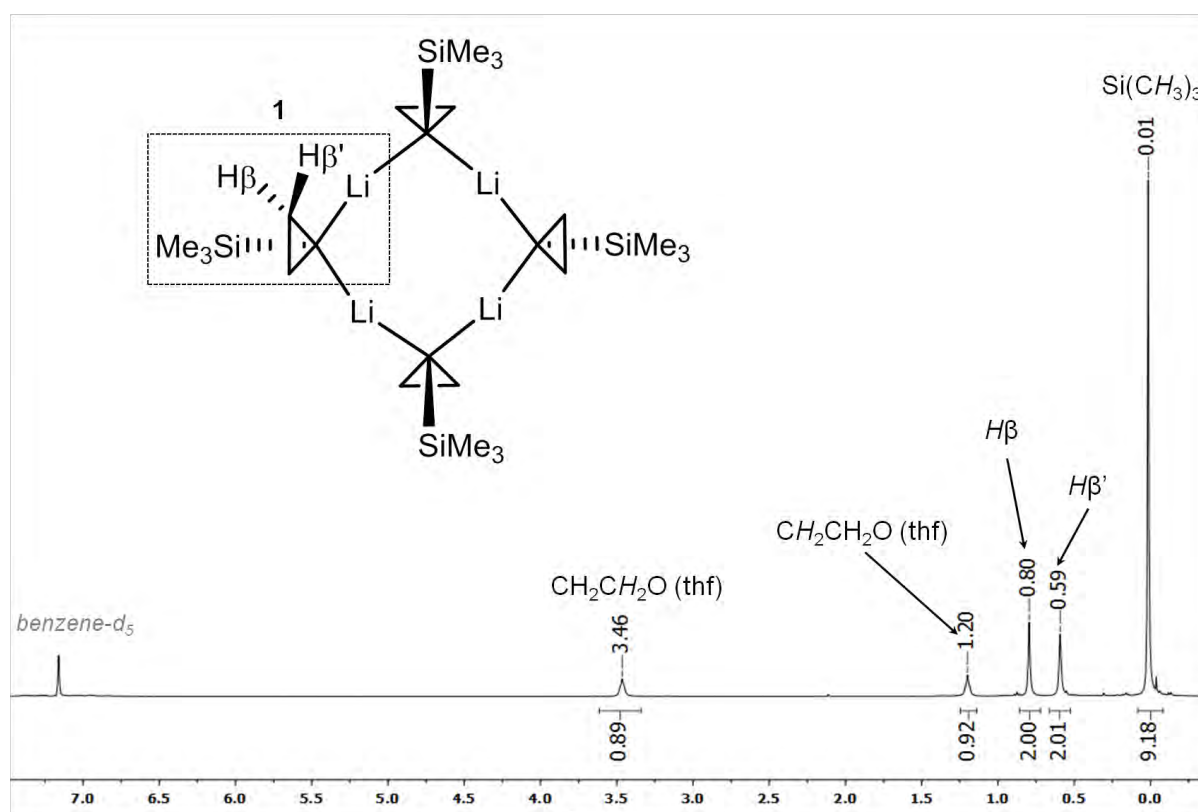


Figure 1.6 ^1H NMR spectrum of **1** in benzene- d_6 .

The ^{13}C NMR spectrum contains the expected resonance for the tms group appearing as a quadruplet centred at $\delta -1.5$ ($^1J_{\text{CH}} = 117$ Hz). The β -carbons of the cyclopropyl ring appeared as a triplet centred at $\delta 7.2$ ($^1J_{\text{CH}} = 156$ Hz) and the α -carbon (found thanks to a HMBC experiment) resonates as a singlet at $\delta 4.9$.

e. Conclusion

1 is the first fully characterised example of a cyclopropyl lithium derivative (*i.e.* by XRD, 1 and 2-D NMR). It is also the first example of an α -C–C agostic structure in an organolithium complex. The interaction has been well characterised by mean of XRD and is currently investigated by DFT calculations. The cyclopropyl moiety is particularly well adapted to the stabilisation of low-valent Li centres. Indeed, even if synthesised in thf, **1** lost its coordinated thf to form a favoured bis- α -C–C agostic compound with low-valent coordinated Li centres. This gives a qualitative estimation of the strength of these C–C agostic distortions, compared to that of thf coordination, when it comes to stabilise Li^+ .

1.2. 1-phenylcyclopropyllithium

a. The phenyl moiety

Introducing a phenyl group at the α -position of a carbanion is a well-established procedure to stabilise a negative charge. The benzylic (bn) anion has the ability to delocalise its lone pair from the p orbital of the α -carbon to the π -system of the aromatic ring. The resonance structures obtained by this mesomeric effect are shown in Figure 1.7.

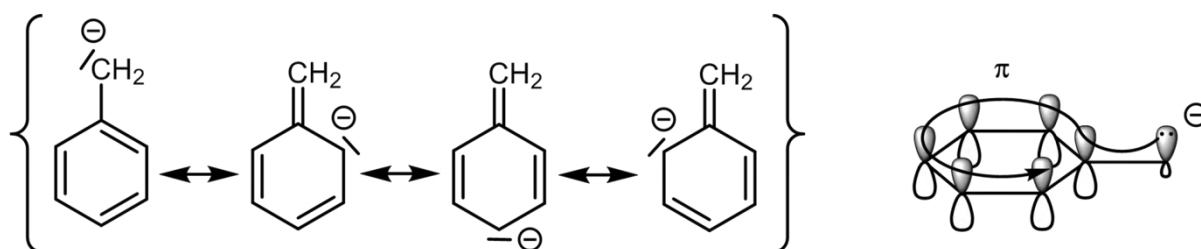


Figure 1.7 Resonance structures of the benzylic carbanion.

As a result of the delocalisation of the negative charge, the pK_a decreases as the number of phenyl groups attached to a saturated carbon increases (e.g. for methane *vs.* benzyl derivatives - Figure 1.8).

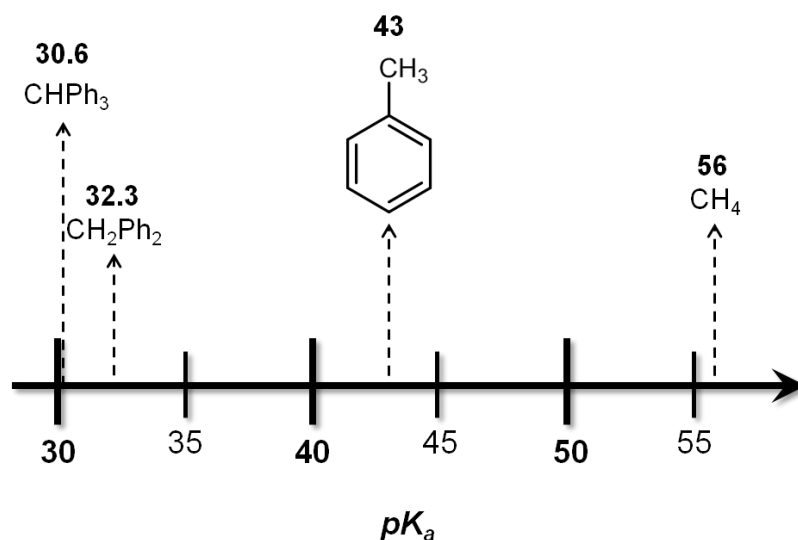
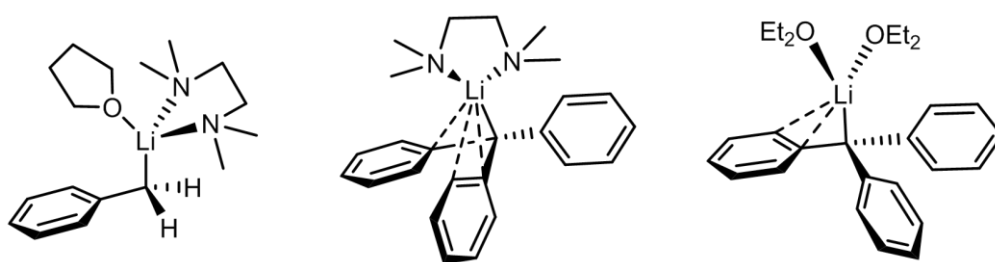


Figure 1.8 pK_a values of methane and phenyl substituted derivatives in DMSO.¹¹⁷

BnLi often crystallises as polymers (with coordinating solvents such as 1,4-diazabicyclo[2.2.2]octane,¹³⁸ diethyl ether,¹³⁹ or thf¹⁴⁰). In the presence of chelating polyamines (the bidentate tmeda (Scheme 1.22, left),¹⁴¹ the tridentate N,N,N-trimethyl-1,4,7-triazacyclononane¹⁴² and the tetradentate tris(N,N-dimethyl-2-aminoethyl)-amine)¹⁴³ monomeric BnLi complexes have been obtained. Moving from mono- to tri-substituted phenyl complexes allows crystallisation of monomeric $[\text{Ph}_3\text{CLi}(\text{tmeda})]$ (Scheme 1.22, centre)¹⁴⁴ and $[\text{Ph}_3\text{CLi}(\text{Et}_2\text{O})_2]$ (Scheme 1.22, right).¹⁴⁵ In these two complexes, short contacts were observed between the lithium cation and *Cipso* and *Cortho* of one or two of the phenyl groups. This testifies the delocalisation of the negative charge on the aromatic rings.

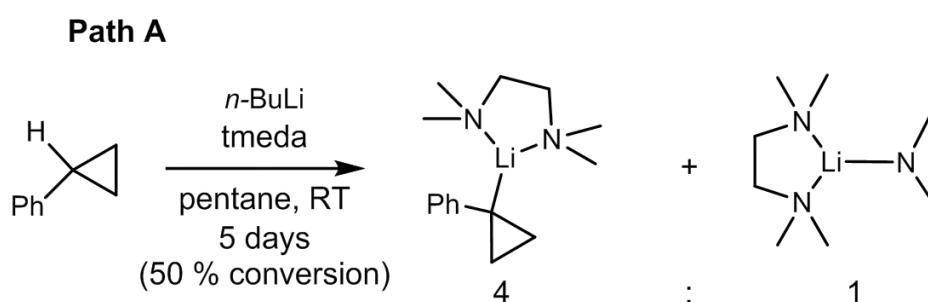


Scheme 1.22 Monomeric structures in the solid state of $[\text{PhCH}_2\text{Li}(\kappa^2\text{-tmeda})(\text{thf})]$ (left), $[\text{Ph}_3\text{CLi}(\kappa^2\text{-tmeda})]$ (centre) and $[\text{Ph}_3\text{CLi}(\text{Et}_2\text{O})_2]$ (right). Secondary $\pi \cdots \text{Li}$ interactions are depicted as dashed lines.⁴⁷

The aggregation of benzyllithium complexes in solution has not been extensively studied. Benzyllithium is monomeric in thf, cryoscopic measurements establishing the formula $[\text{PhCH}_2\text{Li}(\text{thf})_3]$.⁷² A detailed two dimensional ^1H - ^6Li HOESY NMR experiment on the benzyl derivative $[\text{PhCH}(\text{SPh})\text{Li}]$ in thf revealed a monomeric structure with three coordinated thf as well.¹⁴⁶⁻¹⁴⁸ Even on the basis of only two examples, full deaggregation of benzyllithium derivatives could constitute the standard behaviour in thf.

b. Synthesis

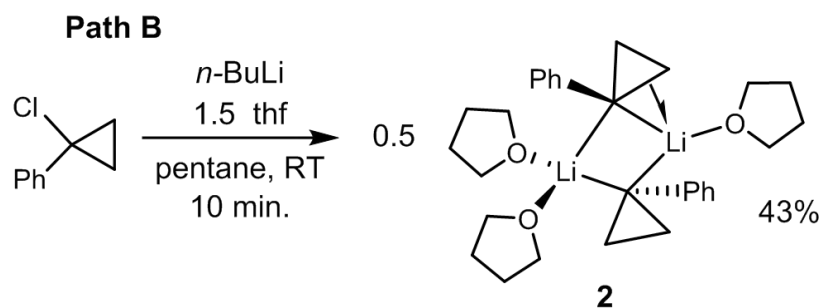
Unlike (trimethylsilyl)cyclopropane, Schlosser and Schneider reported the deprotonation of the proton at the α -position respect to the phenyl group in phenylcyclopropane, with the Lochmann-Schlosser superbases¹⁴⁹⁻¹⁵¹ ($n\text{-BuLi}$ /potassium tert-butoxide) in thf.¹⁵² However, while the potassium complex was described, no data were available on the lithiated compound. Realising phenylcyclopropane is a benzylic derivative, we developed a synthetic procedure similar to that for BnLi ,⁷⁹ which uses $n\text{-BuLi}$ in the presence of tmeda in pentane (Scheme 1.23, path A). While for the synthesis of BnLi , 50% conversion was reached in *ca.* one day at RT, a week was necessary to deprotonate about half of a phenylcyclopropane solution under the same conditions. In addition, cleavage of tmeda and formation of an inseparable mixture of $[(c\text{-CPhC}_2\text{H}_4)\text{Li}(\text{tmeda})]$ and $[(\text{NMe}_2)\text{Li}(\text{tmeda})]$ was observed in a *ca.* 4:1 ratio by ^1H NMR experiment. All attempts to separate these two products failed, but an interesting mixed alkyl/amido lithium aggregate was obtained upon crystallisation (see below – part f).



Scheme 1.23 Deprotonation reaction of phenylcyclopropane.

This side reaction was avoided by switching to a halogen/metal exchange reaction. The 1-chloro-1-phenylcyclopropane reagent was synthesised according to a literature procedure.⁴² When treated with $n\text{-BuLi}$ in a pentane/thf mixture (Scheme 1.24, path B), it

quickly and cleanly afforded 1-phenylcyclopropyllithium. Interestingly, only $[\text{Li}(\text{thf})_2(\mu\text{-}c\text{-CPhC}_2\text{H}_4)_2\text{Li}(\text{thf})]$ (**2**) was isolated, regardless of the quantity of thf used. An optimised yield of 43% was obtained using 1.5 equivalent of thf. Lithium-halogen exchange reactions are equilibria and hence we took advantage of the precipitation of **2** as the driving force of the reaction, which only happened when small quantities of thf were used. **2** was fully characterised by NMR spectroscopy, elemental analysis and X-ray diffraction.



Scheme 1.24 Synthesis of **2**.

c. Solid state structure

In the solid state (Figure 1.9), **2** is a dimer with two Li^+ ions bridged by two 1-phenylcyclopropyl groups *via* C1 (group **A**) and C10 (group **B**). The four-atoms ring (Li1–C1–Li2–C10) is puckered along Li1...Li2 [$42.79(15)^\circ$]. Remarkably, each Li^+ ion bears a different number of thf molecules. Although Li2 is bound to two thf molecules (one of which is disordered) in a pseudo tetrahedral arrangement, Li1 is trigonal planar (sum of angles = 360°) with only one coordinated thf. While the Li– μ -C α bond lengths involving Li2 [Li2–C1 2.201(4), Li2–C10 2.263(4) Å] are within the expected range for such compounds, those involving the tricoordinate Li1 [Li1–C1 2.098(4), Li1–C10 2.129(4) Å] are significantly shorter.^{84,109,67}

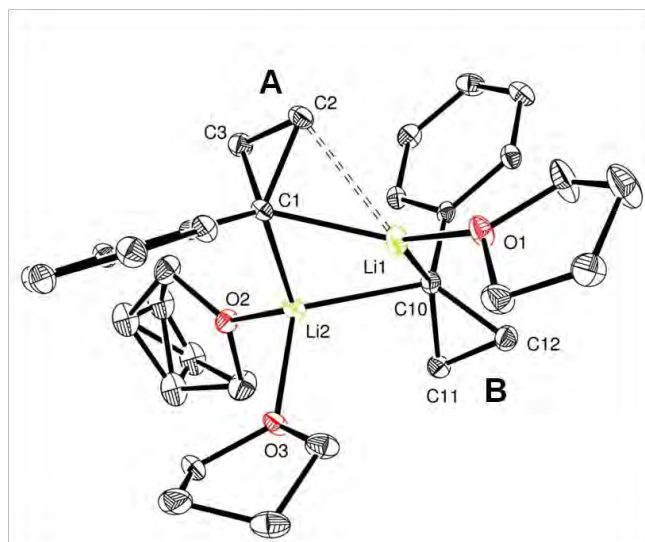


Figure 1.9 ORTEP drawing of $[\text{Li}(\text{thf})_2(\mu\text{-c-CPhC}_2\text{H}_4)_2\text{Li}(\text{thf})]$ (**2**). Ellipsoids at 30% probability level, hydrogens omitted for clarity. Secondary $\text{Li}\cdots\text{C}\cdots\text{C}$ interaction is depicted in double dashed bond. Relevant bond lengths (\AA) and angles ($^\circ$): Li1-C1 2.098(4), Li1-C10 2.129(4), Li2-C1 2.201(4), Li2-C10 2.263(4), $\text{Li1}\cdots\text{C2}$ 2.368(4), C1-C2 1.526(3), C1-C3 1.519(3), C2-C3 1.505(3), C10-C11 1.524(3), C10-C12 1.517(3), C11-C12 1.500(3); Li1-C1-C2 79.89(15), Li1-C1-C3 113.02(16), Li1-C10-C12 100.88(16), Li1-C10-C11 133.02(17), Li2-C1-C2 126.11(16), Li2-C1-C3 93.42(14), Li2-C10-C11 90.53(14), Li2-C10-C12 127.17(16).

This non-symmetric situation is accompanied by a short contact between Li1 and one of the β -carbons (C2) of the cyclopropyl ligand **A** [$\text{Li1}\cdots\text{C2}$ 2.368(4) \AA] and a correspondingly acute $\text{Li-C}\alpha\text{-C}\beta$ angle [Li1-C1-C2 79.89(15) $^\circ$]. These differences are not observed with cyclopropyl group **B**, which appears non-distorted. Other $\text{Li}\cdots\text{C}\beta$ distances are much longer, which precludes any interaction [$\text{Li1}\cdots\text{C12}$ 2.838(4), $\text{Li2}\cdots\text{C3}$ 2.748(4), $\text{Li2}\cdots\text{C11}$ 2.740(4) \AA]. Unlike for **1**, $\text{C}\alpha\text{-C}\beta$ bond lengths are similar within statistical error in both **A** and **B**. The distortion does not seem to be the result of steric pressure since computations indicate a second thf ligand can be accommodated on Li1 (*vide infra*, section e). Steric congestion was proposed to induce a similar unsymmetrical distribution of three thf ligands in $[(\mu\text{-CH}_2\text{NPh}_2)_2\text{Li}_2(\text{thf})_3]$, the only other example of such a dinuclear structure of which we are aware.¹⁵³ Even though a short $\text{Li}\cdots\text{H}\beta$ contact was observed [$\text{Li}\cdots\text{H2}$ 2.05 \AA], we propose the situation results from a $\text{Li}\cdots\text{C}\cdots\text{C}$ agostic distortion, with the help of DFT computation (*vide infra*).

d. Solution behaviour

A ^1H DOSY NMR spectroscopy of **2** in thf- d_8 and in benzene- d_6 was performed. In thf- d_8 , it yielded an estimated FW of 340 ± 34 g/mol (Figure 1.10). Assuming exchange of bound thf with thf- d_8 molecules in solution, a FW of 488.69 g/mol for **2-d₈** would be predicted which is clearly out of the 10% accepted error from the experimental value. Instead, the experimental FW fits nicely with a monomeric four-coordinate lithium structure in solution $[\text{Li}(c\text{-CPhC}_2\text{H}_4)(\text{OC}_4\text{D}_8)_3]$ (**3-d₈**), incorporating three thf- d_8 ligands (FW = 364.6 g/mol, Figure 1.11).

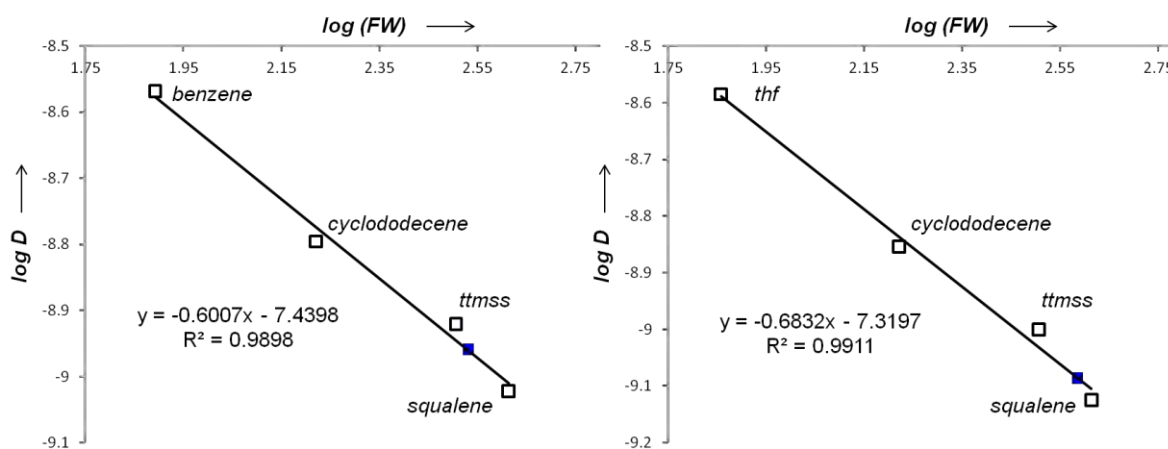


Figure 1.10 Diffusion coefficient-formula weight ^1H DOSY NMR analysis for **2** (blue squares) in thf- d_8 (left) and benzene- d_6 (right). Calibrants (empty squares): thf (72.11 g/mol), benzene (78.11 g/mol), cyclododecene (166.3 g/mol), tetrakis(trimethylsilylsilane), ttmss (320.8 g/mol), squalene (410.7 g/mol).

Other putative mono- and dimeric structures could be ruled out (Figure 1.11). This analysis confirms the tendency toward full deaggregation for benzyllithium compounds in thf. In this solvent, besides $[\text{PhCH}_2\text{Li}(\text{thf})_3]$ and $[\text{PhCH}(\text{SPh})\text{Li}(\text{thf})_3]$ (see above), $[t\text{-BuLi}(\text{thf})_n]$ seems to be the only other clear cut example of a single monomeric species for organolithiums.⁷¹

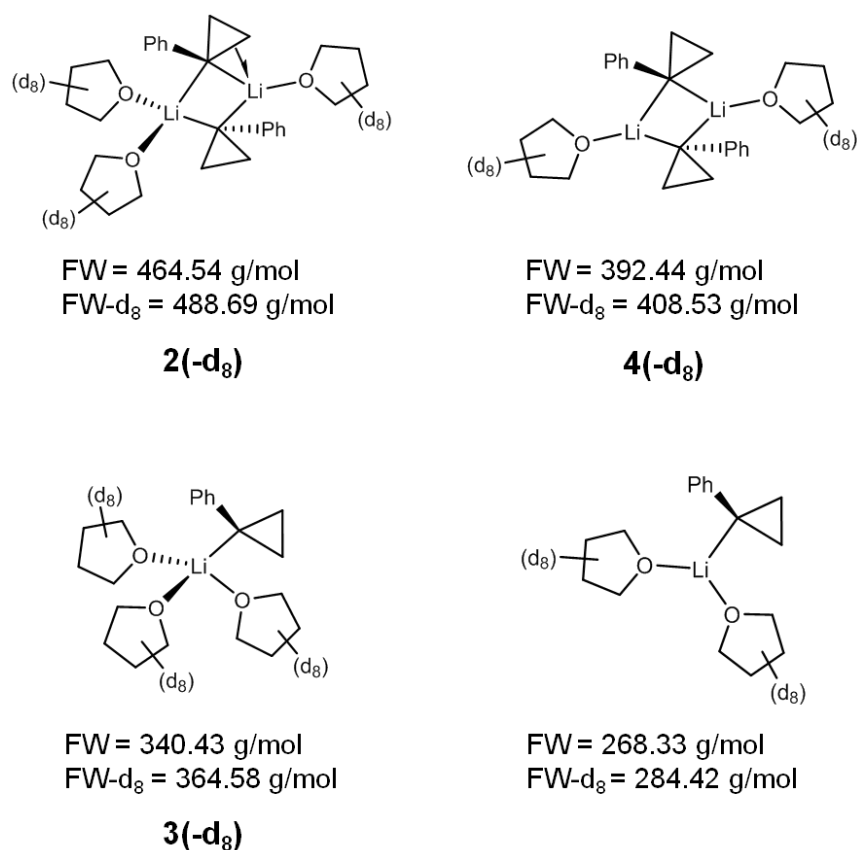
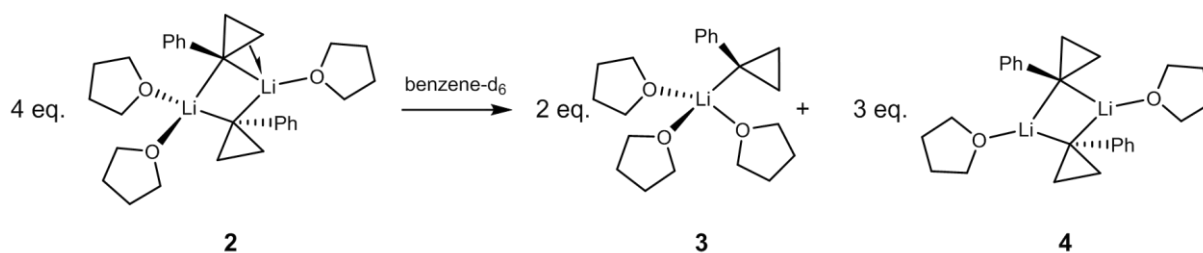


Figure 1.11 Putative structures of **2** in *thf-d₈* or in *benzene-d₆*

In order to evaluate if dimers similar to **2** could exist in solution, we investigated a solvent other than *thf-d₈*. A DOSY experiment was carried out in *benzene-d₆* and yielded an estimated formula weight (FW) of 385 ± 39 g/mol (Figure 1.10). This value is higher than that in *thf-d₈*. This is a consequence of an increased aggregation degree, as expected from a non-coordinating solvent. In this case, displacement of coordinated *thf* by the deuterated benzene is unlikely. The FW for **2** of 464.54 g/mol is once again outside of the 10% error range. **3**, *i.e.* $[\text{Li}(c\text{-CPhC}_2\text{H}_4)(\text{OC}_4\text{H}_8)_3]$ could also be ruled out, because (i) its formula weight does not match the estimated one (FW = 340.43 g/mol), and (ii) there is a ratio of 1.5 *thf* per Li atom in the medium. A dimeric structure in solution with each lithium being three coordinate $[(\mu\text{-}c\text{-CPhC}_2\text{H}_4)\text{Li}(\text{thf})_2]$ (**4**, Figure 1.11) could constitute a good candidate (FW 392.44 g/mol).

However, due to the oxophilicity of lithium, it is unlikely that one *thf* stays free in solution next to two low-coordinate lithium cations. We propose that the estimated formula weight corresponds to an equilibrium between the species **3** and **4**. When **2** is dissolved in *benzene-d₆*, it splits according to the Scheme 1.25 to give **3** and **4** in a 2:3 ratio.



Scheme 1.25 Redistribution reaction of **2** in benzene- d_6 .

Fast exchange between these two compounds gives an average formula weight of 371.64 g/mol (see Equation 1.1).

$$FW_{av.} = \frac{2 \times FW_3 + 3 \times FW_4}{5} = 371.64 \text{ g} \cdot \text{mol}^{-1}$$

Equation 1.1 Calculated average formula weight ($FW_{av.}$) for a 2:3 mixture of **3** and **4**. FW_3 and FW_4 respectively stand for formula weights of **3** and **4**.

The existence of **4** alone would suggest that one equivalent of thf is free in the medium. However, free thf resonances are not observed in the ^1H NMR spectra, even when VT NMR in toluene- d_8 was performed down to -90°C . At low temperature, only one set of resonance is present, confirming the high rate of exchange between **3** and **4**. Consequently no evidence for an $\alpha\text{-C-C}$ agostic distortion can be gained from data in solution. This is in line with known fast intra- and inter-aggregate C–Li bond exchanges in organolithium compounds.⁸⁷

At room temperature, the ^1H NMR spectrum of **2** in thf- d_8 , *i.e.* **3-d₈**, features two resonances in the aromatic region at δ 6.62 (*o*- and *m*- C_6H_5) and 6.08 (*p*- C_6H_5) (Figure 1.12). As in the case of BnLi,¹⁵⁴ the delocalisation of the negative charge on the phenyl ring induces a shielding of the aromatic protons as compared to 1-(phenyl)cyclopropane (δ 7.0–7.3). Interestingly, the β -protons on each enantioface of the cyclopropyl groups in **3-d₈** are equivalent at room temperature and appear as a broad singlet centred at δ 0.4.

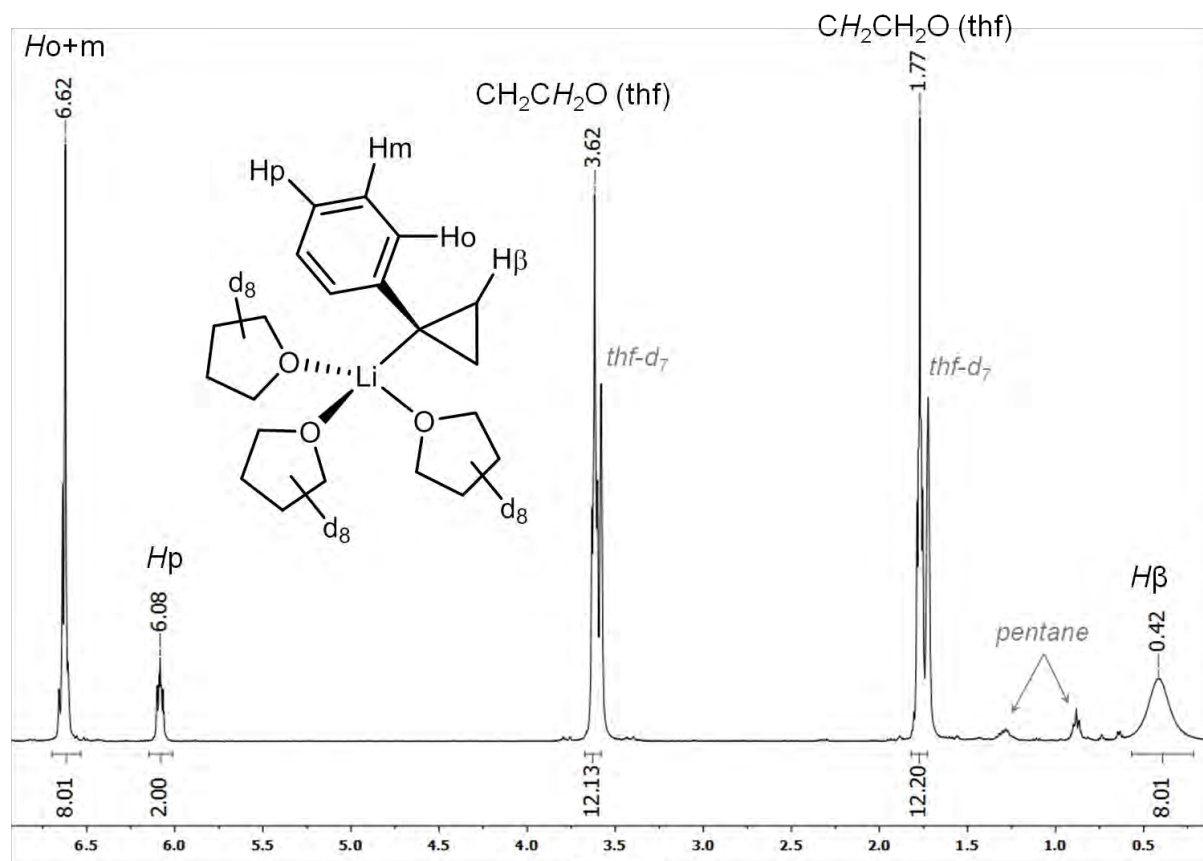


Figure 1.12 ^1H NMR spectrum of $[\text{Li}(\text{thf})_2(\mu\text{-}c\text{-CPhC}_2\text{H}_4)_2\text{Li}(\text{thf})]$ (2) in thf-d_8 .

This signal narrows at high temperature, and splits into two well resolved singlets upon cooling below a coalescence temperature of *ca* 288 K, yielding a low barrier ($\Delta G_{288}^\ddagger = 57$ kJ/mol) for inversion of the carbanionic $\text{C}\alpha$ (Figure 1.13).

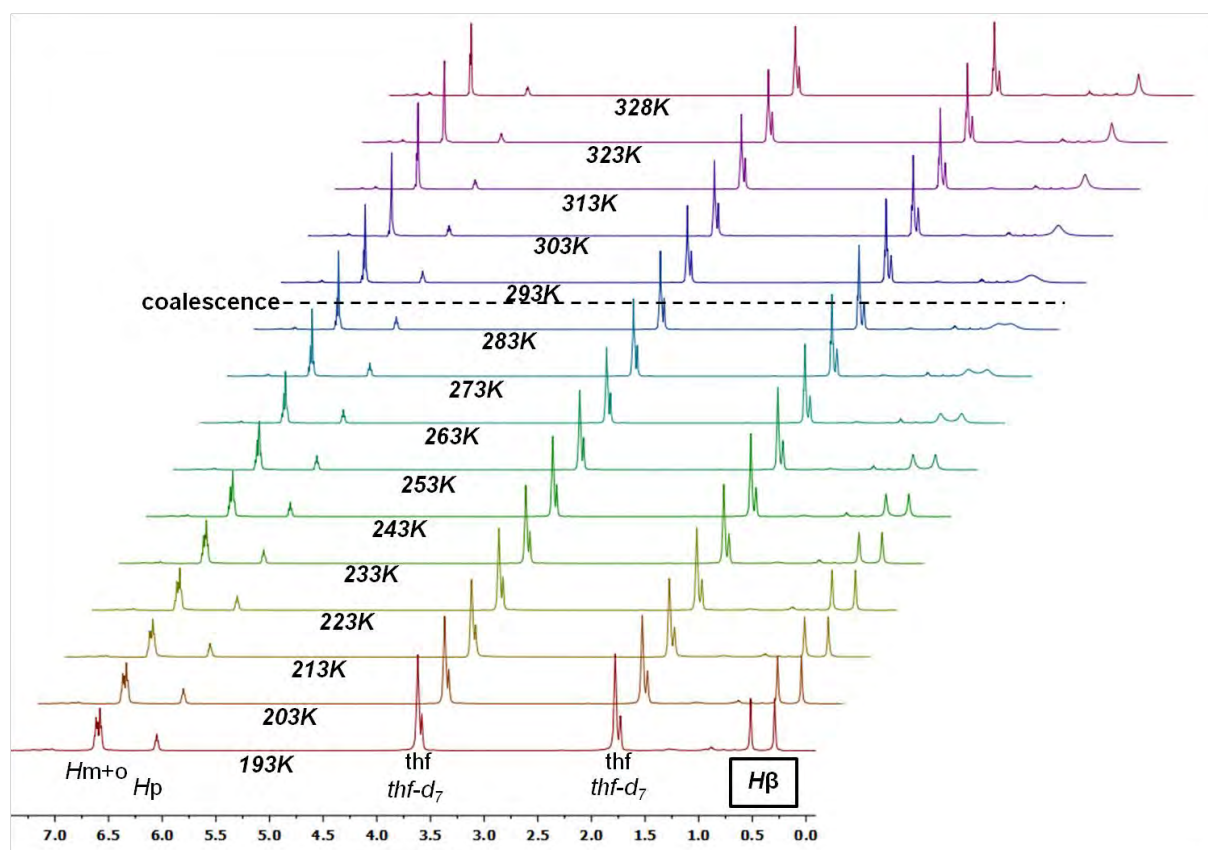


Figure 1.13 Variable-temperature ^1H NMR spectra of **3-d₈** in *thf-d₈*.

A similar behaviour was previously reported for alkyllithium,^{155,156} cyclopropyllithium derivatives^{157,158} and benzyllithium¹⁵⁹ complexes. The presence of a donor solvent as well as delocalisation of the negative charge on phenyl and/or cyclopropyl rings were established to be determining factors that reduce the energy of the inversion barrier of the carbanion.¹⁵⁷ This can be rationalised by the fact that in *thf-d₈*, Li^+ and C^- are solvent separated ion pairs. Thus, the negative charge is free to delocalise on the rings (with a flattened sp^2 $\text{C}\alpha$), the positive charge being stabilised by *thf-d₈* molecules. On the other hand, in non-coordinating solvent, the negative charge stays located on $\text{C}\alpha$ to counterbalance the positive charge of Li^+ .⁴⁷ Indeed, we observe two sets of singlets for the β -protons in benzene- d_6 at RT. A mechanism for the carbanion inversion was proposed for 7-phenylnorbornyllithium and could be extended to **3-d₈** (Figure 1.14).¹⁵⁹

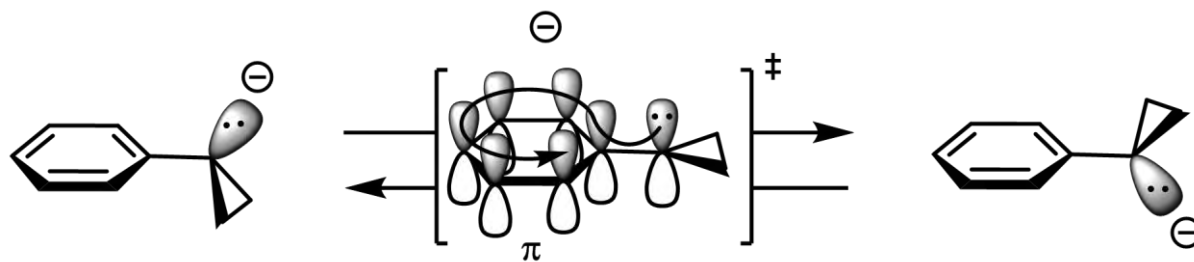


Figure 1.14 Inversion of the 1-phenylcyclopropyl carbanion.

The ^{13}C NMR spectrum in thf-d_8 contains the expected resonances for free protio-thf and the 1-phenylcyclopropyl moiety of **2** with the carbanionic quaternary carbon appearing as a singlet at δ 28.0 and the methylene groups showing a triplet centred at δ 11.2 ($^1J_{\text{CH}} = 153$ Hz).

e. DFT calculations

DFT calculations were carried out in order to probe the electronic structure of **2**. Optimisation (PBE0, def2TZVP) of **2** yielded a non-symmetric structure similar to that observed in the crystal structure (Figure 1.15). This includes the distortion of ring **A** towards the tricoordinate lithium with a $\text{Li}\cdots\text{C}\beta$ distance of 2.33 Å and a $\text{Li}-\text{C}\alpha-\text{C}\beta$ angle of 80° . The shortest distance between Li1 and one H on $\text{C}\beta$ is 2.12 Å which cannot be considered as very short for this kind of complex. This precludes the origin of the distortion as coming from a CH agostic interaction. Evidence for a direct interaction comes from the computed J_{CC} coupling constants which have been used previously as a meaningful parameter to gauge CC agostic structures. Taking $J_{\text{C}_2\text{C}_3}$ as a reference comparable to that for free cyclopropane (12.4 Hz), a significant lowering for $J_{\text{C}\alpha\text{C}\beta}$ ($J_{\text{C}_1\text{C}_2} = -3.4$ Hz) is computed when compared to the three other $J_{\text{C}\alpha\text{C}\beta}$ values in the complex (Figure 1.15). Low J_{CC} (< 0.5 Hz) have been recorded in ^{13}C -enriched *c*-PrLi derivatives.¹⁰⁴ The J_{CH} above has a normal value of 139 Hz. Natural Population Analysis / Natural Bond Orbital analysis indicated the build-up of a stronger negative charge on C2 as compared to C3 in ring **A** but also as compared to both $\text{C}\beta$ s in ring **B**, confirming the electrostatic nature of the interaction between $\text{Li}1\cdots\text{C}2$.

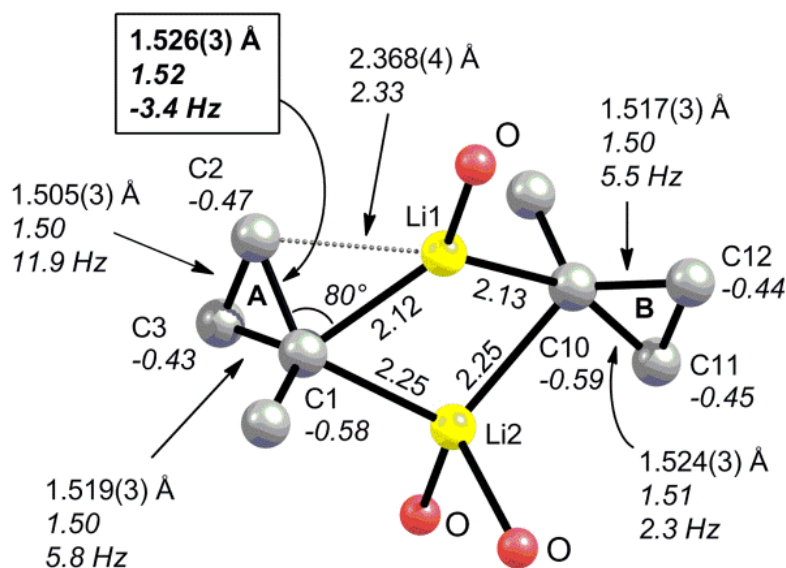


Figure 1.15 Core of the DFT optimised structure of **2**. Legend: experimental bond length (top), computed bond length and J_{CC} (italic). Labels as in the crystal structure with computed Natural Charges (au). For phenyl groups and thf ligands, only ipso-carbon and oxygen atoms, respectively, are depicted for clarity. Hydrogens are omitted for clarity.

We were also able to optimise the putative complex **2-thf** resulting from the addition of one thf ligand to Li1 in **2**. As depicted in Figure 1.16, all bonds between C_{α} and the four-coordinate lithium ions are very similar. The shortest distances between C_{β} and Li are 2.57 and 2.64 Å, which precludes significant interactions. The conformations of the two bridging 1-phenylcyclopropyl groups as well as those of the phenyl rings themselves now minimize steric clashes with the four thf ligands. The Li...Li distance increases from 2.43 Å in the computed structure of **2** to 2.51 Å in **2-thf**. The energy difference between **2-thf** and that of **2** plus one thf molecule is inconsequential (2 kJ/mol). Considering that steric compression can be sustained in **2-thf**, this provides an estimate of the strength of the C–C agostic interaction, since the distortion in **2** overcomes the energy gain provided by the additional thf ligand.

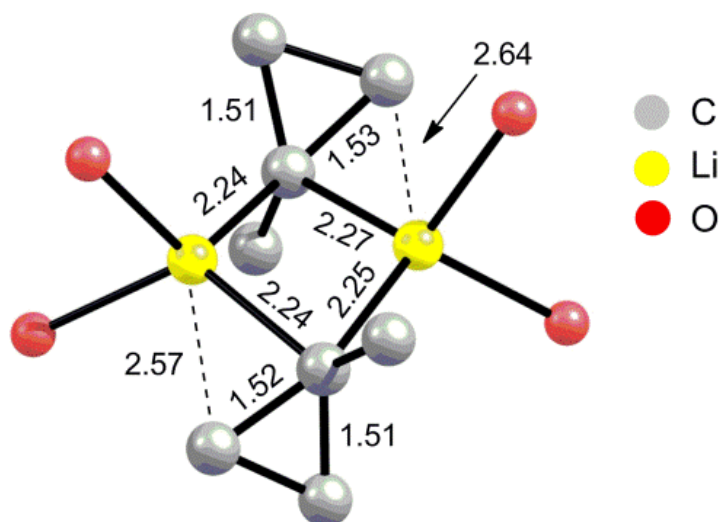
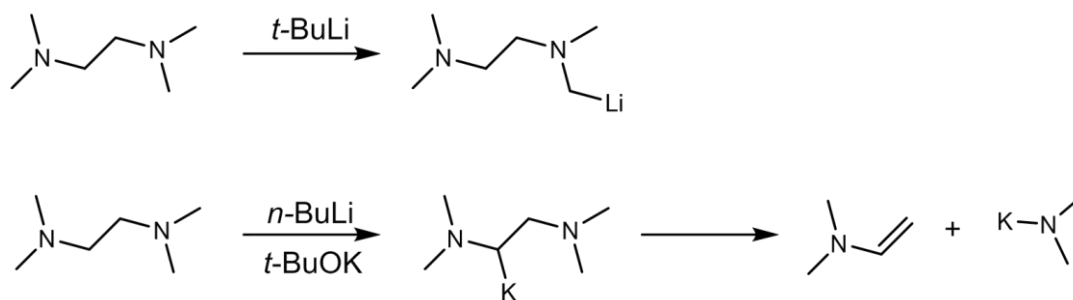


Figure 1.16 Core of the DFT optimised structure of **2-thf** with relevant distances in Å. For phenyl groups and thf ligands, only ipso-carbon and oxygen atoms, respectively, are depicted for clarity. Hydrogens are omitted for clarity.

f. Mixed alkyl/amido lithium complexes

We return to synthetic pathway A (Scheme 1.23), which consisted of deprotonation of phenylcyclopropane by *n*-BuLi in the presence of tmeda in pentane. Cleavage of tmeda was observed and ^1H NMR in benzene- d_6 or thf- d_8 showed mixtures of $[(c\text{-CPhC}_2\text{H}_4)\text{Li}(\text{tmeda})]$ (**5**) and $[(\text{NMe}_2)\text{Li}(\text{tmeda})]$ (**6**) in *ca* 4:1 ratios. Upon solubilisation in thf- d_8 , the coordinated tmeda is displaced by the deuterated solvent, and the ^1H NMR spectrum of **5** presents the same resonances as for **2** (*i.e.* **3-d₈** is generated) together with free tmeda. **6** appears as a singlet at δ 2.74 and has also lost its coordinated tmeda.

As stated above, in the introduction, metalation of tmeda at the methyl group by organolithiums is a well-established reaction, but selective deprotonation at the methylene group followed by C–N bond cleavage as observed here is normally restricted to more reactive superbases systems (Scheme 1.26).^{82,83,160}



Scheme 1.26 Metalation of tmeda, by *t*-BuLi, at the methyl group (top). Metallation of tmeda, by the Lochmann-Schlosser superbase, at the methylene group, and subsequent cleavage of the C–N bond (bottom).

When cooling a thf/hexane solution of **5** and **6**, crystals of at least three different species were obtained. **2** was the most often seen but sometimes an alkyl-amido mixed-aggregate $[(\mu\text{-}c\text{-CPhC}_2\text{H}_4)_2(\mu_3\text{-NMe}_2)\text{Li}_3(\kappa^2\text{-tmeda})_2]$ (**7**) was obtained (Figure 1.17). This is the only structure we have obtained with tmeda coordinated to the lithium instead of thf. However, since the crystals were of poor quality, molecular parameters are not discussed.

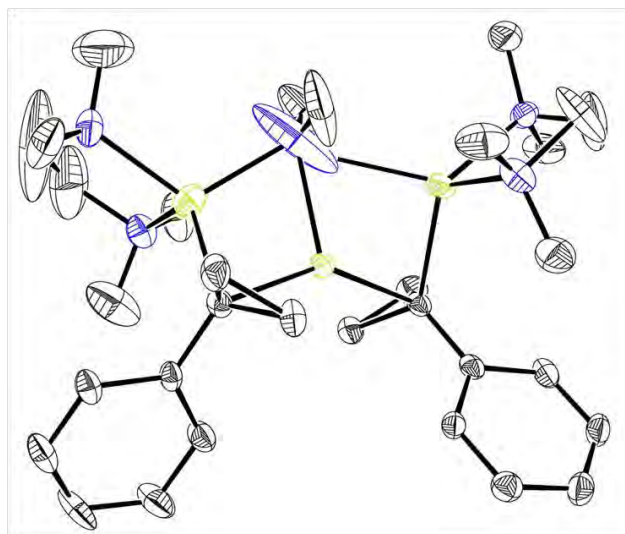


Figure 1.17 ORTEP drawing of **7** (ellipsoids at 30% probability level, hydrogens omitted for clarity). C (grey), Li (yellow), N (blue).

Eventually, in one case, a mixed-aggregate dimeric structure $[\text{Li}(\text{thf})_2(\mu_2\text{-}c\text{-CPhC}_2\text{H}_4)(\mu_3\text{-NMe}_2)\text{Li}]_2$ (**8**) was obtained (Figure 1.18).

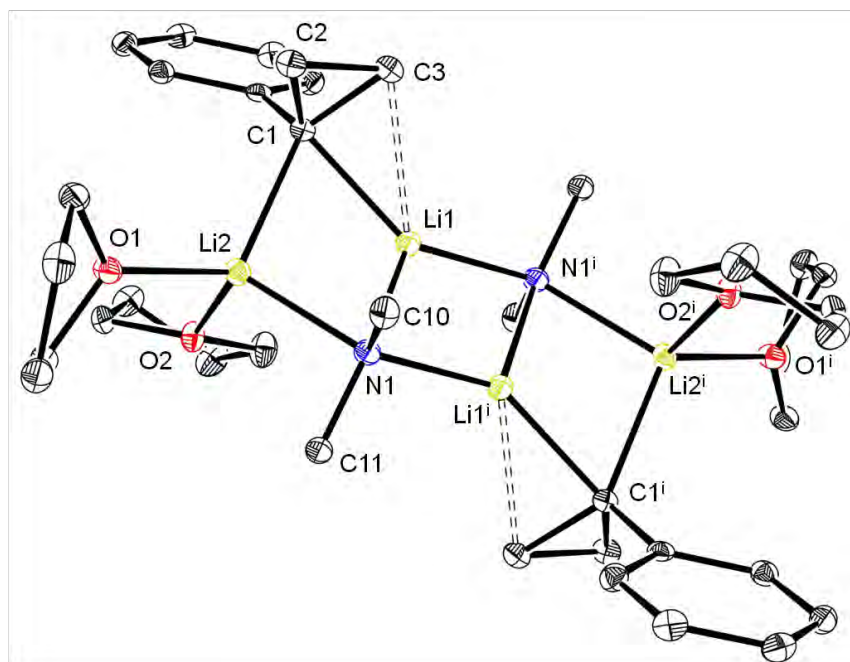


Figure 1.18 ORTEP drawing of structure $[\text{Li}(\text{thf})_2(\mu_2\text{-}c\text{-CPhC}_2\text{H}_4)(\mu_3\text{-NMe}_2)\text{Li}]_2$ (**8**) (ellipsoids at the 30% probability level, hydrogens omitted for clarity). Secondary $\text{Li}\cdots\text{C}-\text{C}$ interactions are depicted in double dashed bonds. Relevant bond lengths (\AA) and angles ($^\circ$): $\text{Li1}-\text{C1}$ 2.131(3), $\text{Li2}-\text{C1}$ 2.216(3), $\text{Li1}-\text{N1}$ 2.014(3), $\text{Li2}-\text{N1}$ 2.133(3), $\text{Li1}-\text{N1}^i$ 2.045(3), $\text{Li1}\cdots\text{C3}$ 2.455(3), $\text{C1}-\text{C2}$ 1.5218(18), $\text{C1}-\text{C3}$ 1.5257(18), $\text{C2}-\text{C3}$ 1.5012(19); $\text{Li1}-\text{C1}-\text{C3}$ 82.55(10), $\text{Li2}-\text{C1}-\text{C2}$ 102.49(10), $\text{Li2}-\text{N1}-\text{Li1}^i$ 137.75(10).

8 adopts a typical ladder-type dimeric structure of two dilithium moieties related by a centre of inversion.^{161,162} The outermost lithium Li1 and Li2 (Li1^i and Li2^i) are spanned by two bridging ligands, one 1-phenylcyclopropyl ligand and one N1-based dimethylamido ligand with the four-membered ring $\text{Li1}-\text{C1}-\text{Li2}-\text{N1}$ being puckered along the $\text{Li1}\cdots\text{Li2}$ axis [$28.92(12)^\circ$]. Li1 is then connected to the symmetric N1^i -based dimethyl amino ligand and Li1^i . Each dimethylamido ligand bridges three lithium centres with a central planar $\text{Li1}-\text{N1}-\text{Li1}^i-\text{N1}^i$ motif. Li2 is four-coordinate bearing two additional thf ligands whereas Li1 is formally three-coordinate. Accordingly, bond lengths between the bridging C and N atoms and the lithium cations are shorter to Li1 . Again, the 1-phenylcyclopropyl group is not symmetrically bound to the two lithiums. It is tilted towards Li1 as evidenced by the acute $\text{Li}-\text{C}\alpha-\text{C}\beta$ angle [$\text{Li1}-\text{C1}-\text{C3}$ $82.55(10)^\circ$] and the short distance between $\text{C}\beta$ and Li1 [$\text{Li1}\cdots\text{C3}$ 2.455(3) \AA]. The latter is not as short as that in **2**. As observed for **2**, the $\text{C}\alpha-\text{C}\beta$ bond lengths remain equal. Most probably the two hard dimethyl amino groups interact strongly with Li1 decreasing the electrostatic $\text{C}\beta\cdots\text{Li}$ interaction in **8**. DFT computations

modelled faithfully the overall structure of **7**. A reduced $J_{C\alpha C\beta}$ (−1.4 Hz) is computed. Overall the interaction appears weaker than in **1** and **2**.

g. Conclusion

Introduction of a phenyl moiety on the cyclopropyl ring allowed isolation and characterisation of two α -C–C agostic complexes (**2** and **8**). The compounds and their secondary interactions have been characterised by means of XRD and DFT calculations. The behaviour of **2** in solution has been extensively studied by 1- and 2-dimensional NMR spectroscopy.

The study of **2** and **8** has led to an enhanced understanding of the α -C–C agostic interaction. This latter is responsible for the favoured crystallisation of an asymmetric structure bearing one formally tricoordinate lithium cation as in **2**. As for **1**, this shows that the C–C-agostic interaction brought by a cyclopropyl group can compete with the donation of a thf molecule, and by doing so can hardly still be considered as “weak” or “secondary”. This is emphasized in the structure of **8**, where C–C agostic interactions still contribute to the stabilisation of three-coordinate Li^+ centres, even in presence of thf and amido donors.

1.3. 1-(phenylthio)cyclopropyllithium

We first defined the objective of this study as the establishment and understanding of C–C agostic interactions in organolithium complexes, *via* the cyclopropyl moiety. With the encouraging results obtained in the presence of strong/hard donors (thf, amido ligands) and since a softer sulfur substituted cyclopropyl was available from the synthesis of **1** (*i.e.* the (phenylthio)cyclopropane), we decided to study its lithiated version. We do not detail the reported examples of sulfur α -substituted carbanions, but it is noteworthy that the phenylthio moiety can stabilise a negative charge by hyperconjugation in a similar way than the SiMe_3 group (delocalisation in the $\sigma^*(\text{S}-\text{C})$). Also, as this work is still ongoing, we only discuss the solid state structure of this compound.

From the synthesis of 1-(phenylthio)-1-(trimethylsilyl)cyclopropane, detailed in part I.1,b, we could isolate crystals of 1-(phenylthio)cyclopropyllithium. Again, a remarkable non-symmetrical structure $[\text{Li}(\text{thf})_2(\mu\text{-}c\text{-CSPHC}_2\text{H}_4)_2\text{Li}(\text{thf})]$ (**9**) was obtained even if the crystals were obtained from a thf/pentane mixture.

In the solid state, **9** is similar to **2** (Figure 1.19), with two Li^+ bridged by two 1-(phenylthio)cyclopropyl moieties arranged around a puckered $[24.73(19)^\circ]$ four atom ring (Li1-C1-Li2-C10). Again, the number of thf on each Li atom is uneven (Li1 being formally three- and Li2 four-coordinate). The Li-C α bond lengths are in the same range as for **2** [Li1-C1 2.120(4), Li1-C10 2.094(3), Li2-C1 2.271(3), Li2-C10 2.240(3) Å]. The C β -S distances are in a normal range for this kind of compound [S1-C4 1.759(2), S2-C13 1.762(2) Å].¹⁶³ However, the C α -S bonds [S1-C1 1.821(2), S2-C10 1.820(2) Å] are longer than in other phenylthio substituted alkyls [range: 1.75(1)-1.78(1) Å].¹⁶³ The previously reported short C α -S were rationalised in terms of the negative hyperconjugation induced by the S atom, which suggests that this effect is less pronounced in **9**.

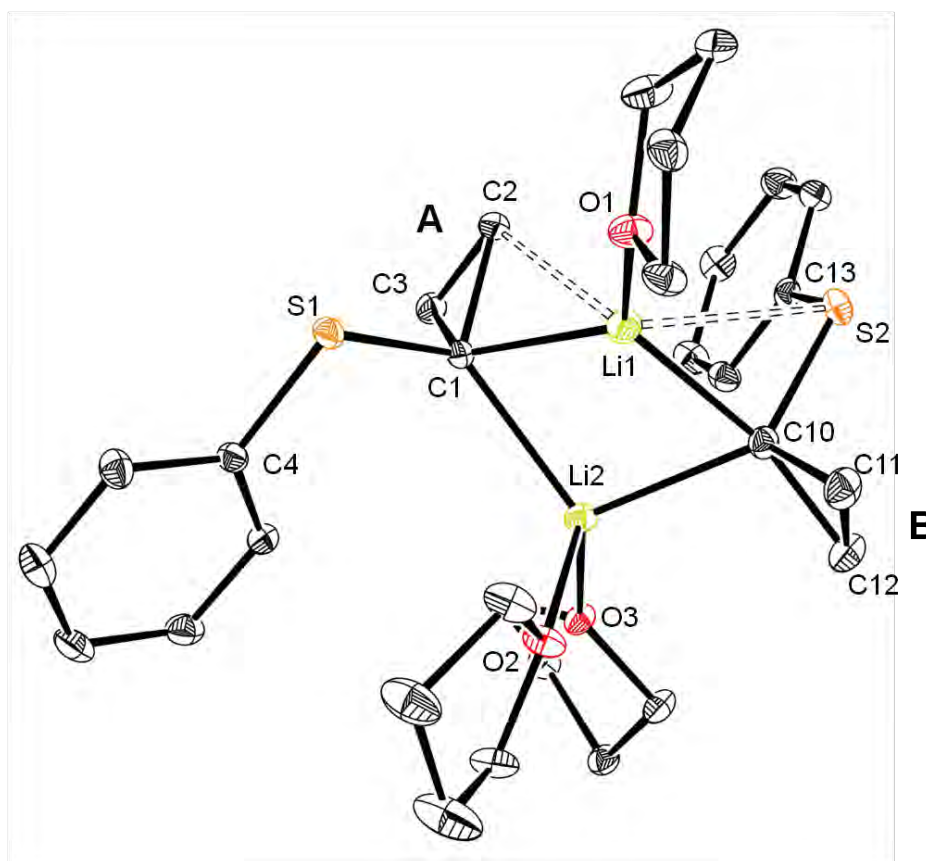


Figure 1.19 ORTEP drawing of $[\text{Li}(\text{thf})_2(\mu\text{-}c\text{-CSPhC}_2\text{H}_4)_2\text{Li}(\text{thf})]$ (**9**) (ellipsoids at 30% probability level, hydrogens omitted for clarity). Secondary $\text{Li}\cdots\text{C}-\text{C}$ and $\text{Li}\cdots\text{S}$ interactions are depicted in double dashed bonds. Relevant bond lengths (Å) and angles ($^\circ$): Li1-C1 2.120(4), Li1-C10 2.094(3), Li2-C1 2.271(3), Li2-C10 2.240(3), $\text{Li1}\cdots\text{C2}$ 2.392(4), $\text{Li1}\cdots\text{S2}$ 2.682(3) S1-C1 1.821(2), S1-C4 1.759(2), S2-C10 1.820(2), S2-C13 1.762(2), C1-C2 1.561(2), C1-C3 1.524(2), C2-C3 1.490(3), C10-C11 1.537(2), C10-C12 1.528(2), C11-C12 1.493(3); Li1-C1-C2 79.47(13), Li1-C1-C3 128.04(15), Li1-C10-C11 108.56(15), Li1-C10-C12 159.66(16), Li2-C1-C2 127.05(13), Li2-C1-C3 114.62(13), Li2-C10-C11 121.04(14), Li2-C10-C12 103.63(14).

As for **2**, this non-symmetric situation is accompanied by a C–C agostic distortion of the cyclopropyl group **A** toward Li1. Indeed, the structure of **9** presents an acute Li1–C1–C2 [79.47(13)°], with respect to Li2–C1–C3 [114.62(13)°], accompanied by a short Li1⋯C2 distance [2.392(4) Å]. Remarkably, this time, a significant elongation of the C1–C2 [1.561(2) Å] vs. C1–C3 [1.524(2) Å] and C2–C3 [1.490(3) Å] bonds is noticed, which confirms the agostic nature of this interaction. The cyclopropyl group **B** does not present any of these differences and Li⋯C β distances [Li1⋯C11 2.967(4) Å; Li2⋯C12 2.994(4) Å] indicate no interaction. Interestingly, the presence of S donor atoms does not disturb the agostic distortion of group **A**, even though S2 interacts with Li1 as shown by the short Li1⋯S2 distance [2.682(3) Å].¹⁶⁴ The Li⋯H distances are in a range (>2.25 Å) where C–H agostic distortions cannot compete with the C–C agostic distortion.

C. Conclusion and perspectives

We have described the synthesis and characterisation of three *c*-PrLi derivatives: [*c*-C(SiMe₃)C₂H₄}Li] (**1**), [Li(thf)₂(μ-*c*-CPhC₂H₄)₂Li(thf)] (**2**) and [Li(thf)₂(μ-*c*-CSPHC₂H₄)₂Li(thf)] (**9**). The structure of a mixed alkyl/amido lithium complex [Li(thf)₂(μ₂-*c*-CPhC₂H₄)(μ₃-NMe₂)Li]₂ (**8**) was also studied. **2** has been fully characterised by the combined use of XRD, NMR spectroscopy and computational modelling.

All complexes exhibit α-C–C agostic distortions in the solid state. These interactions have been identified by crossed XRD/DFT calculation studies for **2** and **8**, and DFT calculations are ongoing for complexes **1** and **9**. In complexes **2**, **8** and **9**, a competition between donor moieties (thf, -NMe₂, -SPh) and agostic interactions has emphasised the strength of the latter with respect to coordination to Li⁺. Notably, the non-symmetrical structures of **2** and **9** are favoured over their symmetrical pendants with an added thf ligand. Compound **1** also easily loses coordinated thf which we attribute to the presence of C–C agostic interactions.

These examples demonstrate the ability of a purely hydrocarbon moiety, *i.e.* the cyclopropyl group, to stabilise an electropositive centre by means of the C–C agostic distortion. Even though there is still on-going work on the magnitude of this interaction, it seems to be favoured over other secondary interactions such as π coordination or C–H agostic distortions.

D. Experimental part

All operations were performed with rigorous exclusion of air and moisture, using standard Schlenk techniques and an Ar filled Jacomex glovebox ($O_2 < 5$ ppm, $H_2O < 1$ ppm). (Phenylthio)cyclopropane, trimethylsilylchloride, phenylcyclopropane, tmeda and *n*-butyllithium (2.5 M solution in hexanes) were purchased from Aldrich. All solvents were pre-dried by passing through a Puresolv MD 7 solvent purification machine, dried over molecular sieves, filtered and degassed by freeze-pump-thaw cycles. Deuterated solvents, (phenylthio)cyclopropane, (trimethylsilyl)chloride, and phenylcyclopropane were dried over molecular sieves, filtered, and degassed by several freeze-pump-thaw cycles and stored in sealed ampoules in the glovebox. Tmeda was distilled over Na and further degassed by freeze-pump-thaw cycles. 1-chlorophenylcyclopropane was prepared according to a literature procedure.⁴²

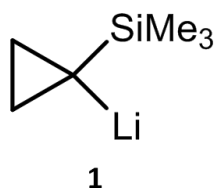
The chemical shifts are given in ppm. NMR spectra were recorded by using J. Young valve NMR tubes using Bruker Avance III 400 (1H , 400.16; 7Li , 155.52; ^{13}C , 100.6; ^{29}Si , 79.5 MHz) or Avance 500 (1H , 500.33; ^{13}C 125.82 MHz) spectrometers. Chemical shifts for 1H NMR were determined using residual proton signals in the deuterated solvents and reported vs. $SiMe_4$. Chemical shifts for ^{13}C NMR spectra were that of the solvent referenced to $SiMe_4$. 7Li NMR spectra were referenced vs. external $LiCl$. ^{29}Si NMR spectra were referenced vs. external $SiMe_4$. DOSY NMR experiments were carried out on a Bruker Avance 400 spectrometer equipped with a 5 mm triple resonance inverse Z-gradient probe (TBI 1H , ^{31}P , BB). The DOSY spectra were acquired at room temperature, without temperature regulation to avoid convection, with the *stebpgp1s* pulse program from Bruker *topspin* software. All spectra were recorded with 16 K time domain data point in the t_2 dimension and 16 t_1 increments. The strength of the gradient was linearly incremented in 16 steps from 2 up to 95% of the maximum gradient strength. All measurements were performed with a compromise diffusion delay D ranging from 90 to 130 ms and a gradient pulse length d ranging from 1.8 to 2.4 ms. Elemental analyses (Analytical service of the LCC) are the average of at least two independent measurements.

XRD data were collected at low temperature (100 K) on a Bruker Kappa Apex II diffractometer using a $Mo-K\alpha$ radiation ($\lambda = 0.71073 \text{ \AA}$) micro-source and equipped with an Oxford Cryosystems Cryostream Cooler Device. The structures have been solved by direct methods using *SIR92*¹⁶⁵ or *SHELXS-97*,¹⁶⁶ and refined by means of least-squares procedures

on F^2 with the aid of the program SHELXL97¹⁶⁶ included in the software package WinGX version 1.63.¹⁶⁷ All hydrogens atoms were placed geometrically, and refined by using a riding model. All non-hydrogens atoms were anisotropically refined, and in the last cycles of refinement a weighting scheme was used, where weights are calculated from the following formula: $w=1/[\sigma^2(F_o^2)+(aP)^2+bP]$ where $P=(F_o^2+2F_c^2)/3$.

Calculations were performed at the DFT level with the PBE1PBE functional as implemented in Gaussian09, revision D.01,¹⁶⁸ using the def2TZVP basis set (N, O, C, Li and H).¹⁶⁹ Structure optimisations were carried out without symmetry constraints. The nature of the stationary points was ascertained by a vibrational analysis within the harmonic approximation (1 atm and 298 K). Minima were identified by a full set of real frequencies. Electronic and free energies are reported in hartree with zero-point energy correction. Computation of NMR coupling constants used the same functional associated with the IGLO-II basis set for C and H.¹⁷⁰ NBO calculations were carried out with NBO 6.0 as implemented in Gaussian 09.¹⁷¹

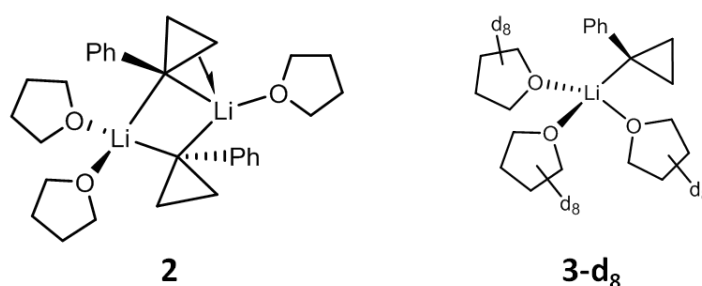
Synthesis of [$\{c\text{-C}(\text{SiMe}_3)\text{C}_2\text{H}_4\}\text{Li}$] (**1**)



A solution of lithium naphthalenide in thf (4.6 mL, 2.46 mmol) was added dropwise *via* a syringe pump at -70°C to a solution of 1-(phenylthio)-1-(trimethylsilyl)cyclopropane (274 mg, 1.23 mmol) in thf (4 mL). The resulting golden yellow solution was allowed to warm up slowly and the solvent was removed under vacuum when the temperature reached 0°C (*ca* 2 hours). Naphthalene was removed by sublimation under higher vacuum (10 hours, $P < 10^{-3}$ mbar, RT). The residue was extracted with toluene (3 x 5 mL). Drying this solution under vacuum afforded a brown solid of [$\{c\text{-C}(\text{SiMe}_3)\text{C}_2\text{H}_4\}\text{Li}(\text{thf})_x$] ($0 < x < 0.3$) (121 mg, 81%, traces of lithium thiophenolate). Single crystals of **1** suitable for XRD analysis were grown by cooling a toluene solution at -40°C (< 5 mg). Further attempts to purify **1** failed either due to its high solubility in toluene, or because of co-crystallization of lithium thiophenolate in toluene/pentane mixtures. No elemental analysis was obtained.

^1H NMR (benzene- d_6 , 298 K, $x = 0.23$) δ 3.46 (s, 0.9 H, $\text{CH}_2\text{CH}_2\text{O}$ -thf), 1.20 (s, 0.9 H, $\text{CH}_2\text{CH}_2\text{O}$ -thf), 0.80 (s, 2 H, $H\beta$), 0.59 (s, 2 H, $H\beta'$), 0.01 (s, 9H, $\text{Si}(\text{CH}_3)_3$). ^7Li NMR (benzene- d_6 , 298 K) δ 2.08 (s, Li). ^{19}Si NMR (benzene- d_6 , 298 K) δ 0.21 (s, Si). ^{13}C NMR (benzene- d_6 , 298 K, $x = 0.23$) δ 68.8 (t, $\text{CH}_2\text{CH}_2\text{O}$ -thf), 25.3 (t, $\text{CH}_2\text{CH}_2\text{O}$ -thf), 7.2 (t, $J_{\text{CH}} = 156$ Hz, $C\beta$), -1.6 (q, $J_{\text{CH}} = 117$ Hz, $\text{Si}(\text{CH}_3)_3$), -4.9 (s, $C\alpha$).

Synthesis of $[\text{Li}(\text{thf})_2(\mu\text{-c-CPhC}_2\text{H}_4)_2\text{Li}(\text{thf})]$ (2**) and $[\text{Li}(\text{c-CPhC}_2\text{H}_4)(\text{OC}_4\text{D}_8)_3]$ (**3-d₈**)**

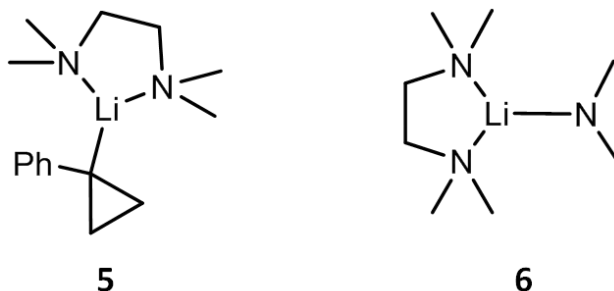


1-chloro-1-phenylcyclopropane (200 mg, 1.31 mmol), *n*-BuLi in hexanes (0.6 mL, 1.5 mmol) and pentane (4 mL) were mixed together in a Schlenk flask. Thf (0.2 mL, 2.5 mmol) was quickly added *via* a syringe and the reaction mixture was stirred at room temperature. A white solid started to precipitate almost immediately and stirring was maintained for 10 min. The reaction slurry was then stored at -40°C overnight. After filtration, the solid was washed with pentane and dried under vacuum, to give an analytically pure white powder (130 mg, 0.280 mmol, 43%). Anal. Calcd for $\text{C}_{30}\text{H}_{42}\text{Li}_2\text{O}_3$: C, 77.57; H, 9.11; N 0.00. Found: C, 77.70; H, 9.18; N 0.00. **2** gave **3-d₈** upon solubilisation in thf- d_8 . Single crystals of **2** suitable for XRD analysis were obtained directly from the reaction mixture after storage at -40°C . **2** reacted slowly with protio-thf (several hours at room temperature, $t_{1/2} \approx 24$ h) according to classical thf cleavage pathways.

^1H NMR (thf- d_8 , 298 K) δ 6.62 (m, 8 H, (*o,m*)- C_6H_5), 6.08 (tt, 2 H, $^3J_{\text{HH}} = 6.3$, $^4J_{\text{HH}} = 1.9$ Hz, *p*- C_6H_5), 3.62 (m, 12 H, $\text{CH}_2\text{CH}_2\text{O}$ -thf), 1.77 (m, 12 H, $\text{CH}_2\text{CH}_2\text{O}$ -thf), 0.42 (br s, 8 H, $H\beta$). ^7Li NMR (thf- d_8 , 298 K) δ 0.35 (s, Li). ^{13}C NMR (thf- d_8 , 298 K) δ 167.9 (s, *ipso*- C_6H_5), 127.6 (d, $J_{\text{CH}} = 151$ Hz, *m*- C_6H_5), 125.2 (d, $J_{\text{CH}} = 152$ Hz, *o*- C_6H_5), 113.6 (d, $J_{\text{CH}} = 157$ Hz, *p*- C_6H_5), 68.4 (t, $J_{\text{CH}} = 144$ Hz, $\text{CH}_2\text{CH}_2\text{O}$ -thf), 28.0 (s, $C\alpha$) 26.5 (t, $J_{\text{CH}} = 132$ Hz,

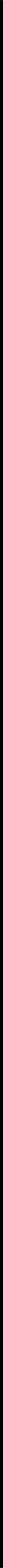
$\text{CH}_2\text{CH}_2\text{O-thf}$), 11.2 (t, $J_{\text{CH}} = 153$ Hz, $\text{C}\beta$). The *ipso*- C_6H_5 , *m*- C_6H_5 , *o*- C_6H_5 , *p*- C_6H_5 and $\text{C}\alpha$ were assigned thanks to a HMBC analysis.

Synthesis of [(*c*-CPhC₂H₄)Li(tmeda)] (**5**) and [(NMe₂)Li(tmeda)] (**6**)



Phenylcyclopropane (505 mg, 4.27 mmol), tmeda (494 mg, 4.25 mmol) and pentane (6 mL) were mixed together. The mixture was cooled down to 0°C and *n*-BuLi in hexanes (2.4 mL, 6.0 mmol) was slowly added. The mixture was gradually warmed to room temperature affording a red solution from which a yellow solid gradually precipitated over a period of 5 days. The precipitate was collected by filtration and washed with cold (−40°C) pentane (3 x 1 mL) to give a *ca* 4:1 mixture of **5** and **6** (548 mg, 1.94 mmol in **5**, 45% for **5**). Single crystals of **2** and **7** suitable for XRD analysis were obtained by suspending the mixture of **5** and **6** in hexane followed by slow addition of thf until solubilisation and storage at −40°C overnight.

¹H NMR (benzene-*d*₆, 298 K) δ 7.47 (br s, 2 H, *o/m*-C₆H₅), 7.30 (t, 2 H, *o/m*-C₆H₅), 6.88 (t, 1 H, *p*-C₆H₅), 2.95 (br s, 1.5 H, LiN(CH₃)₂), 1.82 (s, 12 H, CH₃N-tmeda), 1.67 (s, 4 H, CH₂N-tmeda), 1.26 (br s, 2 H, *H*β), 0.95 (br s, 2 H, *H*β). ¹H NMR (thf-*d*₈, 298 K) δ 6.63 (m, 4 H, (*o,m*)-C₆H₅), 6.09 (tt, 1 H, ³*J*_{HH} = 6.3 Hz, ⁴*J*_{HH} = 1.9 Hz, *p*-C₆H₅), 2.74 (br s, 1.6 H, LiN(CH₃)₂), 2.30 (s, 4 H, CH₂N-tmeda), 2.15 (s, 12 H, CH₃N-tmeda), 0.43 (br s, 4 H, *H*β).



CHAPTER 2

Chapter 2. Cyclopropylcalcium complexes

A. Introduction

This chapter deals with the organometallic chemistry of Ca. Extending the chemistry developed in the previous chapter, here we aimed at the synthesis and characterisation of a new class of cyclopropyl calcium compounds that could display C–C⋯Ca agostic interactions. The synthesis of organometallic species bearing a reactive Ca–C bond is challenging and we detail here the most used synthetic routes to these complexes, presenting the benchmark compounds that have been previously characterised. We focus on the most reactive organocalcium species, *i.e.* the complexes bearing exclusively σ Ca–Csp² and Ca–Csp³ bonds. In addition, we mainly discuss herein the complexes that have been isolated and whose XRD structures are known.

1.1. The organocalcium complexes

In the context of resource depletion and sustainable development, there is a current trend in organometallic and coordination chemistry to move to more abundant, less expensive and less toxic alternatives. Ca constitute a good candidate as it is an abundant (3.4% of the earth's crust¹⁷²), biocompatible, and cheap metal. Ca is the twentieth element of the periodic table and the third alkaline earth metal below Mg. Ca is very oxophilic, electropositive [$\chi(\text{Ca}) = 1.04 \approx \chi(\text{Li}) = 0.97 < \chi(\text{Mg}) = 1.23$, electronegativity according to Allred-Rochow]¹⁷³ and redox-inert at the oxidation state +2. Due to its large ionic radius [$r(\text{Ca}^{2+}) = 1.00 \text{ \AA}$]⁵⁰ and to the high ionic character of the Ca–C bond (e.g.: Me₂Ca is calculated to be 89% ionic),⁵⁶ Ca can afford a wide variety of coordination numbers in a similar fashion to lanthanides, the most common being 4 and 6.

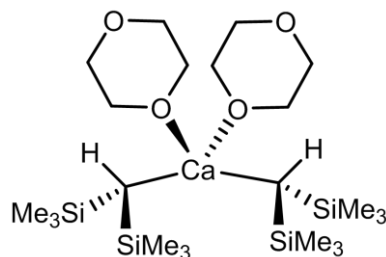
As a consequence of these properties, organocalcium compounds can be employed as new reagents in group transfer and metallation reactions. Nonetheless, access to organocalcium compounds is difficult, mostly because: (i) metallic Ca is inert and activation may require harsh conditions and (ii) organocalcium compounds are very reactive and prone to redistribution (such as the well-known Schlenk equilibrium, Scheme 2.1) or ether cleavage reactions.¹⁷⁴ These features require carefully chosen and well-controlled reaction conditions. This explains why the chemistry of Ca has attracted attention only in recent decades,^{174–178}

whereas the organometallic chemistry of Mg has been extensively developed since the first report by Victor Grignard more than one century ago.¹⁷⁹



Scheme 2.1 *The Schlenk equilibrium.*

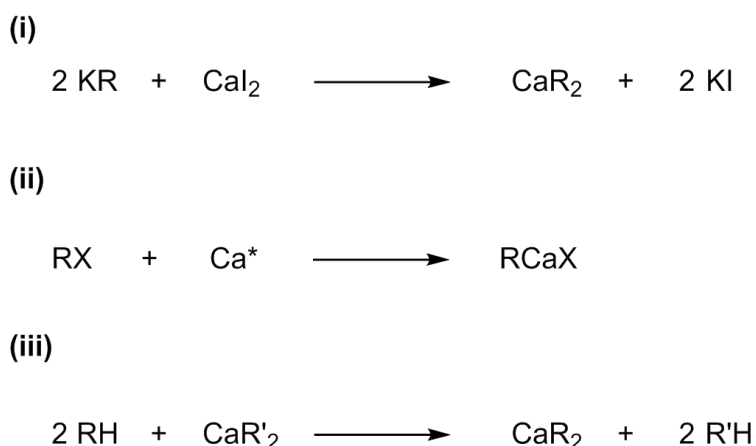
Several synthetic strategies have been used to overcome the problem of Ca inertness. A common entry point is the use of CaI_2 salts in ethereal solvents, although organocalcium complexes can also be prepared directly from $\text{Ca}(0)$ by dissolving the metal in liquid ammonia (details are given below in part I.2). As the $\sigma(\text{Ca}-\text{C})$ bond is essentially ionic, the same strategy used for organolithium compounds (*cf.* chapter 1) to prevent side reactions, *i.e.* the use of the bulky and charge stabilising SiMe_3 and/or Ph groups,¹⁷⁶ can be employed here for Ca. This is best exemplified by the breakthrough work of Lappert *et al.*, who crystallised the first alkylcalcium complex, $[\{\text{CH}(\text{SiMe}_3)_2\}_2\text{Ca}(1,4\text{-dioxane})_2]$ (Scheme 2.2).¹⁸⁰



Scheme 2.2 *Solid state structure of $[\{\text{CH}(\text{SiMe}_3)_2\}_2\text{Ca}(1,4\text{-dioxane})_2]$.*

I.2. Synthesis of organocalcium complexes

The three most common techniques to synthesise organocalcium are depicted in Scheme 2.3 and include: (i) Salt metathesis between an organopotassium (RK) and calcium diiodide (CaI_2), (ii) oxidative addition of an organohalide (RX) on activated calcium metal (Ca^*), (iii) deprotonation of an alkane (RH) by an alkylcalcium (CaR'_2).¹⁷⁴⁻¹⁷⁷



Scheme 2.3 Common routes to organocalcium compounds.

We focus only on the two first routes (i) and (ii). Pathway (iii) requires a group R' more basic than R. Although this method is very convenient for the synthesis of amido, acetylide or alcoolate calcium complexes, it is not suitable for highly basic alkyls such as the cyclopropyl group.

a. Salt metathesis from organopotassium and CaI_2

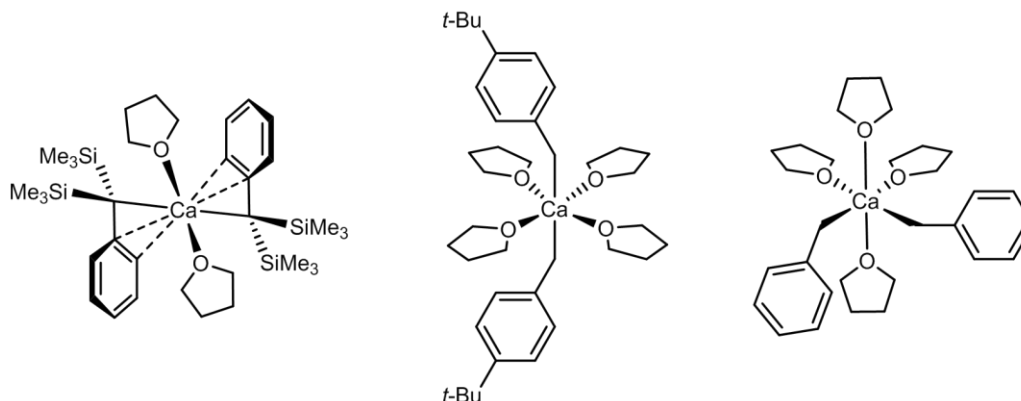
Salt metathesis is the most extensively used reaction to synthesise alkyl-, benzyl- and allylcalcium compounds.¹⁷⁵ By using CaI_2 as the Ca source, metal activation can be achieved easily. This reaction takes place mainly in ethereal media (usually thf) as both CaI_2 and RK precursors are generally not soluble in hydrocarbon solvents. The CaI_2 must be extremely pure (>99%). CaI_2 is generally stirred in the solvent *prior* to use, in order to form the more reactive $[\text{CaI}_2(\text{L})_4]$ complex (L= thf, Et_2O). The advantage of the salt metathesis is the precipitation of potassium iodide (KI) which is easily separated from the ether soluble organocalcium compounds, driving the reaction toward the formation of the products. This approach has two drawbacks: highly pure CaI_2 is expensive (*ca* 20 € / g for 99.999% purity) and the organopotassium precursor must be well-defined and isolated as pure as possible.

Herein we present the benchmark organocalcium complexes that have been obtained by the salt metathesis reaction.

i. Benzylcalcium compounds

As reported by the team of Harder, salt metathesis between benzylpotassium compounds and CaI_2 in thf afforded the benzylcalcium complexes $[\{\alpha,\alpha-$

$(\text{SiMe}_3)_2\text{PhC}\}_2\text{Ca}(\text{thf})_2$ ¹⁸¹, $[\{(4-t\text{-Bu-C}_6\text{H}_4)\text{CH}_2\}_2\text{Ca}(\text{thf})_4]$ ¹⁸² and $[(\text{PhCH}_2)_2\text{Ca}(\text{thf})_4]$ ¹⁸² (Scheme 2.4).



Scheme 2.4 Solid state structures of $[\{\alpha,\alpha\text{-(SiMe}_3)_2\text{PhC}\}_2\text{Ca}(\text{thf})_2]$ (left), $[\{(4\text{-}t\text{-Bu-C}_6\text{H}_4)\text{CH}_2\}_2\text{Ca}(\text{thf})_4]$ (centre) and $[(\text{PhCH}_2)_2\text{Ca}(\text{thf})_4]$ (right). Short $\text{C}\cdots\text{Ca}$ contacts are depicted in dashed lines.

Short *Cipso/Cortho*...Ca distances were observed in the structure of $[\{\alpha,\alpha\text{-(SiMe}_3)_2\text{PhC}\}_2\text{Ca}(\text{thf})_2]$. In the structures of the *t*-Bu-substituted and unsubstituted benzylcalcium complexes, on the other hand, no short distances are present, probably due to the filling of the Ca coordination sphere by two extra thf molecules. For the unsubstituted dibenzylcalcium compound, the formation of the *cis*-isomer vs. the *trans*-isomer was explained by the presence of an intermolecular network of $\text{C-H}\cdots\pi$ interactions which would favour the *cis*-geometry. The *trans*-geometry was calculated by DFT to be slightly less stable than the *cis*-one.

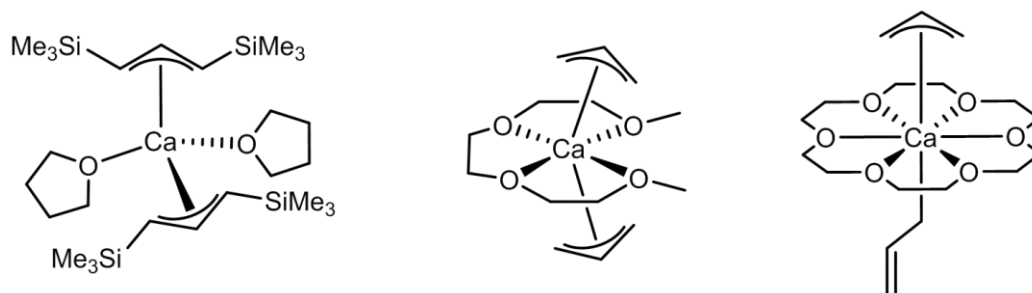
Interestingly a similar dibenzylcalcium compound was synthesised from deprotonation of toluene by a Ca(I) 2,4,6-triphenylbenzene compound and was crystallised as a 1,3,5-trimethyl-1,3,5-triazinane (tmta) adduct of formula $[(\text{PhCH}_2)_2\text{Ca}(\text{tmta})_2]$.¹⁸³

The benzylcalcium compounds are of great interest for synthetic applications as they are easy to synthesise and are potent deprotonating or group transfer agents.^{182,184–188}

ii. Allylcalcium compounds

Salt metathesis between allylpotassium compounds and CaI_2 in thf allowed the crystallisation of the allylcalcium complexes $[\{\eta^3\text{-}1,3\text{-(SiMe}_3)_2\text{C}_3\text{H}_3\}_2\text{Ca}(\text{thf})_2]$,¹⁸⁹ $[(\eta^3\text{-}$

$C_3H_5)_2Ca(\kappa^4\text{-triglyme})]^{190}$ and $[(\eta^1\text{-}C_3H_5)(\eta^3\text{-}C_3H_5)Ca(18\text{-crown-}6)]^{191}$ depicted in Scheme 2.5.

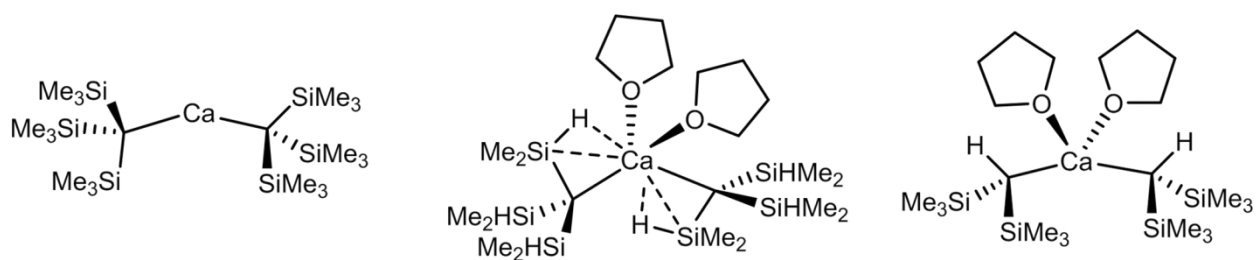


Scheme 2.5 Solid state structures of $[\{\eta^3\text{-}1,3\text{-}(\text{SiMe}_3)_2\text{C}_3\text{H}_3\}_2\text{Ca}(\text{thf})_2]$ (left), $[(\eta^3\text{-}C_3H_5)_2Ca(\kappa^4\text{-triglyme})]$ (centre) and $[(\eta^1\text{-}C_3H_5)(\eta^3\text{-}C_3H_5)Ca(18\text{-crown-}6)]$ (right).

In the SiMe_3 substituted diallylcalcium complex, the η^3 coordination mode is favoured, probably for steric reasons. In the case of non-substituted diallylcalcium complexes, it was shown by the team of Okuda that the hapticity of the allyl ligands depends on the coordination number around the Ca metal and on the steric hindrance of the donor base. DFT optimisation of the tetra(pyridine)diallylcalcium adduct leads to the expulsion of one pyridine ligand favouring the trispyridine complex $[(\eta^3\text{-}C_3H_5)_2Ca(\text{pyridine})_3]$. To maintain the coordination of the four pyridines, a haptotropic shift from π to σ of one or two allyl groups is required, leading to $[(\eta^1\text{-}C_3H_5)(\eta^3\text{-}C_3H_5)Ca(\text{pyridine})_4]$ and $[(\eta^1\text{-}C_3H_5)_2Ca(\text{pyridine})_4]$. This was confirmed by ^1H NMR in pyridine- d_5 where an η^1 bonding mode was observed.¹⁹⁰ This also explains the favoured mixed hapticity in the crystal structure of $[(\eta^1\text{-}C_3H_5)(\eta^3\text{-}C_3H_5)Ca(18\text{-crown-}6)]$. The diallylcalcium complex without coordinated ligand was isolated as a white powder and characterised by NMR and elemental analysis.¹⁹⁰

iii. Alkylcalcium compounds

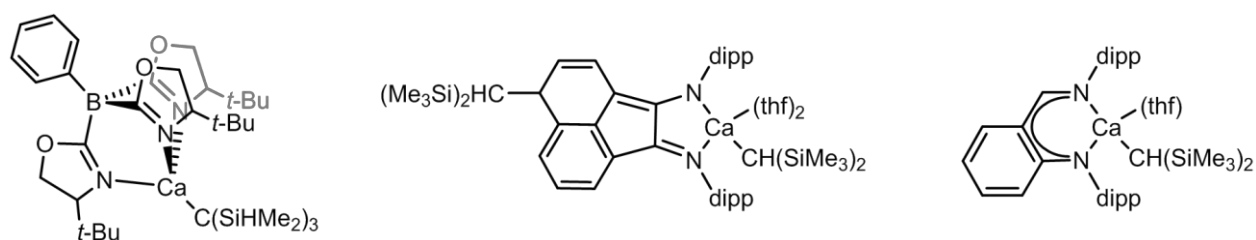
The complex $[\{C(\text{SiMe}_3)_3\}_2Ca]$ was synthesised and crystallised from $[\{C(\text{SiMe}_3)_3\}K]$ and CaI_2 in benzene (Scheme 2.6),¹⁹² a rare example of a salt metathesis reaction in hydrocarbon rather than in ethereal medium. This compound is the only solvent-free crystallised alkylcalcium complex. When $[\{C(\text{SiHMe}_2)_3\}K]$ was used instead of $[\{C(\text{SiMe}_3)_3\}K]$, the salt metathesis reaction with CaI_2 in thf afforded the bis-Si-H agostic calcium complex $[\{C(\text{SiHMe}_2)_3\}_2Ca(\text{thf})_2]$, also presented in Scheme 2.6.^{193,194}



Scheme 2.6 Solid state structures of $[\{C(SiMe_3)_3\}_2Ca]$ (left), $[\{C(SiHMe_2)_3\}_2Ca(thf)_2]$ (centre) and $[\{CH(SiMe_3)_2\}_2Ca(thf)_2]$ (right). Short $Si\cdots Ca$ and $H\cdots Ca$ contacts are depicted in dashed lines.

The complex $[\{CH(SiMe_3)_2\}_2Ca(thf)_2]$, was initially synthesised by the team of Lappert under specialised metal-vapour reaction conditions.¹⁸⁰ A new synthetic pathway employing a wet method, *i.e.* the salt metathesis of $[\{CH(SiMe_3)_2\}K]$ with CaI_2 in thf, was later reported by Hill *et al.*¹⁹⁵

Both $[\{C(SiHMe_2)_3\}_2Ca(thf)_2]$ and $[\{CH(SiMe_3)_2\}_2Ca(thf)_2]$ were used as precursors for the synthesis of rare heteroleptic alkyl complexes of formula $[(To^T)Ca\{C(SiHMe_2)_3\}]$ (To^T = tris(4-*t*-butyl-2-oxazoliny)phenylborate),¹⁹⁶ $[\{(Me_3Si)_2CH-BIAN\}Ca\{CH(SiMe_3)_2\}]$ (BIAN = bis(imino)acenaphthene)^{197,198} and $[(N^N)Ca\{CH(SiMe_3)_2\}]$ (N^N = iminoanilide)¹⁹⁹ (Scheme 2.7). The latter was obtained by a one pot reaction between $(N^N)H$, $[\{CH(SiMe_3)_2\}K]$ and CaI_2 . None of these complexes have been characterised by XRD. These three heteroleptic complexes were used for catalytic hydroelementation reactions (especially hydroamination).

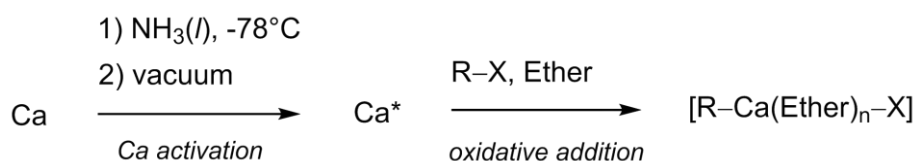


Scheme 2.7 Proposed formula for heteroleptic calcium complexes, $[(To^T)Ca\{C(SiHMe_2)_3\}]$ (left), $[\{(Me_3Si)_2CH-BIAN\}Ca\{CH(SiMe_3)_2\}]$ (centre) and $[(N^N)Ca\{CH(SiMe_3)_2\}]$ (right).

b. Synthesis from metallic Ca

The Grignard reaction with metallic Ca is difficult due to its inertness. Several techniques to activate Ca have been investigated, such as: co-condensation between Ca vapour and the suitable organohalide,¹⁸⁰ solubilisation of Ca in ethereal solvents saturated with ammonia gas,^{200,201} purification and activation of Ca by vacuum distillation at 870°C/7.10⁻⁵ mbar,²⁰² reduction of CaI₂ by potassium in thf or toluene (Rieke method),^{203,204} formation of an anthracene calcium complex in thf followed by its decomposition in hot toluene (Bogdanović method),^{205,206} and reduction of CaI₂ or CaBr₂ by lithium biphenylide in thf.²⁰⁷ Due to the limited substrate choice and/or the harsh conditions employed, these methods are not always suitable.

Herein, we emphasise the convenient route developed by the team of Westerhausen: metallic Ca is dissolved in liquid ammonia at -78°C and subsequent drying leads to finely divided activated Ca* powder.²⁰⁸⁻²¹⁰ The activated Ca* is then suspended in ethereal medium and the oxidative addition of an organohalide RX affords the expected [R-Ca-X] complex (Scheme 2.8).

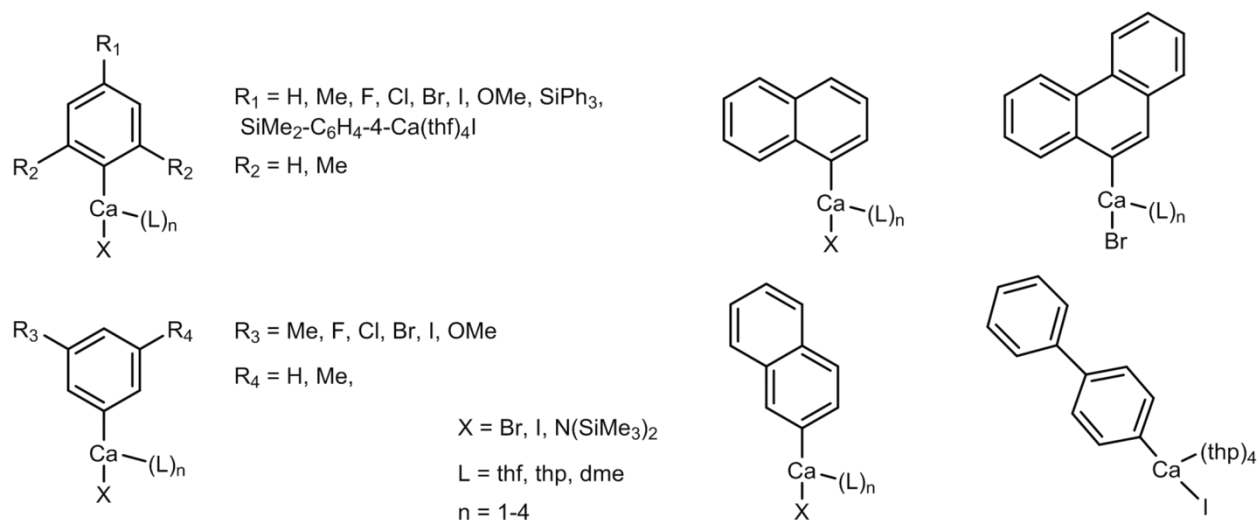


Scheme 2.8 Activation of Ca followed by oxidative addition of an organohalide.

One advantage of this route is that neither Ca nor NH₃ needs extensive purification prior to use (e.g.: we worked with 99% purity reagents). In addition, the ammonia can be easily trapped and recycled. The oxidative addition reaction on Ca* has now been developed for several classes of organocalcium, notably aryl- but also vinyl- and more recently alkylcalcium complexes as described below.

i. Arylcalcium compounds

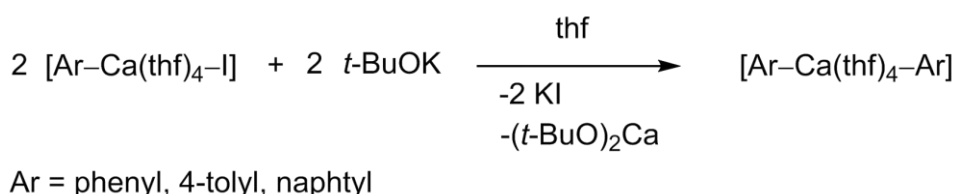
Oxidative addition of arylhalides on Ca* afforded a plethora of compounds presented in Scheme 2.9, including the simplest heteroleptic phenylcalcium complex [(C₆H₅)Ca(thf)₄Br].^{208,209,211-218} All these complexes have been isolated in fair to high yields and most of them have been characterised by XRD.



Scheme 2.9 Heteroleptic arylcalcium complexes obtained from the oxidative addition reaction on Ca^* . Thp = tetrahydropyran, dme = 1,2-dimethoxyethane.

The choice of the solvent and the nature of the halide are crucial. The best yields are obtained in thf and sometimes in thp. Iodoarenes are the most reactive species toward Ca^* . Bromoarenes react more slowly and less selectively whereas chloroarenes and fluoroarenes do not react.¹⁷⁴

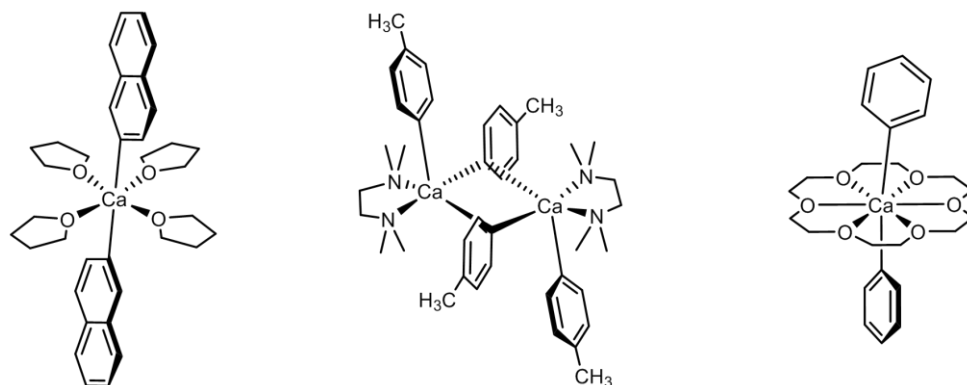
In the case of arylcalcium derivatives, the Schlenk equilibrium in thf is generally displaced toward the formation of the heteroleptic compounds. Besides, just like addition of dioxane converts heteroleptic magnesium complexes into their homoleptic pendants, addition of *t*-BuOK allows the isolation of diaryl compounds (Scheme 2.10).^{219,220} The equilibrium is displaced towards the homoleptic diaryl Ca species by the precipitation of KI and the ill-characterised $(t\text{-BuO})_2\text{Ca}$.



Scheme 2.10 Synthesis of diarylcalcium complexes.

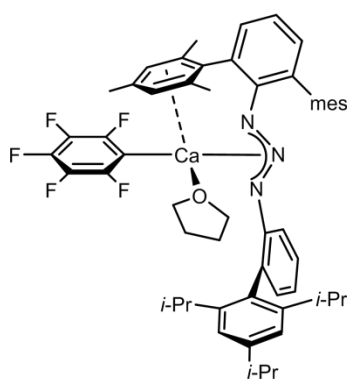
By using this method, diphenyl, di(4-tolyl) and dinaphthyl calcium complexes are obtained. Due to the high solubility of these compounds, only the $[(\alpha\text{-Napht})_2\text{Ca(thf)}_4]$ and

$[(\beta\text{-Naph})_2\text{Ca}(\text{thf})_4]$ complexes have been crystallised with thf donors. In order to reduce their solubility, polyamines and 18-crown-6 are used, affording crystallisation of other arylcalcium complexes (some of them are depicted in Scheme 2.11).



Scheme 2.11 Solid state structures of $[(\beta\text{-Naph})_2\text{Ca}(\text{thf})_4]$ (left), $[(4\text{-CH}_3\text{C}_6\text{H}_4)_2\text{Ca}(\text{tmeda})]_2$ (centre) and $[\text{Ph}_2\text{Ca}(18\text{-crown-6})]$ (right).

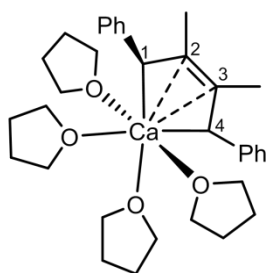
A unique heteroleptic fluorinated arylcalcium complex $[(\text{C}_6\text{F}_5)\text{Ca}(\text{N}_3\text{ArAr}')(\text{thf})]$ ($\text{N}_3\text{ArAr}' = 1,3\text{-diaryltriazenide}$, $\text{Ar} = 2,6\text{-dimesitylphenyl}$, $\text{Ar}' = 2\text{-(2,4,6-tri-}i\text{-Pr-phenyl)phenyl}$) is obtained in a one-pot reaction from non-activated metallic calcium, $\text{Hg}(\text{C}_6\text{F}_5)_2$ and the triazene precursor (Scheme 2.12).²²¹ This compound is stabilised by π -bonding between the crowded triazene ligand and the metal centre.



Scheme 2.12 Solid state structure of $[(\text{C}_6\text{F}_5)\text{Ca}(\text{N}_3\text{ArAr}')(\text{thf})]$. A short $\pi \cdots \text{Ca}$ contact is depicted by a dashed line.

ii. Butadiendiylcalcium compound

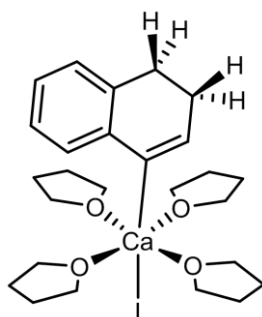
An isolated example of a butadiendiyl complex was reported early on by Nakamura *et al.*²²² Reaction of 2,3-dimethyl-1,4-diphenylbutadiene with non-activated calcium metal in thf afforded the red $[(C_4H_2Me_2Ph_2)Ca(thf)_4]$ (Scheme 2.13) in 67% yield. The coordination mode of the but-2-ene-1,4-diide ligand was unveiled by a XRD analysis: the Ca atom binds the two 1,4-carbanions and extra stabilisation is provided by a π interaction with the 2,3-carbon bond.



Scheme 2.13 Solid state structure of $[(C_4H_2Me_2Ph_2)Ca(thf)_4]$. Short $\pi \cdots Ca$ contacts are depicted in dashed line.

iii. Vinylcalcium compounds

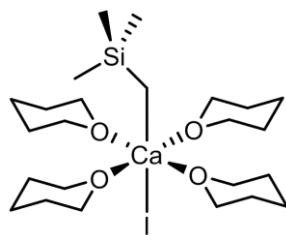
By applying the Ca^* method, the team of Westerhausen isolated the first vinylcalcium complex of formula $[(1,2\text{-dihydronaphth-4-yl})Ca(thf)_4I]$ (Scheme 2.14).²²³ 1-cyclohexenylcalcium iodide was also detected. Even if the latter was not isolated, its formation was confirmed by the formation of the corresponding 1-cyclohexen-1-carboxylic acid after quenching with CO_2 .



Scheme 2.14 Solid state structure of $[(1,2\text{-dihydronaphth-4-yl})Ca(thf)_4I]$.

iv. Alkylcalcium compounds

The Westerhausen method was recently extended to the synthesis of the alkyl compound $[(\text{SiMe}_3\text{CH}_2)\text{Ca}(\text{thp})_4\text{I}]$,²²⁴ which was obtained from the oxidative addition of iodomethyltrimethylsilane on Ca^* in thf. Single crystals could be grown in thp (Scheme 2.15). This compound constitutes a new step toward non-substituted alkylcalcium chemistry, as only one SiMe_3 group is present to stabilise the carbanion.



Scheme 2.15 Solid state structure of $[\text{SiMe}_3\text{CH}_2\text{Ca}(\text{thp})_4\text{I}]$.

B. Results and discussion

In this part, we aimed at the synthesis and characterisation of a cyclopropylcalcium complex. Two strategies were investigated: we first used stabilised α -substituted cyclopropyl groups that are introduced on Ca(II) *via* the salt metathesis reaction. We then studied the oxidative addition between iodocyclopropane and activated Ca(0)*.

I.1.Salt metathesis reaction

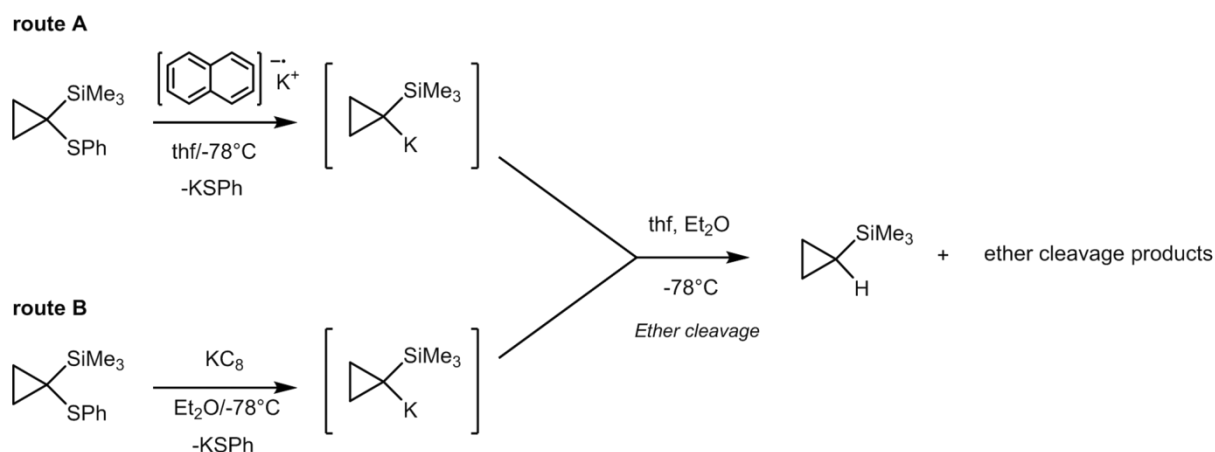
a. Synthesis of cyclopropylpotassium derivatives

The synthesis of cyclopropylpotassium has never been reported. As presented for Li in chapter 1, therefore, we decided to investigate the synthesis of similar cyclopropylpotassium derivatives stabilised by trimethylsilyl and phenyl moieties.

i. (Trimethylsilyl)cyclopropyl group

As (trimethylsilyl)cyclopropane cannot be deprotonated (*cf.* chapter 1), the same strategy employed for complex **1** [$\{c\text{-C}(\text{SiMe}_3)\text{C}_2\text{H}_4\}\text{Li}$] was used here. The 1-(phenylthio)-1-(trimethylsilyl)cyclopropane was successfully reduced by potassium naphthalenide in thf at -78°C , as attested by the disappearance of the characteristic colour of the latter (Scheme 2.16, route A). Due to thf degradation, however, the only observed product was (trimethylsilyl)cyclopropane.

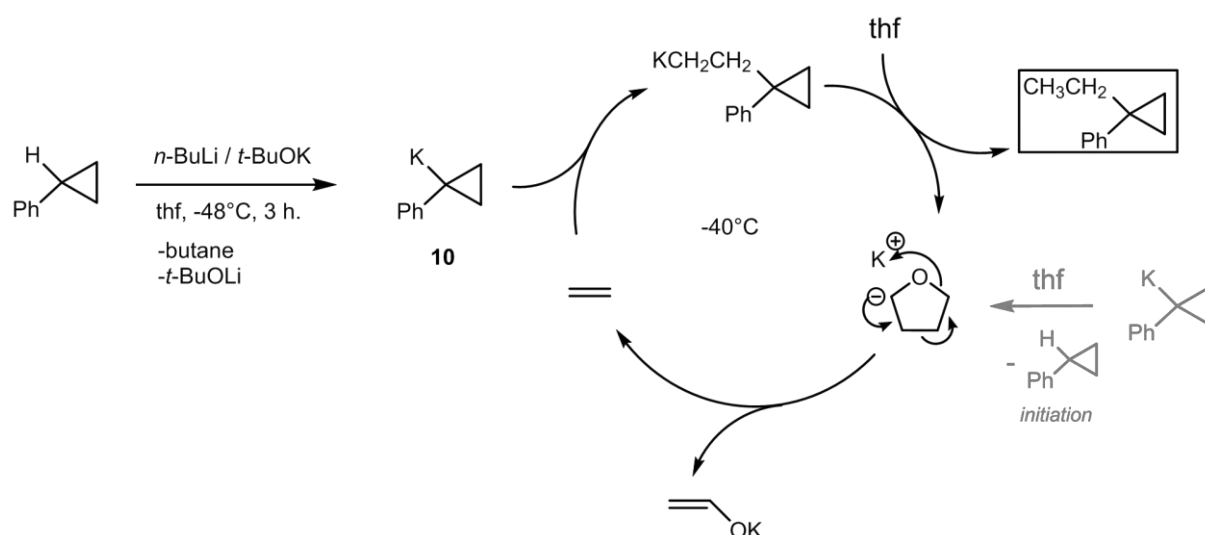
We next decided to carry out the reaction in Et_2O which is less prone to degradation and has a lower boiling point, allowing its removal under vacuum at -78°C . As potassium naphthalenide could not be prepared in Et_2O , we used instead KC_8 as reducing agent (Scheme 2.16, route B). Immediate formation of graphite was observed, indicating that reduction of the C–S bond had occurred. However, after drying of the mixture at -78°C , only (trimethylsilyl)cyclopropane was observed, as the result of the fast protonation of [$\{c\text{-C}(\text{SiMe}_3)\text{C}_2\text{H}_4\}\text{K}$], even at low temperature. As all attempts to synthesise a SiMe_3 substituted cyclopropylpotassium failed, we moved to the phenyl substituted cyclopropylpotassium compounds.



Scheme 2.16 C–S reduction of 1-phenylthio-1-(trimethylsilyl)cyclopropane by potassium naphthalenide (route A) and potassium graphite (route B).

ii. Phenylcyclopropyl group

The synthesis of 1-phenylcyclopropylpotassium (**10**) was reported by Schlosser and Schneider, using the Lochmann-Schlosser superbases in thf at -48°C for 3 hours.¹⁵² When the temperature rose above -40°C , formation of 1-ethyl-1-phenylcyclopropane (51% yield) was observed. This product was proposed to result from the addition of the organopotassium on the ethylene generated by the thf cleavage reaction. This gives rise to the self-catalysed reaction shown in Scheme 2.17.

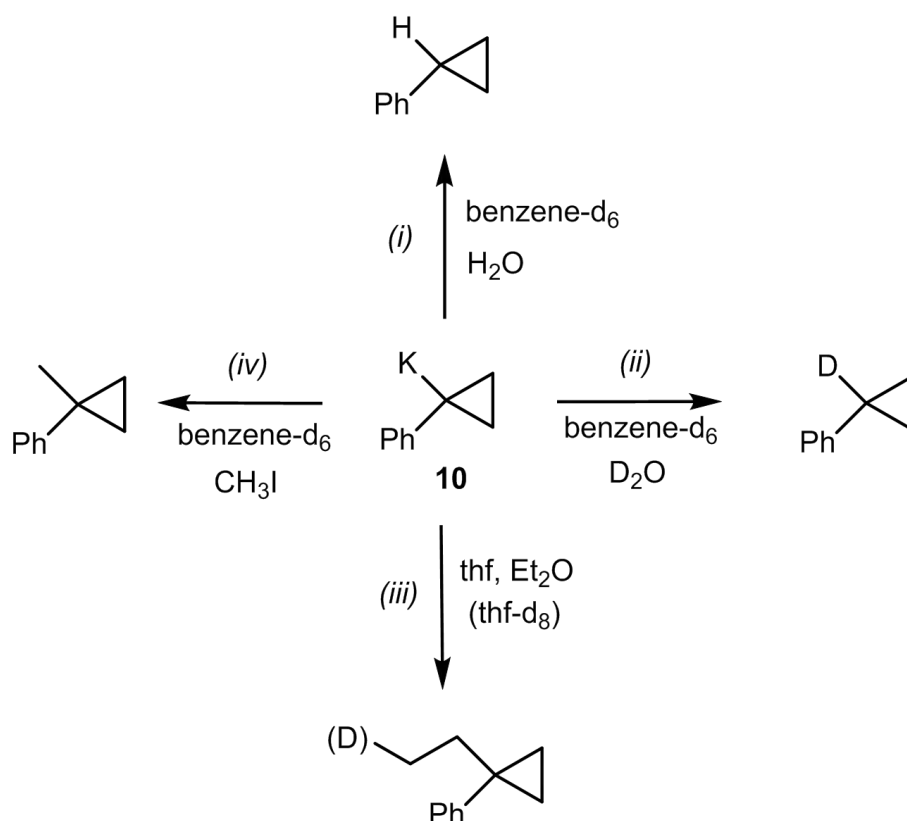


Scheme 2.17 Synthesis of 1-phenylcyclopropylpotassium and 1-ethyl-1-phenyl-cyclopropane.

The regioselectivity of the phenylcyclopropane deprotonation depends on the choice of the solvent.¹⁵² In hydrocarbons, a mixture of α , *ortho*, *meta* and *para* deprotonated phenylcyclopropyl products was observed, whereas in thf, high selectivity for the deprotonation of the cyclopropyl α -position was reported.

We followed therefore the procedure described by Schlosser and Schneider carefully maintaining the temperature below -48°C . Formation of **10** was attested by the intense red colour of the medium upon addition of *n*-BuLi to the *t*-BuOK/phenylcyclopropane mixture in thf at -48°C . After 3 hours stirring, the mixture was placed under vacuum keeping the temperature below -45°C . Subsequent washing with pentane and filtration to remove *t*-BuOLi afforded **10** as a brown powder in *ca* 55% yield.

Compound **10** was not directly characterised by NMR since it readily reacts with ethers above -40°C and is not soluble in hydrocarbons (probably because it is polymeric, as is $[\{\alpha,\alpha\text{-}(\text{SiMe}_3)_2\text{PhC}\}\text{K}]_{\infty}$).¹⁸¹ Its formation was confirmed by derivatisation reactions (Scheme 2.18):



Scheme 2.18 Derivatisation reactions of **10**.

(i) Hydrolysis of **10** led to the formation of phenylcyclopropane as observed by ^1H NMR. Small amounts of *t*-butanol (0.09 eq.) and 1-ethyl-1-phenyl-cyclopropane (0.13 eq.), however, were also observed. Subsequent washing of **10** with pentane did not decrease the *t*-BuOH or 1-ethyl-1-phenyl-cyclopropane ratios measured after hydrolysis, suggesting that *t*-BuOK and $[(\text{Ph-}i>c\text{-C}_3\text{H}_4)\text{CH}_2\text{CH}_2\text{K}]$ are mixed with **10** probably as adducts. Formation of adducts between *t*-BuOK and benzylopotassium compounds has been reported, although only when *t*-BuOK was introduced in excess.¹⁵⁰ The outcome of the reaction was not altered by the use of different experimental conditions. All purification attempts have failed so far.

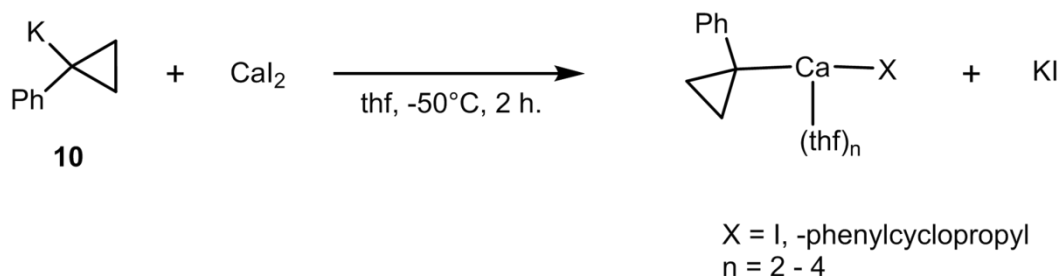
(ii) The regioselectivity for the deprotonation of phenylcyclopropane at the α -position was unambiguously confirmed by hydrolysis of **10** with D_2O . This led to the formation of α -deuterated phenylcyclopropane ($\text{Ph-}i>c\text{-C}_3\text{H}_4\text{D}$) as observed by ^1H NMR (broad signals comparable to those of phenylcyclopropane with the exception of the H_α resonance), together with the deuterated analogues of the by-products mentioned above.

(iii) Solubilisation of **10** in thf and Et_2O at RT afforded the ethylene addition product, 1-ethyl-1-phenyl-cyclopropane as attested by ^1H NMR.¹⁵² Solubilisation of **10** in thf- d_8 afforded $(\text{Ph-}i>c\text{-C}_3\text{H}_4)\text{CH}_2\text{CH}_2\text{D}$.

(iv) The reaction of **10** with iodomethane (CH_3I) afforded 1-methyl-1-phenyl-cyclopropane as ascertained by ^1H NMR in benzene- d_6 .²²⁵

b. Salt metathesis reaction

Although product **10** could not be obtained pure, the salt metathesis reaction with CaI_2 was investigated. Addition of **10** to CaI_2 in thf at -50°C led to precipitation of a white solid (KI) (Scheme 2.19). After 2 hours of reaction, the volatiles were removed at -45°C . Extraction of the product with toluene at RT and washing with pentane afforded a red powder.



Scheme 2.19 Reaction between **10** and CaI_2 .

^1H NMR analyses in thf-d_8 of the extraction product revealed that at least 3 different compounds were present, always in different ratios. One example of such a spectrum containing a mixture of two of these products is presented in Figure 2.1. The resonances that can be attributed to metallated phenylcyclopropyl complexes are: *Hortho+meta* (range: δ 6.79-6.62), *Hpara* (range: δ 6.35-6.08) and *H β* (two ranges of resonances: δ 0.64-0.60 and 0.36-0.33). The chemical shifts are in the same range as for the lithiated phenylcyclopropyl complex **2**.

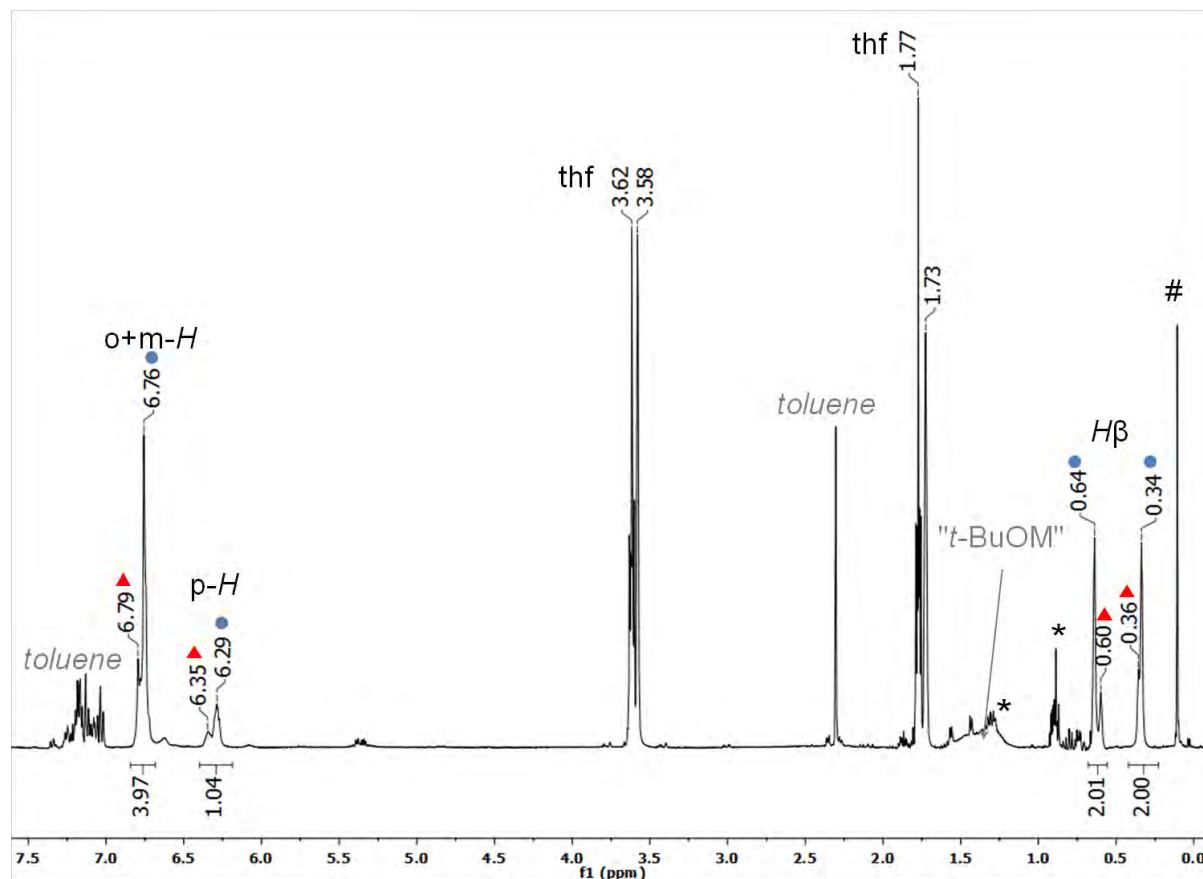


Figure 2.1 ^1H NMR spectrum in thf-d_8 of the mixture containing two purported phenylcyclopropyl Ca compounds. * = residual pentane, # = residual silicon grease. $M = \text{K}, \text{Ca}$. The two different compounds are labelled as blue circles and red triangles.

Interestingly these new products were much less sensitive to ether degradation than **10**. Indeed, upon quenching with H_2O , recovery of phenylcyclopropane together with *t*-BuOH (*ca* 0.10 eq.) was observed but no 1-ethyl-1-phenyl-cyclopropane was detected. In addition, the species presented in Figure 2.1 were fully converted to phenylcyclopropane within *ca* 25 days at RT in thf-d_8 .

It is therefore likely we have obtained new phenylcyclopropyl Ca complexes of the type $[(c\text{-CPhC}_2\text{H}_4)\text{CaX}(\text{thf})_n]$ ($X = \text{I}$, phenylcyclopropyl; $n = 2\text{-}4$). However, although partially characterised, the solubility of these compounds has prevented their isolation and crystallisation.

1.2. Oxidative addition on Ca*

As the cyclopropyl group resembles the aryl and vinyl groups, we investigated the synthesis of a non-substituted cyclopropyl calcium complex by oxidative addition of iodocyclopropane on Ca*. This work was started during a month stay at the Institut für Anorganische und Analytische Chemie, Jena, Germany, thanks to a collaboration with the team of the Professor Matthias Westerhausen. We had the opportunity to learn, then to transfer in our own laboratory, the calcium activation technique of which a detailed procedure is provided herein.^{208–210}

a. Activation of calcium

(i) Metallic Ca chunks (99% purity) and glass balls (diameter 4 mm) are placed in a Schlenk flask (Figure 2.2). (ii) Gaseous ammonia (99% purity) is then condensed at -78°C and the mixture is vigorously shaken. Quick solubilisation of Ca leads to a dark blue solution of the electride salt $\{\text{Ca}(\text{NH}_3)_x^{2+} + 2e(\text{NH}_3)_y^-\}$. This characteristic blue colour is due to the presence of solvated electrons, as typically observed upon solubilisation of alkali or alkaline earth metals in liquid ammonia.^{226–229} (iii) Ammonia is evaporated by heating the medium above -33°C . This affords “bronze calcium” which is attributed to the Ca(0) complex $[\text{Ca}(\text{NH}_3)_6]$.²³⁰ (iv) Under vacuum, “bronze calcium” loses its weakly coordinated ammonia to give highly dispersed and activated calcium powder (Ca*). Ca* is pyrophoric and quickly degrades upon exposition to air and moisture. Under inert gas, however, it can be stored for several months at RT.

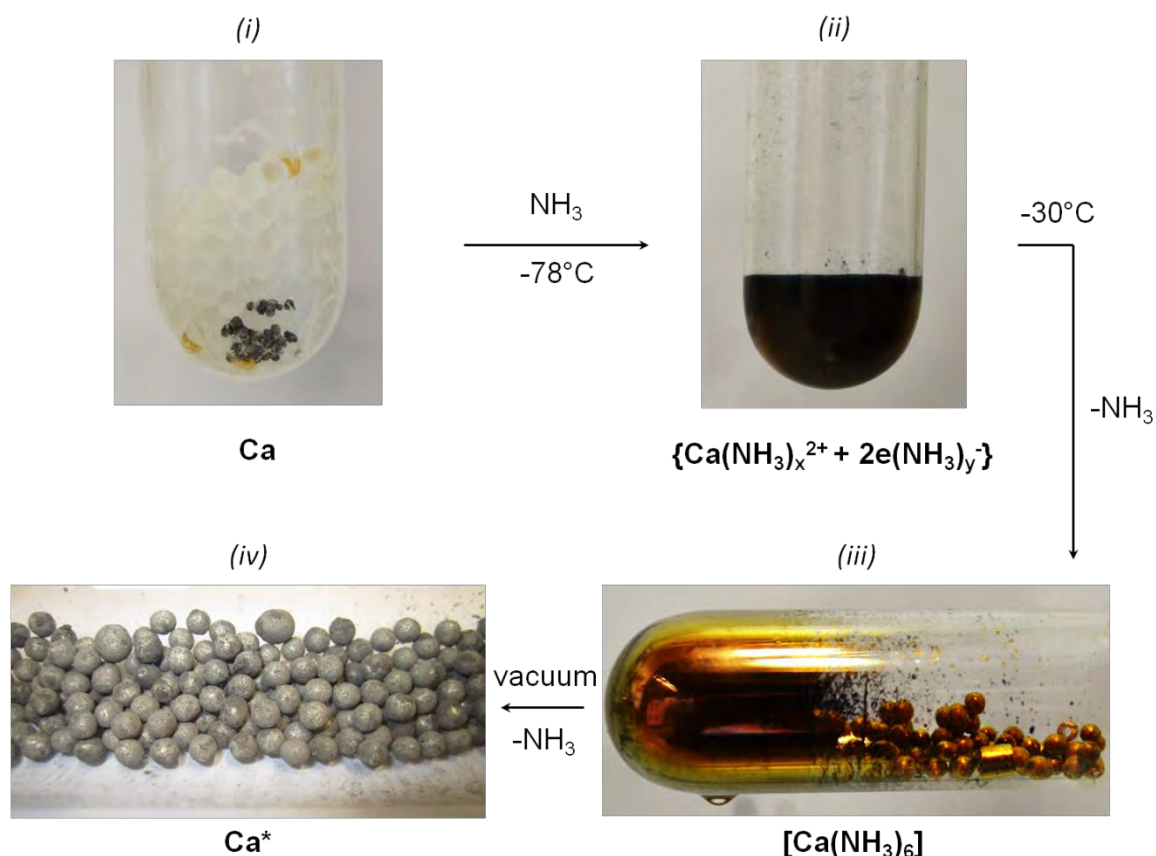
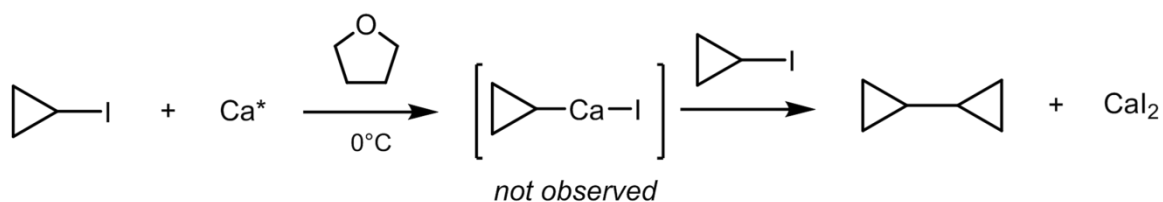


Figure 2.2 Formation of activated calcium. (Photography: Alexander Koch and Sven Krieck, Friedrich-Schiller-Universität Jena).

b. Synthesis of cyclopropyl calcium

i. Reaction in thf

The oxidative addition of iodocyclopropane on Ca^* in thf at 0°C is exothermic, inducing a colour change of the suspension from colourless to yellow. However, only bicyclopropyl and CaI_2 were observed by NMR and XRD. Their formation can be attributed to the Wurtz coupling reaction as depicted in Scheme 2.20. By changing the reaction temperature (from -80°C to RT), the iodocyclopropane/ Ca^* ratio and the time of addition and reaction, we could not change the course of the reaction. As depicted in Scheme 2.20, nonetheless, the formation of bicyclopropyl constitutes a strong indication that the expected cyclopropyl calcium complex has been formed.

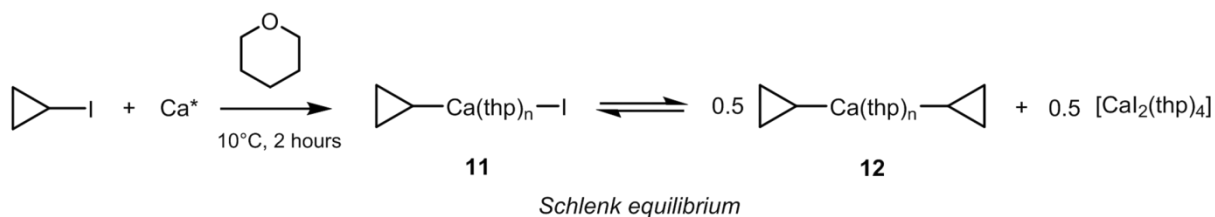


Scheme 2.20 Formation of bicyclopropyl compound by the Wurtz coupling reaction.

The full conversion of iodocyclopropane and the absence of any other by-products indicate that the bicyclopropyl compound was obtained in high yield, even though it has not been precisely determined. The best reported yield for the bicyclopropyl synthesis is 20% from the Simmons-Smith cyclopropanation reaction of butadiene.²³¹ Interestingly, the Wurtz coupling reaction between cyclopropylmagnesium bromide and cyclopropyl bromide affords bicyclopropyl in only 10% yield.²³¹

ii. Reaction in thp

In order to avoid the Wurtz coupling, we decided to change the reaction conditions by using the less donating thp solvent instead of thf. Slow addition of iodocyclopropane on Ca* led, after 2 hours shaking at 10°C and subsequent filtration, to a red solution of heteroleptic $[c\text{-PrCa}(\text{thp})_x\text{I}]$ (**11**) and/or homoleptic $[(c\text{-Pr})_2\text{Ca}(\text{thp})_x]$ (**12**) (Scheme 2.21) as evidenced by ^1H NMR analysis. **11** and **12** are related by a Schlenk equilibrium (see below). Acidimetric titration of an aliquot of this solution after quenching with H_2O indicated that 70% of iodocyclopropane had transformed into **11** and **12**. Despite the use of thp, we still obtained the Wurtz coupling products bicyclopropyl and $[\text{CaI}_2(\text{thp})_4]$, which accounted for the remaining 30% of the conversion of iodocyclopropane. Although this solution could be potentially used directly for subsequent acid/base or group transfer reactions (as for classical Grignard), we tried to obtain **11** and **12** as solid compounds. Reducing the volume and cooling down the solution resulted in crystallisation of $[\text{CaI}_2(\text{thp})_4]$ as attested by ^1H NMR and XRD. When most of $[\text{CaI}_2(\text{thp})_4]$ had precipitated, the solvent of the mother liquor was removed under vacuum to afford a red powder containing **11** and **12** which was characterised by ^1H and ^{13}C NMR. Upon hydrolysis of this powder, ^1H NMR spectroscopy showed full conversion to thp and cyclopropane. These organocalcium complexes slowly degrade in thp (<10% degradation after 3 days at RT) to give cyclopropane and the corresponding ether decomposition products.



Scheme 2.21 Synthesis of complexes **11** and **12**.

11 and/or **12** are very soluble in ethers (Et₂O, thp, thf) and toluene but not in pentane. Due to their high solubility, crystallisation of **11** or **12** has failed so far. Upon addition of coordinating polyamines (tmeda, pmdta) or polyethers (triglyme, 18-crown-6) to **11** or **12**, the coordinated thp is displaced leading to less soluble complexes. However, crystals suitable for XRD have not been obtained so far.

Interestingly, the amount of [CaI₂(thp)₄] obtained during the purification process far exceeded what we expected from the Wurtz coupling reaction only. We therefore propose that this excess testifies to the existence of the Schlenk equilibrium between **11** and **12**. However, as some [CaI₂(thp)₄] already precipitated during the reaction, it was difficult to estimate its precise amount, and thus to quantify the equilibrium shift between **11** and **12**.

iii. NMR analyses

A typical ¹H NMR spectrum of **11** and/or **12** after work up is presented in Figure 2.3. The apparent 1:1 ratio between the two set of signals is random and could not be repeated.

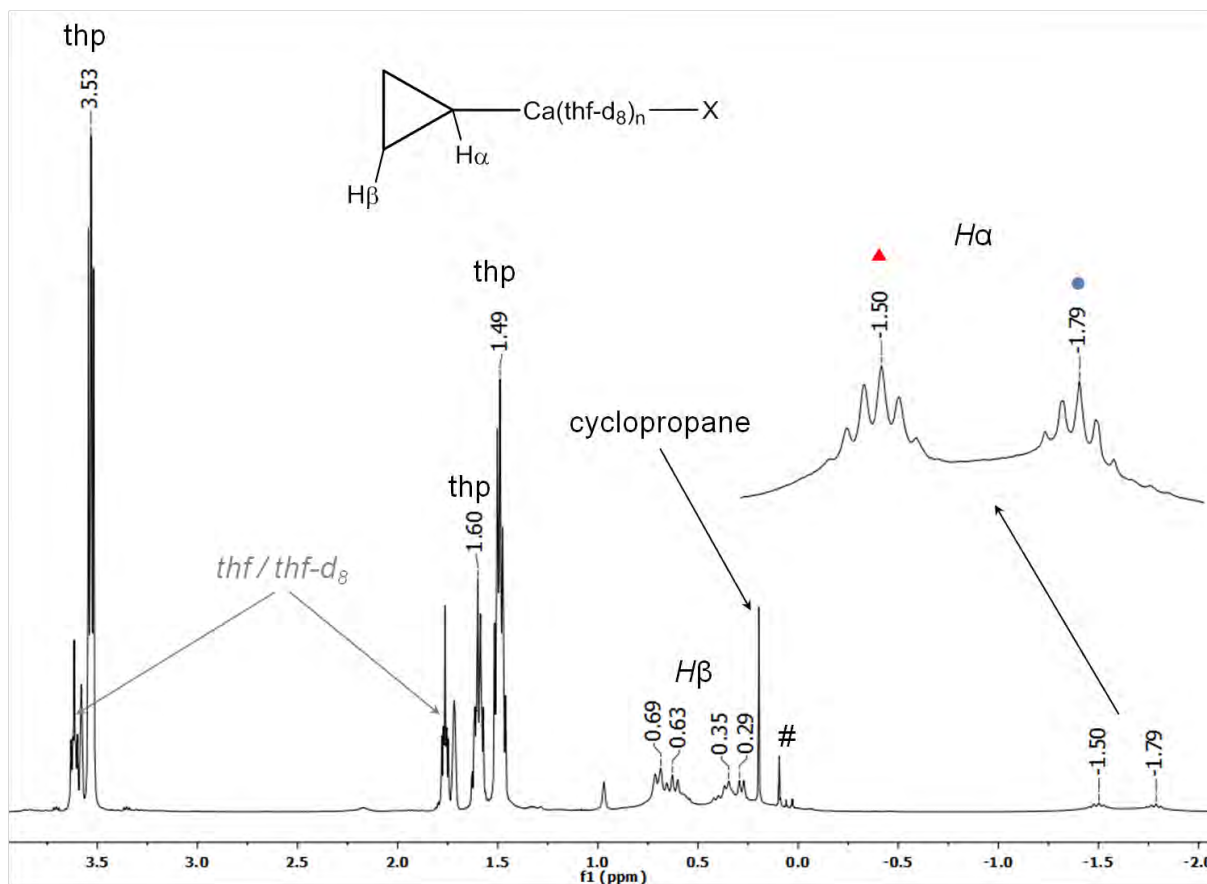


Figure 2.3 ^1H NMR spectrum of a mixture of **11** and/or **12** in thf-d_8 . # = residual silicon grease. The signals of the two different compounds are labelled as blue circles and red triangles. $X = \text{I}, \text{C}_3\text{H}_5$.

The relevant resonances can be observed in thf-d_8 : the coordinated thp has been displaced by the thf-d_8 and appears as a free molecule at δ 3.53 ($\text{O-CH}_2\text{-CH}_2\text{-CH}_2$), 1.60 ($\text{O-CH}_2\text{-CH}_2\text{-CH}_2$) and 1.49 ($\text{O-CH}_2\text{-CH}_2\text{-CH}_2$); two sets of H_β , H_β' and H_α signals of bound cyclopropyl groups appear in the range δ 0.75-0.50, δ 0.40-0.20 and δ -1.50 - -1.80, respectively. The strong shielding of the H_α signal is characteristic of the cyclopropyl anion. In thf-d_8 , H_α of cyclopropyllithium and cyclopropylmagnesium bromide resonates at δ -2.53 and -2.04, respectively.²³² The integrations between the H_β , H_β' and H_α signals are consistent with a 2:2:1 ratio. The amount of coordinated thp in the cyclopropyl Ca complexes could not be estimated by integration due to the presence of small amounts of $[\text{CaI}_2(\text{thp})_4]$ in the mixture. The broadness of the cyclopropyl signals could be attributed to ligand scrambling between **11**, **12**, and their potential monomer/dimer forms.

^1H NMR spectra were also recorded in benzene- d_6 . The spectra are similar to those in thf- d_8 , except for the resonances of the thp which is now coordinated to the Ca centre (broad signals at δ 3.65, 1.33 and 1.27). In benzene- d_6 , the signals of the cyclopropyl moieties are broader than in thf- d_8 .

A RT $^{13}\text{C}\{^1\text{H}\}$ NMR experiment in thf- d_8 displayed a very broad resonance in the range δ 4-9, that was attributed to $C\beta$ thanks to a HMQC experiment. No correlation was observed for $C\alpha$. When the same analyses were carried out at -60°C , narrow resonances at δ 7.9 ($C\alpha$) and δ 7.0 ($C\beta$) were observed amongst the broad signals. The chemical shift for $C\alpha$ is in the range of other alkylcalcium complexes.²²⁴

C. Conclusion and perspectives

The salt metathesis reaction of 1-phenylcyclopropylpotassium and CaI_2 likely generates new 1-phenylcyclopropylcalcium derivatives. However, the high solubility of these compounds have for now hampered their isolation. Furthermore, a new synthetic procedure to access pure 1-phenylcyclopropylpotassium reagent is needed. While we were developing this research, the synthesis of the new, highly basic, alkylcalcium $[(\text{SiMe}_3\text{CH}_2)\text{Ca}(\text{thp})_4\text{I}]$ was published.²²⁴ The isolation of this compound therefore opens new synthetic perspectives since the acid/base reaction between $[(\text{SiMe}_3\text{CH}_2)\text{Ca}(\text{thp})_4\text{I}]$ and phenylcyclopropane might lead to the formation of pure 1-phenylcyclopropylcalcium directly.

The oxidative addition of iodocyclopropane to activated calcium in thp leads to an unprecedented cyclopropylcalcium species. This straightforward synthesis could provide a means of generating a new metallating or group transfer reagent, even though its potential in such reactions has to be studied further. It is also possible to isolate these cyclopropylcalcium complexes as a solid.

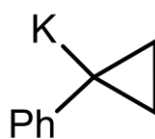
One major difficulty of the organometallic chemistry of calcium is the need for XRD structures. Due to the presence of broad signals, NMR techniques give limited information. In addition, since the alkyl calcium compounds are very sensitive to air and moisture, and can be mixed with traces of CaI_2 , their elemental analysis is often not possible. Derivatisation reactions and acidimetric titration indicate the presence of reactive carbanions but the true nature of the organometallic species remains unclear.

D. Experimental part

All operations were performed with rigorous exclusion of air and moisture, using standard Schlenk techniques and an Ar filled Jacomex glovebox ($O_2 < 5$ ppm, $H_2O < 1$ ppm). Phenylcyclopropane (97%), metallic calcium (granular, 99%), calcium diiodide (99.999%), potassium tert-butoxide (98%), tmeda (99.5%), pmdta (99%), triglyme (99%), 18-crown-6 (99%), tetrahydropyran (99%), *n*-butyllithium (2.5 M solution in hexanes) and glass balls (\varnothing 4 mm) were purchased from Aldrich. Bromocyclopropane (99%) was purchased from Alfa Aesar and ammonia (99%) was purchased from Air Liquide. All solvents were pre-dried by passing through a Puresolv MD 7 solvent purification machine, furtherdried over molecular sieves, filtered and degassed by freeze–pump–thaw cycles. Deuterated solvents, phenylcyclopropane, triglyme and bromocyclopropane were dried over molecular sieves, filtered, and degassed by several freeze–pump–thaw cycles and stored in sealed ampoules in the glovebox. Tmeda, pmdta and thp were distilled over Na and further degassed by freeze–pump–thaw cycles. Potassium tert-butoxide was purified by sublimation at $150^\circ/10^{-1}$ mbar. 18-crown-6 was recrystallised from an acetonitrile solution.

The chemical shifts are given in ppm. NMR spectra were recorded by using J. Young valve NMR tubes using Bruker Avance III 400 (1H , 400.16; ^{13}C , 100.6 MHz) or Avance 500 (1H , 500.33; ^{13}C 125.82 MHz) spectrometers. Chemical shifts for 1H NMR were determined using residual proton signals in the deuterated solvents and are reported vs. $SiMe_4$. Chemical shifts for ^{13}C NMR spectra were that of the solvent referenced to $SiMe_4$.

Synthesis of 1-phenylcyclopropylpotassium



10

To a stirred suspension of phenylcyclopropane (300 mg, 2.54 mmol) and *t*-BuOK (342 mg, 3.05 mmol) in thf (3 mL) a solution of *n*-BuLi in hexane (1,5 mL, 3.75 mmol) was added dropwise at $-80^\circ C$. The mixture was stirred at $-50^\circ C$ for three hours, leading to a colour change from colourless to red together with gas evolution and full solubilisation of the reagents. The volatiles were pumped off while maintaining the temperature below $-45^\circ C$.

After washing with pentane (3 x 5 mL) and subsequent drying, **10** was obtained as a brown powder (252 mg, 55%).

Typical procedure for reactivity studies with 1-phenylcyclopropylpotassium

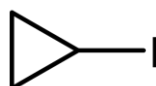
10 (ca 30 mg) was suspended in benzene- d_6 (0.6 mL) in a NMR tube and an excess of the reactant, H_2O , D_2O , Et_2O , thf and CH_3I , respectively, was added at RT. The resulting solution was analysed by 1H NMR.

Synthesis of 1-phenylcyclopropylcalcium compounds

CaI_2 (195 mg, 0.66 mmol) was suspended in thf (8 mL) and heated to $60^\circ C$ for 3 hours. **10** (200 mg, ca 1.2 mmol) was slowly added at $-50^\circ C$ leading to a darkening of the solution and precipitation of a white powder. The mixture was stirred at $-50^\circ C$ for two hours and the volatiles were removed under vacuum at the same temperature. The resulting red-brown slurry was extracted with toluene (3 x 5 mL) and dried under vacuum at RT. A subsequent washing with pentane afforded a red powder (190 mg).

1H NMR (thf- d_8 , 298 K) δ 6.79-6.62 (4H, Hortho+meta), 6.35-6.08 (1H, Hpara), 0.64-0.60 (2H, H β) 0.36-0.33 (2H, H β). The NMR spectrum contains resonances for free thf, but the integrations were never reproducible.

Synthesis of iodocyclopropane



In an argon filled glovebox, a Li ribbon (1.5 g, 0.22 mol) was cut into small pieces and placed in a Schlenk flask filled with Et_2O (150 mL). A solution of bromocyclopropane (10.0 g, 0.0826 mol) in Et_2O (150 mL) was added dropwise at $0^\circ C$ for 3 hours. The slurry was then stirred at RT overnight to afford a cloudy suspension with unreacted Li chunks. The suspension was filtered and the resulting solution was cooled down to $-78^\circ C$. A solution of I_2 (20 g, 0.079 mol) in Et_2O (150 mL) was then added dropwise, until the persistence of a brown colour. The solution was warmed to RT and treated first with water then with an aqueous Na_2SO_3 solution. The organic phase was separated and dried over $MgSO_4$. Et_2O was removed by distillation at atmospheric pressure and the brown residue was purified by trap-to-trap distillation to afford a colourless liquid. The liquid was degassed by freeze-pump-thaw cycles and dried over 4 Å molecular sieves (8.94 g, 64%). Iodocyclopropane is slightly light

sensitive as testified by the yellow colour observed after storing the product in daylight for a few days.

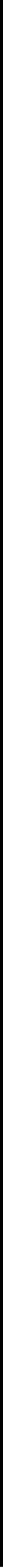
^1H NMR (benzene- d_6 , 298 K) δ 1.80 (tt, 1 H, $J_{\text{HH}} = 11.8, 5.2$ Hz, $H\alpha$), 0.44 (m, 4 H, $H\beta$). ^{13}C NMR (benzene- d_6 , 298 K) δ 9.9 (t, $^1J_{\text{CH}} = 166$ Hz, $C\beta$), -21.2 (d, $^1J_{\text{CH}} = 188$ Hz, $C\alpha$). MS m/z 168.95 (MH^+).

Synthesis of cyclopropylcalcium complexes



In a Schlenk partially filled with glass balls, iodocyclopropane (1.53 g, 9.13 mmol) was added to a suspension of Ca^* (366 mg, 9.13 mmol) in thp (20 mL). The slurry was shaken for two hours at 10°C . The reaction mixture was then warmed to room temperature and unreacted Ca^* was removed by filtration over celite. Acidimetric titration of an aliquot of the resulting red solution gave a conversion of 70%. Repeated concentration of the solution by evaporation under vacuum and cooling to -40°C afforded several crops of colourless crystals of $[\text{CaI}_2(\text{thp})_4]$. Once no more precipitate was obtained, the mother liquor was evaporated to dryness to afford, after several washing with pentane, a brown solid of the cyclopropylcalcium compounds **11** and **12** (400 mg).

^1H NMR (thf- d_8 , 298 K) δ 3.53 (t, $\text{O-CH}_2\text{-CH}_2\text{-CH}_2$), 1.60 (m, $\text{O-CH}_2\text{-CH}_2\text{-CH}_2$), 1.49 (q, $\text{O-CH}_2\text{-CH}_2\text{-CH}_2$), 0.75-0.50 (bm, 2H, $H\beta/\beta'$), 0.40-0.20 (bm, 2H, $H\beta/\beta'$), (-1.50) - (-1.80) (bm, 1H, $H\alpha$). ^1H NMR (benzene- d_6 , 298 K) δ 3.65 (bs, $\text{O-CH}_2\text{-CH}_2\text{-CH}_2$), 1.33 (bs, $\text{O-CH}_2\text{-CH}_2\text{-CH}_2$), 1.27 (bs, $\text{O-CH}_2\text{-CH}_2\text{-CH}_2$), 1.2-1.0 (bs, 2H, $H\beta/\beta'$), 1.0-0.8 (bs, 2H, $H\beta/\beta'$), (-0.8) - (-1.9) (bs, 1H, $H\alpha$). $^{13}\text{C}\{^1\text{H}\}$ NMR (thf- d_8 , 213 K) δ 69.1 ($\text{O-CH}_2\text{-CH}_2\text{-CH}_2$), 27.7 ($\text{O-CH}_2\text{-CH}_2\text{-CH}_2$), 24.6 ($\text{O-CH}_2\text{-CH}_2\text{-CH}_2$), 7.9 ($C\alpha$), 7.0 ($C\beta$).



CHAPTER 3

Chapter 3. Group 4 dicyclopropyl metallocenes

A. Introduction

In this chapter we report our study of the reactivity of the dicyclopropyl zirconocene complex $[\text{Cp}_2\text{Zr}(c\text{-C}_3\text{H}_5)_2]$ (from now on $c\text{-Pr} = c\text{-C}_3\text{H}_5$). This complex has recently proved interesting for C–H bond activation of thiophene, furan and benzene,³¹ and we therefore wished to extend its reactivity scope to pyridine and derivatives. Also, as group 4 metallocene complexes have been extensively used for C–F bond cleavage reactions,²³³ the reactivity of $[\text{Cp}_2\text{M}(c\text{-C}_3\text{H}_5)_2]$ ($\text{M} = \text{Ti}, \text{Zr}$) towards fluorinated pyridines is investigated.

The presented work was initiated by Nuria Romero during her PhD (October 2011 – December 2014), especially concerning the reactivity of $[\text{Cp}_2\text{Zr}(c\text{-C}_3\text{H}_5)_2]$ toward pyridines. The activation of fluorinated pyridines by $[\text{Cp}_2\text{Ti}(c\text{-C}_3\text{H}_5)_2]$ was realised thanks to Anthony Pujol during his master thesis (January - June 2015).

1.1. Reactive early transition metals complexes

Despite significant progress, the activation of strong and inert bonds (such as C–H²³⁴ or C–F²³⁵) remains a topical subject. A crucial aspect is the control of the selectivity within the available bonds of the target molecules. One way to address this issue is to use well-defined molecular coordination complexes of transition metals. In this part, we focus mainly on Early Transition Metals (ETM) complexes and on the mechanisms and scope of fundamental reactions.

a. σ -bond metathesis / α -H abstraction

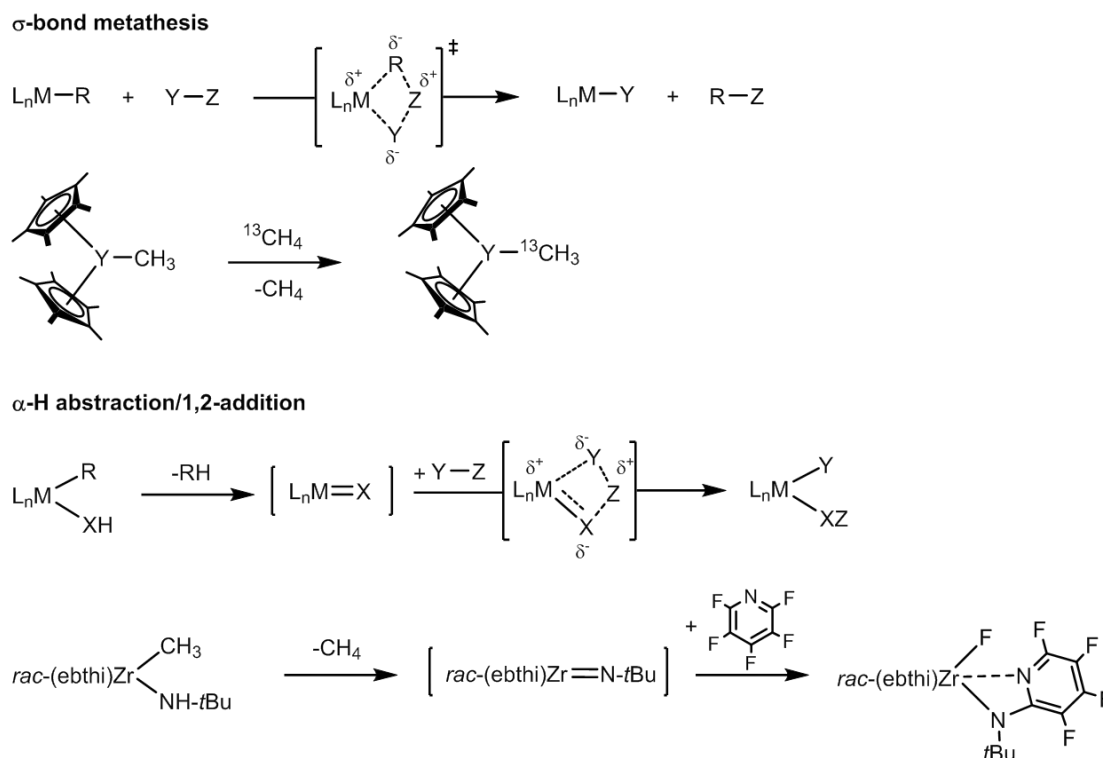
Cleavage of strong and inert bonds necessarily implies the presence of highly reactive species during the activation processes. Two mechanisms usually occur for ETM complexes:

- L_nMR type complexes ($\text{M} = \text{Sc}, \text{R} = \text{H}, \text{alkyl}, \text{aryl}, \text{silyl}$; $\text{M} = \text{Zr}, \text{R} = \text{H}, \text{alkyl}$; $\text{M} = \text{Hf}, \text{Y}, \text{R} = \text{alkyl}$) are usually reactive enough to activate the target bonds *via* a σ -bond metathesis mechanism (Scheme 3.1).^{236–241}

- $\text{L}_n\text{MR}(\text{XH})$ type complexes ($\text{R} = \text{alkyl}, \text{XH} = \text{alkyl}, \text{alkylidene}, \text{amido}$) can undergo intramolecular α -H abstraction to generate reactive transient $[\text{L}_n\text{MX}]$ species such as imido

$M=NR$ ($M = \text{Sc, Ti, Zr, V, Ta, W}$),^{242–248} alkylidene $M=CRR'$ ($M = \text{Ti, V, Nb, Cr, Mo}$)^{249–254} or alkylidyne $Ti\equiv CR$ complexes,^{255–257} that add the desired bond in a 1,2-fashion (Scheme 3.1).

The formation of the transient species, which is the rate-determining step of the overall transformation, is generally thermally activated.

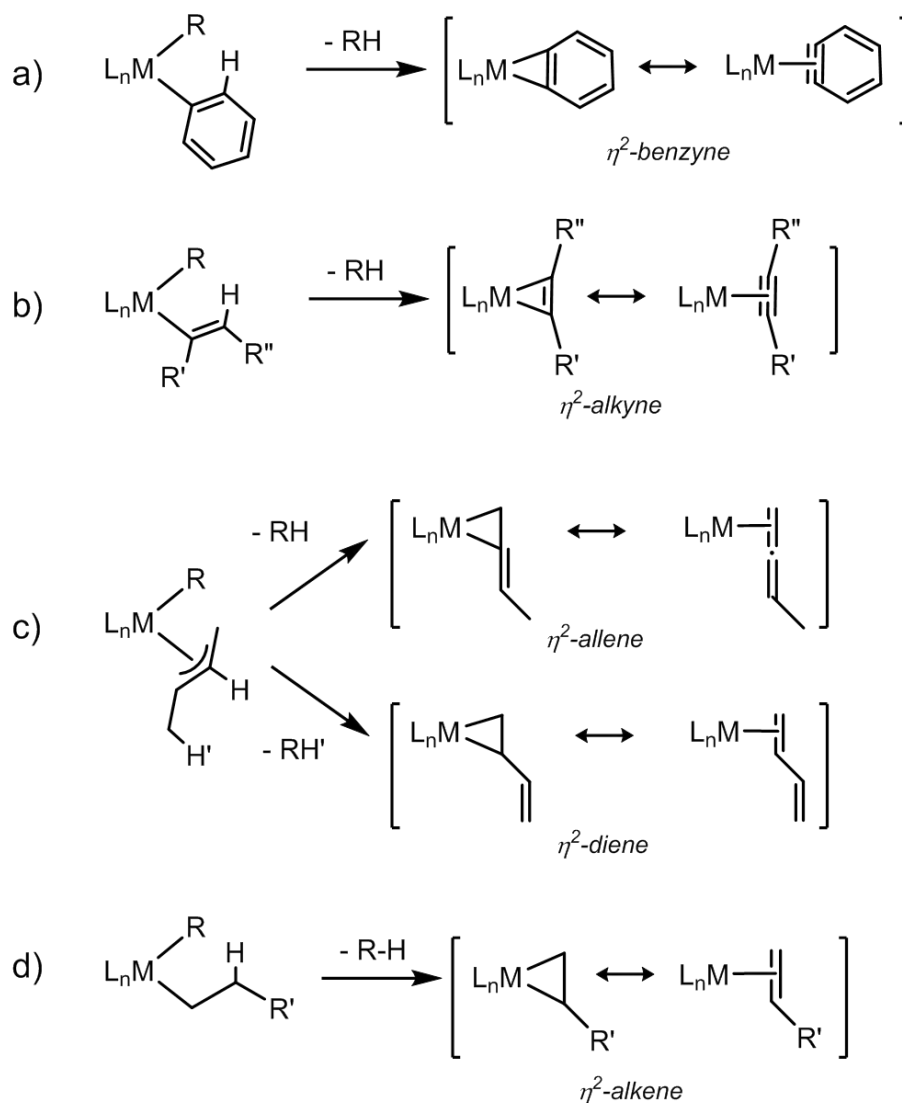


Scheme 3.1 The σ -bond metathesis mechanism with the example of methane activation by $[Cp^*_2Y(CH_3)]$ ²⁴¹ (top) and the α -H abstraction/1,2-addition mechanism with the example of pentafluoropyridine activation by $[rac\text{-}(ebthi)ZrMe(NHt-Bu)]$ ²⁴⁵ (bottom). *ebthi* = ethylenebis(tetrahydro)indenyl.

b. β -H abstraction

Another pathway that generates reactive complexes of ETM is the less common β -H abstraction mechanism. It was first reported on a diaryl titanocene complex, which upon thermal treatment could react with a variety of molecules such as diphenylacetylene,²⁵⁸ CO_2 ,²⁵⁹ or even N_2 .²⁶⁰ The reaction occurs by intramolecular abstraction of a β -H, loss of benzene and formation of a transient $[Cp_2Ti(\eta^2\text{-benzyne})]$ complex.^{258,261,262} A few years later, Erker reported a similar behaviour for the analogous $[Cp_2Zr(\text{tolyl})_2]$ complex, which was able to activate the C–H bond of benzene through a transient η^2 -aryne intermediate.²⁶³

This reaction is now well-documented for η^2 -benzyne of several early transition metals (Scheme 3.2, a).^{252,254,264–267} Highly reactive, similar η^2 -alkyne complexes of Ti,^{268–270} Zr,^{268,271,272} and W^{273,274} have also been reported (Scheme 3.2, b).



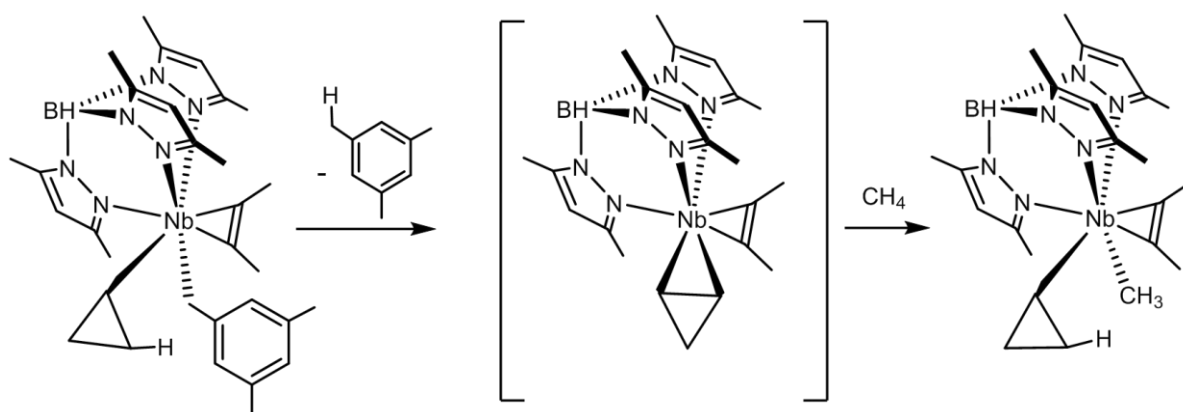
Scheme 3.2 The different types of β -H abstraction in dihydrocarbyl ETM complexes.

This reaction is straightforward in diaryl, aryl/alkyl or alkyl/vinyl systems where α -protons are absent. Yet, this mechanism is also viable in complexes bearing α -protons. Examples include η^2 -allene and η^2 -diene intermediates (Scheme 3.2, c) generated from alkyl allyl complexes of the type $[Cp^*M(NO)R(\eta^3-CH_2CHCHR')]$ ($M = W, Mo$)^{275–277} and η^2 -alkene intermediates (Scheme 3.2, d) generated from dialkyl complexes of Ti,²⁷⁸ Zr,^{268,278–282} Hf,²⁸³ Nb,²⁸⁴ and W.²⁸⁵ The transient species generated by β -H abstraction can activate strong and inert bonds by 1,3-addition, or can react with unsaturated molecules to form C–C

bonds by insertion in the M–C bond. Albeit very reactive, those transient species can be trapped and characterised by addition of a Lewis base, such as PMe_3 or pyridine.

A well-known complex that generates this kind of transient species is the Negishi reagent $[\text{Cp}_2\text{Zr}(n\text{-Bu})_2]$.²⁸¹ Upon thermal treatment, it forms an η^2 -alkene intermediate $[\text{Cp}_2\text{Zr}(\eta^2\text{-1,2-butene})]$, which behaves as a source of $[\text{Cp}_2\text{Zr}(\text{II})]$. $[\text{Cp}_2\text{Zr}(\text{II})]$ reacts with a plethora of substrates such as alkenes, alkynes, ketones, aldehydes, silanes to form coupling products and zirconacycles. Although the formation of the transient $[\text{Cp}_2\text{Zr}(\eta^2\text{-1,2-butene})]$ was initially attributed to a β -H abstraction mechanism,²⁸⁶ a subsequent study highlighted the intricacy of the mechanism, which actually starts from a γ -H abstraction, followed by isomerisation.²⁸⁷

In the group, the β -H abstraction mechanism was also reported for cyclopropyl ETM complexes. The complexes $[\text{Tp}^{\text{Me}_2}\text{NbR}(c\text{-C}_3\text{H}_5)(\text{MeC}\equiv\text{CMe})]$ ($\text{R} = \text{CH}_3, \text{CH}_2\text{-3,5-C}_6\text{H}_3\text{Me}_2$) undergo β -H abstraction of a cyclopropyl hydrogen by R to give methane or mesitylene and an unsaturated η^2 -cyclopropene intermediate $[\text{Tp}^{\text{Me}_2}\text{Nb}(\eta^2\text{-}c\text{-C}_3\text{H}_4)(\text{MeC}\equiv\text{CMe})]$. This intermediate is reactive enough to undergo 1,3-CH bond activation of benzene, toluene, xylene (all isomers), mesitylene and methane across the Nb–cyclopropene bond.^{267,284,288,289} This mechanism is shown for the activation of methane in Scheme 3.3.



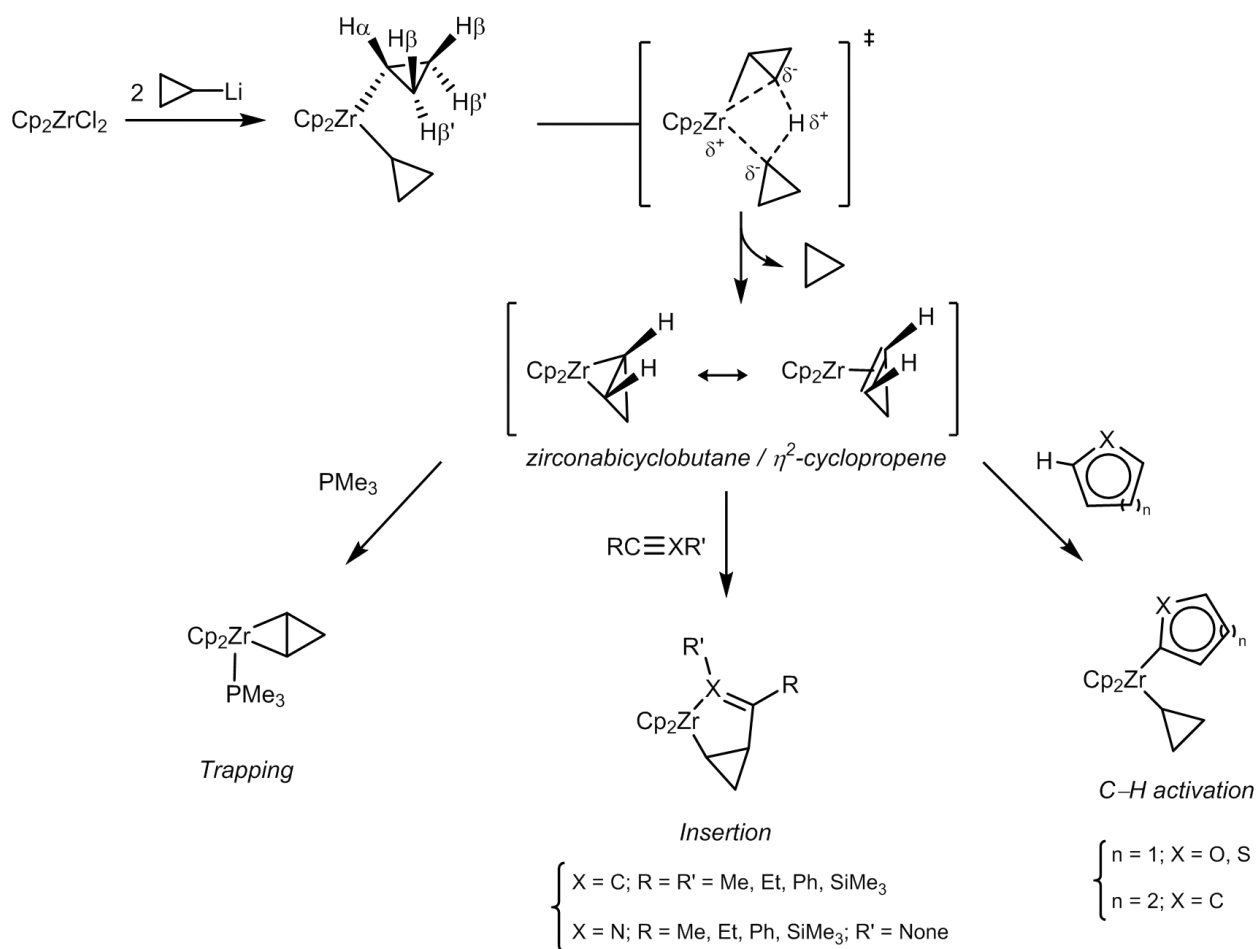
Scheme 3.3 Activation of methane by $[\text{Tp}^{\text{Me}_2}\text{Nb}(\text{CH}_2\text{-3,5-C}_6\text{H}_3\text{Me}_2)(c\text{-C}_3\text{H}_5)(\text{MeC}\equiv\text{CMe})]$.

c. Dicyclopolyzirconocene complex

The first report of a cyclopropylzirconocene complex was published by Buchwald and Nielsen.²⁶⁸ The authors showed that the complex $[\text{Cp}_2\text{ZrMe}(c\text{-C}_3\text{H}_5)]$ gives a transient η^2 -cyclopropene intermediate $[\text{Cp}_2\text{Zr}(\eta^2\text{-}c\text{-C}_3\text{H}_4)]$ by β -H abstraction of methane, which could be

trapped by PMe_3 to yield the phosphine adduct (Scheme 3.4). Insertion reactions of nitriles and alkynes in the Zr–C bond of $[\text{Cp}_2\text{Zr}(\eta^2\text{-}c\text{-C}_3\text{H}_4)]$ were performed (Scheme 3.4), but the reactivity toward strong and inert bonds was not reported. Dicyclopopylzirconocene $[\text{Cp}_2\text{Zr}(c\text{-C}_3\text{H}_5)_2]$ undergoes β -H abstraction of cyclopropane to generate $[\text{Cp}_2\text{Zr}(\eta^2\text{-}c\text{-C}_3\text{H}_4)]$ as well, and is easier to prepare (Scheme 3.4).²⁸⁰

Recently, our group described the CH activation of benzene, thiophene and furan by $[\text{Cp}_2\text{Zr}(c\text{-C}_3\text{H}_5)_2]$ in mild conditions.³¹ Kinetic studies, isotope labelling and DFT calculations of the reaction profile support a rate-determining intramolecular β -H abstraction step followed by a fast stereospecific 1,3-CH bond addition across the Zr–C bond of $[\text{Cp}_2\text{Zr}(\eta^2\text{-}c\text{-C}_3\text{H}_4)]$; the reaction is regioselective at the 2-position for thiophene and furan (Scheme 3.4).

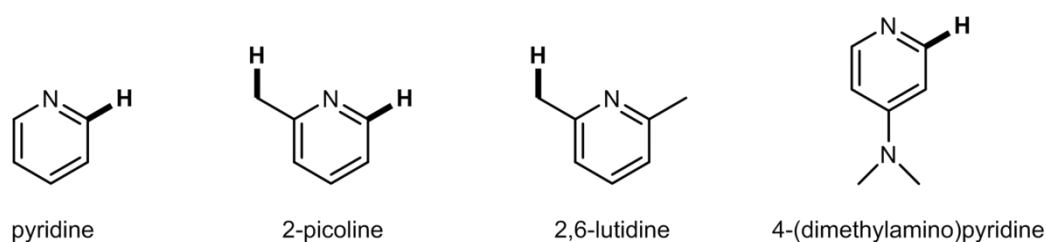


Scheme 3.4 Synthesis and reactivity of dicyclopopylzirconocene $[\text{Cp}_2\text{Zr}(c\text{-C}_3\text{H}_5)_2]$.

As in the Nb case, it is remarkable that the cyclopropyl moiety only reacts *via* a β -H rather than α -H abstraction pathway. Although $[\text{Tp}^{\text{Me}_2}\text{NbR}(c\text{-C}_3\text{H}_5)(\text{MeC}\equiv\text{CMe})]$ shows an α -C–C agostic interaction in the cyclopropyl group, there is no evidence that this unusual property⁶ is at the origin of the rate-determining β -H abstraction reaction. *Per contra*, while $[\text{Cp}_2\text{Zr}(c\text{-C}_3\text{H}_5)_2]$ does not present such a distortion in the crystal structure, DFT calculations suggest that an α -C–C agostic rotamer assists the β -H abstraction of cyclopropane. Although it is difficult to conclude what influence the agostic interaction has on the reaction pathway, the selectivity for β -hydrogens is always observed.

As $[\text{Cp}_2\text{Zr}(c\text{-C}_3\text{H}_5)_2]$ activates the C–H bond of heteroaromatics, we study herein its reactivity toward pyridine and derivatives, which are important building blocks in organic synthesis. The typical reactivity between pyridine derivatives and Zr complexes can be roughly classified into two types:

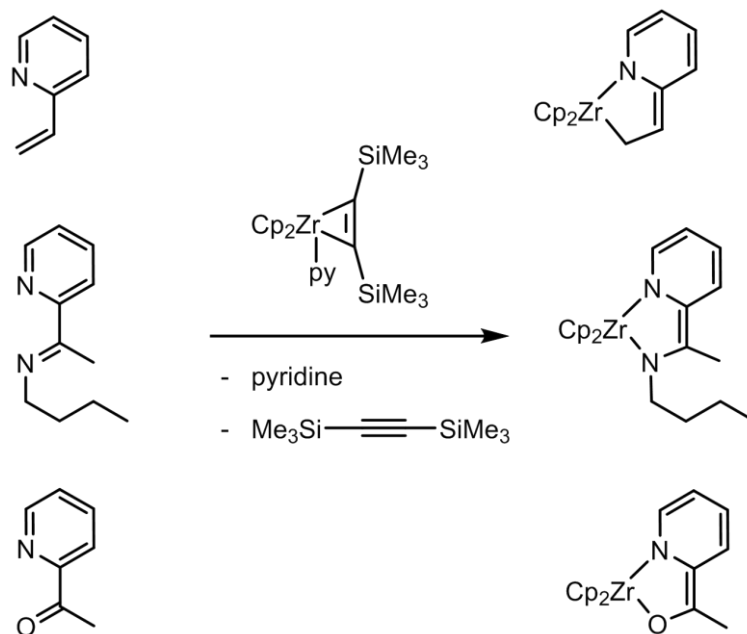
- C–H activation reactions, mostly by cationic alkyl complexes,^{290–294} and in one case by a neutral benzyl complex.²⁹⁵ As depicted in Scheme 3.5, pyridine activation is selective at the 2-position,^{290,291,294,295} whereas 2-picoline can be activated either at the aromatic C–H bond in the 2-position^{291,292} or at both the CH₃ group and the 2-position.²⁹⁵ The activation of 2,6-lutidine occurs at one of the CH₃ groups.²⁹⁰ 4-(dimethylamino)pyridine is activated at the 2-position.²⁹³



Scheme 3.5 *Substituted pyridines. The activated C–H bonds by zirconium complexes are depicted in bold.*

- Dearomatisation reactions by $[\text{Cp}_2\text{Zr(II)}]$ type complexes. For instance, $[\text{Cp}_2\text{Zr}(\text{py})(\eta^2\text{-Me}_3\text{SiC}\equiv\text{CSiMe}_3)]$ reacts with 2-substituted pyridines (vinyl-, N-*n*-butylmethylimino-, and acetylpyridine) by oxidative addition to yield the dearomatised products presented in Scheme 3.6 below.^{296,297} Sometimes only coordination of pyridine is observed

like in $[\text{Cp}_2\text{Zr}(\eta^2\text{-Me}_3\text{SiC}\equiv\text{CSiMe}_3)(\text{py})]$.²⁹⁸ Interestingly, $[\text{Cp}_2\text{Zr}(\text{CH}_3)_2]$ does not react with pyridine or substituted pyridines.²⁹⁹



Scheme 3.6 Dearomatization of vinyl-, *N*-*n*-butyl-methylimino-, and acetyl-pyridine by $[\text{Cp}_2\text{Zr}(\text{py})(\eta^2\text{-Me}_3\text{SiC}\equiv\text{CSiMe}_3)]$.

1.2. C–F activation by early transition metals complexes

There is a growing demand for fluorinated organic compounds (e.g.: 9 of 27 drugs approved by the U.S. Food and Drug Administration (FDA) in 2013 contained a C–F bond in their structure).³⁰⁰ Two pathways toward partially fluorinated molecules can be investigated: (i) selective fluorination of non-fluorinated substrates or (ii) selective defluorination of perfluorinated molecules. The C–F bond is both inert and strong (it is the strongest single bond between carbon and another element, $\text{BDE} = 536 \pm 21 \text{ kJ/mol}$),³⁰¹ seemingly making route (ii) the less accessible. Yet, perfluorinated molecules are now readily accessible, and hence the development of complexes able to selectively cleave C–F bonds is of great interest.

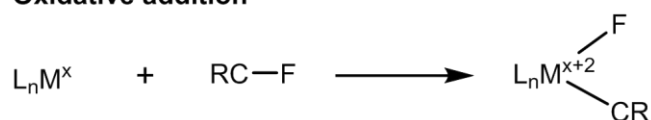
Reviews on the activation of C–F bonds depict the prevalence of alkaline and late transition metal complexes vs. ETM complexes for this aim.^{235,300,302–306} We therefore focus on the latter, in the hope of widening this still restricted field of research.

a. Stoichiometric activation of C–F bonds by ETM complexes

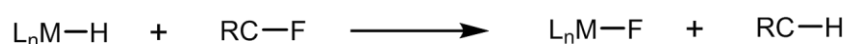
Prior to reaching the catalytic stage, we first focused on the stoichiometric C–F bond cleavage, which is generally the rate-determining step of the overall catalytic cycle.

C–F bond cleavage by ETM complexes can be roughly classified in three main reaction types as depicted in Scheme 3.7, but the associated mechanisms are not always fully elucidated and can still be subject to debate. Oxidative addition of C–F bond to low valent metals (Scheme 3.7, top), the most common pathway for late transition metals,^{303,307,308} was reported for group 4 “[Cp’₂M(II)]” (M = Ti, Cp’ = Cp, Cp*^{*}; M = Zr, Cp’ = Cp, *rac*-*ebthi*)^{233,309–311}, the cationic [Cp*₂Ti][BPh₄]³¹² and group 6 [M(CO)₃(EtCN)] (M = Mo, W)^{306,313} complexes. Hydrodefluorination reactions by hydride complexes (Scheme 3.7, middle) have been reported for [Cp*ScH],³⁰⁶ [(PNP)Ti(CH-*t*-Bu)(CH₂-*t*-Bu)] (PNP = N[2-P(CHMe₂)₂-4-methylphenyl]₂),³¹⁴ [Cp’₂ZrHX] (X = H, Cp’ = Cp, Cp*^{*}; X = Cl, Cp’ = Cp),^{315–319} [*rac*-(*ebthi*)₂ZrH(μ-H)]₂,³²⁰ [Cp*₂HfH₂]³²¹ and [Cp₂NbH₃].^{322,323} When the activated substrate is an aliphatic fluorocarbon, the reaction generally follows a radical mechanism. When the substrate is a fluoroarene/alkene, σ-bond metathesis or hydride nucleophilic substitution followed by F elimination are possible mechanisms.^{233,318,319,324} Finally, there is less than a handful of examples of α-H abstraction reactions followed by 1,2-addition that lead to C–F activation (Scheme 3.7, bottom). They involve the alkylidene [(PNP)Ti(CH-*t*-Bu)(CH₂-*t*-Bu)]^{255,325,326} and amido [*rac*-(*ebthi*)ZrMe(NH-*t*-Bu)]²⁴⁵ complexes (Scheme 3.1, above).

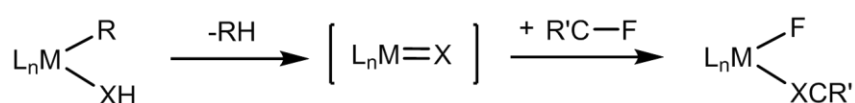
Oxidative addition



Hydrodefluorination



α-H abstraction/1,2-CF addition



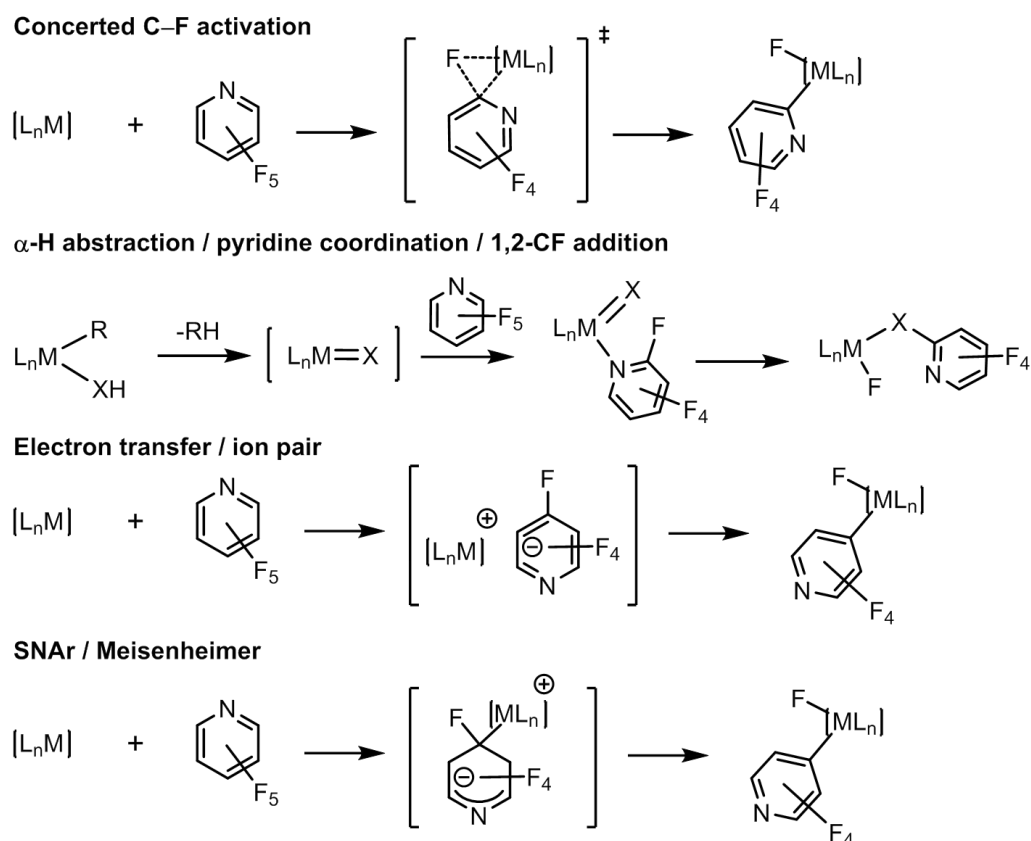
Scheme 3.7 C–F bond cleavage reactions by ETM complexes.

Other isolated reports mentioned hereafter complement the examples of ETM mediated C–F bond cleavage. Upon thermal treatment, an intramolecular reaction converted $[\text{Cp}_2\text{Zr}(\text{C}_6\text{F}_5)_2]$ into $[\text{Cp}_2\text{Zr}(\text{C}_6\text{F}_5)\text{F}]$ and tetrafluorobenzene.³²⁷ Serendipitous C–F activation was observed when $[\text{Ti}(\text{NMe}_2)_4]$ reacted with (pentafluorophenyl)cyclopentadiene ($\text{C}_6\text{F}_5\text{-CpH}$) to yield $[\{2\text{-(NMe}_2\text{)C}_6\text{F}_4\text{-Cp}\}\text{TiF}(\text{NMe}_2)_2]$.³²⁸ A similar reaction was reported upon addition of $[\text{Hf}(\text{NMe}_2)_4]$ on $[\{(2,6\text{-F}_2\text{C}_6\text{H}_3)\text{NCH}_2\}_2\text{C}(\text{CH}_3)(2\text{-C}_5\text{H}_4\text{N})\text{H}_2$ ($\text{Ar}_{\text{F}_2}\text{N}_{\text{Py}}\text{H}_2$) to yield $[(\text{Ar}_{\text{F}_2}\text{N}_{\text{Me}_2}\text{N}_{\text{Py}})\text{HfF}(\text{NMe}_2)_2]$.³²⁹ Complex $[(\text{C}_6\text{F}_5\text{NCH}_2\text{CH}_2\text{OCH}_2)_2\text{Zr}(\text{CH}_2\text{Ph})_2]$ underwent photolytic benzyl zirconium bond cleavage followed by C–F activation to yield $[(\text{C}_6\text{F}_5\text{NCH}_2\text{CH}_2\text{OCH}_2)_2\text{ZrF}_2]$ and $[(\text{C}_6\text{F}_4\text{NCH}_2\text{CH}_2\text{OCH}_2\text{CH}_2\text{OCH}_2\text{CH}_2\text{NC}_6\text{F}_5)\text{Zr}(\text{CH}_2\text{Ph})_2]$.³³⁰

A single example of C–F activation by a β -abstraction mechanism (attributed to Buchwald) was briefly mentioned in a review by Richmond.³⁰⁶ $[\text{Cp}_2\text{Zr}(\eta^2\text{-cyclohexyne})(\text{PMe}_3)]$, generated from $[\text{Cp}_2\text{ZrMe}(1,2\text{-cyclohexene})]$, cleaved the C–F bond of 1,1-difluoroethylene.

We focus our discussion on fluorinated pyridines which have been used in our experiments. Among the fluoroaromatics, fluorinated azaheterocycles, such as fluorinated pyridines or pyrimidines, have found various applications as liquid crystals, herbicides, insecticides, anti-cancer agents and antibiotics.³³¹

Fluorinated pyridines can be activated at the 2-position^{245,255,302,307–309,314,332–336} or at the 4-position.^{302,308,311,330,332,333,335,337–349} Mechanistic issues have been addressed through both experimental and DFT investigations.^{255,302,303,307,311,333,335,345,346} For several metals, the selectivity for the 2-position provides indirect evidence for a concerted oxidative addition *via* a three-centred transition state (Scheme 3.8). Selectivity for the 2-position was also attributed to pre-coordination of the fluorinated pyridine *prior* to the C–F activation (Scheme 3.8).^{245,255} Selectivity for the 4-position can follow either electron-transfer or nucleophilic substitution.



Scheme 3.8 General mechanisms with possible intermediates and transition states for the C–F activation of pentafluoropyridine by transition metal complexes.

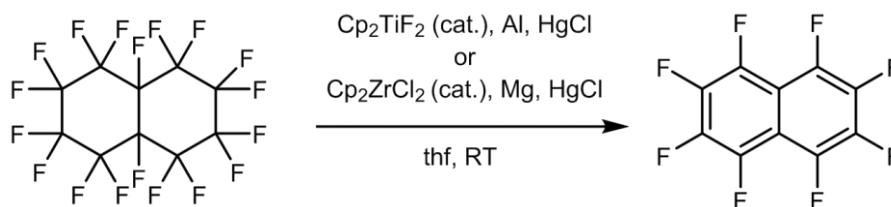
b. Catalytic activation of C–F bonds

Only a few ETM mediated catalytic reactions have been reported. As ETM are electropositive, hard metals, they form stable fluoride complexes upon C–F bond cleavage, which provides not only a thermodynamic driving force for the reaction, but also a barrier to the regeneration of the active species. The best way to address this issue is to add reagents to the catalytic medium that are able to form comparable or even stronger bonds with fluorine, and therefore act as “fluorine sinks”. Various M–F Bond enthalpies are gathered in Table 3.1.³⁵⁰

Table 3.1 Bond enthalpies in gaseous diatomic species.

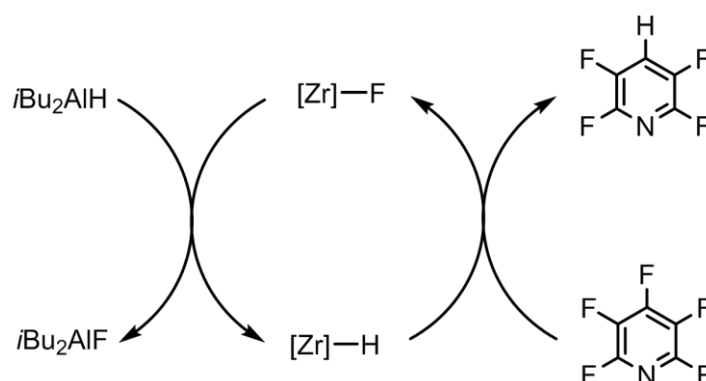
Bond	C–F	Ti–F	Zr–F	Ta–F	Li–F	Mg–F	Si–F	Al–F
ΔH (kJ/mol)	536 ± 21	569 ± 34	623 ± 63	573 ± 13	577 ± 21	462 ± 21	540 ± 13	664 ± 6

Richmond and Kiplinger reported the first examples of this approach with the catalytic defluorination of perfluorodecalin into octafluoronaphthalene (Scheme 3.9) and of perfluoro-(tetradecahydrophenanthrene) into decafluorophenanthrene using $[\text{Cp}_2\text{MX}_2]$ ($\text{M} = \text{Ti}$, $\text{X} = \text{F}$; $\text{M} = \text{Zr}$, $\text{X} = \text{F}$, Cl) complexes along with with mercury activated Mg or Al fluorine sinks.³⁵¹ They achieved turnover numbers (TONs) of 3 and 8 for Zr and Ti complexes, respectively.



Scheme 3.9 Catalytic defluorination of perfluorodecalin by Ti or Zr complexes.

Catalytic hydrodefluorination of pentafluoropyridine by $[\text{Cp}'_2\text{ZrH}(\mu\text{-H})_2]$ ($\text{Cp}' = \text{Cp}$, *rac*-ebthi) was reported in 2007 by the team of Rosenthal.³⁴⁹ In presence of $[\text{Cp}'_2\text{ZrH}(\mu\text{-H})_2]$, pentafluoropyridine is stoichiometrically activated in the 4-position to give 2,3,5,6-tetrafluoropyridine and $[\text{Cp}'_2\text{ZrF}_2]$. Addition of two equivalents of $[i\text{-Bu}_2\text{AlH}]$ (which is unreactive toward pentafluoropyridine) allows regeneration of $[\text{Cp}'_2\text{ZrH}(\mu\text{-H})_2]$ and formation of $[i\text{-Bu}_2\text{AlF}]$, the reaction being driven by the formation of the strong Al–F bond. This leads to the catalytic cycle presented in Scheme 3.10. A TON of 67 in the case of $[\text{rac}(\text{ebthi})_2\text{ZrH}(\mu\text{-H})_2]$ is achieved after 24 hours at RT, the hitherto known record for this hydrodefluorination reaction.²³³ The transformation is initiated either by starting from the hydride $[\text{Cp}'_2\text{ZrH}(\mu\text{-H})_2]$ or the fluoride $[\text{Cp}'_2\text{ZrF}_2]$ complexes.



Scheme 3.10 Proposed catalytic cycle for the C–F activation of pentafluoropyridine by $[\text{Cp}'_2\text{ZrH}(\mu\text{-H})_2]$.

Takahashi and Akiyama concurrently reported the catalytic C–F activation of various fluoroarenes.^{352–354} They used several ETM halides as catalysts (TiCl_3 , TiCl_4 , ZrCl_4 , VCl_3 , NbCl_5 , TaCl_5 , WCl_6) or metallocene complexes ($[\text{CpTiCl}_3]$, $[\text{Cp}_2\text{TiCl}_2]$, $[\text{CpZrCl}_3]$, $[\text{Cp}^*\text{ZrCl}_3]$). In the works of Takahashi, Grignard reagents (RMgCl) are used as fluorine sinks, which leads to arene–R coupling products. Akiyama describes hydrodefluorination reactions using LiAlH_4 as the fluorine transfer agent. The best TON are achieved using $[\text{CpTiCl}_3]$ or TaCl_5 for coupling reactions with 1-fluoronaphthalene (8.5) and using NbCl_5 for hydrodefluorination reactions with various monofluoroarenes (20). When metallocenes are used instead of halide complexes, the catalytic activities increase, but this was not generalised to all the precatalysts.

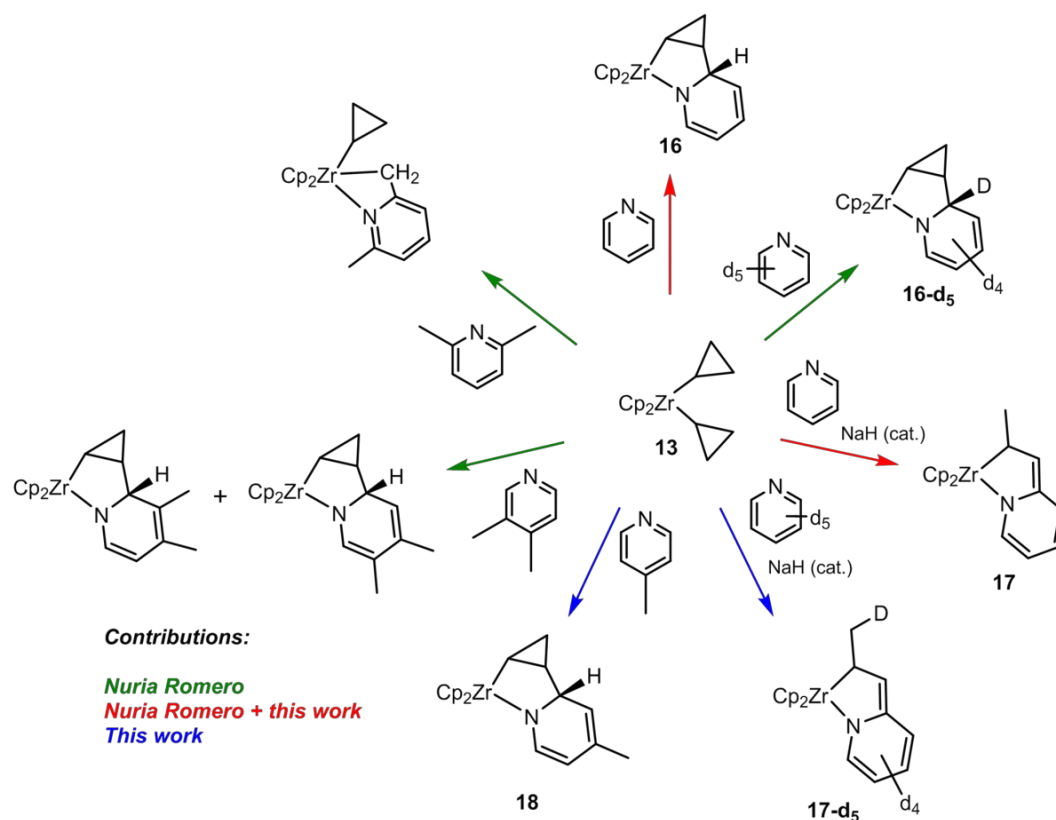
In the last 5 years, only three other examples of C–F catalytic activation by ETM have been reported. Lentz *et al.* developed a hydrodefluorination catalysis similar to that of Rosenthal, but with $[\text{Cp}_2\text{TiH}]$ as the active species and silanes as fluorine sinks.³⁵⁵ They managed to cleave C–F bonds of perfluorovinyl compounds with TON up to 125. Hydrodefluorination of perfluoroarenes was achieved by the team of Crimmin with $[\text{Cp}_2\text{ZrCl}_2]$ and an Al sink (best TON = 64 for pentafluoropyridine).³⁴⁸ The same system was also used to perform C–F cleavage of trifluoropropene.³⁵⁶ Addition of $[\text{CPh}_3][\text{B}(\text{C}_6\text{F}_5)_4]$ to the medium generated cationic complexes *in situ*, which constituted the first report of C–F catalytic activation by group 4 cationic species with TON up to 117.

B. Results and discussion

In this part, the results are presented as follow: (i) general reaction scheme, (ii) mechanistic study and (iii) characterisation of the involved compounds.

I.1. Reaction with pyridine

As stated in the introduction, this work was started by Nuria Romero. In her thesis,³⁵⁷ she reported the reaction of $[\text{Cp}_2\text{Zr}(c\text{-C}_3\text{H}_5)_2]$ with pyridine and substituted pyridines. Our respective contributions to this work are summarised in the Scheme 3.11 below. I focused particularly on better understanding the mechanism involved in the reaction between pyridine and the zirconocene complex. The syntheses of the various substituted pyridines (with the exception of the synthesis of 4-picoline) are not detailed because they have been already reported by Nuria Romero.



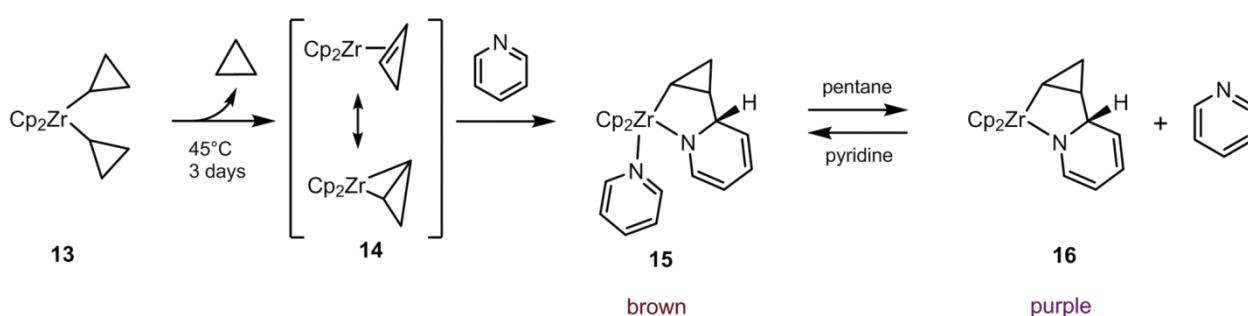
Scheme 3.11 Summary of $[\text{Cp}_2\text{Zr}(c\text{-C}_3\text{H}_5)_2]$ reactions with pyridine derivatives.

a. Formation of C–C coupling product

i. Reaction

Although C–H bond activation of pyridine has been previously reported by early and late transition metal complexes including Zr species, the experiments presented herein showed that C–H bond activation of pyridine by $[\text{Cp}_2\text{Zr}(\eta^2\text{-}c\text{-C}_3\text{H}_5)_2]$ (**13**) did not occur, at least as a primary reaction.

When complex **13** was dissolved in pure pyridine at 45°C, cyclopropane release was observed by ^1H NMR, suggesting the formation of $[\text{Cp}_2\text{Zr}(\eta^2\text{-}c\text{-C}_3\text{H}_4)]$ (**14**), as described above. Evaporation of the volatiles, extraction and recrystallisation from pentane at –40 °C afforded the purple complex $[\text{Cp}_2\text{Zr}\{\kappa^2\text{-N,C}^8\text{-(2-}c\text{-C}_3\text{H}_4\text{)-C}_5\text{H}_5\text{N}\}]$ (**16**) in 89% yield (Scheme 3.12). Interestingly, when complex **16** was recrystallised from pyridine/pentane mixtures, dark brown crystals of an 18-electron zirconocene complex $[\text{Cp}_2\text{Zr}(\text{py})\{\kappa^2\text{-N,C}^8\text{-(2-}c\text{-C}_3\text{H}_4\text{)-C}_5\text{H}_5\text{N}\}]$ (**15**) were obtained. This reaction can be defined either as a C–C oxidative coupling between the cyclopropene and the pyridine or as an insertion reaction of the pyridine in the Zr–C bond of the zirconabicyclobutane. As a consequence of the geometry of **14**, the reaction is stereospecific with the dearomatised pyridine (2-substituted-pyridido) ring and the Zr atom always being *syn* to the cyclopropyl. Upon solubilisation in a solvent other than pyridine, **15** readily gives **16** and free pyridine as evidenced by ^1H NMR and by the immediate colour change from brown to deep purple (Scheme 3.12). Both **15** and **16** are air and moisture sensitive, and although **15** is stable at 45°C for several days, **16** decomposes quickly at room temperature to give an intractable mixture of products.



Scheme 3.12 Reaction of **13** with pyridine to give **15** and **16**.

ii. Mechanism

The thermal reaction of **13** and deuterated pyridine conducted under the same conditions as mentioned above yielded complex $[\text{Cp}_2\text{Zr}\{\kappa^2\text{-N,C}^8\text{-(2-}i\text{-C}_3\text{H}_4\text{)-C}_5\text{D}_5\text{N}\}]$ (**16-d₅**) as ascertained by ^1H and ^2H NMR (Figure 3.1). This experiment confirmed that the oxidative coupling/insertion reaction mechanism proceeds with the absence of a C–H bond activation step.

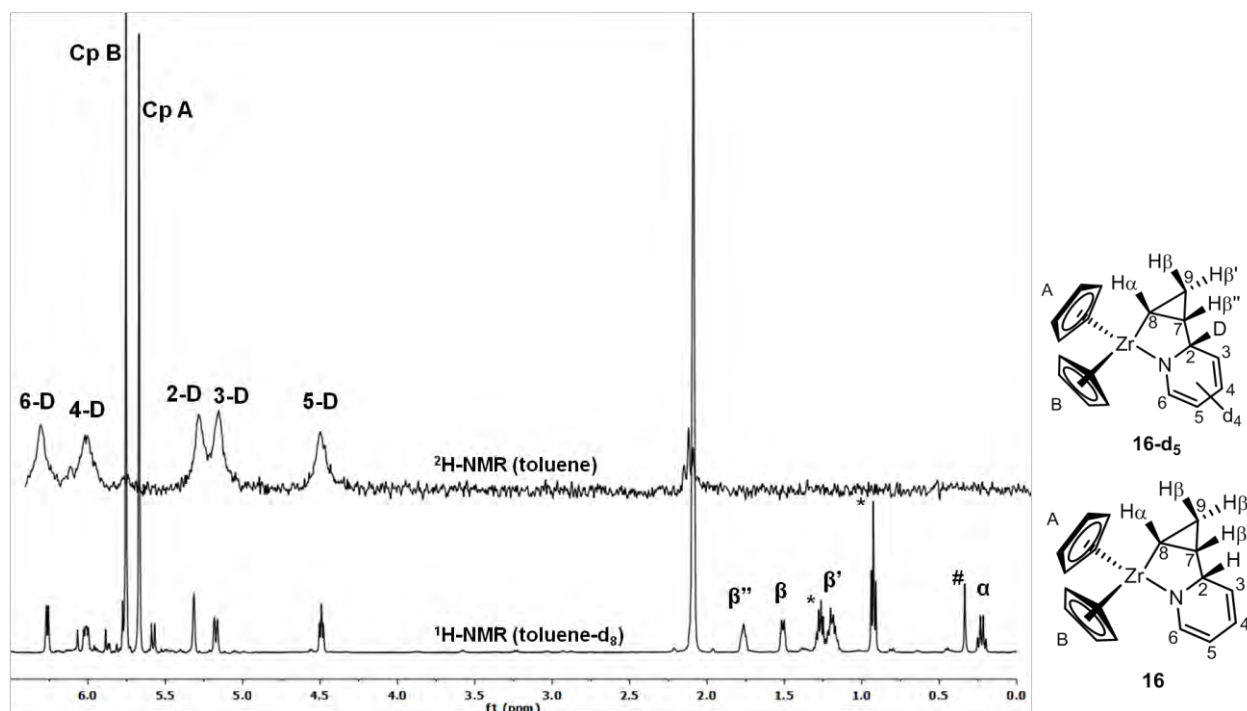
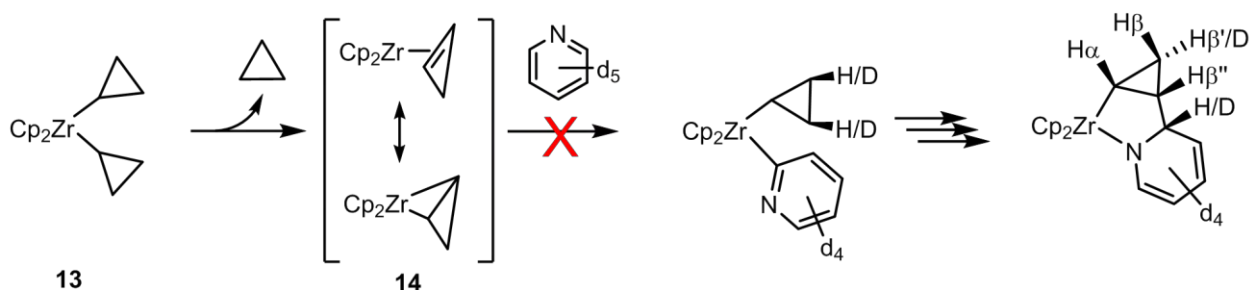


Figure 3.1 Comparison of the ^2H NMR of complex **16-d₅** in toluene (top) and ^1H NMR of complex **16** in toluene- d_8 (bottom). * = residual pentane, # = residual silicon grease.

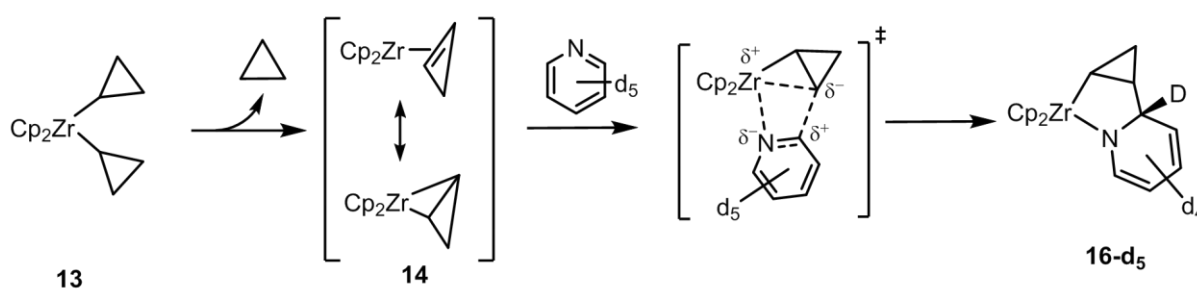
There is no kinetic isotope effect from a qualitative point of view, as no marked difference in reaction time between the formation of **16** and **16-d₅** was observed. In complex **16-d₅**, no deuterium incorporation was observed in the cyclopropyl moiety, which differentiates both mechanisms proposed in Scheme 3.13. The formation of two regioisomers, one of which would incorporate deuterium in the β' -position of the cyclopropyl group, would have been expected had a C–D bond cleavage occurred initially (Scheme 3.13, mechanism A). On the contrary, the five deuterium atoms in **16-d₅** were found exclusively on the 2-substituted-pyridido ring, including the 2-position, which confirmed that the mechanism is a direct coupling (Scheme 3.13, mechanism B).

The selectivity for the 2-position might be attributed to pre-coordination of pyridine as reported in the case of pyridine C–H activation by the complex $[(\text{PNP})\text{Sc}(\text{NH}-[\text{DIPP}])(\text{CH}_3)]$ ($\text{PNP}^- = \text{bis}(2\text{-diisopropylphosphino-4-tolyl})\text{amide}$, $\text{DIPP} = 2,6\text{-diisopropylphenyl}$).²⁴³

Mechanism A: C–H bond activation



Mechanism B: Oxidative coupling / Insertion

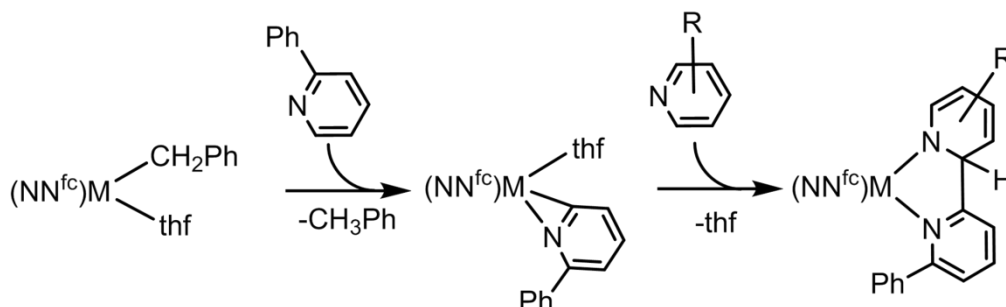


Scheme 3.13 Possible mechanisms for the reaction of **13** with pyridine. Experiments with deuterated pyridine confirmed the mechanism B (oxidative coupling/insertion).

Dearomatisation of pyridine and derivatives has been reported for late transition metal complexes.^{358,359} ETM complexes,³⁶⁰ s-block metal complexes, and rare earth complexes that dearomatise pyridine (sometimes catalytically) include Ca allyl,³⁶¹ Mg hydrides,^{362,363} Sc and Y alkyl,³⁶⁴ Ti hydrides,³⁶⁵ and, as seen in the introduction, $[\text{Cp}_2\text{Zr}(\text{II})]$ complexes (Scheme 3.6).^{296,297}

Y, Sc and Lu benzyl systems have been reported to activate the *ortho*-C–H bond of 2-phenylpyridine by σ -bond metathesis.³⁶⁶ As observed for complexes **15** and **16**, the newly formed pyridyl complexes underwent subsequent insertion reactions with various substituted pyridines to give dearomatized 2-substituted-pyridido ligands (Scheme 3.14).³⁶⁷ A zirconium complex of formula $[(\text{Cbzdiphos}^{i\text{-Pr}})\text{Zr}(\eta^6\text{-toluene})\text{Cl}]$ ($\text{Cbzdiphos}^{i\text{-Pr}} = 1,8\text{-bis}(\text{di-}i\text{-propylphosphino})\text{-3,6-di-}t\text{-butyl-9}H\text{-carbazole}$) similarly first cleaved the C–H bond of

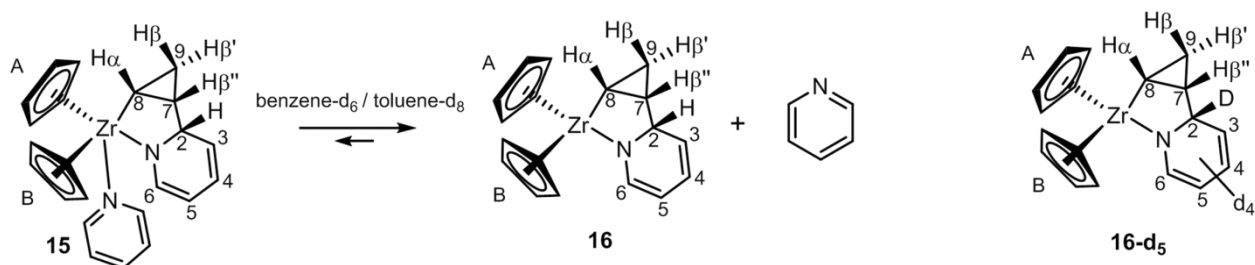
pyridine, and then gave a bi-pyridido ligand by C–C coupling with another pyridine molecule.³⁶⁸



Scheme 3.14 C–H bond activation of 2-phenylpyridine by $[(NN^{fc})M(CH_2Ar)(thf)]$ and subsequent insertion of substituted pyridines, $M = Sc, Y$, $(NN^{fc}) = fc[NSi-(t-BuMe_2)]_2$, $fc = 1,1'$ -ferrocenylene.

iii. Characterisation

$[\text{Cp}_2\text{Zr}(\text{C}_5\text{H}_5\text{N})\{\kappa^2\text{-N,C}^8\text{-(2-}c\text{-C}_3\text{H}_4\text{)-C}_5\text{H}_5\text{N}\}]$ (**15**), $[\text{Cp}_2\text{Zr}\{\kappa^2\text{-N,C}^8\text{-(2-}c\text{-C}_3\text{H}_4\text{)-C}_5\text{H}_5\text{N}\}]$ (**16**) and $[\text{Cp}_2\text{Zr}\{\kappa^2\text{-N,C}^8\text{-(2-}c\text{-C}_3\text{H}_4\text{)-C}_5\text{D}_5\text{N}\}]$ (**16-d₅**)



Scheme 3.15 Equilibrium between complexes **15** and **16** and labelling sequence (left), complex **16-d₅** (right).

All the NMR analyses have been carried out in benzene- d_6 or toluene- d_8 . In these solvents, the equilibrium between **15** and **16** is totally shifted toward **16** (Scheme 3.15). Therefore, the NMR spectra of **15** are identical to those of **16** plus one equivalent of free pyridine.

The remarkable feature of the NMR spectra of **16** in toluene- d_8 is the non-equivalent Cp rings. Their resonances are observed at δ 5.74 and 5.66 in the ^1H NMR spectrum, which indicates the absence of a plane of symmetry (Scheme 3.15). Protons 3-*H* (δ 5.17, d, $^3J_{HH} = 10.1$ Hz), 4-*H* (δ 6.01, dd, $^3J_{HH} = 9.7, 5.7$ Hz), 5-*H* (δ 4.49, ddd, $^3J_{HH} = 6.8, 5.3, 1.3$ Hz) and 6-*H* (δ 6.26, d, $^3J_{HH} = 7.1$ Hz) and the corresponding carbons were identified by ^1H COSY and HMQC experiments. The resonance for 2-*C* appears at δ 56.7 in the ^{13}C NMR spectrum and correlates by HMQC with 2-*H* (δ 5.31, d, $J_{HH\beta''} = 2.3$ Hz). We suggest that the other coupling constants are not observed as a result of the constrained five-membered metallacycle and torsion angles.³⁶⁹ 2-*H* correlates with $H\beta''$ in a COSY experiment and a HMBC experiment shows a strong correlation between 7-*C* (δ 42.4) and 2-*H*. The cyclopropyl group has four protons instead of five. $H\beta$ and $H\beta'$ at δ 1.20 and 1.51, respectively are geminal non equivalents diastereotopic protons bound to 9-*C* (δ 16.0). $H\beta'$ is *syn* to the Zr and to the 2-substituted-pyridido ring whereas $H\alpha$, $H\beta$ and $H\beta''$ are *anti*, as ascertained by NOESY NMR. Because of its proximity to Zr, $H\alpha$ resonates upfield (δ 0.22) in the ^1H NMR spectrum and correlates by HMQC with 8-*C* (δ 41.2).

The ^1H NMR of **16-d₅** features resonances for the cyclopropyl protons $H\alpha$, $H\beta$, $H\beta'$ and $H\beta''$ and the $\eta^5\text{-C}_5\text{H}_5$ moieties which are identical to those observed for **16**. Signals for the deuterated 2-substituted-pyridido ring are absent in the ^1H NMR, but they are all observed in the ^2H NMR at the same chemical shifts. No other deuterium signals were observed in the ^2H NMR spectrum.

Single crystals of complex **15** suitable for XRD were obtained from a concentrated pyridine/pentane solution of **16** cooled to -40°C . The ORTEP plot of **15** is shown in Figure 3.2 with relevant bond distances and angles.

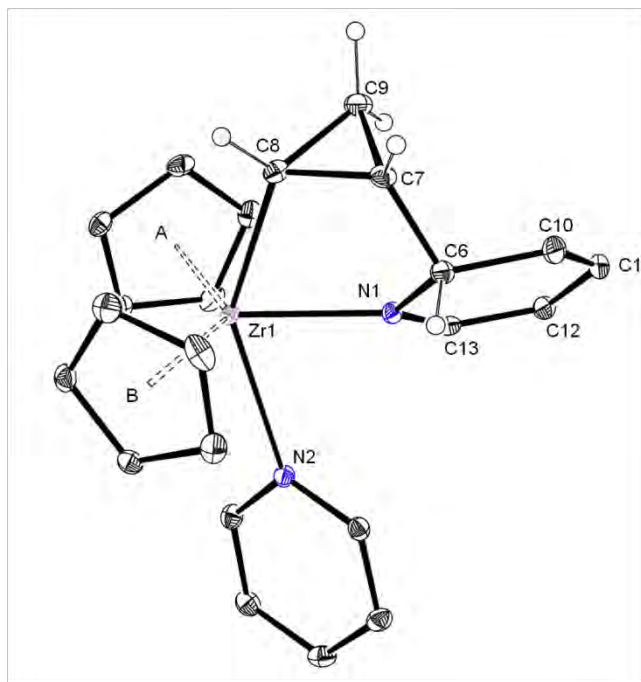


Figure 3.2 ORTEP drawing of **15**. Ellipsoids at 30% probability level, only selected hydrogen atoms are depicted for clarity. Relevant bond lengths (Å) and angles (°): Zr1–N1 2.2054(14), Zr1–N2 2.6091(14), Zr1–C8 2.3062(19), C11–C12 1.447(3), C12–C13 1.355(2), C6–C7 1.522(2), C7–C8 1.510(2), C7–C9 1.505(2), C8–C9 1.508(3), Cp^o–Zr1–Cp^o 128.8, N1–Zr1–C8 72.27(5), Zr1–C8–C7 113.48(11), Zr1–N1–C6 116.45(9), N2–Zr1–C8 147.12(5), N2–Zr1–N1 75.31(4).

The structure features a pentacoordinated Zr centre with Zr1, N1, C8 and N2 being nearly coplanar (torsion angle N2–Zr1–C8–N1 10(1)°). The Zr atom and the 2-substituted-pyridido ring are *syn* to the cyclopropyl, forming a zirconacycle Zr1–N1–C6–C7–C8, which is puckered along the N1⋯C8 axis. The Zr1–C8 distance [2.3062(19) Å] is slightly longer than the Zr–C distances in complex **13** (Zr–C = 2.256(3) and 2.261(3) Å)³¹ and in complex [Cp₂Zr(N,C-2-vinylpyridido)] (Zr–C = 2.272(5)).²⁹⁶ The Zr–N1 distance [2.2054(14) Å] is slightly longer than Zr–N_{amido} σ-bond for others pyridido zirconocene compounds (e.g.: [Cp₂Zr(N,C-2-vinylpyridido)], Zr–N = 2.163(4) Å,²⁹⁶ [Cp₂Zr(N,N'-bi-pyridido)], Zr–N = 2.164(8) and 2.160(8) Å,³⁷⁰ [Cp₂Zr(N,N'-2-(N-*n*-butyl-methylamido)pyridido)] Zr–N = 2.144(2) Å²⁹⁷). The Zr–N2 distance [2.6091(14) Å] is much longer than for Zr–N_{coordinated pyridine} of other Zr complexes, which are typically in the range [2.30–2.50 Å].^{371,372} As C6 is now a sp³ hybridised carbon, the N1–C6 bond [1.496(2) Å] is longer than N1–C13 [1.365(2) Å], and C6–C10 [1.503(3) Å] is longer than the other C–C bonds of the 2-substituted-pyridido cycle.

The absence of a plane of symmetry explains the non-equivalence of the Cp rings observed in the NMR spectra. The N1–Zr1–C8 angle [$72.27(5)^\circ$] is acute for a d^0 metallocene complex [typical value *ca* $94\text{--}97^\circ$]³⁷³ or even for a zirconacycle [typical value *ca* $82\text{--}90^\circ$].^{374–376} This constrained geometry can be attributed to the presence of wide angles in the zirconacycle, themselves imposed by the strained cyclopropyl ring (Zr1–C8–C7 [$113.48(11)^\circ$]; C6–C7–C8 [$115.17(15)^\circ$]) and the nitrogen of the 2-substituted-pyridido ligand (Zr1–N1–C6 [$116.45(9)^\circ$]). This results in a decrease in the overlap between the σ -donor ligand orbitals and the b_2 orbitals of the metal (Figure 3.3). Hence, a pyridine can coordinate, probably interacting mainly with the now available $1a_1$ orbital of the “Cp₂Zr” fragment, leading to an 18-electron pentacoordinated zirconocene complex. Furthermore, this explains the coplanarity of Zr1, N1, C8 and N2 (which is the plan *yz* of the Figure 3.3). The elongated Zr–N2 bond accounts for the lability of the coordinated pyridine, easily leading from **15** to **16**. Also, the instability of **16** at RT can perhaps be explained by the decrease in overlap between the orbitals of the metal and of the ligands, and by this acute N1–Zr1–C8 angle, which exposes the Zr centre to further reactions.

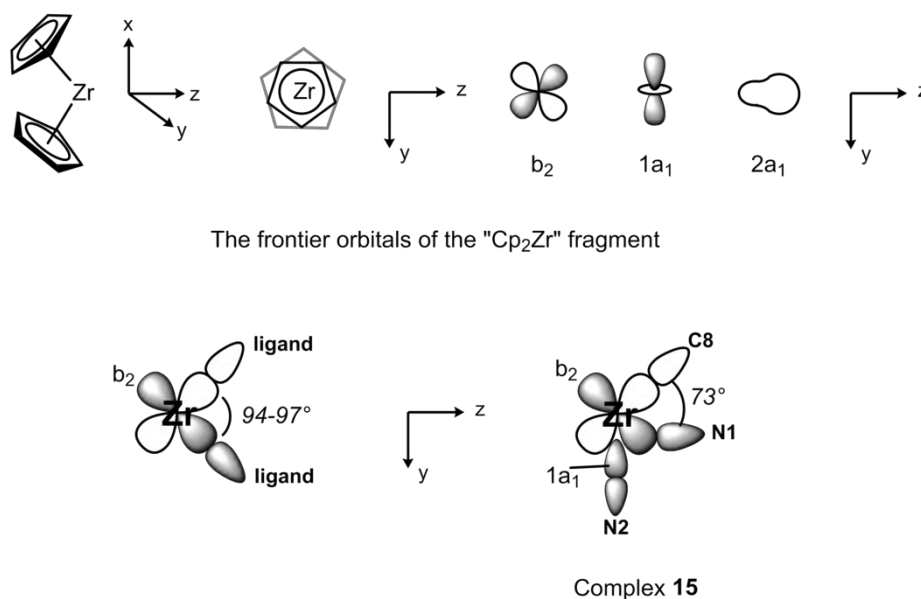


Figure 3.3 The frontier orbitals of zirconocene (up) and a proposal for binding in complex **15** (down).

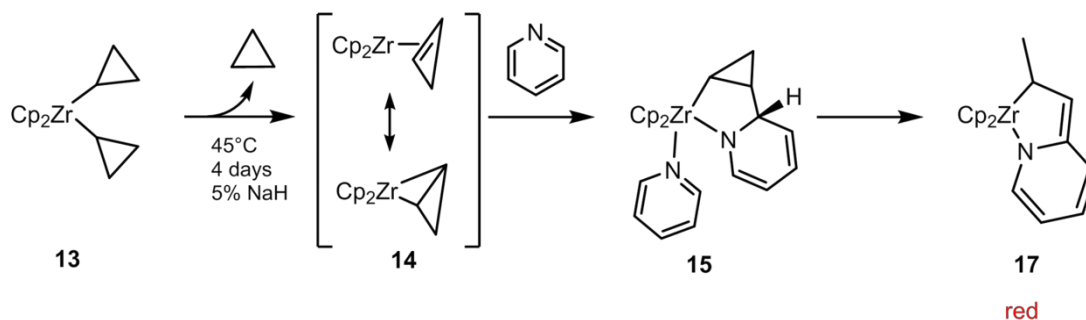
Other 18-electron zirconocene complexes have been reported, see for instance the $[\text{Cp}_2\text{Zr}(\text{Me})(\kappa^2\text{-N,N-Ph}_2\text{C=N-NMe})]$,³⁷⁷ $[\text{Cp}_2\text{Zr}\{\kappa^3\text{-C,N,N-C}(\text{SiMe}_3)=\text{C}(\text{SiMe}_3)\text{CHPhN-N=CHPh}\}]$,³⁷⁸ and $[\text{Cp}_2\text{Zr}(\text{N=C=CPh}_2)(\kappa^2\text{-C,N-C}(\text{SiMe}_3)=\text{C}(\text{Me})\text{C}(\text{CHPh}_2)=\text{NH})]$.³⁷⁹ All of

them present constrained geometry with 3 or 5 membered zirconacycles, and acute angles between the κ^n -coordinated ligands.

b. Opening of the cyclopropyl ring

i. Reaction

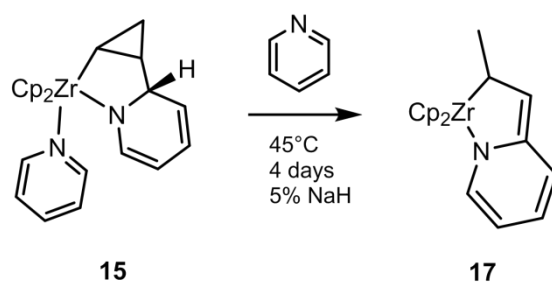
When the reaction of **13** with pyridine was performed in presence of a catalytic amount of a strong base, the new complex $[\text{Cp}_2\text{Zr}\{\kappa^2\text{-N,C}^8\text{-(2-C}_3\text{H}_5\text{)-C}_5\text{H}_4\text{N}\}]$ (**17**) was formed (Scheme 3.16). The formation of **17** was attested by the colour change of the medium from brown to red and confirmed by ^1H and ^{13}C NMR spectroscopy. Ring opening of the cyclopropyl moiety in **15**, accompanied by the migration of a H atom, resulted in extended conjugation with the 2-substituted-pyridido ring. **17** was obtained in 95% yield and was fully characterised by NMR, XRD and elemental analysis.



Scheme 3.16 Reaction of **13** with pyridine in presence of NaH to give **17**.

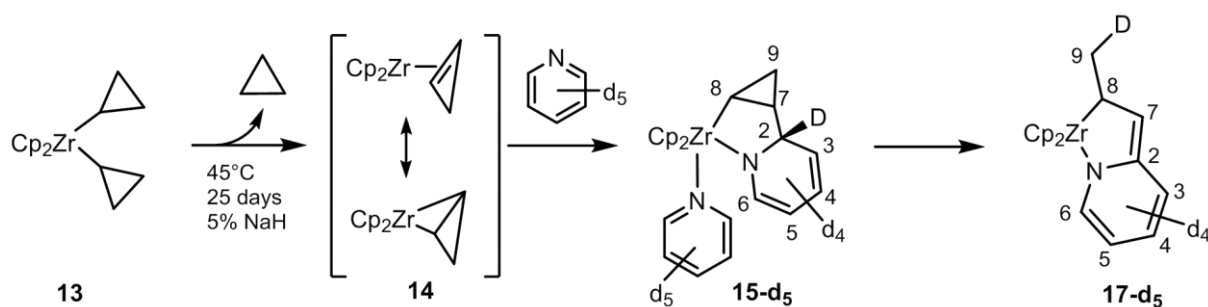
ii. Mechanism

In an effort to confirm that the generation of **17** from **13** proceeds *via* the formation of **15**, the latter complex was dissolved in pyridine and treated with NaH. Heating the reaction for 4 days at 45°C confirmed the complete conversion of **15** into **17** (Scheme 3.17).



Scheme 3.17 Rearrangement of **15** in presence of NaH to give **17**.

The reaction of **13** with deuterated pyridine in the presence of NaH yielded $[\text{Cp}_2\text{Zr}\{\kappa^2\text{-N,C}^8\text{-(2-C}_3\text{H}_4\text{D)-C}_5\text{D}_4\text{N}\}]$ (**17-d₅**) (Scheme 3.18). The reaction was sluggish with an overall reaction time of *ca* 25 days, compared with the formation of **17** in only 4 days. Although qualitative, this marked kinetic isotope effect arose from the transformation of **15-d₅** into **17-d₅** as no C–D bond cleavage was observed during the formation of **15-d₅** (*vide supra*). This suggests a rate-determining step of C–D activation (deprotonation) by the base prior to opening of the cyclopropyl ring.



Scheme 3.18 Reaction of **13** with pyridine-*d*₅ in presence of NaH to give **17-d₅**.

Formation of **17-d₅** was established by ²H NMR, which showed the presence of a single deuterium atom in the methyl group C9, which appears to come from the 2-position of **15-d₅** (Figure 3.4).

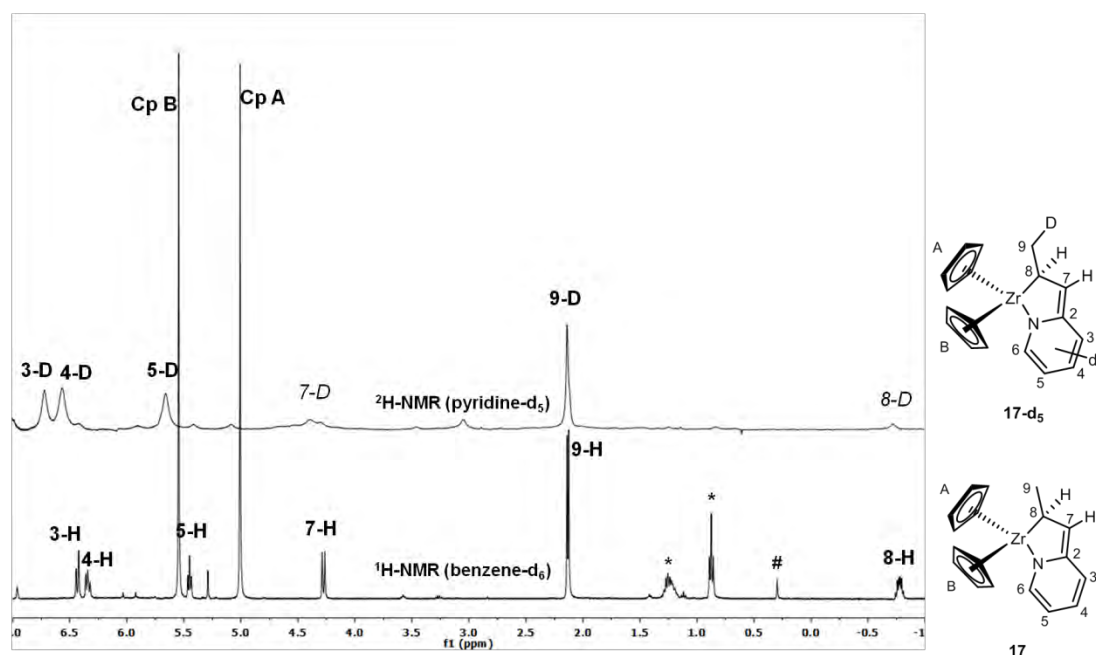


Figure 3.4 Comparison of the ^2H NMR of complex **17-d₅** in pyridine- d_5 (top) and ^1H NMR of complex **5** in benzene- d_6 (bottom). * = residual pentane, # = residual silicon grease.

Even if **17-d₅** is the major product, the ^2H NMR spectrum of the reaction mixture showed that deuteration at the 7- and 8-positions has occurred to some extent as well (ca 5-10% each by integration of the ^2H NMR spectrum). We propose that this is the result of deuterium migration in **17-d₅** over longer reaction times.

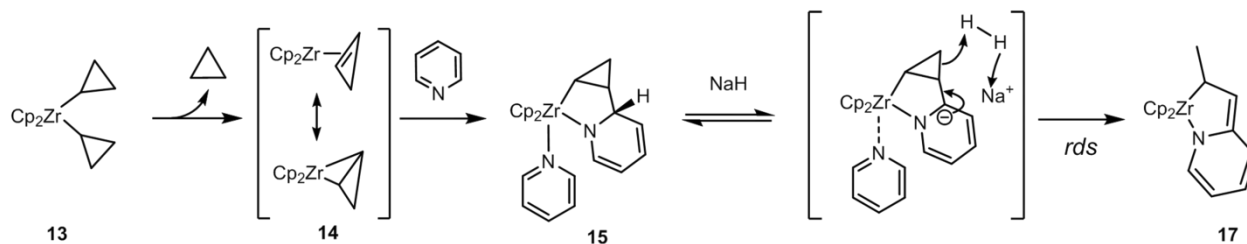
The pKa of the base strongly influences the outcome of the reaction (Table 3.2). Weak bases like pyridine or tmeda have no influence, whereas *t*-BuOK and NaH catalyse the formation of **17**, albeit more slowly in the case of *t*-BuOK.

Table 3.2 Influence of the base on the reaction between **13** and pyridine.

Base	pKa	Reaction time	Yield in 17^d
pyridine ^a	5	6 days	-
tmeda ^b	9	6 days	< 5%
<i>t</i> -BuOK ^c	17	6 days	75%
NaH ^c	35	4 days	95%

All reactions were carried out in pyridine at 45°C, in NMR tubes equipped with benzene- d_6 filled capillaries. ^a Solvent. ^b 5% loading. ^c <5% loading due to solubility issues. ^d NMR yields.

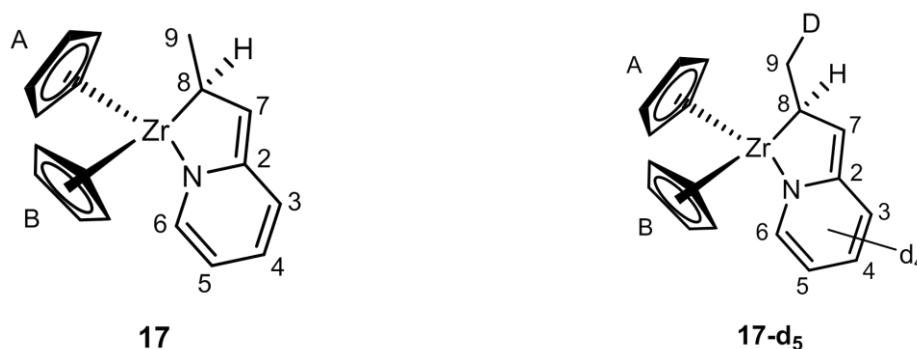
This suggests the existence of an acid-base pre-equilibrium, whose displacement would rule the rate of the reaction by the mechanism depicted in the Scheme 3.19 below.



Scheme 3.19 Proposed mechanism for the formation of **17**.

iii. Characterisation

$[\text{Cp}_2\text{Zr}\{\kappa^2\text{-N,C}^8\text{-(2-C}_3\text{H}_5\text{)-C}_5\text{H}_4\text{N}\}]$ (**17**) and $[\text{Cp}_2\text{Zr}\{\kappa^2\text{-N,C}^8\text{-(2-C}_3\text{H}_4\text{D)-C}_5\text{D}_4\text{N}\}]$ (**17-d**₅)



Scheme 3.20 Complex **17**, complex **17-d**₅, and labelling sequence.

In the ^1H NMR spectrum, the 2-substituted-pyridido moiety and $\eta^5\text{-C}_5\text{H}_5$ moieties of **17** are similar to **16** except for the absence of 2-*H*. The *CH* of the alkene 7-*H* resonates at δ 4.20 ($^3J_{\text{HH}} = 9.2$ Hz). Remarkably, 8-*H* from the *CHCH*₃ aliphatic moiety gives rise to signals at δ -0.85 and 65.0 ($^1J_{\text{CH}} = 129$ Hz) in the ^1H and ^{13}C NMR spectra respectively. The terminal *CH*₃ group appears at δ 2.10 as a doublet in the ^1H NMR spectrum ($^3J_{\text{HH}} = 5.9$ Hz) and as a quartet at δ 22.2 ($^1J_{\text{CH}} = 125$ Hz) in the ^{13}C NMR spectrum.

The ^1H NMR of **17-d₅** shows the same chemical shifts and integration as **17** for the vinylic protons 7-*H* and 8-*H*, and for the $\eta^5\text{-C}_5\text{H}_5$ moieties. As the methyl group bears a deuterium (CH_2D), the signal for the 9-*H* (δ 2.17) now integrates for two protons and has changed from a doublet to an unresolved multiplet resulting from $^2J_{\text{HD}}$ and $^2J_{\text{HH}}$ couplings. Signals for the deuterated 2-substituted-pyridido ring are absent in the ^1H NMR, but they are all observed in the ^2H NMR at similar chemical shifts. A signal corresponding to 9-*D* resonates at δ 2.10 in the ^2H NMR spectrum. Weak resonances are also observed in the ^2H NMR at the chemical shifts of respectively 7-*H* and 8-*H*. 9-*C* appeared as a triplet at δ 22.2 in the $^{13}\text{C}\{^1\text{H}\}$ NMR spectrum, as a consequence of the coupling with deuterium ($^1J_{\text{CD}} = 19$ Hz).

The solid-state molecular structure of **17** is shown in Figure 3.5.

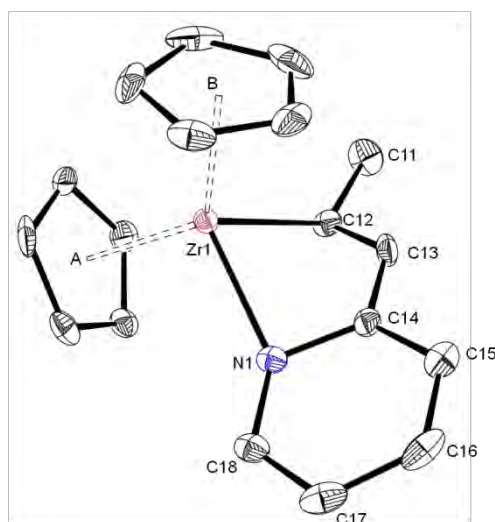


Figure 3.5 ORTEP drawing of **17**. Ellipsoids at 30% probability level, hydrogen atoms omitted for clarity. Relevant bond lengths (Å) and angles (°): Zr1–N1 2.180(4), Zr1–C12 2.269(4), Zr1–C13 2.573(5), Zr1–C14 2.666(7), N1–C14 1.383(6), N1–C18 1.376(6), C12–C13 1.458(7), C13–C14 1.391(7), C14–C15 1.431(6), C15–C16 1.349(7), C16–C17 1.416(8), C17–C18 1.347(7), $\text{Cp}^\circ\text{-Zr1-Cp}^\circ$ 127, Zr1–C12–C13 84.3(3), C11–C12–C13 117.1(4), C12–C13–C14 126.5(5), Zr1–C11–C12 135.3(3), Zr1–N1–C14 94.2(3), N(1)–Zr1–C12 82.21(16), C11–C12–C13 117.1(4)°, Zr–C12–C13 84.3(3).

The structure of a very similar complex [$\text{Cp}_2\text{Zr}\{\eta^2\text{-N,C-(2-C}_2\text{H}_3\text{)-C}_5\text{H}_4\text{N}\}$] (**17'**) was previously reported by the team of Rosenthal. **17'** only differs from **17** by the absence of a methyl group on $\text{C}\alpha$.²⁹⁶ The bond distances for Zr1–C12 [2.269(4) Å] (alkyl) and Zr1–N1 [2.180(4) Å] (amido) are unremarkable, being similar to those for **15** and **17'**. As for **17'**, we

observe a distinctive alternation of short and long bond distances in the metallacycle [C12–C13 1.458(7); C13–C14 1.391(7)] and in the conjugated 2-substituted-pyridido system.

The Zr1–C13 [2.573(5) Å] and Zr1–C14 [2.666(7) Å] distances, together with the puckering of the Zr1–C12–C13–C14–N1 cycle along N1⋯C12, could suggest a weak Zr- π (C13=C14) interaction. This results in an envelope structure (Figure 3.6), characterised by a β angle (*ca* 123°) much smaller than 180° (β being the angle between the plane N1Zr1C12 and the mean plane C12C13C14N1), together with a small torsion angle for C12–C13–C14–N1 (12°). This envelope conformation was observed in **17'** and other similar zirconocene complexes such as [Cp₂Zr(N,N'-bi-pyridido)]³⁷⁰ and [Cp₂Zr(N,N'-2-(N-*n*-butylmethylamido)pyridido)].²⁹⁷

The C12–Zr–N1 angle [82.21(16)°] is larger than in complex **15** [72.27(5)°], which probably prevents coordination of a pyridine molecule.

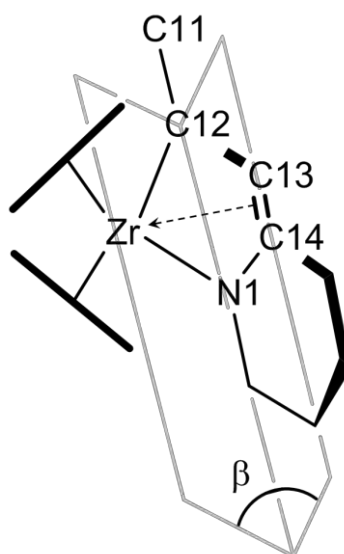
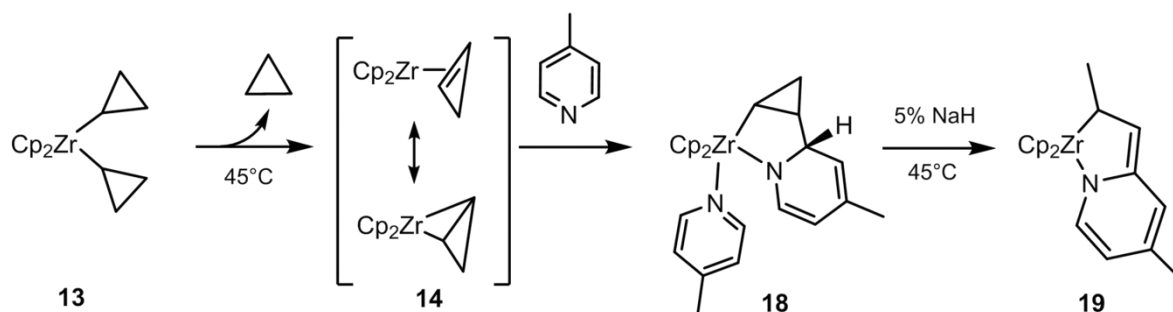


Figure 3.6 The envelope structure of **17**. Zr- π (C=C) interaction depicted by a dashed arrow.

c. Reactions with substituted pyridines

We complemented the previously reported reactions between **13** and substituted pyridines, namely 2,6-dimethylpyridine and 3,4-dimethylpyridine,³⁵⁷ by investigating the reaction with 4-methylpyridine (4-picoline). This yielded a complex analogous to **15**,

$[\text{Cp}_2\text{Zr}(4\text{-picoline})\{\kappa^2\text{-N,C}^8\text{-(2-}i\text{-C}_3\text{H}_4\text{)-(4-CH}_3\text{)C}_5\text{H}_5\text{N}\}]$ (**18**) (Scheme 3.21). Furthermore, in presence of base the analogue of **17**, $[\text{Cp}_2\text{Zr}\{\kappa^2\text{-N,C}^8\text{-(2-C}_3\text{H}_5\text{)-(4-CH}_3\text{)C}_5\text{H}_4\text{N}\}]$ (**19**), was obtained. The experimental parameters and yields were identical to those for **15** and **17** (>90% by NMR).



Scheme 3.21 Reaction of **13** with 4-picoline to give **18** and **19**.

Apart from the absence of the *Hpara* and presence of the new methyl resonances, the ^1H and ^{13}C NMR spectra for **18** and **19** are very similar to those of **15** and **17**.

When **18** was crystallised in a pyridine/pentane mixture, the pyridine adduct $[\text{Cp}_2\text{Zr}(\text{py})\{\kappa^2\text{-N,C}^8\text{-(2-}i\text{-C}_3\text{H}_4\text{)-(4-CH}_3\text{)C}_5\text{H}_5\text{N}\}]$ (**18-py**) was obtained. No exchange between the coordinated pyridine and the 4-methyl-2-substituted-pyridido ring was observed, which suggests that the rearrangement from **18** to **19** (and **15** to **17**) follows an intramolecular process, as previously proposed.

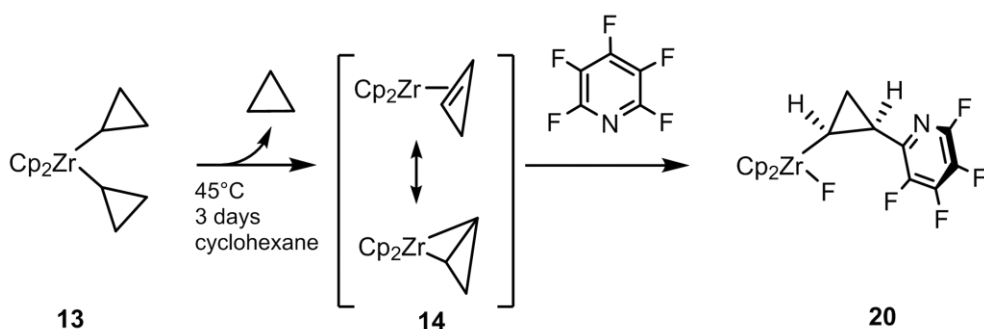
1.2. C–F activation of fluorinated pyridines

This work was also started by Nuria Romero, who was the first to realise that dicyclopropyl zirconocene was able to cleave the C–F bond of pentafluoropyridine.

a. Stoichiometric activation by $[\text{Cp}_2\text{Zr}(i\text{-C}_3\text{H}_5)_2]$

i. Reaction

Although complex **13** does not activate the C–F bond of fluoroaromatics such as C_6F_6 or $\text{C}_6\text{H}_5\text{F}$, it reacted cleanly with the more reactive pentafluoropyridine. When **13** was heated with pentafluoropyridine, C–F activation occurred selectively at the 2-position to give $[\text{Cp}_2\text{ZrF}\{(2\text{-C}_5\text{F}_4\text{N})\text{-}i\text{-C}_3\text{H}_4\}]$ **20** as depicted in Scheme 3.22.

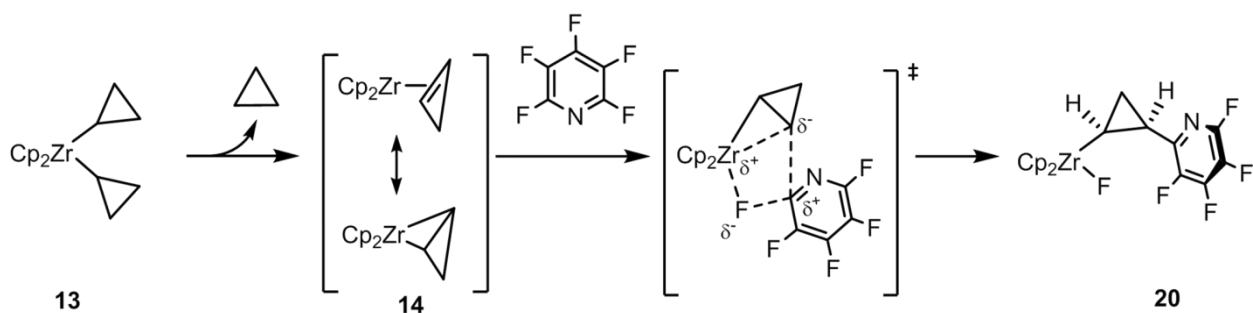


Scheme 3.22 *Synthesis of product 20.*

The reaction was performed in cyclohexane at 45°C for 3 days. Formation of cyclopropane, total consumption of **13** together with a change of colour from yellow to light brownish and the formation of a precipitate were observed. Extraction of the solid with toluene and removal of the volatiles gave **20** as a pure air and moisture sensitive beige solid in 85% yield. The selective C–F bond activation at the 2-position of the pentafluoropyridine implies formation of both a Zr–F bond and a cyclopropyl-2-pyridyl C–C bond. Complex **20** has been characterised by multinuclear NMR, elemental analysis and XRD.

ii. Mechanism

The mechanism involves intramolecular β -H abstraction from **13** to give the η^2 -cyclopropene intermediate **14** as the rate-determining step. It is followed by the 1,3-C–F addition through a four centre transition state involving the C–F bond of the fluorinated pyridine and the Zr–C bond in **14**. This mechanism is depicted in Scheme 3.23 and is similar to that for α -H abstraction followed by 1,2-C–F described in the introduction. The driving force of the reaction is the formation of the strong Zr–F bond.



Scheme 3.23 *Proposed mechanism for the formation of complex 20.*

The mechanism for this reaction was investigated by computational studies at the DFT PBE1PBE/ SDD (Zr)/TZVP (F, C, H) level of theory. Since reactions were carried out in nonpolar cyclohexane, energies were not corrected for solvent influence. The energy profile of the reaction between pentafluoropyridine and **13** displays various intermediates and transition states (Figure 3.7). The β -H abstraction TS is found 108 kJ/mol higher than complex **13** while the gap between intermediate **14**/ C_5F_5N and the second activation barrier is only of 37 kJ/mol. This profile provides further evidence that β -H abstraction is the rate-determining step. The product of the reaction is considerably more stable compared to the other species involved, with compound **20** being 268 kJ/mol lower in energy than **13**. The DFT calculations does not show pre-coordination of pentafluoropyridine that could have explained the selectivity at the 2-position.

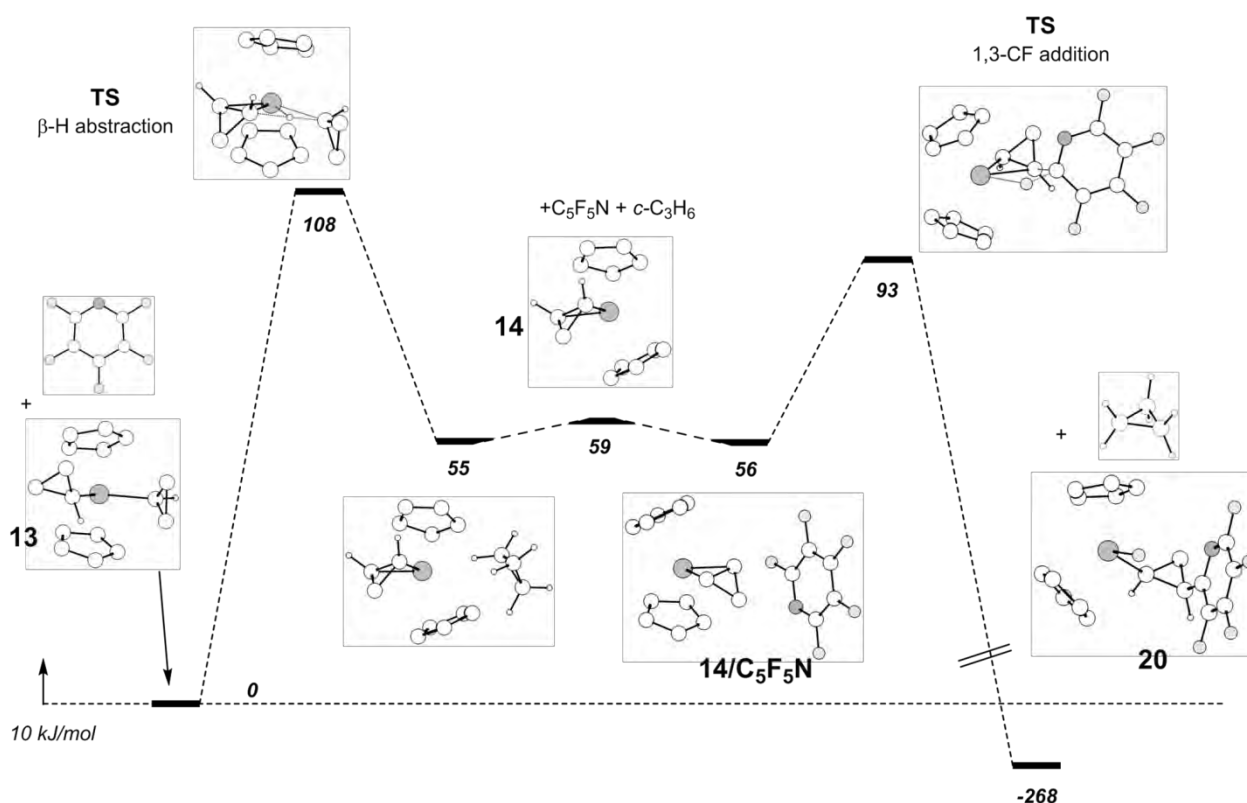
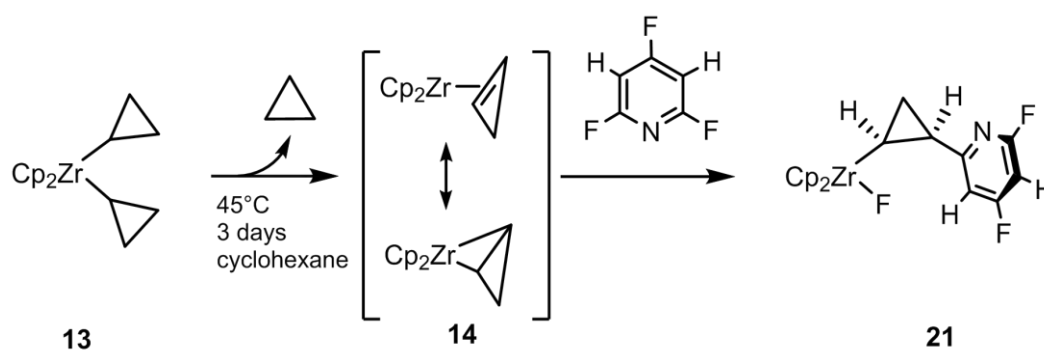


Figure 3.7 Potential energy surface (ΔE) for the reaction between pentafluoropyridine and **13** (kJ/mol). Colour code: white = C,H; light grey = F; dark grey = Zr, N.

iii. Other fluorinated pyridines

Braun *et al.* established that the strength of the C–F bonds of fluoroaromatics increase as the number of fluorines on the aromatic ring decreases.²³⁵ We therefore decided to investigate the reaction of **13** with 2,4,6-trifluoropyridine, 2,4-difluoropyridine and 2-fluoropyridine in order to probe the ability of intermediate **14** to cleave different types of C–F bonds.

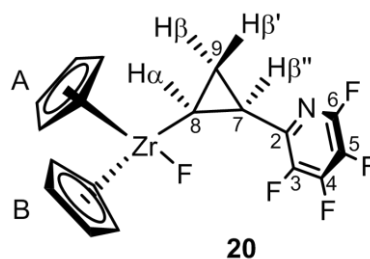
The activation of 2,4,6-trifluoropyridine occurred in the exact same way as pentafluoropyridine and gave $[\text{Cp}_2\text{ZrF}\{(2\text{-C}_3\text{F}_2\text{H}_2\text{N})\text{-}c\text{-C}_3\text{H}_4\}]$ (**21**) as depicted in Scheme 3.24. **21** was fully characterised by multinuclear NMR, elemental analysis and XRD. This experiment showed that **14** is able to activate selectively stronger C–F bonds.



Scheme 3.24 Synthesis of product **21**.

We investigated the reaction between **13** and 2,4-difluoropyridine. Preliminary results have established that C–F bond cleavage occurred, as suggested by two characteristic Zr–F (δ 59.00 and 56.25) resonances in the ^{19}F NMR spectrum of the reaction mixture. The ^1H and ^{19}F NMR spectra present many resonances that have not yet been assigned, but attest for a mixture of products. This could originate from the fact that 2,4-difluoropyridine presents stronger C–F bonds than the penta- and tri-fluorinated pyridines as well as a *Hortho* potentially leading to selectivity issues. This work is still ongoing.

When **13** was mixed with 2-fluoropyridine, no C–F activation products were detected in the reaction mixture, and the formation of an insoluble polymeric product has, for now, precluded further investigations.

iv. *Characterisation*

Scheme 3.25 Complex **20** and labelling sequence.

A full NMR characterisation of **20** (^1H , ^{19}F and ^{13}C NMR) was performed in benzene- d_6 or toluene- d_8 . ^1H NMR showed two inequivalent Cp signals (δ 5.82 and 5.76 for $\eta^5\text{-C}_5\text{H}_5$ A and $\eta^5\text{-C}_5\text{H}_5$ B respectively) which were differentiated by a ^1H - ^{19}F HOESY experiment. Four inequivalent multiplets for the $c\text{-C}_3\text{H}_4$ moiety were observed similarly to product **16** at δ 2.42 ($H\beta''$), 1.62 ($H\beta$), 1.47 ($H\beta'$) and 0.09 ($H\alpha$) by ^1H NMR and δ 38.09 (8-C), 21.45 (7-C), 20.96 (9-C) by ^{13}C NMR. In the ^{19}F NMR spectrum, a characteristic Zr–F signal³¹⁷ was observed at δ 64 as a broad singlet together with four aromatic signals at δ –86.48, –142.78, –151.66 and –163.80. Out of the 4 signals, only one corresponds to a fluorine present at the *ortho*-position (δ –86.48) of a fluorinated pyridine, indicating that C–F activation had occurred selectively at the 2-position of the pyridine ring. ^{13}C NMR experiments including $^{13}\text{C}\{^1\text{H}\}$, $^{13}\text{C}\{^1\text{H}\}\{^{19}\text{F}\}$, HMQC and HMBC were conclusive for the assignment of all the signals and allowed to determine J_{CH} and J_{CF} (see experimental part).

The ORTEP of complex **20**, obtained from an XRD crystal structure, is depicted in Figure 3.8.

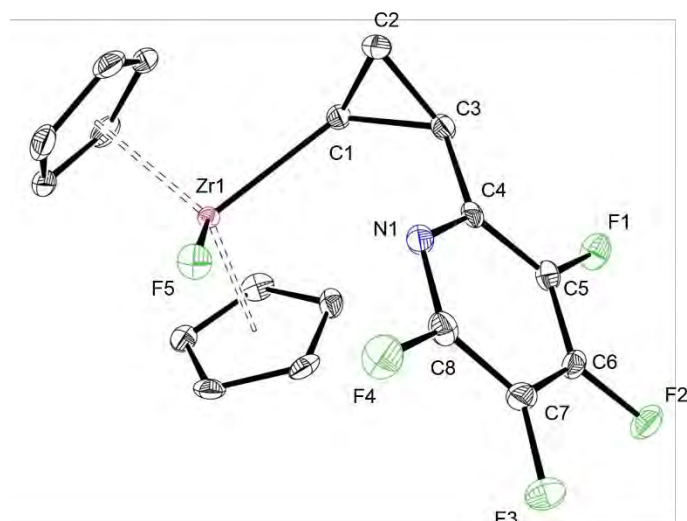
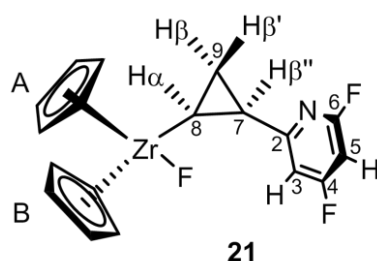


Figure 3.8 ORTEP drawing of **20**. Ellipsoids at 30% probability level, hydrogen atoms omitted for clarity. Relevant bond lengths (Å) and angles (°): Zr1–F5 1.950(2), Zr1–C1 2.301(2), C3–C4 1.474(3), C1–C2 1.503(3), C1–C3 1.544(3), C2–C3 1.508(3), F5–Zr1–C1 105.44(6), Cp°–Zr1–Cp° 133.1.

The first remarkable feature is the absence of coordination of the fluorinated pyridine moiety. The fluorinated pyridyl moiety is bound to the cyclopropyl ring *via* the C3–C4 bond, and is *syn* to the Zr center. The Zr1–F5 distance of 1.950(2) Å is similar to that in [Cp₂ZrF(2,3,5,6-tetrafluoropyrid-4-yl)] (1.946(2) Å)³¹¹ or in [Cp₂ZrF₂] (1.98(1) Å).³⁸⁰ The Zr1–C1 distance [2.301(2) Å] is slightly shorter than in [Cp₂ZrF(2,3,5,6-tetrafluoropyrid-4-yl)] [2.347(3) Å]. The C1–Zr–F5 angle of 105.44(6)° is larger than 99.38(9)° in [Cp₂ZrF(2,3,5,6-tetrafluoropyrid-4-yl)], likely due to the steric repulsion between the Cp ligands and the pyridyl moiety.



Scheme 3.26 Complex **21** and labelling sequence.

A NMR characterisation of **21** (^1H , ^{19}F and ^{13}C NMR) was performed in benzene- d_6 . The spectra are similar to those of **20**, with two new signals for 3-*H* and 5-*H* in the ^1H NMR spectrum at δ 6.50 and 5.88 (hidden by the Cp A signal), respectively. Three resonances are observed in the ^{19}F NMR spectrum, including the characteristic fluorine bonded to the Zr atom at δ 59.6. The 3-*C* and 5-*C* carbon bearing hydrogens have shifted upfield to δ 106.8 and 93.4 respectively.

The XRD structure of **21** is similar to that of **20** (Figure 3.9), except for the different torsion angles $\text{F3-Zr1-C1-C3} = 161(1)^\circ$ in **21** vs. $\text{F5-Zr1-C1-C3} = 46(1)^\circ$ in **20**.

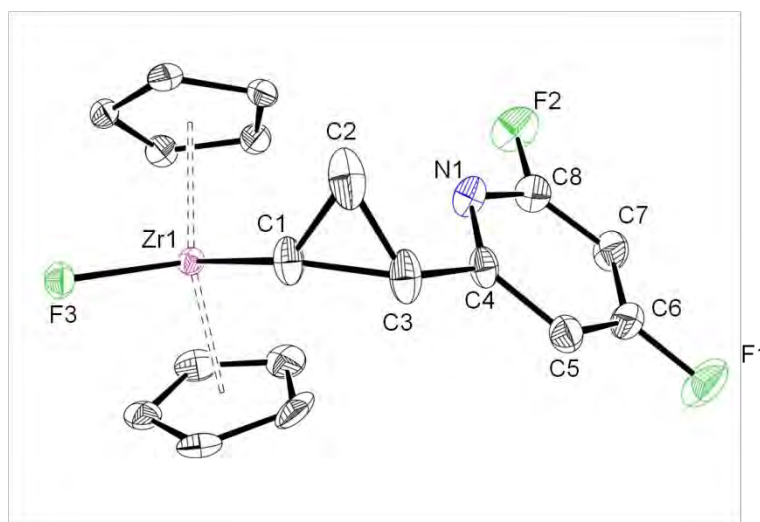
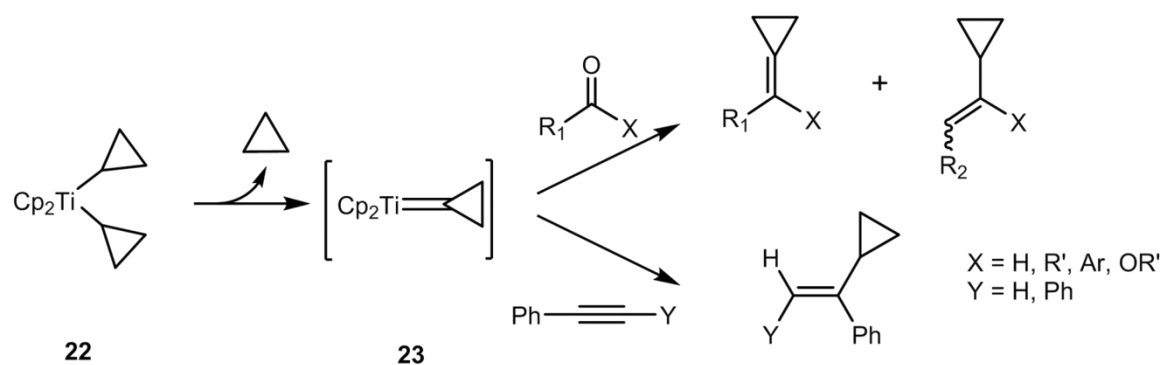


Figure 3.9 ORTEP drawing of **21**. Ellipsoids at 30% probability level, hydrogen atoms omitted for clarity. Relevant bond lengths (\AA) and angles ($^\circ$): Zr1-F3 1.967(2), Zr1-C1 2.260(4), C3-C4 1.483(6), C1-C2 1.475(7), C1-C3 1.520(6), C2-C3 1.483(7), F3-Zr1-C1 94.42(12), $\text{Cp}^\circ\text{-Zr1-Cp}^\circ$ 131.2.

b. Stoichiometric activation by $[\text{Cp}_2\text{Ti}(\text{c-C}_3\text{H}_5)_2]$

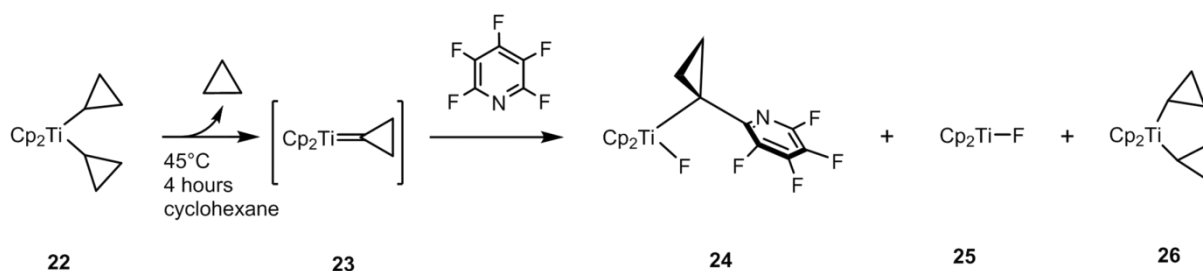
i. Reaction

For comparison purposes, we investigated the reactivity of the related dicyclopentyl titanocene complex $[\text{Cp}_2\text{Ti}(\text{c-C}_3\text{H}_5)_2]$ (**22**) toward C-F activation of pentafluoropyridine. A notable feature of **22** is its ability to undergo α - rather than β -CH abstraction leading to the formation of a transient cyclopropylidene complex $[\text{Cp}_2\text{Ti}=\text{C}(\text{C}_2\text{H}_4)]$ (**23**) (Scheme 3.27). This compound was previously described by the team of Petasis, and used for the Wittig-like cyclopropylideneation of aldehydes, ketones or esters and formation of vinyl cyclopropanes from alkynes (Scheme 3.27).²⁴⁹



Scheme 3.27 Olefination of carbonyl compounds and addition of alkynes on **22**.

The reactivity of **22** with pentafluoropyridine is summarised in Scheme 3.28. Complex **22** reacted in the presence of 10 equivalents of pentafluoropyridine in cyclohexane to give selectively the beige product $[\text{Cp}_2\text{TiF}\{(2\text{-C}_5\text{F}_4\text{N})\text{-}\eta\text{-C}_3\text{H}_4\}]$ (**24**) along with cyclopropane. C–F activation has occurred selectively at the 2-position.



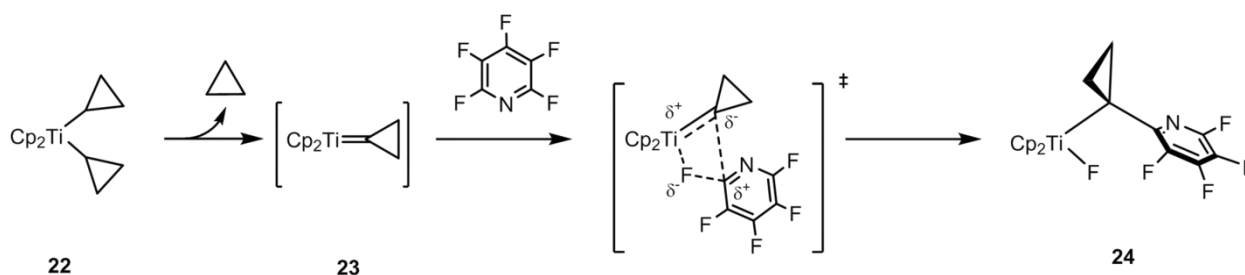
Scheme 3.28 Reaction of **22** with pentafluoropyridine.

This α -H abstraction reaction was complete after only 4 h at 45°C , significantly faster than the analogous β -H abstraction transformation seen with **13**. Formation of the green titanocene(III) fluoride $[\text{Cp}_2\text{TiF}]$ (**25**) and a complex tentatively formulated as $[\text{Cp}_2\text{Ti}(\kappa^2\text{-C}_3\text{H}_4\text{-C}_3\text{H}_4)]$ (**26**) (*vide infra*) was also observed. Despite repeated efforts, we have experienced difficulties in separating of complexes **24** and **25** from **26**. Hence, the yields of **24** (44%) and **26** (20% - assuming that the proposed formula is correct) were determined by ^1H NMR relative to benzene as an internal standard. Complex **24** has been characterised by multinuclear NMR, elemental analysis and XRD. As **24** and **25** co-crystallised as beige and green crystals, respectively, pure **24** was separated by hand from **25** under a microscope for

the elemental analysis. Complex **25** has been characterized by EPR spectroscopy and XRD and **26** by multinuclear NMR.

ii. Mechanism

We propose that the mechanism for the formation of **24** is an α -H abstraction followed by a 1,2-CF bond addition as described in the introduction (Scheme 3.29). Nonetheless, trapping of the transient cyclopropylidene **23** has never been reported and our own attempts have failed so far.



Scheme 3.29 Proposed mechanism for the formation of complex **24**.

The driving force of the reaction is the formation of a strong Ti–F bond. In order to have a better insight into this mechanism, computational studies have been carried out at the DFT PBE1PBE/ SDD (Ti)/TZVP (F, C, H) level of theory. Since reactions were carried out in nonpolar cyclohexane, energies were not corrected for solvent influence. Three rotamers of **22**, *i.e.* **22-1**, **22-2**, and **22-3**, were computed within a 7 kJ/mol energy range (Figure 3.10). No efforts were invested in finding the rotational barriers. We focused our study on the rate-determining step of the reaction, namely the elimination of cyclopropane from **22**, and more specifically on understanding why this process occurs through α -H abstraction (pathway **A**) instead of β -H abstraction (pathway **B**). The computed energy profile for the conversion of **22** to intermediates **23-A** or **23-B** *via* transition state **TS-A** or **TS-B** is shown in Figure 3.10. **TS-B** is higher in energy than **TS-A** (≈ 15 kJ/mol) indicating that **23-A** is formed preferentially. Remarkably, the η^2 -cyclopropene titanocene **23-B**, formed after β -H abstraction, is significantly more stable than the cyclopropylidene intermediate **23-A** by about 35 kJ/mol. Since compound **24** results from the C-F activation of pentafluoropyridine by intermediate **23-A**, one can say the reaction follows the kinetically controlled pathway.

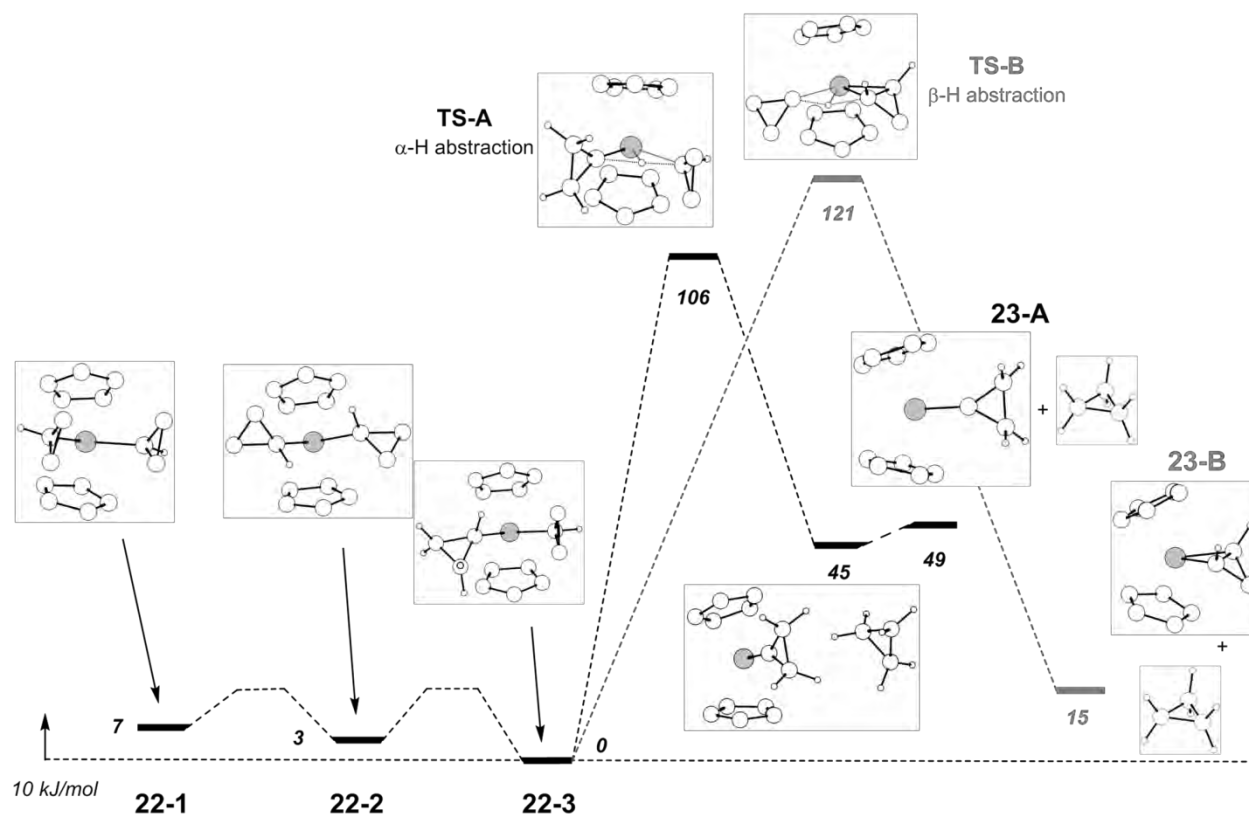


Figure 3.10 Potential energy surface (ΔE) for the loss of cyclopropane in **22** (kJ/mol). Colour code: white = C,H; light grey = F; dark grey = Ti.

The energy profile of the reaction between pentafluoropyridine and **22** is quite similar to that reported in the case of Zr (complex **13**) (Figure 3.11). The main difference is of course the α -H rather than β -H abstraction TS, which is found 106 kJ/mol higher than complex **22**. The gap between intermediate **23-A**/ C_5F_5N and the second TS is only 54 kJ/mol. This profile confirms that α -H abstraction is the rate-determining step. The product of the reaction is considerably more stable compared to the other species involved, with compound **24** being 261 kJ/mol lower in energy than the most stable rotamer of **22**. It is worth noting that **23-A** has a C_s -symmetric structure with the cyclopropylidene moiety included in one of the two mirror planes. As for the formation of **20**, no pre-coordination of pentafluoropyridine that could explain the selectivity for the 2-position was calculated.

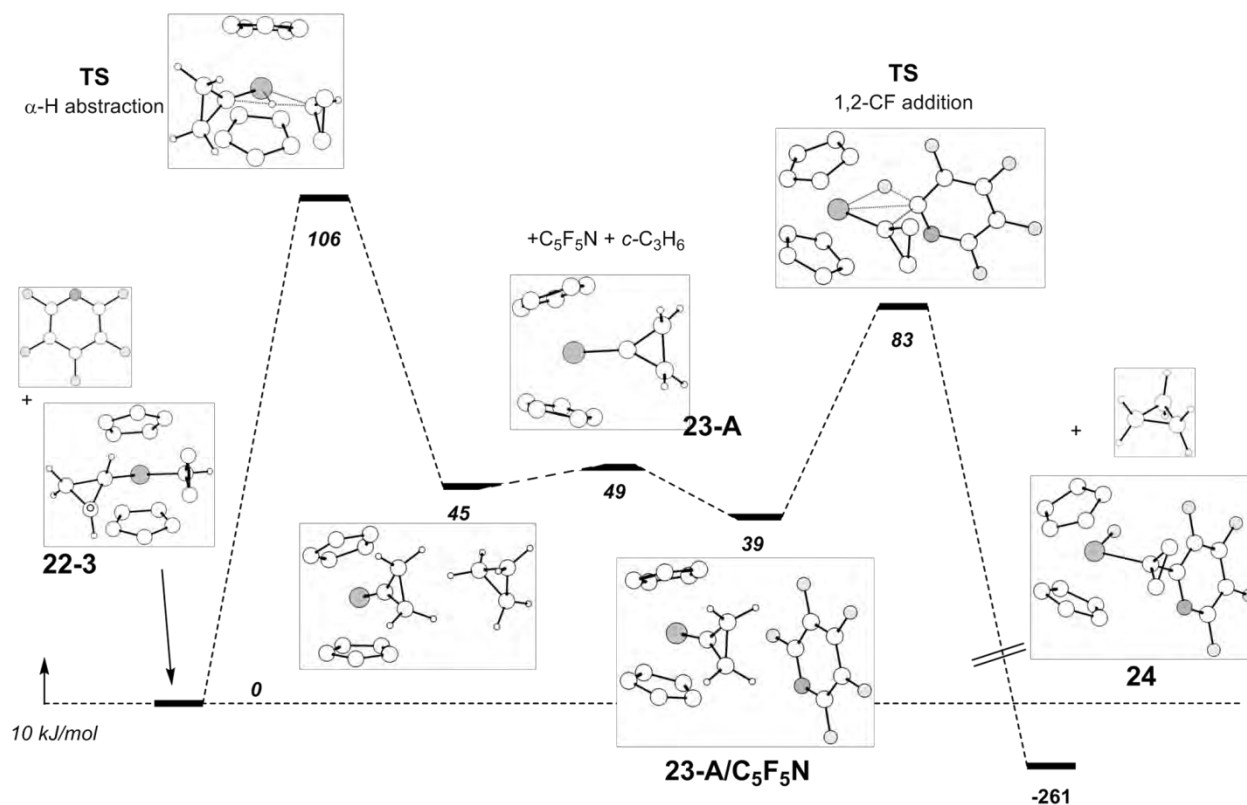
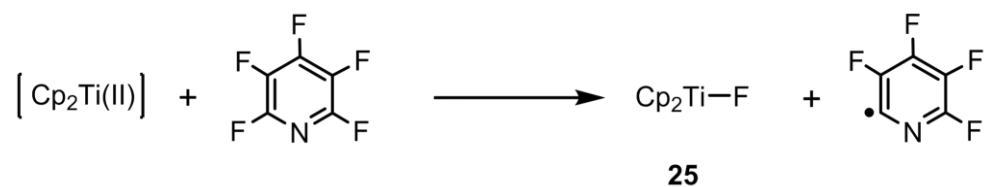


Figure 3.11 Potential energy surface (ΔE) for the reaction between pentafluoropyridine and **22** (kJ/mol). Colour code: white = C,H; light grey = F; dark grey = Ti, N.

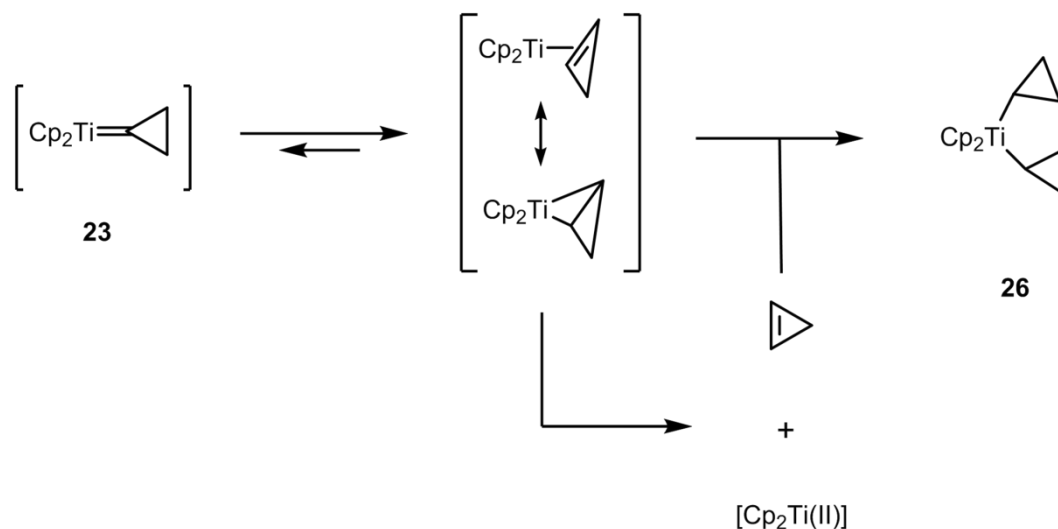
The mechanism by which **25** is formed is unknown. One hypothesis would be the binding of one fluorine atom to a reduced $[\text{Cp}_2\text{Ti(II)}]$ fragment, followed by the homolytic cleavage of the C–F bond yielding Cp_2TiF with a titanium (III) metal centre and a tetrafluoropyridyl radical (Scheme 3.30). However, the presence of the latter was never observed.



Scheme 3.30 Proposed mechanism for the formation of complex **25**.

If the structure of **26** displayed in Scheme 3.28 proved to be true, one possibility for its formation would be the isomerisation of the cyclopropylidene intermediate **23** into the η^2 -

cyclopropene titanocene along with the 1,3-CC bond addition of a hypothetically free cyclopropene (Scheme 3.31). This latter could possibly arise from decomposition of the η^2 -cyclopropene intermediate. Isomerisation of an alkylidene into an η^2 -alkene is a well-known process for ETM.^{381–383} The mechanism generally follows a 1,2-hydride migration and is shifted toward the formation of the alkene complex (Figure 3.10).³⁸³



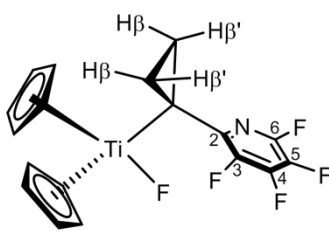
Scheme 3.31 Proposed mechanism for the formation of complex **26**.

[Cp₂Ti(II)], involved in the reaction presented in Scheme 3.30, might result from the decomposition of η^2 -cyclopropene complex (Scheme 3.31). Nevertheless, no experimental evidence for these hypotheses was collected.

iii. Characterisation

A whole NMR characterisation of **24** (¹H, ¹⁹F and ¹³C NMR) was performed in benzene-d₆. **26** was easily separated from **24** by extraction with pentane, but the NMR analyses have been realised on mixtures of **24** and **25**. The latter being paramagnetic (d¹ metal), only resonances attributable to **24** are present in the NMR spectra, and no broadening of the signal due to the presence of **25** was noticed.





24

Scheme 3.32 Complex **24** and labelling sequence.

In the ^1H NMR spectrum of **24**, all 10 hydrogens of the Cp rings appear at δ 5.91 as a singlet, indicating the existence of a plane of symmetry. Two signals are observed at δ 1.49 and 1.23 as broad singlets, corresponding to the $\text{H}\beta$ of the cyclopropyl fragment, equivalent hydrogen atoms being the ones on the same face (see Scheme 3.32). The ^{19}F NMR spectrum of **24** is similar to that of **20**, except for a typical Ti–F resonance at δ 156.6.^{384–386} The four other resonances correspond to one *Fpara* (δ –141.39), two *Fmeta* (δ –142.24 and –164.01) and only one *Fortho* (δ –84.72), indicating the selective activation of the pyridine ring in the 2-position. In the ^{13}C NMR spectrum, salient features include (i) $\text{C}\alpha$, a quaternary carbon appearing as a singlet at δ 48.5 (ii) the two equivalent $\text{C}\beta$ s showing up as a triplet at δ 23.0 ($^1J_{\text{CH}} = 161$ Hz) (iii) high $^1J_{\text{CF}}$ coupling constants (230–260 Hz) for carbon bearing fluorine atoms.

The molecular X-ray crystal structure of **24** is displayed in Figure 3.12 below.

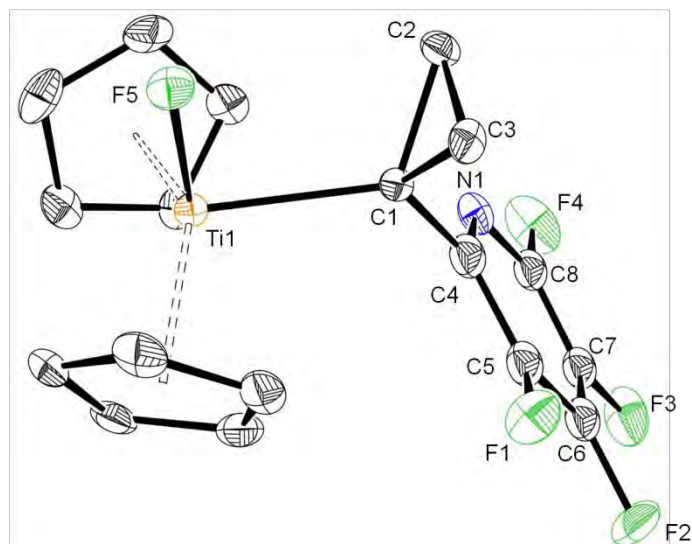
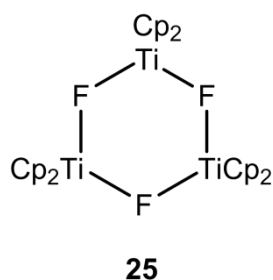
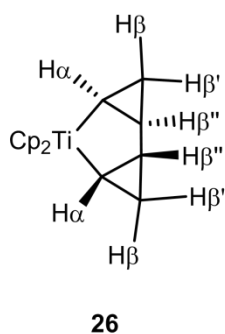


Figure 3.12 ORTEP drawing of **24**. Ellipsoids at 30% probability level, hydrogen atoms omitted for clarity. Relevant bond lengths (Å) and angles (°): Ti1–F5 1.853(3), Ti1–C1 2.226(4), C1–C2 1.538(6), C1–C3 1.526(6), C2–C3 1.516(7), C4–C1 1.465(6), F5–Ti1–C1 91.83(16), C4–C1–Ti1 122.0(3), C3–C1–C2 59.3(3), C3–C2–C1 59.9(3), C2–C3–C1 60.7(3), Cp^o–Ti–Cp^o 131.

As in the structure of **20**, there is no coordination of the fluorinated pyridine moiety on the Ti centre. A new cyclopropyl-2-pyridyl C–C bond can be observed between the carbon C1 at the α -position of the titanium and C4 at the 2-position of the pyridyl ring, confirming the regioselectivity of the reaction. The Ti1–F5 distance of 1.853 (3) Å is similar to that in [Cp₂Ti(CH=CH₂)F] 1.847(3) Å³⁸⁵ or in [Cp'₂TiF₂] (Cp' = 1,3-bis(trimethylsilyl)cyclopentadienyl) 1.832(2) Å.³⁸⁷ The Ti1–C1 distance of 2.226(4) Å is longer than 2.098(6) Å in [Cp₂Ti(CH=CH₂)F] probably because C1 is quaternary. The F5–Ti1–C1 angle is 91.83(16)° which is within the typical range for d⁰ titanocenes bearing σ -bonded ligands (Cp₂TiXX').^{373,384,385}

[Cp₂TiF] (25)**Scheme 3.33** Trimer of Complex 25.

The characterisation of complex **25** was reported by the team of Lentz.^{388,389} We observed the same ESR analysis with a signal $g = 1.983(4)$ and super hyperfine splittings (sextet, A (⁴⁷Ti, 7.75%, $I = 5/2$) = 9.2 G and octet A (⁴⁹Ti, 5.51%, $I = 7/2$) = 8.6 G). Also we have obtained a XRD structure of the complex **25** as a trimer of formula [Cp₂TiF]₃ similar to that previously reported, but in a different crystal system (space group for **25**: *Pnma*, space group for the previously reported structure: *P2₁2₁2₁*; no significant differences in metrical parameters were observed between the two structures).³⁸⁸

[Cp₂Ti-κ²-(C₃H₄-C₃H₄)] (26)**Scheme 3.34** Proposed structure for complex 26.

Compound **26** was found in the crude material and it could be extracted with pentane but was not isolated. The other products were also partly soluble and crystallization attempts were unsuccessful due to a greater solubility of **26** (compared to **24** and **25**) in different solvents.

From ^1H , ^{19}F and ^{13}C NMR spectroscopy, we managed to deduce that **26** contains: (i) two equivalent Cp rings and no fluorine atom, (ii) ^1H NMR signals from δ 0.45 to 1.45, typical of a 1,2-disubstituted cyclopropyl ring (Figure 3.13), comparable to the cyclopropyl resonances for **16** and **20**, which integrate with a 1:1 ratio with respect to the Cp rings. We suggest the C_2 -symmetric structure for **26**, displayed in Scheme 3.34 and in Figure 3.13.

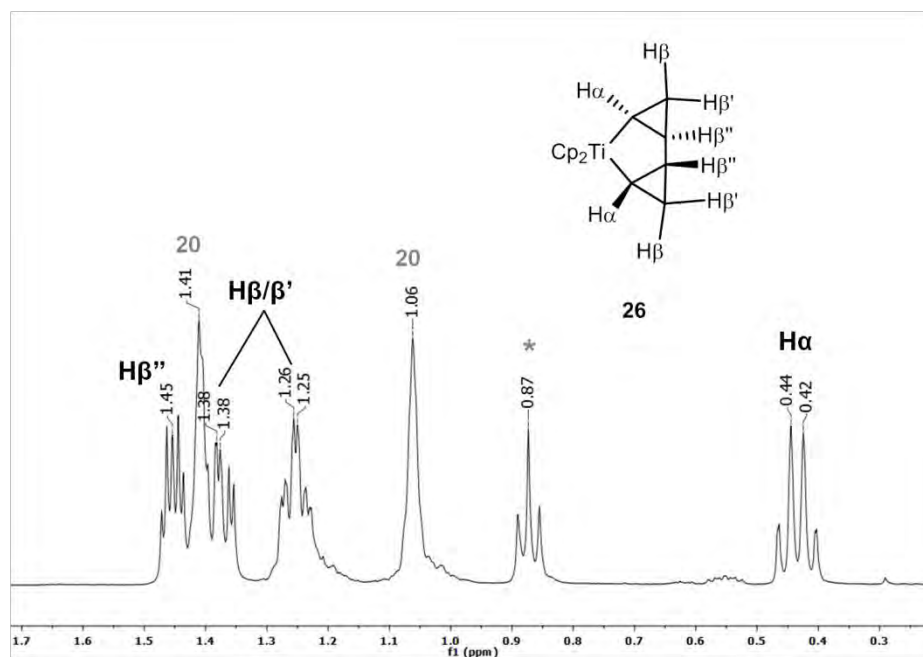
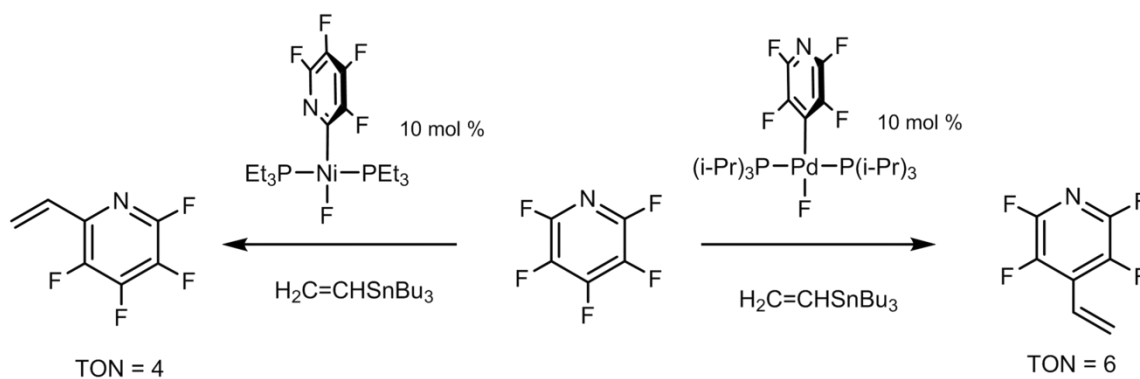


Figure 3.13 ^1H NMR of a mixture of complexes **24** and **26** in toluene- d_8 with tentative assignment of the **26** resonances. * = residual pentane

c. Toward catalysis

No example of catalytic C–F bond cleavage of pentafluoropyridine, followed by C–C bond formation, has been reported for ETM complexes (for hydrodefluorination reactions, see introduction). Only two complexes of late transition metals are able to realise such a transformation (Scheme 3.35).^{340,390} *trans*-[NiF(2- $\text{C}_5\text{F}_4\text{N}$)(PEt_3) $_2$] and *trans*-[PdF(4- $\text{C}_5\text{F}_4\text{N}$)(*P*-*i*-Pr $_3$) $_2$] catalyse the C–C coupling between pentafluoropyridine and vinyltributyltin regioselectively at the 2- (Ni) or 4-position (Pd). TON are 4 and 6, respectively.



Scheme 3.35 Catalytic pentafluoropyridine activation by late transition metal complexes.

Catalytic introduction of a cyclopropyl moiety is of synthetic interest. Indeed, not only three carbons are linked at once to the pyridine ring, but subsequent ring opening, cycloadditions and ring enlargement of the cyclopropyl group can yield a wide variety of compounds.²⁵ For this reason, we investigated the catalytic cycle presented in Figure 3.14 below. This cycle was inspired by the work of Rosenthal (see introduction), where an alkyl aluminium was used as the fluorine sink (transmetallating agent).

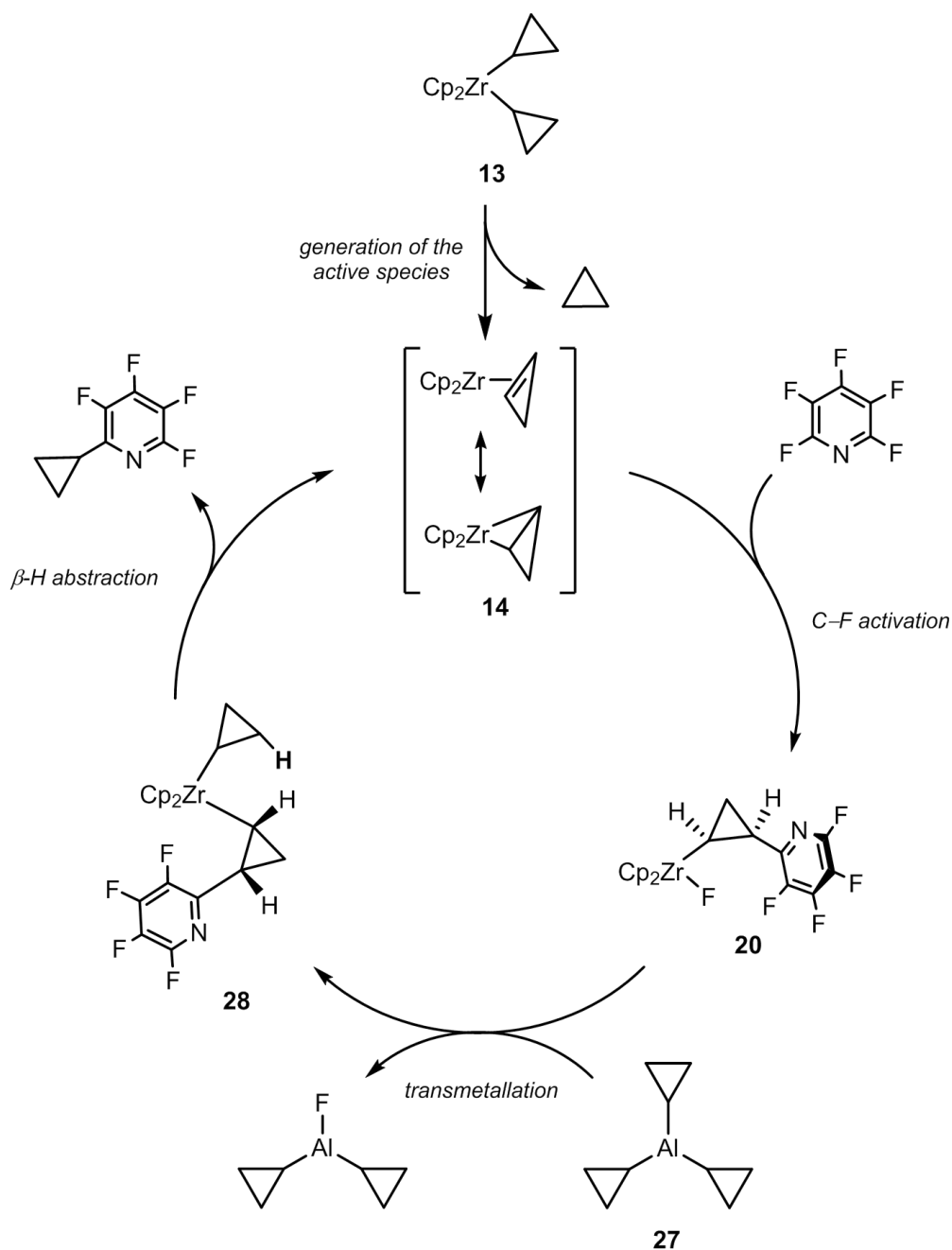


Figure 3.14 Proposed catalytic cycle for the formation of 2-cyclopropyltetrafluoropyridine.

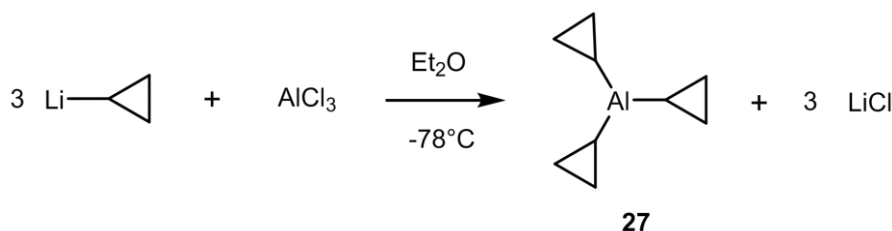
The catalytic cycle would start with the generation of the active species **14** from **13**. Reaction with pentafluoropyridine would result in C–C coupling *via* the cleavage of the C–F bond at the 2-position, yielding compound **20**. Tricyclopropylaluminium [$(c\text{-C}_3\text{H}_5)_3\text{Al}$] (**27**) would function as the transmetalating agent, abstracting the fluorine bound to the zirconium centre and forming a new σ -bond between the Zr atom and a cyclopropyl group (complex **28**). The last step would be the regeneration of the η^2 -cyclopropene intermediate through β -H

abstraction and the release of 2-cyclopropyltetrafluoropyridine. As described below, we have been able to complete each step of this cycle independently.

i. Synthesis of tricyclopropyl aluminium

Alkyl aluminiums are able to defluorinate Zr complexes because of the stronger Al–F vs. Zr–F BDE (664 vs. 623 kJ/mol) and because of the stronger Zr–C vs. Al–C (561 vs. 255 kJ/mol).³⁵⁰ Yet, that BDE for the Al–F bond is valid when the two other substituents on Al are alkyls, *ie* for AlR₂F complex. A second transmetallation reaction is less likely to happen, as the BDE of the second Al–F bond in AlRF₂ drops to 546 kJ/mol, less than that of the Zr–F bond. Hence, only one alkyl from the aluminium complex could potentially be transferred to the Zr fluoride complex.

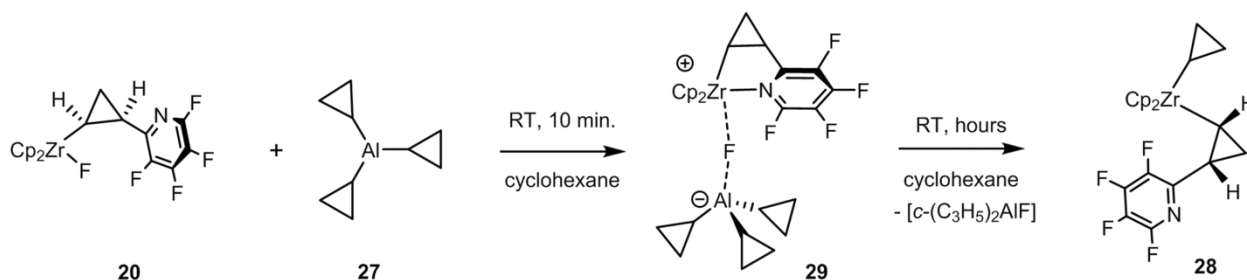
The synthesis and characterisation of tricyclopropylaluminium **27** was reported by Thomas and Oliver.³⁹¹ As they use toxic dicyclopropylmercury as the starting material, we investigated another synthetic procedure similar to that for [Ph₃Al].³⁹² The salt metathesis of AlCl₃ with [*c*-C₃H₅Li] in diethyl ether (Scheme 3.36) followed by sublimation yielded **17** as white crystals in a non-optimized 30% yield. There is no coordinated Et₂O molecule.



Scheme 3.36 Synthesis of complex **27**.

ii. Stoichiometric transmetallation

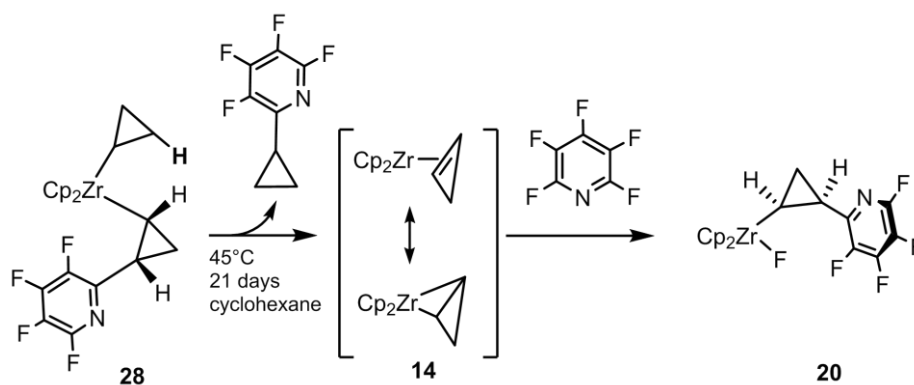
The reaction between **20** and **27**, in cyclohexane, yielded [*c*-(C₃H₅)₂AlF] and the transmetallation Zr product [Cp₂Zr(*c*-C₃H₅){(2-C₅F₄N)-*c*-C₃H₄}] (**28**) (Scheme 3.37). Due to its poor solubility in cyclohexane, we were also able to isolate a zwitterionic Zr/Al intermediate of formula [Cp₂Zr(2-C₅F₄N)-*c*-C₃H₄]⁺[(μ-F)-(c-C₃H₅)₃Al]⁻ (**29**). **29** quickly forms and then reacts more slowly (over several hours) to give **28** and [*c*-(C₃H₅)₂AlF] at room temperature. As this work is still ongoing, the yields have not been determined yet, but by ¹H NMR we observed total conversion of **27** to **29**, followed by **29** to **28**. **28** and **29** were characterised by XRD and multinuclear NMR analyses.



Scheme 3.37 Synthesis of complexes **28** and **29**.

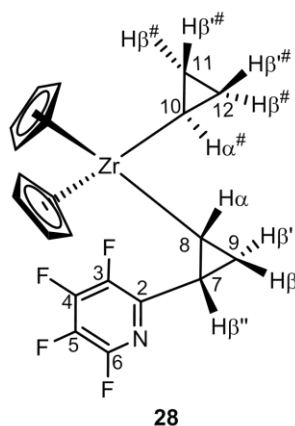
iii. C–F activation of pentafluoropyridine by complex 28

In a NMR tube equipped with a benzene- d_6 capillary, complex **28** was placed with 10 equivalents of pentafluoropyridine in cyclohexane and was heated to 45°C. The reaction was monitored by ^1H and ^{19}F NMR. We observed the full conversion of **28** over a period of 21 days, and appearance of Zr–F and Cp resonances that belong to complex **20**. The reaction medium was then dried under vacuum, washed with pentane, and ^1H and ^{19}F NMR were recorded in benzene- d_6 . They confirm the formation of complex **20** (Scheme 3.38) which demonstrates the feasibility of the proposed catalytic cycle (Figure 3.14). Investigations are now ongoing in order to reach the genuine catalytic stage.



Scheme 3.38 Formation of complex **20** from C–F bond cleavage of pentafluoropyridine by complex **28**.

iv. Characterisation



Scheme 3.39 Complex **28** and labelling sequence.

A full NMR characterisation of **28** (^1H , ^{19}F and ^{13}C NMR) was performed in benzene- d_6 . Four inequivalent multiplets for the $(\text{C}_5\text{F}_4\text{N})\text{-}c\text{-C}_3\text{H}_4$ moiety were observed similarly to complex **8** with an upfield resonance for $\text{H}\alpha$ (δ -1.08), together with three new resonances at δ 0.84 ($\text{H}\beta'^{\#}$), 0.38 ($\text{H}\beta^{\#}$) and 0.35 ($\text{H}\alpha^{\#}$) for the $c\text{-C}_3\text{H}_5$ group (Scheme 3.39). These proton assignments were made with the aid of data from COSY and NOESY experiments. The ^{19}F NMR spectrum is similar to that of **20** with four aromatic signals at δ -87.19, -141.86, -151.42 and -163.76; there is no resonance corresponding to a Zr-bound fluorine. ^{13}C NMR experiments including $^{13}\text{C}\{^1\text{H}\}$, HMQC and HMBC allowed for the assignment of all the signals of the cyclopropyl and cyclopentadienyl carbons but the resonances of the pyridine carbons were not observed (see experimental section).

The molecular XRD structure of **28** is presented in Figure 3.15.

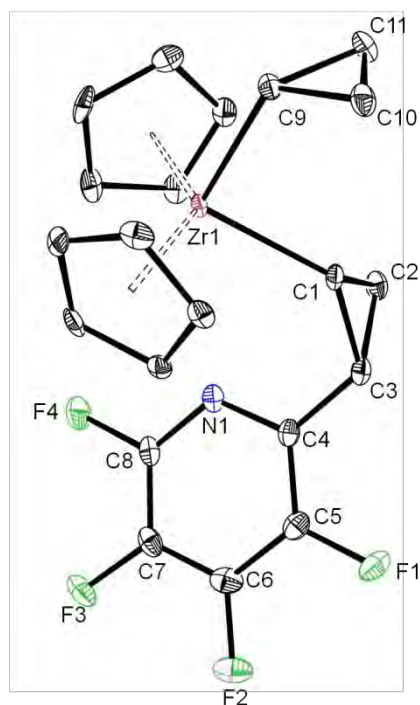
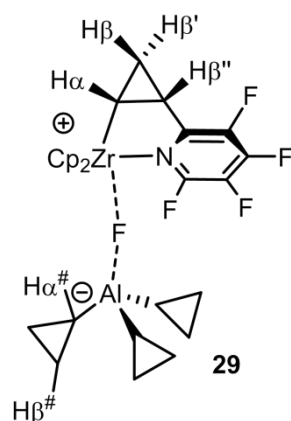


Figure 3.15 ORTEP drawing of **28**. Ellipsoids at 30% probability level, hydrogen atoms omitted for clarity. Relevant bond lengths (Å) and angles (°): Zr1–C1 2.288(1), Zr1–C9 2.266(3), C3–C4 1.470(4), C1–C2 1.502(4), C1–C3 1.548(4), C2–C3 1.506(5), C9–C10 1.516(4), C9–C11 1.508(4), 1.492(5), C1–Zr1–C9 95.47(11), Cp^o–Zr–Cp^o 133.

The structure of **28** is similar to that of **20**, with the F atom previously bounded to the Zr now substituted by a cyclopropyl ring. There is still absence of coordination of the fluorinated pyridine moiety; even if N1 points toward Zr1, the Zr–N1 [>3.5 Å] distance is in a range that precludes interaction. The Zr1–C1 [2.288(1) Å] and Zr–C9 [2.266(3) Å] distances are in the same range as Zr–C bonds in **20** [2.301(2) Å] and **13** [2.256(3) and 2.261(3) Å].³¹ The C1–Zr1–C9 angle of 95.47(11)° is in the typical range for this kind of d⁰ compound. Neither distortion nor bond lengthening of the cyclopropyl groups is observed.



Scheme 3.40 Complex **29**.

So far, only RT ^1H and ^{19}F NMR spectra in benzene- d_6 have been recorded. As complex **29** yields **28** and $[(c\text{-C}_3\text{H}_5)_2\text{AlF}]$ readily, resonances attributable to complex **28** are present in the spectra at RT. Complex **29** exhibits a broad Cp resonance at δ 5.96 in the ^1H NMR spectrum. Other resonances were tentatively assigned as follow: δ 2.25 ($\text{H}\beta''$), 1.48 ($\text{H}\beta$ or $\text{H}\beta'$), 0.83 ($\text{H}\beta^\#$ or $\text{H}\beta''^\#$), 0.71 ($\text{H}\beta^\#$ or $\text{H}\beta''^\#$), 0.66 ($\text{H}\beta$ or $\text{H}\beta'$), 0.32 ($\text{H}\alpha$) and -0.95 ($\text{H}\alpha^\#$). The ^{19}F NMR spectrum is too intricate for a tentative assignment of the signals but no resonance for a Zr–F bond was observed, confirming the proposed zwitterionic structure of complex **29**.

The X-ray crystal structure of **29** is displayed in Figure 3.16.

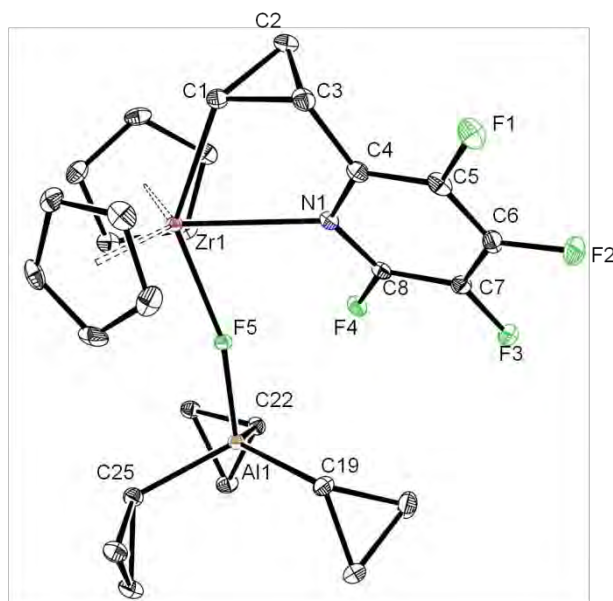


Figure 3.16 ORTEP drawing of **29**. Ellipsoids at 30% probability level, hydrogen atoms omitted for clarity. Relevant bond lengths (Å) and angles (°): Zr1–F5 2.1654(8), Zr1–N1 2.5270(12), Zr1–C1 2.3140(15), Al1–F5 1.8089(9), C3–C4 1.465 (2), C1–C2 1.502(2), C1–C3 1.524(2), C2–C3 1.531(2), N1–Zr1–C1 68.99(5), N1–Zr1–F5 71.00(4).

XRD structures for several zirconocenium aluminate complexes of general formula $[\text{Cp}'_2\text{ZrX}]^+[(\mu\text{-F})\text{-LA}]^-$ (LA: Lewis acid) have been reported.^{393–396} These complexes are generally used as catalysts for alkene polymerisation. To the best of our knowledge, it is the first time that such a species is isolated in a step of a catalytic C–F bond activation reaction.

29 is a zwitterionic complex containing an Al and a Zr centre, linked by a bridging fluoride F5. The Zr–C1 bond [2.3140(15) Å] is comparable to that in complex **20** [2.301(2) Å]. The pyridine ring is coordinated to the Zr with a Zr1–N1 distance of 2.5270(12) Å. The Al–C bonds [Al1–C19 1.9660(15) Å, Al1–C22 1.9702(15) Å, Al1–C25 1.9648(16) Å] are in the same range as that in the dimeric structure of **27** [*ca* 1.94–2.01 Å],⁴³ showing that no cyclopropyl transfer to the Zr centre has occurred yet. There is neither distortion nor significant bond lengthening in any of the cyclopropyl rings.

The most important feature in the structure of **28** is the competition between Zr and Al for the bridging fluoride ligand. The long Zr1–F5 [2.1654(8) Å] and short Al1–F5 [1.8089(9) Å] distances are in the range of the other reported complexes [Zr–F 2.10 to 2.24 Å and Al–F 1.73 to 1.81 Å].^{393–396} By comparison, the Zr–F distance [1.950(1) Å] in **20** is considerably shorter, which shows the greater affinity of fluorine for aluminium than zirconium. We

suggest that the coordination of pyridine stabilises the cationic Zr centre and helps the fluorine transfer from Zr to Al.

C. Conclusion and perspectives

The dicyclopropylzirconocene complex **13** forms a very reactive transient intermediate $[\text{Cp}_2\text{Zr}(\eta^2\text{-}c\text{-C}_3\text{H}_4)]$ **14** by intramolecular β -H abstraction of cyclopropane. Upon insertion of unsaturated molecules in the Zr–C bond of this intermediate, zirconacycles are formed,²⁶⁸ but **14** also activates C–H bonds of thiophene, benzene and furan.³¹

We have shown that **14** is able to dearomatise pyridine by C–C oxidative coupling / insertion reaction in the C–C bond. Subsequent cyclopropyl ring opening and C–H activation are observed upon addition of a catalytic amount of a strong base. A reasonable mechanism has been proposed.

Compound **14** is also able to activate the C–F bond of pentafluoro- and 2,4,6-trifluoropyridine. Only preliminary results have been obtained with the less reactive 2,4-difluoro- and 2-fluoropyridine. We have investigated individual steps of a potential catalytic cycle for a C–F bond cleavage/C–C bond forming reaction. Details of some of these steps have to be further clarified. Genuine catalytic transformations are currently being investigated.

In the case of the analogous dicyclopropyltitanocene, C–F bond cleavage of pentafluoropyridine is also realised, but *via* a cyclopropylidene intermediate $[\text{Cp}_2\text{Ti}=\text{C}(\text{C}_2\text{H}_4)]$ resulting from α -H rather than β -H abstraction of cyclopropane. This behaviour was elucidated by DFT calculations. However, formation of reaction by-products was not accounted for, and efforts in this direction are ongoing.

D. Experimental part

All operations were performed with rigorous exclusion of air and moisture, using standard Schlenk techniques and an Ar filled Jacomex glovebox ($O_2 < 5$ ppm, $H_2O < 1$ ppm). Zirconocene dichloride (98%), titanocene dichloride (97%), metallic lithium (ribbon, 99.9%), potassium tert-butoxide (98%), NaH (95%), aluminium chloride (99.99%), tmeda (99.5%), pyridine (99%), 4-methylpyridine (99%) were purchased from Aldrich. Bromocyclopropane (99%) was purchased from Alfa Aesar. Pentafluoropyridine (99%), 2,4,6-trifluoropyridine (95%), 2,4-difluoropyridine (98%) and 2-fluoropyridine (99%) were purchased from Fluorochem. All solvents were pre-dried by passing through a Puresolv MD 7 solvent purification machine, dried over molecular sieves, filtered and degassed by freeze–pump–thaw cycles. Deuterated solvents, fluorinated pyridines, and bromocyclopropane were dried over molecular sieves, filtered, and degassed by several freeze–pump–thaw cycles and stored in sealed ampoules in the glovebox. Tmeda was distilled over Na and further degassed by freeze–pump–thaw cycles. Pyridine and 4-methylpyridine were distilled over CaH_2 and further degassed by freeze–pump–thaw cycles. Potassium tert-butoxide was purified by sublimation at $150^\circ/10^{-1}$ mbar. Zirconocene dichloride was recrystallised from neat dichloromethane and pentane. Titanocene dichloride was purified by sublimation at $190^\circ/10^{-1}$ mbar. Cyclopropyllithium was prepared from Li and bromocyclopropane in ether from $0^\circ C$ to RT for 12 h from an adapted literature procedure¹¹⁴ and then it was titrated by the Gilman procedure.³⁹⁷ Dicyclopropyl zirconocene³¹ and dicyclopropyl titanocene²⁴⁹ were prepared from literature procedures.

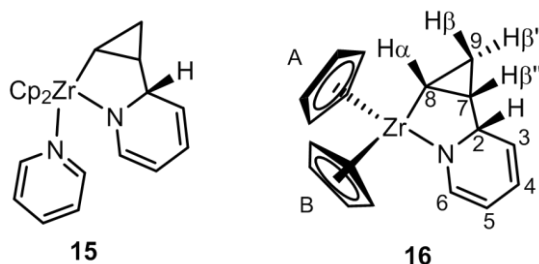
The chemical shifts are given in ppm. NMR spectra were recorded by using J. Young valve NMR tubes using Bruker Avance III 400 (1H , 400.16; ^{19}F , 376.49; 7Li , 155.52; ^{13}C , 100.6 MHz) or Avance 500 (1H , 500.33; 2H , 77.75; ^{13}C 125.82 MHz) spectrometers. Chemical shifts for 1H NMR were determined using residual proton signals in the deuterated solvents and reported *vs.* $SiMe_4$. Chemical shifts for ^{13}C NMR spectra were that of the solvent referenced to $SiMe_4$. ^{19}F NMR spectra were referenced *vs.* external $CFCl_3$. Elemental analyses (Analytical service of the LCC) are the average of at least two independent measurements.

XRD data were collected at low temperature (100 K) on a Bruker Kappa Apex II diffractometer using a Mo- $K\alpha$ radiation ($\lambda = 0.71073 \text{ \AA}$) micro-source and equipped with an Oxford Cryosystems Cryostream Cooler Device. The structures have been solved by direct methods using SIR92¹⁶⁵ or SHELXS-97,¹⁶⁶ and refined by means of least-squares procedures

on F^2 with the aid of the program SHELXL97¹⁶⁶ included in the software package WinGX version 1.63.¹⁶⁷ All hydrogens atoms were placed geometrically, and refined by using a riding model. All non-hydrogens atoms were anisotropically refined, and in the last cycles of refinement a weighting scheme was used, where weights are calculated from the following formula: $w=1/[\sigma^2(F_o^2)+(aP)^2+bP]$ where $P=(F_o^2+2F_c^2)/3$.

Calculations were performed at the DFT level with the PBE1PBE functional as implemented in Gaussian09.¹⁶⁸ The TZVP basis set was used for atoms C, H and F.³⁹⁸ Ti³⁹⁹ and Zr⁴⁰⁰ were described using the Stuttgart/Dresden RECP pseudo-potential (SDD) and its associated basis set. Structure optimisations were carried out without symmetry constraints. The nature of the stationary points was ascertained by a vibrational analysis within the harmonic approximation (1 atm and 298 K). Minima were identified by a full set of real frequencies. Electronic energies are reported in hartree with zero-point energy correction.

Synthesis of $[\text{Cp}_2\text{Zr}(\text{C}_5\text{H}_5\text{N})\{\kappa^2\text{-N,C}^8\text{-(2-}i\text{-C}_3\text{H}_4\text{)-C}_5\text{H}_5\text{N}\}]$ (15**) and $[\text{Cp}_2\text{Zr}\{\kappa^2\text{-N,C}^8\text{-(2-}i\text{-C}_3\text{H}_4\text{)-C}_5\text{H}_5\text{N}\}]$ (**16**).**

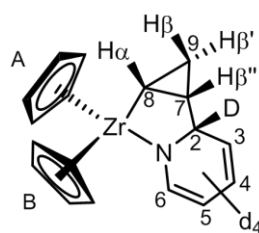


Compound **13** (150 mg, 0.49 mmol) was dissolved in pyridine (2 mL, 21.1 mmol). The mixture was heated to 45 °C for 3 days to give a brown solution. This solution was dried under reduced pressure. After extraction with pentane, the purple solution was kept to -40°C overnight to give a dark purple solid. The solution was removed by filtration and the solid was recrystallised from pentane at -40°C to yield **16** as dark purple crystals (150 mg, 0.441 mmol, 89%). This solid is air, moisture and temperature sensitive. Anal. Calcd. for $\text{C}_{18}\text{H}_{19}\text{NZr}$: C 63.49, H 5.58 N 4.11. Found: C 63.28, H 5.70, N 3.90. Crystals of **15** suitable for XRD were obtained from a pyridine solution of **16**, layered with pentane and stored at -40°C for one week. **15** spontaneously gave **16** upon solubilisation in any other solvent than pyridine.

¹H NMR (toluene-*d*₈, 223 K) δ 6.26 (d, 1 H, ³ J_{HH} = 7.1 Hz, 6-*H*), 6.01 (dd, 1 H, ³ J_{HH} = 9.7, 5.7 Hz, 4-*H*), 5.74 (s, 5 H, $\eta^5\text{-C}_5\text{H}_5\text{B}$), 5.66 (s, 5 H, $\eta^5\text{-C}_5\text{H}_5\text{A}$), 5.31 (q, 1 H, ³ J_{HH} = 2.3 Hz, 2-*H*), 5.17 (d, 1 H, ³ J_{HH} = 10.1 Hz, 3-*H*), 4.49 (ddd, H, ³ J_{HH} = 6.8, 5.3, 1.3 Hz, 5-H).

H), 1.75 (m, 1 H, $H\beta''$), 1.51 (dt, 1 H, $^3J_{HH} = 7.4, 3.4$ Hz, $H\beta'$), 1.20 (ddd, 1 H, $^2J_{HH} = 12.4, ^3J_{HH} = 8.3, 4.2$ Hz, $H\beta$), 0.22 (q, 1 H, $^3J_{HH} = 9.0$ Hz, $H\alpha$). ^{13}C NMR (toluene- d_8 , **223 K**) δ 142.9 (d, $J_{CH} = 165$ Hz, 6-C), 122.6 (d, $J_{CH} = 160$ Hz, 3-C), 122.0 (d, $J_{CH} = 159$ Hz, 4-C), 111.3 (m, $J_{CH} = 172$ Hz, $\eta^5\text{-C}_5\text{H}_5$ A), 110.0 (m, $J_{CH} = 172$ Hz, $\eta^5\text{-C}_5\text{H}_5$ B), 91.2 (d, $J_{CH} = 159$ Hz, 5-C), 56.7 (d, $J_{CH} = 131$ Hz, 2-C), 42.4 (d, $J_{CH} = 144$ Hz, 7-C), 41.2 (d, $J_{CH} = 130$ Hz, 8-C), 16.0 (t, $J_{CH} = 158$ Hz, 9-C).

Synthesis of $[\text{Cp}_2\text{Zr}\{\kappa^2\text{-N,C}^8\text{-(2-}i\text{-C}_3\text{H}_4\text{)-C}_5\text{D}_5\text{N}\}]$ (16-d₅**).**

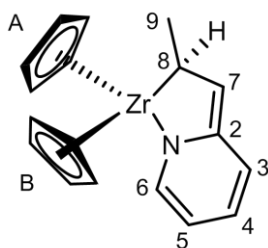


16-d₅

Compound **13** (100 mg, 0.33 mmol) was dissolved in 8 mL of cyclohexane, and pyridine- d_5 (0.40 mL, 4.7 mmol) was added. The mixture was heated at 40°C for 4 days to give a purple solution and a brown solid. The solvent was removed under reduced pressure and the residue was extracted with pentane. After evaporation of the solvent, the solid was crystallised from cold pentane at -40°C to yield **16-d₅** as dark purple crystals (16 mg, 0.046 mmol, 14%). This solid is air, moisture and temperature sensitive.

^1H NMR (benzene- d_6 , **298 K**) δ 5.85 (s, 5 H, $\eta^5\text{-C}_5\text{H}_5\text{B}$), 5.77 (s, 5 H, $\eta^5\text{-C}_5\text{H}_5\text{A}$), 1.73 (ddd, 1 H, $^3J_{HH} = 8.7, 7.1, 3.7$ Hz, $H\beta''$), 1.48 (ddd, 1 H, $^2J_{HH} = 8.4, ^3J_{HH} = 3.5$ Hz, $H\beta'$), 1.15 (m, 1H, $H\beta$), 0.28 (q, 1H, $^3J_{HH} = 9.6$ Hz, $H\alpha$). ^2H NMR (toluene- d_8 , **253 K**) δ 6.38 (s, 6-D), 6.09 (s, 4-D), 5.37 (s, 2-D), 5.24 (s, 3-D), 4.60 (s, 5-D).

Synthesis of $[\text{Cp}_2\text{Zr}\{\kappa^2\text{-N,C}^8\text{-(2-C}_3\text{H}_5\text{)-C}_5\text{H}_4\text{N}\}]$ (17**).**

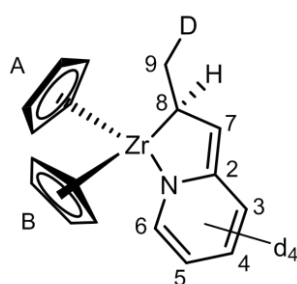


17

Compound **13** (148 mg, 0.487 mmol), NaH (0.6 mg, 0.024 mmol) and pyridine (1.7 mL, 21.1 mmol) were placed in a Schlenk flask. The mixture was heated to 45°C for 4 days to give a red solution. The volatiles were pumped off, and the resulting red powder was washed with pentane to afford **17** (160 mg, 0.470 mmol, 95% NMR). It was extracted with diethyl ether (1 mL), layered with pentane (4 mL), and the Schlenk flask was stored in the fridge at -40°C. After one week, red crystals suitable for XRD were isolated by filtration (45mg, 0.132 mmol, 27%). Anal. Calcd. for C₁₈H₁₉NZr: C 63.49, H 5.58 N 4.11. Found: C 63.26, H 5.66, N 4.35. **5** is air and moisture sensitive.

¹H NMR (toluene-d₈, **298 K**) δ 7.32 (d, 1 H, ³J_{HH} = 6.3 Hz, 6-H), 6.37 (d, 1 H, ³J_{HH} = 9.0 Hz, 3-H), 6.29 (dd, 1 H, ³J_{HH} = 8.7, 5.6 Hz, 4-H), 5.52 (s, 5H, η⁵-C₅H₅B), 5.40 (td, 1 H, ³J_{HH} = 6.0, ⁵J_{HH} = 1.1 Hz, 5-H), 5.01 (s, 5H, η⁵-C₅H₅A), 4.20 (d, 1 H, ³J_{HH} = 9.2 Hz, 7-H), 2.10 (d, 3 H, ³J_{HH} = 5.9 Hz, 9-H), -0.85 (dq, 1 H, ³J_{HH} = 9.6, 5.9 Hz, 8-H). ¹H NMR (toluene-d₈, **233 K**) δ 7.27 (d, 1 H, ³J_{HH} = 6.3 Hz, 6-H), 6.39 (m, 2 H, 3-H + 4-H), 5.46 (s, 6H, η⁵-C₅H₅B + 5-H), 4.92 (s, 5H, η⁵-C₅H₅A), 4.16 (d, 1 H, ³J_{HH} = 9.2 Hz, 7-H), 2.18 (d, 3 H, ³J_{HH} = 5.9 Hz, 9-H), -0.84 (dq, 1 H, ³J_{HH} = 9.6, 5.9 Hz, 8-H). ¹³C NMR (toluene-d₈, **233 K**) δ 146.7 (dt, ¹J_{CH} = 173, ³J_{CH} = 4.7 Hz, 6-C), 136.2 (s, 2-C), 128.1 (d, 4-C), 122.1 (d, ¹J_{CH} = 162 Hz, 3-C), 105.3 (dp, ¹J_{CH} = 171, ³J_{CH} = 7 Hz, η⁵-C₅H₅B), 103.5 (dtd, ¹J_{CH} = 164, ³J_{CH} = 6, 2 Hz, 5-C), 101.1 (dp, ¹J_{CH} = 171, ³J_{CH} = 7 Hz, η⁵-C₅H₅A), 93.3 (dd, ¹J_{CH} = 152, ³J_{CH} = 6 Hz, 7-C), 65.0 (dd, ¹J_{CH} = 129, ³J_{CH} = 6 Hz, 8-C), 22.2 (qd, ¹J_{CH} = 124.6, ³J_{CH} = 6 Hz, 9-C).

Synthesis of [Cp₂Zr{κ²-N,C⁸-(2-C₃H₄D)-C₅D₄N}] (**17-d₅**).

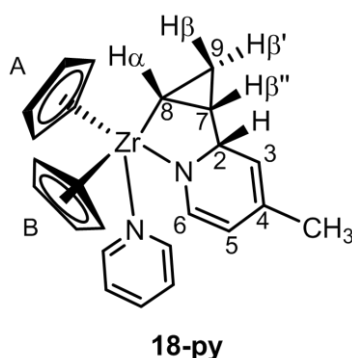


17-d₅

Compound **13** (46 mg, 0.15 mmol), NaH (0.2 mg, 0.008 mmol) and pyridine-d₅ (0.55 mL, 6.9 mmol) were mixed together in a NMR tube equipped with a J.S. Young valve. The mixture was heated to 45°C for 25 days to give a red solution of **17-d₅**. The reaction was monitored by ¹H NMR. The NMR tube was open in the glovebox to allow release of cyclopropane, *prior* to NMR analyses.

^1H NMR (pyridine- d_5 , 298 K) δ 5.95 (s, 5 H, $\eta^5\text{-C}_5\text{H}_5\text{B}$), 5.32 (s, 5 H, $\eta^5\text{-C}_5\text{H}_5\text{A}$), 4.51 (d, 1 H, $^3J_{\text{HH}} = 9.2$ Hz, 7-*H*), 2.17 (m, 2 H, 9-*H*), -0.67 (dt, 1 H, $^3J_{\text{HH}} = 9.3$, 5.8 Hz, 8-*H*). ^2H NMR (pyridine- d_5 , 298 K) δ 6.71 (s, 3-*D*), 6.56 (s, 4-*D*), 5.65 (s, 5-*D*), 2.13 (s, 9-*D*). ^{13}C NMR (pyridine- d_5 , 233 K) δ 147.1 (t, $^1J_{\text{CD}} = 26$ Hz, 6-*C*), 137.2 (s, 2-*C*), 128.5 (t, $^1J_{\text{CD}} = 24$ Hz, 4-*C*), 122.5 (t, $^1J_{\text{CD}} = 26$ Hz, 3-*C*), 106.4 (dp, $^1J_{\text{CH}} = 171$, $^3J_{\text{CH}} = 7$ Hz, $\eta^5\text{-C}_5\text{H}_5\text{B}$), 103.8 (t, $^1J_{\text{CD}} = 24$ Hz, 5-*C*), 102.2 (dp, $^1J_{\text{CH}} = 171$, $^3J_{\text{CH}} = 7$ Hz, $\eta^5\text{-C}_5\text{H}_5\text{A}$), 94.2 (dt, $^1J_{\text{CH}} = 152$, $^3J_{\text{CD}} = 6$ Hz, 7-*C*), 66.1 (dt, $^1J_{\text{CH}} = 129$, $^3J_{\text{CH}} = 6$ Hz, 8-*C*), 22.2 (td, $^1J_{\text{CD}} = 19$, $^3J_{\text{CH}} = 6$ Hz, 9-*C*).

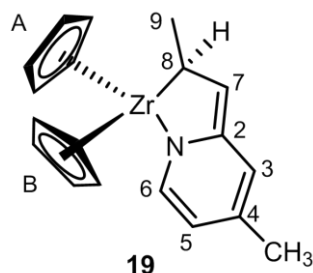
Synthesis of $[\text{Cp}_2\text{Zr}(\text{C}_5\text{H}_5\text{N})\{\kappa^2\text{-N,C}^8\text{-(2-*c*-C}_3\text{H}_4\text{)-(4-CH}_3\text{)C}_5\text{H}_4\text{N}\}]$ (18-py**).**



Compound **13** (159 mg, 0.52 mmol) was dissolved in 4-methylpyridine (1.5 mL, 15.3 mmol). The mixture was stirred at 45°C for 3 days to give a brown solution. The solvent was removed under vacuum and the residue was extracted with 1 mL of pyridine. This solution was then layered with pentane (6 mL) and stored at -40°C. After one week, brown crystals of **18-py** were collected by filtration (154 mg, 68%). This solid is air and moisture sensitive. Anal. Calcd. for $\text{C}_{24}\text{H}_{26}\text{N}_2\text{Zr}$: C 66.46, H 6.04, N 6.46. Found: C 66.17, H 6.24, N 6.51. **18-py** spontaneously loses its coordinated pyridine upon solubilisation in any other solvent than pyridine, and is therefore present in all the NMR spectra.

^1H NMR (benzene- d_6 , 298 K) δ 6.25 (d, 1 H, $^3J_{\text{HH}} = 7.0$ Hz, 6-*H*), 5.87 (s, 5 H, $\eta^5\text{-C}_5\text{H}_5\text{B}$), 5.78 (s, 5H, $\eta^5\text{-C}_5\text{H}_5\text{A}$), 5.31 (broad s, 1 H, 2-*H*), 4.88 (m, 1 H, 3-*H*), 4.42 (dd, 1 H, $^3J_{\text{HH}} = 7.0$ Hz, $^4J_{\text{HH}} = 1.6$ Hz, 5-*H*), 1.78 (t, 3 H, $^4J_{\text{HH}} = 1.5$ Hz, CH_3), 1.76 (m, 1 H, $\text{H}\beta''$), 1.44 (dt, 1 H, $^3J_{\text{HH}} = 8.4$, 3.6 Hz, $\text{H}\beta'$), 1.15 (ddd, 1 H, $^3J_{\text{HH}} = 3.3$, $\text{H}\beta$), 0.30 (q, 1 H, $^3J_{\text{HH}} = 8.5$ Hz, $\text{H}\alpha$). ^{13}C NMR (benzene- d_6 , 298 K) δ = 142.29 (d, $J_{\text{CH}} = 164$ Hz, 6-*C*), 129.4 (s, 4-*C*), 118.5 (d, $J_{\text{CH}} = 157$ Hz, 3-*C*), 111.5 (d, $J_{\text{CH}} = 172$ Hz, $\eta^5\text{-C}_5\text{H}_5\text{A}$), 110.3 (d, $J_{\text{CH}} = 172$ Hz, $\eta^5\text{-C}_5\text{H}_5\text{B}$), 95.4 (d, $J_{\text{CH}} = 161$ Hz, 5-*C*), 57.4 (d, $J_{\text{CH}} = 136$ Hz, 2-*C*), 42.3 (d, $J_{\text{CH}} = 144$ Hz, 8-*C*), 41.1 (d, $J_{\text{CH}} = 157$ Hz, 7-*C*), 21.5 (q, $J_{\text{CH}} = 125$ Hz, CH_3), 16.3 (t, $J_{\text{CH}} = 157$ Hz, 9-*C*).

Synthesis of $[\text{Cp}_2\text{Zr}\{\kappa^2\text{-N,C}^8\text{-(2-C}_3\text{H}_5\text{)-(4-CH}_3\text{)C}_5\text{H}_4\text{N}\}]$ (19**).**



Compound **13** (48 mg, 0.16 mmol), NaH (0.2 mg, 0.008 mmol) and 4-methylpyridine (0.55 mL, 5.7 mmol) were mixed together in a NMR tube equipped with a J.S. Young valve and a benzene- d_6 filled capillary. The mixture was heated to 45°C for 4 days to give a red solution which was dried under vacuum. The resulting red solid was washed with pentane to give **19** (NMR yield > 95%).

$^1\text{H NMR}$ (benzene- d_6 , **298 K**) δ 7.36 (d, 1 H, $^3J_{\text{HH}} = 6.3$ Hz, 6-*H*), 6.27 (s, 1 H, 3-*H*), 5.57 (s, 5 H, $\eta^5\text{-C}_5\text{H}_5\text{B}$), 5.37 (dd, 1 H, $^3J_{\text{HH}} = 6.3$, $^4J_{\text{HH}} = 1.5$ Hz, 5-*H*), 5.03 (s, 5 H, $\eta^5\text{-C}_5\text{H}_5\text{A}$), 4.23 (d, 1 H, $^3J_{\text{HH}} = 9.2$ Hz, 7-*H*), 2.16 (d, 3 H, $^3J_{\text{HH}} = 5.9$ Hz, 9-*H*), 1.86 (s, 3 H, CH_3), -0.66 (dq, 1 H, $^3J_{\text{HH}} = 9.2$, 5.9 Hz, 8-*H*). $^{13}\text{C NMR}$ (benzene- d_6 , **298 K**) δ 146.2 (dd, $^1J_{\text{CH}} = 172$, $^3J_{\text{CH}} = 3.6$ Hz, 6-*C*), 138.3 (q, $^3J_{\text{CH}} = 6.6$ Hz, 4-*C*), 137.8 (m, 2-*C*), 120.2 (dq, $^1J_{\text{CH}} = 158$, $^4J_{\text{CH}} = 4.5$ Hz, 3-*C*), 106.6 (dq, $^1J_{\text{CH}} = 163$, $^4J_{\text{CH}} = 6.3$ Hz, 5-*C*), 105.5 (dp, $^1J_{\text{CH}} = 171$, $^3J_{\text{CH}} = 6.8$ Hz, $\eta^5\text{-C}_5\text{H}_5\text{B}$), 101.4 (dp, $^1J_{\text{CH}} = 171$, $^3J_{\text{CH}} = 6.8$ Hz, $\eta^5\text{-C}_5\text{H}_5\text{A}$), 92.3 (dq, $^1J_{\text{CH}} = 152$, $^4J_{\text{CH}} = 5.7$, 2.1 Hz, 7-*C*), 65.9 (dq, $^1J_{\text{CH}} = 129$, $^3J_{\text{CH}} = 5.9$ Hz, 8-*C*), 22.4 (q, $^1J_{\text{CH}} = 124$ Hz, 9-*C*), 21.2 (q, $^1J_{\text{CH}} = 124$ Hz, CH_3).

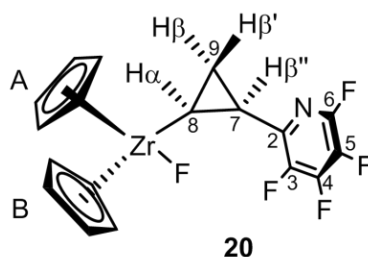
Synthesis of **17 from **16**.**

Compound **16** (18.5 mg, 54.3 μmol), NaH (0.2 mg, 8 μmol) and pyridine (0.6 mL) were placed in a NMR tube equipped with a J.S. Young valve and a capillary filled with benzene- d_6 . The mixture was heated to 45°C for 4 days to give a red solution of **17** (NMR yield > 95%).

Typical procedure for studies of the influence of the base (tmeda, *t*-BuOK, NaH) on the synthesis of **17.**

Compound **13** (50 mg, 0.16 mmol), the base (8 μmol) and pyridine (0.6 mL) were placed in a NMR tube equipped with a J.S. Young valve and a benzene- d_6 filled capillary. The mixture was heated to 45°C. The extent of the reaction was monitored by $^1\text{H NMR}$.

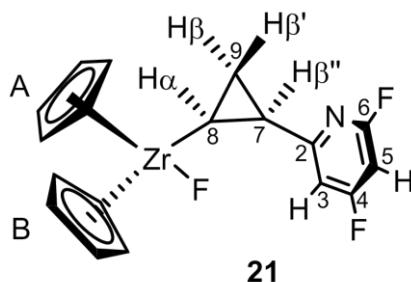
[Cp₂ZrF{(2-C₅F₄N)-*c*-C₃H₄}] (20).



Compound **13** (400 mg, 1.32 mmol) was dissolved in cyclohexane (4 mL) and pentafluoropyridine (2.28 g, 13.5 mmol) was added. The mixture was heated to 45°C for 3 days to give a beige suspension. The volatiles were removed under reduced pressure and the residue was extracted with toluene. After evaporation of the solvent and washing with pentane (3x1 mL), complex **20** was obtained as a beige solid (485 mg, 1.13 mmol, 85%). Anal. Calcd. for C₁₈H₁₄NF₅Zr: C 50.21; H 3.25, N 3.25. Found: C 50.28; H 3.30, N 3.10. Crystals suitable for XRD were obtained by cooling a concentrated toluene solution of **8** to -40°C.

¹H NMR (benzene-d₆, **298 K**) δ 5.82 (s, 5 H, η⁵-C₅H₅A), 5.76 (s, 5 H, η⁵-C₅H₅B), 2.42 (m, 1 H, Hβ'), 1.62 (ddd, 1 H, J_{HH} = 9.9, 4.2, 3.1 Hz, Hβ), 1.47 (ddd, 1 H, J_{HH} = 10.5, 7.5, 2.9 Hz, Hβ'), 0.12 (q, 1 H, J_{HH} = 10.1 Hz, Hα). ¹⁹F NMR. (benzene-d₆, **298 K**) δ 63.67 (s, 1 F, Zr-F), -86.48 (td, 1 F, J_{FF} = 25, 15 Hz, 6-F), -142.78 (dt, 1 F, J_{FF} = 20, 15 Hz, 4-F), -151.66 (dd, 1 F, J_{FF} = 26, 20 Hz, 3-F), -163.80 (dd, 1 F, J_{FF} = 26, 20 Hz, 5-F). ¹³C NMR (toluene-d₈, **223 K**) δ 146.8 (td, J_{CF} = 15, 6 Hz, 2-C), 146.5 (dd, J_{CF} = 232, 10.05 Hz, 6-C), 146.0 (d, J_{CF} = 266 Hz, 5-C), 144.9 (d, J_{CF} = 253 Hz, 4-C), 131.6 (ddd, J_{CF} = 263, 36, 12 Hz, 3-C), 112.9 (dq, J_{CH} = 173, 7 Hz, η⁵-C₅H₅A), 112.5 (dq, J_{CH} = 173, 7 Hz, η⁵-C₅H₅B), 38.1 (d, J_{CH} = 129 Hz, 8-C), 21.5 (d, J_{CH} = 162 Hz, 7-C), 21.0 (t, J_{CH} = 160 Hz, 9-C).

[Cp₂ZrF{(2-C₅F₂H₂N)-*c*-C₃H₄}] (21).

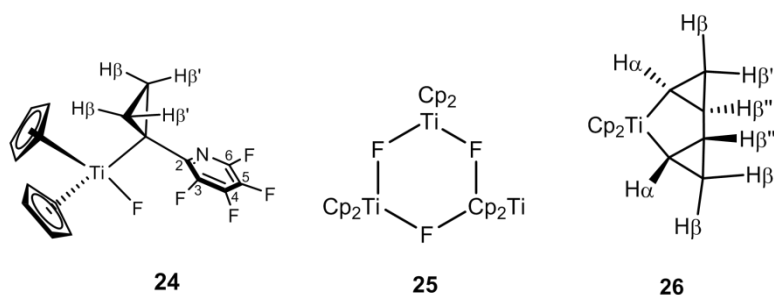


Compound **13** (154 mg, 0.51 mmol) was dissolved in cyclohexane (1.5 mL) and 2,4,6-trifluoropyridine (640 mg, 4.8 mmol) was added. The mixture was heated to 45°C for 3 days

to give a beige suspension. The volatiles were removed under reduced pressure and the residue was extracted with toluene (1 mL). Storage of the solution at -40°C for one week afforded **21** as beige crystals (122 mg, 0.31 mmol, 61%). Anal. Calcd. for $\text{C}_{18}\text{H}_{16}\text{NF}_3\text{Zr}$: C 54.80; H 4.09, N 3.55. Found: C 54.91; H 4.19, N 3.45. Crystals suitable for XRD were obtained directly from the reaction medium set up in a NMR tube.

^1H NMR (benzene- d_6 , **298 K**) δ 6.50 (d, 2 H, $J_{\text{HH}} = 9.2$ Hz, 3-*H*), 5.88 (s, 6 H, $\eta^5\text{-C}_5\text{H}_5\text{A} + 5\text{-H}$), 5.78 (s, 5 H, $\eta^5\text{-C}_5\text{H}_5\text{B}$), 2.30 (m, 1 H, $\text{H}\beta''$), 1.45 (ddd, 1 H, $J_{\text{HH}} = 10.5, 7.4, 3.3$ Hz, $\text{H}\beta$), 1.22 (dt, 1 H, $J_{\text{HH}} = 9.6, 3.7$ Hz, $\text{H}\beta'$), 0.00 (q, 1 H, $J_{\text{HH}} = 10.1$ Hz, $\text{H}\alpha$). ^{19}F NMR (benzene- d_6 , **298 K**) δ 59.64 (s, 1 F, Zr-*F*), -65.06 (d, 1 F, $J_{\text{FF}} = 21.9$ Hz, 6-*F*), -99.62 (dt, 1 F, $J_{\text{FF}} = 22.5$ Hz, $J_{\text{FH}} = 8.7$ Hz, 4-*F*). ^{13}C NMR (benzene- d_6 , **298 K**) δ 171.5 (ddt, $J_{\text{CF}} = 260, 13$ Hz, $J_{\text{CH}} = 5$ Hz, 4-*C*), 169.0 (dd, $J_{\text{CF}} = 17, 9$ Hz, 2-*C*), 164.5 (ddd, $J_{\text{CF}} = 235, 14$ Hz, $J_{\text{CH}} = 4$ Hz, 6-*C*), 113.1 (dp, $J_{\text{CH}} = 173, 6$ Hz, $\eta^5\text{-C}_5\text{H}_5\text{A}$), 112.6 (dp, $J_{\text{CH}} = 173, 6$ Hz, $\eta^5\text{-C}_5\text{H}_5\text{B}$), 106.8 (ddd, $J_{\text{CH}} = 168$ Hz, $J_{\text{CF}} = 18, 5$ Hz, 3-*C*), 93.4 (dddd, $J_{\text{CH}} = 172, 3$ Hz, $J_{\text{CF}} = 43, 23$ Hz, 5-*C*), 40.3 (d, $J_{\text{CH}} = 128$ Hz, 8-*C*), 29.8 (d, $J_{\text{CH}} = 160$ Hz, 7-*C*), 22.1 (t, $J_{\text{CH}} = 160$ Hz, 9-*C*).

[$\text{Cp}_2\text{TiF}\{(2\text{-C}_5\text{F}_4\text{N})\text{-}c\text{-C}_3\text{H}_4\}$] (**24**), [Cp_2TiF] (**25**) and [$\text{Cp}_2\text{Ti-}\kappa^2\text{-(C}_3\text{H}_4\text{-C}_3\text{H}_4)$] (**26**).



Compound **22** (150 mg, 0.58 mmol) was dissolved in cyclohexane (3 mL) and pentafluoropyridine (0.63 mL, 5.8 mmol) was added. The mixture was heated to 45°C for 4h to give a brown-orange slurry. The volatiles were removed under vacuum and the residue was washed with pentane several times to remove **26**. **24** crystallized from cold toluene with complex **25**. Elemental analysis data were collected by hand separation of the crystals of **24** and **25** under a microscope. To obtain the yield of **24** and **26**, the reaction between **22** and pentafluoropyridine was set up at 45°C in a NMR tube equipped with a J.S. young valve and

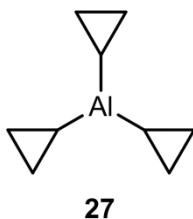
filled with cyclohexane- d_{12} . A benzene-filled capillary was introduced and used as an internal standard. The yields for **24** (44%) and **26** (20%) were determined by integration of the signals in the ^1H NMR spectrum. For **24** anal. Calcd. for $\text{C}_{18}\text{H}_{14}\text{F}_5\text{NTi}$: C 55.84; H 3.64; N 3.62. Found: C 56.54; H 3.53; N 3.44. Crystals of **24** suitable for XRD were obtained directly from the reaction medium set up in a NMR. Crystals of **25** suitable for XRD were obtained from a toluene solution of **24** and **25** stored at -40°C .

For 24: ^1H NMR (benzene- d_6 , 298 K) δ 5.91 (s, 10 H, $\eta^5\text{-C}_5\text{H}_5$), 1.49 (s, 2 H, $H\beta/\beta'$), 1.23 (s, 2 H, $H\beta/\beta'$). ^{19}F NMR (benzene- d_6 , 298 K) δ 156.59 (s, 1 F, Ti-F), -84.72 (td, 1 F, $J_{\text{FF}} = 28, 15$ Hz, 6-F), -141.39 (td, 1 F, $J_{\text{FF}} = 20, 15$ Hz, 4-F), -142.24 (dd, 1 F, $J_{\text{FF}} = 28, 20$ Hz, 3-F), -164.01 (dd, 1 F, $J_{\text{FF}} = 27, 20$ Hz, 5-F). ^{13}C NMR (benzene- d_6 , 298 K) δ 153.5 (m, 2-C), 146.8 (d, $J_{\text{CF}} = 263$ Hz, 5-C), 145.4 (d, $J_{\text{CF}} = 233$ Hz, 6-C), 143.7 (d, $J_{\text{CF}} = 255$ Hz, 4-C), 131.0 (ddd, $J_{\text{CF}} = 263, 36, 12$ Hz, 3-C), 116.1 (dp, $J_{\text{CH}} = 175, 5$ Hz, $\eta^5\text{-C}_5\text{H}_5$), 48.5 (s, C α), 23.0 (t, 2 C, $J_{\text{CH}} = 161$ Hz, C β).

For 25: ESR. A paramagnetic species was observed with $g = 1.983(4)$ and super hyperfine splitting constants of $A(^{47}\text{Ti}, 7.75\%, I = 5/2) = 9.2$ G, sextet and $A(^{49}\text{Ti}, 5.51\%, I = 7/2) = 8.6$ G, octet.

For 26: ^1H NMR (benzene- d_6 , 298 K) tentative assignment δ 5.82 (s, 10 H, $\eta^5\text{-C}_5\text{H}_5$), 1.45 (td, 2 H, $J_{\text{HH}} = 7.5, 3.4$ Hz, $H\beta/\beta'$), 1.37 (tdd, 2 H, $J_{\text{HH}} = 8.8, 3.2, 1.0$ Hz, $H\beta/\beta'$), 1.24 (tdd, 2H, $J_{\text{HH}} = 8.1, 3.5, 1.1$ Hz, $H\beta/\beta'$), 0.45 (tdd, 2 H, $J_{\text{HH}} 8.5, 8.0, 1.2$ Hz, $H\alpha$) ^{13}C NMR (benzene- d_6 , 298 K) δ 113.5 (d, $J_{\text{CH}} 174$ Hz, $\eta^5\text{-C}_5\text{H}_5$), 53.1 (d, $J_{\text{CH}} 146$ Hz, $\alpha\text{-CH}$), 28.5 (t, $J_{\text{CH}} 158$ Hz, $\beta\text{-CH}_2$), 21.6 (d, $J_{\text{CH}} 155$ Hz, $\beta\text{-CH}$).

$[(\text{c-C}_3\text{H}_5)_3\text{Al}]$ (27).

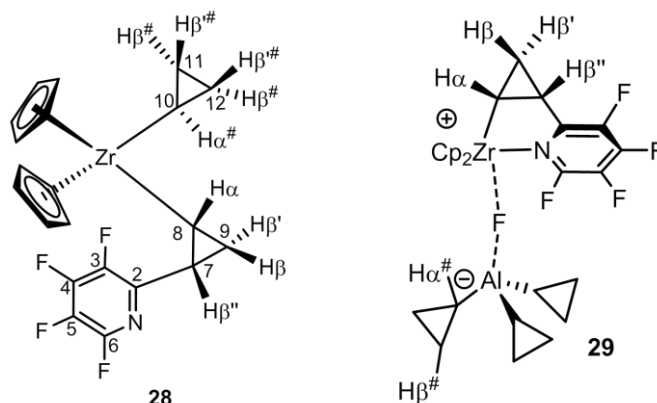


A solution of cyclopropylaluminum (13 mmol) in diethyl ether (20 mL) was added dropwise to a solution of aluminium trichloride (4.1 mmol, 551 mg) in the same solvent (8 mL) at -80°C . The mixture was allowed to warm up to RT and was stirred for 3 hours. It was

filtered and dried under high vacuum ($P < 10^{-4}$ mbar). The resulting yellow powder was sublimed to give **27** as white crystals (180 mg, 1.2 mmol, 30%, non-optimised yield).

Spectroscopic data (^1H and ^{13}C NMR) were identical to those reported previously.^{43,232,391}

[Cp₂Zr(*c*-C₃H₅){(2-C₅F₄N)-*c*-C₃H_{4}}] (**28**) and [Cp₂Zr(2-C₅F₄N)-*c*-C₃H₄]⁺[(μ -F)-(*c*-C₃H₅)₃Al]⁻ (**29**).}



The synthesis of these complexes has not been optimised yet. Compound **27** (45.5 mg, 0.30 mmol) and complex **20** (130 mg, 0.30 mmol) were dissolved in cyclohexane (6 mL). After a few minutes a white solid started to precipitate. The reaction mixture was stirred for one hour at RT, and the precipitate was collected by filtration. This solid is a mixture of complex **29** and [(*c*-C₃H₅)₂AlF]. The mother liquor was dried under vacuum, and washed with pentane to afford **28** as a beige solid (70 mg, 0.15 mmol, 50%). At RT, **29** spontaneously gives **28** and [(*c*-C₃H₅)₂AlF]. Crystals of **28** suitable for XRD were obtained by slow evaporation of a concentrated cyclohexane solution. Crystals of **29** suitable for XRD were obtained by layering a cold toluene solution (-40°C) with pentane. No elemental analysis has been recorded yet as a [(*c*-C₃H₅)₂AlF] co-precipitated during all the crystallisation attempts.

For 28: ^1H NMR (benzene-*d*₆, **298 K**) δ 5.90 (s, 5 H, η^5 -C₅H₅A), 5.59 (s, 5 H, η^5 -C₅H₅B), 2.26 (m, 1 H, H β ''), 1.33 (ddd, 1 H, $J_{\text{HH}} = 9.9, 4.2, 3.1$ Hz, H β), 1.23 (ddd, 1 H, $J_{\text{HH}} = 10.5, 7.5, 2.9$ Hz, H β ''), 0.84 (d, 2 H, $J_{\text{HH}} = 8.8$ Hz, H β ''), 0.38 (t, 2 H, $J_{\text{HH}} = 7.0$ Hz, H β ''), -0.35 (tt, 1 H, $J_{\text{HH}} = 9.8, 8.0$ Hz, H α ''), -1.08 (q, 1 H, $J_{\text{HH}} = 9.7$ Hz, H α). ^{19}F NMR (benzene-*d*₆, **298 K**) δ -87.19 (td, 1 F, $J_{\text{FF}} = 25, 15$ Hz, 6-F), -141.86 (dt, 1 F, $J_{\text{FF}} = 19, 14$ Hz, 4-F), -151.42 (dd, 1 F, $J_{\text{FF}} = 26, 20$ Hz, 3-F), -163.76 (dd, 1 F, $J_{\text{FF}} = 26, 20$ Hz, 5-F). ^{13}C NMR (toluene-*d*₈, **223 K**) δ 111.8 (dq, $J_{\text{CH}} = 172, 7$ Hz, η^5 -C₅H₅A), 110.6 (dp, $J_{\text{CH}} = 173, 7$

Hz, $\eta^5\text{-C}_5\text{H}_5\text{B}$), 44.7 (d, $J_{CH} = 122$ Hz, 8-C), 35.7 (d, $J_{CH} = 134$ Hz, 10-C), 23.5 (t, $J_{CH} = 162$ Hz, 9-C), 21.4 (d, $J_{CH} = 163$ Hz, 7-C), 12.1 (t, $J_{CH} = 158$ Hz, 11/12-C), 11.4 (t, $J_{CH} = 158$ Hz, 11/12-C).

29: ^1H NMR (benzene- d_6 , 298 K) δ 5.96 (bs, 10 H, $\eta^5\text{-C}_5\text{H}_5$), 2.25 (m, 1 H, $H\beta''$), 1.48 (ddd, 1 H, $J_{HH} = 10.1, 4.0, 2.6$ Hz, $H\beta$), 0.83 (d, 6 H, $J_{HH} = 10.0$ Hz, $H\beta^\#$), 0.71 (m, 6 H, $H\beta^\#$), 0.52 (bs, 1 H, $H\beta'$), 0.31 (q, 1 H, $J_{HH} = 9.2$ Hz, $H\alpha$), -0.95 (bs, 3 H, $H\alpha^\#$).

General Conclusion

The cyclopropyl ligand is a fascinating group, and through its prism we have presented the properties and reactivities of some Li, K, Ca, Ti, Zr and Al complexes. In Chapter 1, we described complexes where the cyclopropyl group was able to stabilise low coordinate Li^+ centres *via* rare agostic interactions with its C–C, rather than C–H, bonds. We were surprised to observe that this so-called weak interaction could compete with the coordination of donor bases in the solid state. In Chapter 2, we reported that the uniqueness of cyclopropyl allowed us to synthesise the first non-stabilised alkylcalcium compound. In Chapter 3, we have shown that using the cyclopropyl group as a ligand led to reactive complexes, able to dearomatise and activate the C–H bond of pyridine, and to cleave stronger C–F bonds. These results have complemented previous works on Nb cyclopropyl complexes, and have led to renewed interest in cyclopropyl complexes, regardless of the metal used.

I found it very interesting that my PhD work was divided in three different projects. It gave me the opportunity to learn about different fields of chemistry. I particularly enjoyed the contrast between studying new organocalcium chemistry and working on the well-known yet still surprising and promising organolithium and metallocene topics. Although I started by considering those projects as very different from each other, connections have emerged all throughout this work. I realised the importance of studying organometallic complexes of the alkaline and alkaline-earth metals, as they could be used to synthesise the group 4 complexes, which were in their turn used for the activation of small molecules. Hence, this work constitutes a good depiction of the link connecting fundamental studies to potential applications.

References

- 1 K. B. Wiberg, *Acc. Chem. Res.*, 1996, **29**, 229–234.
- 2 R. F. W. Bader, *Atoms in Molecules: A Quantum Theory*, Clarendon Press, Oxford England : New York, 1st Paperback Edition., 1994.
- 3 P. Chakrabarti, P. Seiler, J. D. Dunitz, A. D. Schluter and G. Szeimies, *J. Am. Chem. Soc.*, 1981, **103**, 7378–7380.
- 4 R. Boese, T. Miebach and A. de Meijere, *J. Am. Chem. Soc.*, 1991, **113**, 1743–1748.
- 5 R. J. Butcher and W. J. Jones, *J. Mol. Spectrosc.*, 1973, **47**, 64–83.
- 6 M. Etienne and A. S. Weller, *Chem. Soc. Rev.*, 2013, **43**, 242–259.
- 7 S. J. Blanksby and G. B. Ellison, *Acc. Chem. Res.*, 2003, **36**, 255–263.
- 8 A. de Meijere, *Angew. Chem. Int. Ed. Engl.*, 1979, **18**, 809–826.
- 9 A. D. Walsh, *Nature*, 1947, **159**, 712–713.
- 10 A. D. Walsh, *Trans. Faraday Soc.*, 1949, **45**, 179–190.
- 11 C. A. Coulson, *Valence*, Clarendon Press, Oxford, 2nd ed., 1961.
- 12 H. Günther, *NMR spectroscopy: an introduction*, Wiley, Chichester, 1980.
- 13 N. Muller and D. E. Pritchard, *J. Chem. Phys.*, 1959, **31**, 768–771.
- 14 N. F. Ramsey, *Phys. Rev.*, 1953, **91**, 303–307.
- 15 M. Stöcker, *Org. Magn. Reson.*, 1982, **20**, 175–179.
- 16 K. Frei and H. J. Bernstein, *J. Chem. Phys.*, 1963, **38**, 1216–1226.
- 17 D. Cremer, E. Kraka, A. Wu and W. Lüttke, *ChemPhysChem*, 2004, **5**, 349–366.
- 18 C. H. DePuy, S. Gronert, S. E. Barlow, V. M. Bierbaum and R. Damrauer, *J. Am. Chem. Soc.*, 1989, **111**, 1968–1973.
- 19 P. G. Wenthold, M. L. Polak and W. C. Lineberger, *J. Phys. Chem.*, 1996, **100**, 6920–6926.
- 20 J. B. Kim, P. G. Wenthold and W. C. Lineberger, *J. Phys. Chem. A*, 1999, **103**, 10833–10841.
- 21 D. Y.-K. Chen, R. H. Pouver and J.-A. Richard, *Chem. Soc. Rev.*, 2012, **41**, 4631–4642.
- 22 D. Arlt, M. Jautelat and R. Lantsch, *Angew. Chem. Int. Ed. Engl.*, 1981, **20**, 703–722.
- 23 A. G. M. Barrett, W. W. Doubleday, D. Hamprecht, K. Kasdorf, G. J. Tustin, A. J. P. White and D. J. Williams, *Chem. Commun.*, 1997, 1693–1700.
- 24 K. Yamada, M. Ojika and H. Kigoshi, *Nat. Prod. Rep.*, 2007, **24**, 798–813.
- 25 T. F. Schneider, J. Kaschel and D. B. Werz, *Angew. Chem. Int. Ed.*, 2014, **53**, 5504–5523.
- 26 H. Lebel, J.-F. Marcoux, C. Molinaro and A. B. Charette, *Chem. Rev.*, 2003, **103**, 977–1050.
- 27 C. F. H. Tipper, *J. Chem. Soc. Resumed*, 1955, 2045–2046.
- 28 K. Ruhland, *Eur. J. Org. Chem.*, 2012, **2012**, 2683–2706.
- 29 R. A. Periana and R. G. Bergman, *Organometallics*, 1984, **3**, 508–510.
- 30 R. A. Periana and R. G. Bergman, *J. Am. Chem. Soc.*, 1984, **106**, 7272–7273.
- 31 Y. Hu, N. Romero, C. Dinoi, L. Vendier, S. Mallet-Ladeira, J. E. McGrady, A. Locati, F. Maseras and M. Etienne, *Organometallics*, 2014, **33**, 7270–7278.
- 32 J. Jaffart, M. Etienne, M. Reinhold, J. E. McGrady and F. Maseras, *Chem. Commun.*, 2003, 876–877.
- 33 W. Noh and G. S. Girolami, *Inorg. Chem.*, 2008, **47**, 10682–10691.

- 34 D. F. Schafer, P. T. Wolczanski and E. B. Lobkovsky, *Organometallics*, 2011, **30**, 6518–6538.
- 35 W. A. Herrmann, F. E. Kühn, C. C. Romão, H. T. Huy, M. Wang, R. W. Fischer, P. Kiprof and W. Scherer, *Chem. Ber.*, 1993, **126**, 45–50.
- 36 C. Boulho, T. Keys, Y. Coppel, L. Vendier, M. Etienne, A. Locati, F. Bessac, F. Maseras, D. A. Pantazis and J. E. McGrady, *Organometallics*, 2009, **28**, 940–943.
- 37 M. A. Esteruelas, A. M. López, F. López, J. L. Mascareñas, S. Mozo, E. Oñate and L. Saya, *Organometallics*, 2013, **32**, 4851–4861.
- 38 P. N. Swepston, N. L. Jones, J. A. Ibers, S. Maoyu, H. Jinling and L. Jiayi, *Acta Crystallogr. Sect. C*, 1984, **40**, 39–41.
- 39 H. Lehmkuhl, C. Naydowski, R. Benn, A. Ruffinska, G. Schroth, R. Mynott and C. Krüger, *Chem. Ber.*, 1983, **116**, 2447–2465.
- 40 N. L. Jones and J. A. Ibers, *Organometallics*, 1982, **1**, 326–330.
- 41 E. G. Perevalova, I. G. Belesov, Y. T. Struchkov, I. F. Leschova, Y. S. Kalyuzhnaya, T. I. Voyevodskaya, Y. L. Slovokhotov and K. I. Granberg, *J. Organomet. Chem.*, 1985, **286**, 129–143.
- 42 C. A. Ogle, P. A. Riley, J. J. Dorchak and J. L. Hubbard, *J. Org. Chem.*, 1988, **53**, 4409–4412.
- 43 W. H. Ilsley, M. D. Glick, J. P. Oliver and J. W. Moore, *Inorg. Chem.*, 1980, **19**, 3572–3577.
- 44 F. Brady, K. Henrick and R. W. Matthews, *J. Organomet. Chem.*, 1979, **165**, 21–30.
- 45 D. V. Airapetyan, V. S. Petrosyan, S. V. Gruener, A. A. Korlyukov, D. E. Arkhipov, A. A. Bowden and K. V. Zaitsev, *Inorganica Chim. Acta*, 2015, **432**, 142–148.
- 46 K. Ruhlandt-Senge, K. W. Henderson and P. C. Andrews, in *Comprehensive Organometallic Chemistry III*, ed. R. H. Crabtree, Elsevier, Oxford, 2007, pp. 1–65.
- 47 A. Harrison-Marchand and F. Mongin, *Chem. Rev.*, 2013, **113**, 7470–7562.
- 48 W. Schlenk and J. Holtz, *Berichte Dtsch. Chem. Ges.*, 1917, **50**, 262–274.
- 49 A. Bondi, *J. Phys. Chem.*, 1964, **68**, 441–451.
- 50 R. D. Shannon, *Acta Crystallogr. Sect. A*, 1976, **32**, 751–767.
- 51 P. v. R. Schleyer, *Pure Appl. Chem.*, 2009, **56**, 151–162.
- 52 W. N. Setzer and P. v. R. Schleyer, in *Advances in Organometallic Chemistry*, ed. F. G. A. S. and R. West, Academic Press, 1985, vol. 24, pp. 353–451.
- 53 E. Kaufmann, K. Raghavachari, A. E. Reed and P. v. R. Schleyer, *Organometallics*, 1988, **7**, 1597–1607.
- 54 R. J. Bushby and H. L. Steel, *J. Organomet. Chem.*, 1987, **336**, C25–C32.
- 55 R. J. Bushby and H. L. Steel, *J. Chem. Soc. Perkin Trans. 2*, 1990, 1169–1176.
- 56 C. Lambert and P. v. R. Schleyer, *Angew. Chem. Int. Ed. Engl.*, 1994, **33**, 1129–1140.
- 57 E. D. Jemmis, J. Chandrasekhar and P. v. R. Schleyer, *J. Am. Chem. Soc.*, 1979, **101**, 2848–2856.
- 58 A. Streitwieser, J. E. Williams, S. Alexandratos and J. M. McKelvey, *J. Am. Chem. Soc.*, 1976, **98**, 4778–4784.
- 59 A. Streitwieser, *J. Organomet. Chem.*, 1978, **156**, 1–3.
- 60 W. Scherer, P. Sirsch, M. Grosche, M. Spiegler, S. A. Mason and M. G. Gardiner, *Chem. Commun.*, 2001, 2072–2073.
- 61 H. Ott, C. Däschlein, D. Leusser, D. Schildbach, T. Seibel, D. Stalke and C. Strohmam, *J. Am. Chem. Soc.*, 2008, **130**, 11901–11911.
- 62 E. Weiss and E. A. C. Lucken, *J. Organomet. Chem.*, 1964, **2**, 197–205.
- 63 E. Weiss and G. Hencken, *J. Organomet. Chem.*, 1970, **21**, 265–268.
- 64 T. Kottke and D. Stalke, *Angew. Chem. Int. Ed. Engl.*, 1993, **32**, 580–582.

- 65 E. Weiss, T. Lambertsen, B. Schubert, J. K. Cockcroft and A. Wiedenmann, *Chem. Ber.*, 1990, **123**, 79–81.
- 66 V. H. Gessner and C. Strohmann, *J. Am. Chem. Soc.*, 2008, **130**, 14412–14413.
- 67 V. H. Gessner, C. Däschlein and C. Strohmann, *Chem. – Eur. J.*, 2009, **15**, 3320–3334.
- 68 R. D. Thomas, R. M. Jensen and T. C. Young, *Organometallics*, 1987, **6**, 565–571.
- 69 R. D. Thomas, M. T. Clarke and T. C. Young, *J. Organomet. Chem.*, 1987, **328**, 239–248.
- 70 C. Su, R. Hopson and P. G. Williard, *Eur. J. Inorg. Chem.*, 2013, **2013**, 4136–4141.
- 71 W. Bauer, W. R. Winchester and P. v. R. Schleyer, *Organometallics*, 1987, **6**, 2371–2379.
- 72 P. West and R. Waack, *J. Am. Chem. Soc.*, 1967, **89**, 4395–4399.
- 73 B. Qu and D. B. Collum, *J. Am. Chem. Soc.*, 2006, **128**, 9355–9360.
- 74 R. E. Dinnebier, U. Behrens and F. Olbrich, *J. Am. Chem. Soc.*, 1998, **120**, 1430–1433.
- 75 H. Hope and P. P. Power, *J. Am. Chem. Soc.*, 1983, **105**, 5320–5324.
- 76 D. Thoennes and E. Weiss, *Chem. Ber.*, 1978, **111**, 3157–3161.
- 77 U. Schümann, J. Kopf and E. Weiss, *Angew. Chem. Int. Ed. Engl.*, 1985, **24**, 215–216.
- 78 M. B. Smith, in *March's Advanced Organic Chemistry: Reactions, Mechanisms, and Structure*, John Wiley & Sons, 2013, pp. 312–343.
- 79 W. N. SMITH, in *Polyamine-Chelated Alkali Metal Compounds*, AMERICAN CHEMICAL SOCIETY, 1974, vol. 130, pp. 23–55.
- 80 R. B. Bates, L. M. Kroposki and D. E. Potter, *J. Org. Chem.*, 1972, **37**, 560–562.
- 81 J. Clayden and S. A. Yasin, *New J. Chem.*, 2002, **26**, 191–192.
- 82 F. H. Köhler, N. Hertkorn and J. Blümel, *Chem. Ber.*, 1987, **120**, 2081–2082.
- 83 S. Harder and M. Lutz, *Organometallics*, 1994, **13**, 5173–5176.
- 84 C. Strohmann and V. H. Gessner, *Angew. Chem. Int. Ed.*, 2007, **46**, 4566–4569.
- 85 B. Conway, A. R. Kennedy, R. E. Mulvey, S. D. Robertson and J. G. Álvarez, *Angew. Chem. Int. Ed.*, 2010, **49**, 3182–3184.
- 86 H. L. Lewis and T. L. Brown, *J. Am. Chem. Soc.*, 1970, **92**, 4664–4670.
- 87 G. Fraenkel, M. Henrichs, J. M. Hewitt, B. M. Su and M. J. Geckle, *J. Am. Chem. Soc.*, 1980, **102**, 3345–3350.
- 88 J. F. McGarrity and C. A. Ogle, *J. Am. Chem. Soc.*, 1985, **107**, 1805–1810.
- 89 L. M. Jackman and L. M. Scarmoutzos, *J. Am. Chem. Soc.*, 1984, **106**, 4627–4629.
- 90 H. J. Reich, D. P. Green, M. A. Medina, W. S. Goldenberg, B. Ö. Gudmundsson, R. R. Dykstra and N. H. Phillips, *J. Am. Chem. Soc.*, 1998, **120**, 7201–7210.
- 91 M. Brookhart, M. L. H. Green and L.-L. Wong, in *Progress in Inorganic Chemistry*, ed. S. J. Lippard, John Wiley & Sons, Inc., 1988, pp. 1–124.
- 92 D. R. Armstrong, R. E. Mulvey, G. T. Walker, D. Barr, R. Snaith, W. Clegg and D. Reed, *J. Chem. Soc. Dalton Trans.*, 1988, 617–628.
- 93 K. Ruhlandt-Senge, J. J. Ellison, R. J. Wehmschulte, F. Pauer and P. P. Power, *J. Am. Chem. Soc.*, 1993, **115**, 11353–11357.
- 94 B. Schiemenz and P. P. Power, *Angew. Chem. Int. Ed. Engl.*, 1996, **35**, 2150–2152.
- 95 S. Duttwyler, Q.-Q. Do, A. Linden, K. K. Baldridge and J. S. Siegel, *Angew. Chem. Int. Ed.*, 2008, **47**, 1719–1722.
- 96 W. Scherer and G. S. McGrady, *Angew. Chem. Int. Ed.*, 2004, **43**, 1782–1806.
- 97 D. Braga, F. Grepioni, K. Biradha and G. R. Desiraju, *J. Chem. Soc. Dalton Trans.*, 1996, 3925–3930.
- 98 R. Zerger, W. Rhine and G. Stucky, *J. Am. Chem. Soc.*, 1974, **96**, 6048–6055.

- 99 J. L. Wardell, in *Comprehensive Organometallic Chemistry*, eds. F. G. A. Stone and E. W. Abel, Pergamon, Oxford, 1982, pp. 43–120.
- 100 G. D. Stucky, M. M. Eddy, W. H. Harrison, R. Lagow, H. Kawa and D. E. Cox, *J. Am. Chem. Soc.*, 1990, **112**, 2425–2427.
- 101 K. N. Houk, N. G. Rondan, P. v. R. Schleyer, E. Kaufmann and T. Clark, *J. Am. Chem. Soc.*, 1985, **107**, 2821–2823.
- 102 U. Siemeling, T. Redecker, B. Neumann and H.-G. Stammer, *J. Am. Chem. Soc.*, 1994, **116**, 5507–5508.
- 103 C. Boulho, T. Keys, Y. Coppel, L. Vendier, M. Etienne, A. Locati, F. Bessac, F. Maseras, D. A. Pantazis and J. E. McGrady, *Organometallics*, 2009, **28**, 940–943.
- 104 D. Seebach, R. Hässig and J. Gabriel, *Helv. Chim. Acta*, 1983, **66**, 308–337.
- 105 B. Goldfuss, P. von R. Schleyer and F. Hampel, *J. Am. Chem. Soc.*, 1996, **118**, 12183–12189.
- 106 Y. Escudié, C. Dinoi, O. Allen, L. Vendier and M. Etienne, *Angew. Chem. Int. Ed.*, 2012, **51**, 2461–2464.
- 107 C. A. Ogle, B. K. Huckabee, H. C. Johnson, P. F. Sims, S. D. Winslow and A. A. Pinkerton, *Organometallics*, 1993, **12**, 1960–1963.
- 108 M. A. Nichols and P. G. Williard, *J. Am. Chem. Soc.*, 1993, **115**, 1568–1572.
- 109 C. Strohmman, V. H. Gessner and A. Damme, *Chem. Commun.*, 2008, 3381–3383.
- 110 C. Su, R. Hopson and P. G. Williard, *J. Am. Chem. Soc.*, 2013, **135**, 12400–12406.
- 111 R. P. Zerger and G. D. Stucky, *J. Chem. Soc. Chem. Commun.*, 1973, 44–45.
- 112 W. Hollstein, K. Harms, M. Marsch and G. Boche, *Angew. Chem. Int. Ed. Engl.*, 1988, **27**, 846–847.
- 113 A. Sekiguchi and M. Tanaka, *J. Am. Chem. Soc.*, 2003, **125**, 12684–12685.
- 114 D. Seyferth and H. M. Cohen, *Inorg. Chem.*, 1963, **2**, 625–629.
- 115 D. Seyferth and H. M. Cohen, *J. Organomet. Chem.*, 1963, **1**, 15–21.
- 116 H. Schmidbaur, A. Schier and U. Schubert, *Chem. Ber.*, 1983, **116**, 1938–1946.
- 117 F. G. Bordwell, *Acc. Chem. Res.*, 1988, **21**, 456–463.
- 118 A. Streitwieser, L. Xie, P. Wang and S. M. Bachrach, *J. Org. Chem.*, 1993, **58**, 1778–1784.
- 119 B. Teclé, A. F. M. Maq sudur Rahman and J. P. Oliver, *J. Organomet. Chem.*, 1986, **317**, 267–275.
- 120 M. F. Lappert, L. M. Engelhardt, C. L. Raston and A. H. White, *J. Chem. Soc. Chem. Commun.*, 1982, 1323–1324.
- 121 C. Eaborn, P. B. Hitchcock, J. D. Smith and A. C. Sullivan, *J. Chem. Soc. Chem. Commun.*, 1983, 827–828.
- 122 S. Halazy, W. Dumont and A. Krief, *Tetrahedron Lett.*, 1981, **22**, 4737–4740.
- 123 L. A. Paquette, K. A. Horn and G. J. Wells, *Tetrahedron Lett.*, 1982, **23**, 259–262.
- 124 L. A. Paquette, G. J. Wells, K. A. Horn and T.-H. Yan, *Tetrahedron*, 1983, **39**, 913–924.
- 125 L. A. Paquette, *Chem. Rev.*, 1986, **86**, 733–750.
- 126 B. Schiemenz and P. P. Power, *Organometallics*, 1996, **15**, 958–964.
- 127 F. Antolini, P. B. Hitchcock, M. F. Lappert and X.-H. Wei, *Organometallics*, 2003, **22**, 2505–2516.
- 128 N. J. Hardman, R. J. Wright, A. D. Phillips and P. P. Power, *J. Am. Chem. Soc.*, 2003, **125**, 2667–2679.
- 129 T. Tatic, S. Hermann, M. John, A. Loquet, A. Lange and D. Stalke, *Angew. Chem. Int. Ed.*, 2011, **50**, 6666–6669.
- 130 D. R. Baker, W. Clegg, L. Horsburgh and R. E. Mulvey, *Organometallics*, 1994, **13**, 4170–4172.

- 131 C. Schade, P. v. R. Schleyer, H. Dietrich and W. Mahdi, *J. Am. Chem. Soc.*, 1986, **108**, 2484–2485.
- 132 D. Bojer, I. Kamps, X. Tian, A. Hepp, T. Pape, R. Fröhlich and N. W. Mitzel, *Angew. Chem. Int. Ed.*, 2007, **46**, 4176–4179.
- 133 C. Eaborn, Z.-R. Lu, P. B. Hitchcock and J. D. Smith, *Organometallics*, 1996, **15**, 1651–1655.
- 134 S. S. Al-Juaid, A. G. Avent, C. Eaborn, S. M. El-Hamruni, S. A. Hawkes, M. S. Hill, M. Hopman, P. B. Hitchcock and J. D. Smith, *J. Organomet. Chem.*, 2001, **631**, 76–86.
- 135 K. Izod, C. Wills, W. Clegg and R. W. Harrington, *Organometallics*, 2006, **25**, 38–40.
- 136 M. S. Hill and P. B. Hitchcock, *Organometallics*, 2002, **21**, 220–225.
- 137 D. Li, I. Keresztes, R. Hopson and P. G. Williard, *Acc. Chem. Res.*, 2009, **42**, 270–280.
- 138 S. P. Patterman, I. L. Karle and G. D. Stucky, *J. Am. Chem. Soc.*, 1970, **92**, 1150–1157.
- 139 M. A. Beno, H. Hope, M. M. Olmstead and P. P. Power, *Organometallics*, 1985, **4**, 2117–2121.
- 140 M. Hage, C. A. Ogle, T. L. Rathman and J. L. Hubbard, *Main Group Met. Chem.*, 2011, **21**, 777–782.
- 141 W. Zarges, M. Marsch, K. Harms and G. Boche, *Chem. Ber.*, 1989, **122**, 2303–2309.
- 142 J. Arnold, V. Knapp, J. A. R. Schmidt and A. Shafir, *J. Chem. Soc. Dalton Trans.*, 2002, 3273–3274.
- 143 M. G. Davidson, D. Garcia-Vivo, A. R. Kennedy, R. E. Mulvey and S. D. Robertson, *Chem. – Eur. J.*, 2011, **17**, 3364–3369.
- 144 J. J. Brooks and G. D. Stucky, *J. Am. Chem. Soc.*, 1972, **94**, 7333–7338.
- 145 R. A. Bartlett, H. V. R. Dias and P. P. Power, *J. Organomet. Chem.*, 1988, **341**, 1–9.
- 146 S. Schade and G. Boche, *J. Organomet. Chem.*, 1998, **550**, 359–379.
- 147 S. Schade and G. Boche, *J. Organomet. Chem.*, 1998, **550**, 381–395.
- 148 M. Kühnen, H. Günther, J.-P. Amoureux and C. Fernández, *Magn. Reson. Chem.*, 2002, **40**, 24–30.
- 149 L. Lochmann, J. Pospíšil and D. Lim, *Tetrahedron Lett.*, 1966, **7**, 257–262.
- 150 L. Lochmann and J. Trekoval, *J. Organomet. Chem.*, 1987, **326**, 1–7.
- 151 M. Schlosser, *Pure Appl. Chem.*, 2009, **60**, 1627–1634.
- 152 M. Schlosser and P. Schneider, *Helv. Chim. Acta*, 1980, **63**, 2404–2410.
- 153 F. Becke, F. W. Heinemann, T. Rüffer, P. Wiegeleben, R. Boese, D. Bläser and D. Steinborn, *J. Organomet. Chem.*, 1997, **548**, 205–210.
- 154 S. Bywater and D. J. Worsfold, *J. Organomet. Chem.*, 1971, **33**, 273–279.
- 155 M. Witanowski and J. D. Roberts, *J. Am. Chem. Soc.*, 1966, **88**, 737–741.
- 156 G. Fraenkel, W. E. Beckenbaugh and P. P. Yang, *J. Am. Chem. Soc.*, 1976, **98**, 6878–6885.
- 157 G. Köbrich, D. Merkel and K. Imkampe, *Chem. Ber.*, 1973, **106**, 2017–2024.
- 158 M. P. Periasamy and H. M. Walborsky, *J. Am. Chem. Soc.*, 1977, **99**, 2631–2638.
- 159 P. R. Peoples and J. B. Grutzner, *J. Am. Chem. Soc.*, 1980, **102**, 4709–4715.
- 160 P. C. Andrews, W. Clegg and R. E. Mulvey, *Angew. Chem. Int. Ed. Engl.*, 1990, **29**, 1440–1441.
- 161 D. R. Armstrong, D. Barr, W. Clegg, R. E. Mulvey, D. Reed, R. Snaith and K. Wade, *J. Chem. Soc. Chem. Commun.*, 1986, 869–870.
- 162 D. R. Armstrong, D. Barr, W. Clegg, S. M. Hodgson, R. E. Mulvey, D. Reed, R. Snaith and D. S. Wright, *J. Am. Chem. Soc.*, 1989, **111**, 4719–4727.
- 163 M. Linnert, C. Bruhn, T. Rüffer, H. Schmidt and D. Steinborn, *Organometallics*, 2004, **23**, 3668–3673.

- 164 W. Bauer, P. A. A. Klusener, S. Harder, J. A. Kanters, A. J. M. Duisenberg, L. Brandsma and P. v. R. Schleyer, *Organometallics*, 1988, **7**, 552–555.
- 165 A. Altomare, G. Cascarano, C. Giacovazzo and A. Guagliardi, *J. Appl. Crystallogr.*, 1993, **26**, 343–350.
- 166 SHELX97 [Includes SHELXS97, SHELXL97, CIFTAB]-Programs for Crystal Structure Analysis (Release 97-2). G. M. Sheldrick, Institut für Anorganische Chemie der Universität, Tammanstrasse 4, D-3400 Göttingen, Germany, 1998.
- 167 L. J. Farrugia, *J. Appl. Crystallogr.*, 1999, **32**, 837–838.
- 168 Gaussian 09, Revision D.01, M. J. Frisch, G. W. Trucks, H. B. Schlegel, G. E. Scuseria, M. A. Robb, J. R. Cheeseman, G. Scalmani, V. Barone, B. Mennucci, G. A. Petersson, H. Nakatsuji, M. Caricato, X. Li, H. P. Hratchian, A. F. Izmaylov, J. Bloino, G. Zheng, J. L. Sonnenberg, M. Hada, M. Ehara, K. Toyota, R. Fukuda, J. Hasegawa, M. Ishida, T. Nakajima, Y. Honda, O. Kitao, H. Nakai, T. Vreven, J. A. Montgomery, Jr., J. E. Peralta, F. Ogliaro, M. Bearpark, J. J. Heyd, E. Brothers, K. N. Kudin, V. N. Staroverov, T. Keith, R. Kobayashi, J. Normand, K. Raghavachari, A. Rendell, J. C. Burant, S. S. Iyengar, J. Tomasi, M. Cossi, N. Rega, J. M. Millam, M. Klene, J. E. Knox, J. B. Cross, V. Bakken, C. Adamo, J. Jaramillo, R. Gomperts, R. E. Stratmann, O. Yazyev, A. J. Austin, R. Cammi, C. Pomelli, J. W. Ochterski, R. L. Martin, K. Morokuma, V. G. Zakrzewski, G. A. Voth, P. Salvador, J. J. Dannenberg, S. Dapprich, A. D. Daniels, O. Farkas, J. B. Foresman, J. V. Ortiz, J. Cioslowski, D. J. Fox, Gaussian, Inc., Wallingford CT, 2013.
- 169 F. Weigend and R. Ahlrichs, *Phys. Chem. Chem. Phys.*, 2005, **7**, 3297–3305.
- 170 M. Schindler and W. Kutzelnigg, *J. Chem. Phys.*, 1982, **76**, 1919–1933.
- 171 NBO 6.0. E. D. Glendening, J. K. Badenhoop, A. E. Reed, J. E. Carpenter, J. A. Bohmann, C. M. Morales, C. R. Landis, and F. Weinhold, Theoretical Chemistry Institute, University of Wisconsin, Madison (2013).
- 172 H. Breuer, M. Meslé-Gribenski, P. Morin, M. Sénéchal-Couvercelle and C. Morin, *Atlas de la chimie*, Librairie générale française, Paris, 2000.
- 173 A. L. Allred and E. G. Rochow, *J. Inorg. Nucl. Chem.*, 1958, **5**, 264–268.
- 174 M. Westerhausen, *Z. Für Anorg. Allg. Chem.*, 2009, **635**, 13–32.
- 175 S. Harder, *Chem. Rev.*, 2010, **110**, 3852–3876.
- 176 W. D. Buchanan, D. G. Allis and K. Ruhlandt-Senge, *Chem. Commun.*, 2010, **46**, 4449–4465.
- 177 S. Harder and J. F. Carpentier, Eds., *Alkaline-earth metal compounds: oddities and applications*, Springer, Berlin, 2013.
- 178 M. S. Hill, D. J. Liptrot and C. Weetman, *Chem. Soc. Rev.*, 2016, **45**, 972–988.
- 179 V. Grignard, *Comptes Rendus Hebd. Séances Académie Sci.*, 1900, **130**, 1322–1324.
- 180 F. G. N. Cloke, P. B. Hitchcock, M. F. Lappert, G. A. Lawless and B. Royo, *J. Chem. Soc. Chem. Commun.*, 1991, 724–726.
- 181 F. Feil and S. Harder, *Organometallics*, 2000, **19**, 5010–5015.
- 182 S. Harder, S. Müller and E. Hübner, *Organometallics*, 2004, **23**, 178–183.
- 183 S. Kriek, H. Görls and M. Westerhausen, *J. Am. Chem. Soc.*, 2010, **132**, 12492–12501.
- 184 P. Jochmann, J. P. Davin, T. P. Spaniol, L. Maron and J. Okuda, *Angew. Chem. Int. Ed.*, 2012, **51**, 4452–4455.
- 185 L. Orzechowski, G. Jansen, M. Lutz and S. Harder, *Dalton Trans.*, 2009, 2958–2964.
- 186 M. A. Guino-o, C. F. Campana and K. Ruhlandt-Senge, *Chem. Commun.*, 2008, 1692–1694.
- 187 T. K. Panda, K. Yamamoto, K. Yamamoto, H. Kaneko, Y. Yang, H. Tsurugi and K. Mashima, *Organometallics*, 2012, **31**, 2268–2274.
- 188 L. Orzechowski and S. Harder, *Organometallics*, 2007, **26**, 2144–2148.

- 189 M. J. Harvey, T. P. Hanusa and V. G. Young, Jr., *Angew. Chem. Int. Ed.*, 1999, **38**, 217–219.
- 190 P. Jochmann, T. S. Dols, T. P. Spaniol, L. Perrin, L. Maron and J. Okuda, *Angew. Chem. Int. Ed.*, 2009, **48**, 5715–5719.
- 191 P. Jochmann, T. P. Spaniol, S. C. Chmely, T. P. Hanusa and J. Okuda, *Organometallics*, 2011, **30**, 5291–5296.
- 192 C. Eaborn and P. B. Hitchcock, *Chem. Commun.*, 1997, 1961–1962.
- 193 K. Yan, B. M. Upton, A. Ellern and A. D. Sadow, *J. Am. Chem. Soc.*, 2009, **131**, 15110–15111.
- 194 K. Yan, G. Schoendorff, B. M. Upton, A. Ellern, T. L. Windus and A. D. Sadow, *Organometallics*, 2013, **32**, 1300–1316.
- 195 M. R. Crimmin, A. G. M. Barrett, M. S. Hill, D. J. MacDougall, M. F. Mahon and P. A. Procopiou, *Chem. – Eur. J.*, 2008, **14**, 11292–11295.
- 196 S. R. Neal, A. Ellern and A. D. Sadow, *J. Organomet. Chem.*, 2011, **696**, 228–234.
- 197 M. Arrowsmith, M. S. Hill and G. Kociok-Köhn, *Organometallics*, 2011, **30**, 1291–1294.
- 198 M. Arrowsmith, M. S. Hill and G. Kociok-Köhn, *Organometallics*, 2014, **33**, 206–216.
- 199 B. Liu, T. Roisnel, J.-F. Carpentier and Y. Sarazin, *Chem. – Eur. J.*, 2013, **19**, 13445–13462.
- 200 S. R. Drake and D. J. Otway, *J. Chem. Soc. Chem. Commun.*, 1991, 517–519.
- 201 S. R. Drake and D. J. Otway, *J. Chem. Soc. Chem. Commun.*, 1991, 1060–1060.
- 202 J. Evers, A. Weiss, E. Kaldis and J. Muheim, *J. Common Met.*, 1973, **30**, 83–95.
- 203 R. D. Rieke, *Science*, 1989, **246**, 1260–1264.
- 204 M. J. McCormick, K. B. Moon, S. R. Jones and T. P. Hanusa, *J. Chem. Soc. Chem. Commun.*, 1990, 778–779.
- 205 B. Bogdanović, N. Janke, H.-G. Kinzelmann and U. Westeppe, *Chem. Ber.*, 1988, **121**, 33–37.
- 206 H. Bönnemann, B. Bogdanović, R. Brinkmann, N. Egeler, R. Benn, I. Topalović and K. Seevogel, *Main Group Met. Chem.*, 1990, **13**, 341–362.
- 207 T. C. Wu, H. Xiong and R. D. Rieke, *J. Org. Chem.*, 1990, **55**, 5045–5051.
- 208 R. Fischer, M. Gärtner, H. Görls and M. Westerhausen, *Angew. Chem. Int. Ed.*, 2006, **45**, 609–612.
- 209 R. Fischer, M. Gärtner, H. Görls and M. Westerhausen, *Organometallics*, 2006, **25**, 3496–3500.
- 210 S. Kriek and M. Westerhausen, *Chem. Unserer Zeit*, 2009, **43**, 384–390.
- 211 M. Gärtner, H. Görls and M. Westerhausen, *Synthesis*, 2007, **2007**, 725–730.
- 212 M. Westerhausen, M. Gärtner, R. Fischer and J. Langer, *Angew. Chem. Int. Ed.*, 2007, **46**, 1950–1956.
- 213 M. Gärtner, H. Görls and M. Westerhausen, *Organometallics*, 2007, **26**, 1077–1083.
- 214 J. Langer, H. Görls and M. Westerhausen, *Inorg. Chem. Commun.*, 2007, **10**, 853–855.
- 215 M. Gärtner, H. Görls and M. Westerhausen, *J. Organomet. Chem.*, 2008, **693**, 221–227.
- 216 M. Köhler, J. Langer, H. Görls and M. Westerhausen, *Organometallics*, 2012, **31**, 8647–8653.
- 217 J. Langer, M. Köhler, R. Fischer, F. Dündar, H. Görls and M. Westerhausen, *Organometallics*, 2012, **31**, 6172–6182.
- 218 M. Köhler, J. Langer, R. Fischer, H. Görls and M. Westerhausen, *Chem. – Eur. J.*, 2013, **19**, 10497–10500.

- 219 J. Langer, S. Kriek, H. Görls and M. Westerhausen, *Angew. Chem. Int. Ed.*, 2009, **48**, 5741–5744.
- 220 J. Langer, M. Köhler, H. Görls and M. Westerhausen, *Chem. – Eur. J.*, 2014, **20**, 3154–3161.
- 221 S.-O. Hauber, F. Lissner, G. B. Deacon and M. Niemeyer, *Angew. Chem. Int. Ed.*, 2005, **44**, 5871–5875.
- 222 K. Mashima, H. Sugiyama, N. Kanehisa, Y. Kai, H. Yasuda and A. Nakamura, *J. Am. Chem. Soc.*, 1994, **116**, 6977–6978.
- 223 M. Köhler, H. Görls, J. Langer and M. Westerhausen, *Chem. - Eur. J.*, 2014, **20**, 5237–5239.
- 224 M. Köhler, A. Koch, H. Görls and M. Westerhausen, *Organometallics*, 2016, **35**, 242–248.
- 225 I. Fleming and C. J. Urch, *J. Organomet. Chem.*, 1985, **285**, 173–191.
- 226 C. A. Kraus, *J. Am. Chem. Soc.*, 1907, **29**, 1557–1571.
- 227 G. E. Gibson and W. L. Argo, *J. Am. Chem. Soc.*, 1918, **40**, 1327–1361.
- 228 J. L. Dye, *Science*, 2003, **301**, 607–608.
- 229 E. Zurek, P. P. Edwards and R. Hoffmann, *Angew. Chem. Int. Ed.*, 2009, **48**, 8198–8232.
- 230 N. Mammano and M. J. Sienko, *J. Solid State Chem.*, 1970, **1**, 534–535.
- 231 C. K. Jankowski, A. Pelletier, E. Diaz, J. M. R. Belanger, J. R. J. Pare, C. Lamouroux and J. Boivin, *J. Mex. Chem. Soc.*, 2009, **53**, 220–228.
- 232 P. A. Scherr and J. P. Oliver, *J. Mol. Spectrosc.*, 1969, **31**, 109–117.
- 233 M. Klahn and U. Rosenthal, *Organometallics*, 2012, **31**, 1235–1244.
- 234 See the special issues: *Chem. Soc. Rev.* 2011, **40** (No. 4); *Acc. Chem. Res.* 2012, **45** (No. 6); *Chem. Rev.* 2010, **110** (No. 2).
- 235 T. Ahrens, J. Kohlmann, M. Ahrens and T. Braun, *Chem. Rev.*, 2015, **115**, 931–972.
- 236 R. Waterman, *Organometallics*, 2013, **32**, 7249–7263.
- 237 H. Tsurugi, K. Yamamoto and K. Mashima, *J. Am. Chem. Soc.*, 2011, **133**, 732–735.
- 238 R. Waterman, *Organometallics*, 2007, **26**, 2492–2494.
- 239 A. D. Sadow and T. D. Tilley, *J. Am. Chem. Soc.*, 2005, **127**, 643–656.
- 240 M. E. Thompson, S. M. Baxter, A. R. Bulls, B. J. Burger, M. C. Nolan, B. D. Santarsiero, W. P. Schaefer and J. E. Bercaw, *J. Am. Chem. Soc.*, 1987, **109**, 203–219.
- 241 P. L. Watson, *J. Am. Chem. Soc.*, 1983, **105**, 6491–6493.
- 242 J. R. Webb, S. A. Burgess, T. R. Cundari and T. B. Gunnoe, *Dalton Trans.*, 2013, **42**, 16646–16665.
- 243 B. F. Wicker, H. Fan, A. K. Hickey, M. G. Crestani, J. Scott, M. Pink and D. J. Mindiola, *J. Am. Chem. Soc.*, 2012, **134**, 20081–20096.
- 244 C. C. Cummins, C. P. Schaller, G. D. Van Duyne, P. T. Wolczanski, A. W. E. Chan and R. Hoffmann, *J. Am. Chem. Soc.*, 1991, **113**, 2985–2994.
- 245 H. M. Hoyt, F. E. Michael and R. G. Bergman, *J. Am. Chem. Soc.*, 2004, **126**, 1018–1019.
- 246 J. de With and A. D. Horton, *Angew. Chem. Int. Ed. Engl.*, 1993, **32**, 903–905.
- 247 C. P. Schaller and P. T. Wolczanski, *Inorg. Chem.*, 1993, **32**, 131–144.
- 248 D. F. Schafer and P. T. Wolczanski, *J. Am. Chem. Soc.*, 1998, **120**, 4881–4882.
- 249 N. A. Petasis and E. I. Bzowej, *Tetrahedron Lett.*, 1993, **34**, 943–946.
- 250 H. van der Heijden and B. Hessen, *J. Chem. Soc. Chem. Commun.*, 1995, 145–146.
- 251 J. G. Andino, U. J. Kilgore, M. Pink, A. Ozarowski, J. Krzystek, J. Telser, M.-H. Baik and D. J. Mindiola, *Chem. Sci.*, 2010, **1**, 351–356.
- 252 J. K. Cockcroft, V. C. Gibson, J. A. K. Howard, A. D. Poole, U. Siemeling and C. Wilson, *J. Chem. Soc. Chem. Commun.*, 1992, 1668–1670.

- 253 M. P. Coles, V. C. Gibson, W. Clegg, M. R. J. Elsegood and P. A. Porrelli, *Chem. Commun.*, 1996, 1963–1964.
- 254 K. Wada, C. B. Pamplin, P. Legzdins, B. O. Patrick, I. Tsyba and R. Bau, *J. Am. Chem. Soc.*, 2003, **125**, 7035–7048.
- 255 H. Fan, A. R. Fout, B. C. Bailey, M. Pink, M.-H. Baik and D. J. Mindiola, *Dalton Trans.*, 2013, **42**, 4163–4174.
- 256 J. A. Flores, V. N. Cavaliere, D. Buck, B. Pintér, G. Chen, M. G. Crestani, M.-H. Baik and D. J. Mindiola, *Chem. Sci.*, 2011, **2**, 1457–1462.
- 257 B. C. Bailey, H. Fan, E. W. Baum, J. C. Huffman, M.-H. Baik and D. J. Mindiola, *J. Am. Chem. Soc.*, 2005, **127**, 16016–16017.
- 258 J. Dvorak, R. J. O'Brien and W. Santo, *J. Chem. Soc. Chem. Commun.*, 1970, 411–412.
- 259 I. S. Kolomnikov, T. S. Loveeva, V. V. Gorbachevskaya, G. G. Aleksandrov, Y. T. Struchkov and M. E. Vol'pin, *J. Chem. Soc. Chem. Commun.*, 1971, 972–973.
- 260 V. B. Shur, E. G. Berkovitch, L. B. Vasiljeva, R. V. Kudryavtsev and M. E. Vol'Pin, *J. Organomet. Chem.*, 1974, **78**, 127–132.
- 261 C. P. Boekel, J. H. Teuben and H. J. de Liefde Meijer, *J. Organomet. Chem.*, 1974, **81**, 371–377.
- 262 C. P. Boekel, J. H. Teuben and H. J. de Liefde Meijer, *J. Organomet. Chem.*, 1975, **102**, 161–165.
- 263 G. Erker, *J. Organomet. Chem.*, 1977, **134**, 189–202.
- 264 C. B. Pamplin and P. Legzdins, *Acc. Chem. Res.*, 2003, **36**, 223–233.
- 265 S. J. McLain, R. R. Schrock, P. R. Sharp, M. R. Churchill and W. J. Youngs, *J. Am. Chem. Soc.*, 1979, **101**, 263–265.
- 266 J. K. F. Buijink, K. R. Kloetstra, A. Meetsma, J. H. Teuben, W. J. J. Smeets and A. L. Spek, *Organometallics*, 1996, **15**, 2523–2533.
- 267 C. Boulho, P. Oulié, L. Vendier, M. Etienne, V. Pimienta, A. Locati, F. Bessac, F. Maseras, D. A. Pantazis and J. E. McGrady, *J. Am. Chem. Soc.*, 2010, **132**, 14239–14250.
- 268 S. L. Buchwald and R. B. Nielsen, *Chem. Rev.*, 1988, **88**, 1047–1058.
- 269 V. V. Burlakov, A. V. Polyakov, A. I. Yanovsky, Y. T. Struchkov, V. B. Shur, M. E. Vol'pin, U. Rosenthal and H. Görls, *J. Organomet. Chem.*, 1994, **476**, 197–206.
- 270 U. Rosenthal, P.-M. Pellny, F. G. Kirchbauer and V. V. Burlakov, *Acc. Chem. Res.*, 2000, **33**, 119–129.
- 271 S. L. Buchwald, B. T. Watson and J. C. Huffman, *J. Am. Chem. Soc.*, 1987, **109**, 2544–2546.
- 272 U. Rosenthal, A. Ohff, M. Michalik, H. Görls, V. V. Burlakov and V. B. Shur, *Angew. Chem. Int. Ed. Engl.*, 1993, **32**, 1193–1195.
- 273 J. D. Debad, P. Legzdins, S. A. Lumb, R. J. Batchelor and F. W. B. Einstein, *J. Am. Chem. Soc.*, 1995, **117**, 3288–3289.
- 274 J. D. Debad, P. Legzdins, S. A. Lumb, S. J. Rettig, R. J. Batchelor and F. W. B. Einstein, *Organometallics*, 1999, **18**, 3414–3428.
- 275 J. Y. K. Tsang, M. S. A. Buschhaus, P. M. Graham, C. J. Semiao, S. P. Semproni, S. J. Kim and P. Legzdins, *J. Am. Chem. Soc.*, 2008, **130**, 3652–3663.
- 276 R. A. Baillie, R. W. Y. Man, M. V. Shree, C. Chow, M. E. Thibault, W. S. McNeil and P. Legzdins, *Organometallics*, 2011, **30**, 6201–6217.
- 277 R. A. Baillie and P. Legzdins, *Acc. Chem. Res.*, 2014, **47**, 330–340.
- 278 M. Kamitani, K. Searles, C.-H. Chen, P. J. Carroll and D. J. Mindiola, *Organometallics*, 2015, **34**, 2558–2566.
- 279 R. A. Fisher and S. L. Buchwald, *Organometallics*, 1990, **9**, 871–873.
- 280 J. Yin and W. M. Jones, *Organometallics*, 1993, **12**, 2013–2014.

- 281 E.-I. Negishi and T. Takahashi, *Acc. Chem. Res.*, 1994, **27**, 124–130.
- 282 D. Kissounko, A. Epshteyn, J. C. Fettinger and L. R. Sita, *Organometallics*, 2006, **25**, 531–535.
- 283 S. L. Buchwald, K. A. Kreuzer and R. A. Fisher, *J. Am. Chem. Soc.*, 1990, **112**, 4600–4601.
- 284 P. Oulié, C. Boulho, L. Vendier, Y. Coppel and M. Etienne, *J. Am. Chem. Soc.*, 2006, **128**, 15962–15963.
- 285 S.-Y. S. Wang, K. A. Abboud and J. M. Boncella, *J. Am. Chem. Soc.*, 1997, **119**, 11990–11991.
- 286 E. Negishi, D. R. Swanson and T. Takahashi, *J. Chem. Soc. Chem. Commun.*, 1990, 1254–1255.
- 287 V. K. Dioumaev and J. F. Harrod, *Organometallics*, 1997, **16**, 1452–1464.
- 288 C. Boulho, L. Vendier, M. Etienne, A. Locati, F. Maseras and J. E. McGrady, *Organometallics*, 2011, **30**, 3999–4007.
- 289 C. Li, C. Dinoi, Y. Coppel and M. Etienne, *J. Am. Chem. Soc.*, 2015, **137**, 12450–12453.
- 290 R. F. Jordan and A. S. Guram, *Organometallics*, 1990, **9**, 2116–2123.
- 291 R. F. Jordan, D. F. Taylor and N. C. Baenziger, *Organometallics*, 1990, **9**, 1546–1557.
- 292 A. L. Lincoln, G. M. Wilmes and R. M. Waymouth, *Organometallics*, 2005, **24**, 5828–5835.
- 293 C. A. Bradley, E. Lobkovsky and P. J. Chirik, *J. Am. Chem. Soc.*, 2003, **125**, 8110–8111.
- 294 S. Bi, Z. Lin and R. F. Jordan, *Organometallics*, 2004, **23**, 4882–4890.
- 295 S. Kuppuswamy, I. Ghiviriga, K. A. Abboud and A. S. Veige, *Organometallics*, 2010, **29**, 6711–6722.
- 296 D. Thomas, W. Baumann, A. Spannenberg, R. Kempe and U. Rosenthal, *Organometallics*, 1998, **17**, 2096–2102.
- 297 F. Reiß, K. Altenburger, L. Becker, K. Schubert, H. Jiao, A. Spannenberg, D. Hollmann, P. Arndt and U. Rosenthal, *Chem. – Eur. J.*, 2016, **22**, 3361–3369.
- 298 U. Rosenthal, A. Ohff, W. Baumann, A. Tillack, H. Görls, V. V. Burlakov and V. B. Shur, *Z. Für Anorg. Allg. Chem.*, 1995, **621**, 77–83.
- 299 K. C. Jantunen, B. L. Scott and J. L. Kiplinger, *J. Alloys Compd.*, 2007, **444–445**, 363–368.
- 300 J. Weaver and S. Senaweera, *Tetrahedron*, 2014, **70**, 7413–7428.
- 301 R. N. Perutz, *Science*, 2008, **321**, 1168–1169.
- 302 E. Clot, O. Eisenstein, N. Jasim, S. A. Macgregor, J. E. McGrady and R. N. Perutz, *Acc. Chem. Res.*, 2011, **44**, 333–348.
- 303 H. Amii and K. Uneyama, *Chem. Rev.*, 2009, **109**, 2119–2183.
- 304 H. Torrens, *Coord. Chem. Rev.*, 2005, **249**, 1957–1985.
- 305 J. Burdeniuc, B. Jedicka and R. H. Crabtree, *Chem. Ber.*, 1997, **130**, 145–154.
- 306 J. L. Kiplinger, T. G. Richmond and C. E. Osterberg, *Chem. Rev.*, 1994, **94**, 373–431.
- 307 T. Braun and R. N. Perutz, *Chem. Commun.*, 2002, 2749–2757.
- 308 S. Burling, P. I. P. Elliott, N. A. Jasim, R. J. Lindup, J. McKenna, R. N. Perutz, S. J. Archibald and A. C. Whitwood, *Dalton Trans.*, 2005, 3686–3695.
- 309 I. M. Piglosiewicz, S. Kraft, R. Beckhaus, D. Haase and W. Saak, *Eur. J. Inorg. Chem.*, 2005, **2005**, 938–945.
- 310 M. Fujiwara, J. Ichikawa, T. Okauchi and T. Minami, *Tetrahedron Lett.*, 1999, **40**, 7261–7265.
- 311 U. Jäger-Fiedler, P. Arndt, W. Baumann, A. Spannenberg, V. V. Burlakov and U. Rosenthal, *Eur. J. Inorg. Chem.*, 2005, **2005**, 2842–2849.

- 312 M. W. Bouwkamp, J. de Wolf, I. del Hierro Morales, J. Gercama, A. Meetsma, S. I. Troyanov, B. Hessen and J. H. Teuben, *J. Am. Chem. Soc.*, 2002, **124**, 12956–12957.
- 313 C. E. Osterberg, M. A. King, A. M. Arif and T. G. Richmond, *Angew. Chem. Int. Ed. Engl.*, 1990, **29**, 888–890.
- 314 A. R. Fout, J. Scott, D. L. Miller, B. C. Bailey, M. Pink and D. J. Mindiola, *Organometallics*, 2009, **28**, 331–347.
- 315 B. L. Edelbach, A. K. Fazlur Rahman, R. J. Lachicotte and W. D. Jones, *Organometallics*, 1999, **18**, 3170–3177.
- 316 L. A. Watson, D. V. Yandulov and K. G. Caulton, *J. Am. Chem. Soc.*, 2001, **123**, 603–611.
- 317 B. M. Kraft, R. J. Lachicotte and W. D. Jones, *J. Am. Chem. Soc.*, 2001, **123**, 10973–10979.
- 318 E. Clot, C. Mégret, B. M. Kraft, O. Eisenstein and W. D. Jones, *J. Am. Chem. Soc.*, 2004, **126**, 5647–5653.
- 319 B. M. Kraft, E. Clot, O. Eisenstein, W. W. Brennessel and W. D. Jones, *J. Fluor. Chem.*, 2010, **131**, 1122–1132.
- 320 P. Arndt, U. Jäger-Fiedler, M. Klahn, W. Baumann, A. Spannenberg, V. V. Burlakov and U. Rosenthal, *Angew. Chem. Int. Ed.*, 2006, **45**, 4195–4198.
- 321 R. D. Rieth, W. W. Brennessel and W. D. Jones, *Eur. J. Inorg. Chem.*, 2007, **2007**, 2839–2847.
- 322 J. Sala-Pala, J. Amaudrut, J. E. Guerchais, R. Mercier and M. Cerutti, *J. Fluor. Chem.*, 1979, **14**, 269–271.
- 323 J. Sala-Pala, J. Amaudrut, J. E. Guerchais, R. Mercier, J. Douglade and J. G. Theobald, *J. Organomet. Chem.*, 1981, **204**, 347–359.
- 324 W. D. Jones, *Dalton Trans.*, 2003, 3991–3995.
- 325 B. C. Bailey, H. Fan, J. C. Huffman, M.-H. Baik and D. J. Mindiola, *J. Am. Chem. Soc.*, 2007, **129**, 8781–8793.
- 326 J. G. Andino, H. Fan, A. R. Fout, B. C. Bailey, M.-H. Baik and D. J. Mindiola, *J. Organomet. Chem.*, 2011, **696**, 4138–4146.
- 327 B. L. Edelbach, B. M. Kraft and W. D. Jones, *J. Am. Chem. Soc.*, 1999, **121**, 10327–10331.
- 328 P. A. Deck, M. M. Konaté, B. V. Kelly and C. Sleboznick, *Organometallics*, 2004, **23**, 1089–1097.
- 329 R. R. Schrock, J. Adamchuk, K. Ruhland and L. P. H. Lopez, *Organometallics*, 2003, **22**, 5079–5091.
- 330 P. E. O'Connor, D. J. Berg and T. Barclay, *Organometallics*, 2002, **21**, 3947–3954.
- 331 T. Hiyama, *Organofluorine Compounds*, Springer Berlin Heidelberg, Berlin, Heidelberg, 2000.
- 332 T. Braun and F. Wehmeier, *Eur. J. Inorg. Chem.*, 2011, **2011**, 613–625.
- 333 J. A. Hatnean and S. A. Johnson, *Organometallics*, 2012, **31**, 1361–1373.
- 334 S. J. Archibald, T. Braun, J. A. Gaunt, J. E. Hobson and R. N. Perutz, *J. Chem. Soc. Dalton Trans.*, 2000, 2013–2018.
- 335 A. Nova, M. Reinhold, R. N. Perutz, S. A. Macgregor and J. E. McGrady, *Organometallics*, 2010, **29**, 1824–1831.
- 336 L. Cronin, C. L. Higgitt, R. Karch and R. N. Perutz, *Organometallics*, 1997, **16**, 4920–4928.
- 337 N. A. Jasim, R. N. Perutz, A. C. Whitwood, T. Braun, J. Izundu, B. Neumann, S. Rothfeld and H.-G. Stammler, *Organometallics*, 2004, **23**, 6140–6149.
- 338 J. Vela, J. M. Smith, Y. Yu, N. A. Ketterer, C. J. Flaschenriem, R. J. Lachicotte and P. L. Holland, *J. Am. Chem. Soc.*, 2005, **127**, 7857–7870.

- 339 D. Noveski, T. Braun, B. Neumann, A. Stammler and H.-G. Stammler, *Dalton Trans.*, 2004, 4106–4119.
- 340 T. Braun, J. Izundu, A. Steffen, B. Neumann and H.-G. Stammler, *Dalton Trans.*, 2006, 5118–5123.
- 341 D. Breyer, T. Braun and A. Penner, *Dalton Trans.*, 2010, **39**, 7513–7520.
- 342 G. Ung and G. Bertrand, *Chem. – Eur. J.*, 2012, **18**, 12955–12957.
- 343 F. Lu, H. Sun, A. Du, L. Feng and X. Li, *Org. Lett.*, 2014, **16**, 772–775.
- 344 A. L. Raza, J. A. Panetier, M. Teltewskoi, S. A. Macgregor and T. Braun, *Organometallics*, 2013, **32**, 3795–3807.
- 345 A. Nova, S. Erhardt, N. A. Jasim, R. N. Perutz, S. A. Macgregor, J. E. McGrady and A. C. Whitwood, *J. Am. Chem. Soc.*, 2008, **130**, 15499–15511.
- 346 B. Procacci, R. J. Blagg, R. N. Perutz, N. Rendón and A. C. Whitwood, *Organometallics*, 2014, **33**, 45–52.
- 347 H. Lv, Y.-B. Cai and J.-L. Zhang, *Angew. Chem. Int. Ed.*, 2013, **52**, 3203–3207.
- 348 S. Yow, S. J. Gates, A. J. P. White and M. R. Crimmin, *Angew. Chem. Int. Ed.*, 2012, **51**, 12559–12563.
- 349 U. Jäger-Fiedler, M. Klahn, P. Arndt, W. Baumann, A. Spannenberg, V. V. Burlakov and U. Rosenthal, *J. Mol. Catal. Chem.*, 2007, **261**, 184–189.
- 350 J. Speight, *Lange's Handbook of Chemistry, 70th Anniversary Edition*, McGraw-Hill Professional, New York, 16th edn., 2005.
- 351 J. L. Kiplinger and T. G. Richmond, *J. Am. Chem. Soc.*, 1996, **118**, 1805–1806.
- 352 H. Guo, F. Kong, K. Kanno, J. He, K. Nakajima and T. Takahashi, *Organometallics*, 2006, **25**, 2045–2048.
- 353 K. Fuchibe and T. Akiyama, *J. Am. Chem. Soc.*, 2006, **128**, 1434–1435.
- 354 K. Fuchibe, Y. Ohshima, K. Mitomi and T. Akiyama, *J. Fluor. Chem.*, 2007, **128**, 1158–1167.
- 355 M. F. Kühnel and D. Lentz, *Angew. Chem. Int. Ed.*, 2010, **49**, 2933–2936.
- 356 D. Lanzinger, I. M. Höhle, S. B. Weiß and B. Rieger, *J. Organomet. Chem.*, 2015, **778**, 21–28.
- 357 N. Romero Fernandez, phd, Université de Toulouse, Université Toulouse III - Paul Sabatier, 2014.
- 358 G. E. Dobereiner, A. Nova, N. D. Schley, N. Hazari, S. J. Miller, O. Eisenstein and R. H. Crabtree, *J. Am. Chem. Soc.*, 2011, **133**, 7547–7562.
- 359 K. Oshima, T. Ohmura and M. Sugimoto, *J. Am. Chem. Soc.*, 2011, **133**, 7324–7327.
- 360 P. L. Diaconescu, *Acc. Chem. Res.*, 2010, **43**, 1352–1363.
- 361 P. Jochmann, V. Leich, T. P. Spaniol and J. Okuda, *Chem. – Eur. J.*, 2011, **17**, 12115–12122.
- 362 M. S. Hill, G. Kociok-Köhn, D. J. MacDougall, M. F. Mahon and C. Weetman, *Dalton Trans.*, 2011, **40**, 12500–12509.
- 363 J. Intemann, M. Lutz and S. Harder, *Organometallics*, 2014, **33**, 5722–5729.
- 364 K. L. Miller, B. N. Williams, D. Benitez, C. T. Carver, K. R. Ogilby, E. Tkatchouk, W. A. Goddard and P. L. Diaconescu, *J. Am. Chem. Soc.*, 2010, **132**, 342–355.
- 365 L. Hao, J. F. Harrod, A.-M. Lebus, Y. Mu, R. Shu, E. Samuel and H.-G. Woo, *Angew. Chem. Int. Ed.*, 1998, **37**, 3126–3129.
- 366 C. T. Carver and P. L. Diaconescu, *J. Am. Chem. Soc.*, 2008, **130**, 7558–7559.
- 367 C. T. Carver, D. Benitez, K. L. Miller, B. N. Williams, E. Tkatchouk, W. A. Goddard and P. L. Diaconescu, *J. Am. Chem. Soc.*, 2009, **131**, 10269–10278.
- 368 G. T. Plundrich, H. Wadepohl, E. Clot and L. H. Gade, *Chem. – Eur. J.*, 2016, **22**, 9283–9292.

- 369 M. Hesse, H. Meier and B. Zeeh, *Méthodes spectroscopiques pour la chimie organique*, Masson, 1997.
- 370 J. R. Nitschke and T. D. Tilley, *Angew. Chem. Int. Ed.*, 2001, **40**, 2142–2145.
- 371 R. Kempe, S. Brenner and P. Arndt, *Organometallics*, 1996, **15**, 1071–1074.
- 372 K. Nienkemper, G. Kehr, S. Kehr, R. Fröhlich and G. Erker, *J. Organomet. Chem.*, 2008, **693**, 1572–1589.
- 373 J. W. Lauher and R. Hoffmann, *J. Am. Chem. Soc.*, 1976, **98**, 1729–1742.
- 374 D. F. Taber, J. P. Louey, Y. Wang, W. A. Nugent, D. A. Dixon and R. L. Harlow, *J. Am. Chem. Soc.*, 1994, **116**, 9457–9463.
- 375 R. Fischer, D. Walther, P. Gebhardt and H. Görls, *Organometallics*, 2000, **19**, 2532–2540.
- 376 M. Klahn, W. Baumann, P. Arndt, V. V. Burlakov, T. Schareina, A. Spannenberg and U. Rosenthal, *Organometallics*, 2009, **28**, 915–918.
- 377 S. Gambarotta, C. Floriani, A. Chiesi-Villa and C. Guastini, *Inorg. Chem.*, 1983, **22**, 2029–2034.
- 378 T. Zippel, P. Arndt, A. Ohff, A. Spannenberg, R. Kempe and U. Rosenthal, *Organometallics*, 1998, **17**, 4429–4437.
- 379 J. Zhao, S. Zhang, W.-X. Zhang and Z. Xi, *Organometallics*, 2011, **30**, 3464–3467.
- 380 M. A. Bush and G. A. Sim, *J. Chem. Soc. Inorg. Phys. Theor.*, 1971, 2225–2229.
- 381 J. A. Marsella, K. Folting, J. C. Huffman and K. G. Caulton, *J. Am. Chem. Soc.*, 1981, **103**, 5596–5598.
- 382 J. H. Freudenberger and R. R. Schrock, *Organometallics*, 1985, **4**, 1937–1944.
- 383 C. Roger, G. S. Bodner, W. G. Hatton and J. A. Gladysz, *Organometallics*, 1991, **10**, 3266–3274.
- 384 F. L. Taw, B. L. Scott and J. L. Kiplinger, *J. Am. Chem. Soc.*, 2003, **125**, 14712–14713.
- 385 R. Beckhaus, J. Sang, J. Oster and T. Wagner, *J. Organomet. Chem.*, 1994, **484**, 179–190.
- 386 N. A. Barnes, A. K. Brisdon, I. R. Crossley, R. G. Pritchard and J. E. Warren, *Organometallics*, 2004, **23**, 2680–2685.
- 387 C. H. Winter, X. X. Zhou and M. J. Heeg, *Inorg. Chem.*, 1992, **31**, 1808–1815.
- 388 M. F. Kuehnel, P. Holstein, M. Kliche, J. Krüger, S. Matthies, D. Nitsch, J. Schutt, M. Sparenberg and D. Lentz, *Chem. – Eur. J.*, 2012, **18**, 10701–10714.
- 389 C. Ehm, J. Krüger and D. Lentz, *Chem. – Eur. J.*, 2016, **22**, 9305–9310.
- 390 T. Braun, R. N. Perutz and M. I. Sladek, *Chem. Commun.*, 2001, 2254–2255.
- 391 R. D. Thomas and J. P. Oliver, *Organometallics*, 1982, **1**, 571–579.
- 392 S. Krieck, H. Görls and M. Westerhausen, *Organometallics*, 2008, **27**, 5052–5057.
- 393 Y.-X. Chen, C. L. Stern and T. J. Marks, *J. Am. Chem. Soc.*, 1997, **119**, 2582–2583.
- 394 Y.-X. Chen, M. V. Metz, L. Li, C. L. Stern and T. J. Marks, *J. Am. Chem. Soc.*, 1998, **120**, 6287–6305.
- 395 M.-C. Chen, J. A. S. Roberts and T. J. Marks, *J. Am. Chem. Soc.*, 2004, **126**, 4605–4625.
- 396 P. Arndt, A. Spannenberg, W. Baumann, V. V. Burlakov, U. Rosenthal, S. Becke and T. Weiss, *Organometallics*, 2004, **23**, 4792–4795.
- 397 H. Gilman and F. K. Cartledge, *J. Organomet. Chem.*, 1964, **2**, 447–454.
- 398 A. Schäfer, C. Huber and R. Ahlrichs, *J. Chem. Phys.*, 1994, **100**, 5829–5835.
- 399 M. Dolg, U. Wedig, H. Stoll and H. Preuss, *J. Chem. Phys.*, 1987, **86**, 866–872.
- 400 D. Andrae, U. Häußermann, M. Dolg, H. Stoll and H. Preuß, *Theor. Chim. Acta*, 1990, **77**, 123–141.

Crystallographic Data

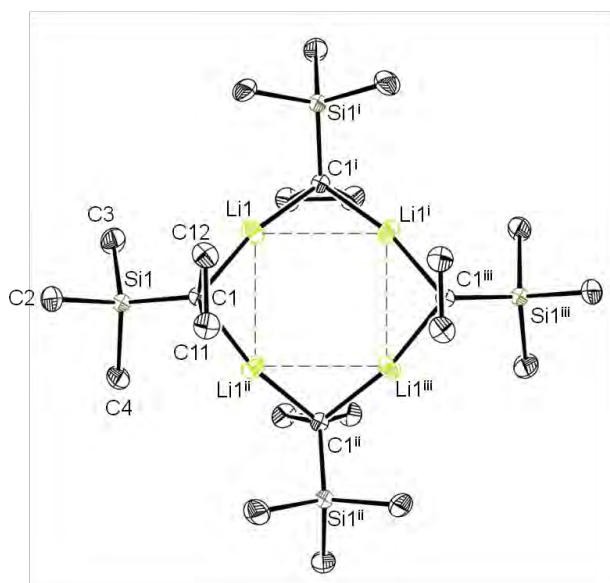


Table 3 Crystal data and structure refinement for **1**.

Formula	C ₆ H ₁₃ LiSi
Mol. wt.	120.19
Crystal system	Tetragonal
Space group	<i>I</i> -4
<i>a</i> (Å)	15.7073(4)
<i>b</i> (Å)	15.7073(4)
<i>c</i> (Å)	6.9282(3)
α (°)	90.0
β (°)	90.0
γ (°)	90.0
<i>V</i> (Å ³)	1709.32(11)
<i>Z</i>	8
Density (g/cm ³)	0.934
Abs. coeff., (mm ⁻¹)	0.182
<i>F</i> (000)	528
Crystal size, mm	0.480 x 0.100 x 0.08
θ range, deg	3.214 to 26.356
<i>R</i> (int)	0.0362
Reflections collected	4946
Reflec. Unique [<i>I</i> >2 σ (<i>I</i>)]	1743
Completeness to θ	99.4%
Data/restraints/param.	1743 / 0 / 88
Goodness-of-fit	1.010
<i>R</i> ₁ [<i>I</i> >2 σ (<i>I</i>)] (all data)	0.0450
w <i>R</i> ₂ [<i>I</i> >2 σ (<i>I</i>)] (all data)	0.0856
Largest diff. e ⁻ Å ⁻³	0.221 and -0.133

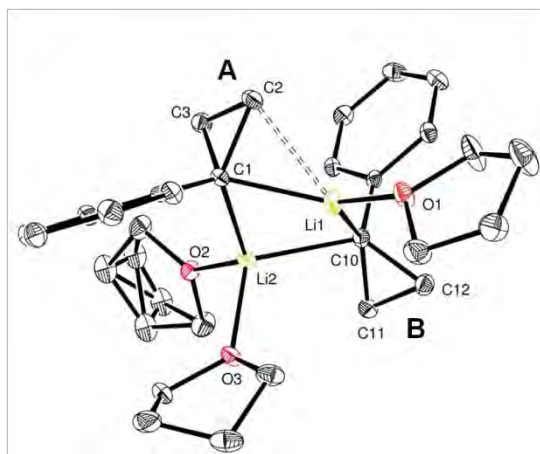
Table 4 Bond lengths [\AA] for **1**.

C(1)-Li(1)	2.033(5)	C(1)-Li(1)#1	2.025(5)
C(12)-Li(1)	2.405(6)	C(11)-Li(1)#1	2.413(6)
Li(1)-Li(1)#2	2.959(6)	Li(1)-Si(1)	3.181(4)
C(1)-Si(1)	1.836(2)	C(2)-Si(1)	1.874(3)
C(3)-Si(1)	1.872(3)	C(4)-Si(1)	1.874(3)
C(1)-C(12)	1.528(4)	C(11)-C(12)	1.480(5)
C(1)-C(11)	1.529(4)		

Table 5 Angles [$^\circ$] for **2**.

C(11)-C(1)-C(12)	57.9(2)	C(12)-Li(1)-Li(1)#2	114.3(3)
C(11)-C(1)-Si(1)	118.1(2)	C(11)#2-Li(1)-Li(1)#2	72.4(2)
C(12)-C(1)-Si(1)	116.9(2)	C(1)#2-Li(1)-Li(1)#1	124.8(2)
C(11)-C(1)-Li(1)#1	84.3(2)	C(1)-Li(1)-Li(1)#1	43.10(18)
C(12)-C(1)-Li(1)#1	126.3(3)	C(12)-Li(1)-Li(1)#1	71.9(2)
Si(1)-C(1)-Li(1)#1	114.1(2)	C(11)#2-Li(1)-Li(1)#1	113.4(3)
C(11)-C(1)-Li(1)	127.5(3)	Li(1)#2-Li(1)-Li(1)#1	89.987(9)
C(12)-C(1)-Li(1)	83.7(2)	C(1)#2-Li(1)-Si(1)	154.5(3)
Si(1)-C(1)-Li(1)	110.5(2)	C(1)-Li(1)-Si(1)	32.73(10)
Li(1)#1-C(1)-Li(1)	93.6(3)	C(12)-Li(1)-Si(1)	59.97(12)
C(12)-C(11)-C(1)	61.0(2)	C(11)#2-Li(1)-Si(1)	116.1(2)
C(12)-C(11)-Li(1)#1	107.0(2)	Li(1)#2-Li(1)-Si(1)	153.61(16)
C(1)-C(11)-Li(1)#1	56.63(17)	Li(1)#1-Li(1)-Si(1)	63.63(16)
C(11)-C(12)-C(1)	61.08(19)	C(1)-Si(1)-C(3)	107.93(13)
C(11)-C(12)-Li(1)	108.7(2)	C(1)-Si(1)-C(4)	109.48(13)
C(1)-C(12)-Li(1)	57.16(19)	C(3)-Si(1)-C(4)	109.31(16)
C(1)#2-Li(1)-C(1)	167.5(3)	C(1)-Si(1)-C(2)	114.86(15)
C(1)#2-Li(1)-C(12)	143.4(3)	C(3)-Si(1)-C(2)	107.30(15)
C(1)-Li(1)-C(12)	39.16(14)	C(4)-Si(1)-C(2)	107.86(16)
C(1)#2-Li(1)-C(11)#2	39.09(14)	C(1)-Si(1)-Li(1)	36.78(13)
C(1)-Li(1)-C(11)#2	141.1(3)	C(3)-Si(1)-Li(1)	71.47(14)
C(12)-Li(1)-C(11)#2	172.0(2)	C(4)-Si(1)-Li(1)	118.03(15)
C(1)#2-Li(1)-Li(1)#2	43.30(17)	C(2)-Si(1)-Li(1)	131.84(17)
C(1)-Li(1)-Li(1)#2	125.4(2)		

Symmetry code: #1 $-y+3/2, x+1/2, -z+3/2$ #2 $y-1/2, -x+3/2, -z+3/2$

**Table 6** Crystal data and structure refinement for **2**.

Formula	$C_{30}H_{42}Li_2O_3 \cdot 0.5(C_6H_{14})$
CCDC	1465291
Mol. wt.	507.60
Crystal system	Triclinic
Space group	<i>P</i> -1
<i>a</i> (Å)	8.5802(5)
<i>b</i> (Å)	9.4380(5)
<i>c</i> (Å)	20.2265(11)
α (°)	80.998(2)
β (°)	82.494(2)
γ (°)	70.198(2)
<i>V</i> (Å ³)	1516.79(15)
<i>Z</i>	2
Density (g/cm ³)	1.111
Abs. coeff., (mm ⁻¹)	0.068
<i>F</i> (000)	554
Crystal size, mm	0.2 x 0.12 x 0.03
θ range, deg	2.31 to 25.35
Limiting indices	-10 ≤ <i>h</i> ≤ 9, -11 ≤ <i>k</i> ≤ 11, -24 ≤ <i>l</i> ≤ 24
<i>R</i> (int)	0.0362
Reflections collected	27496
Reflec. Unique [<i>I</i> > 2σ(<i>I</i>)]	5557
Completeness to θ	99.9%
Data/restraints/param.	5557 / 0 / 346
Goodness-of-fit	1.040
<i>R</i> ₁ [<i>I</i> > 2σ(<i>I</i>)] (all data)	0.0548
w <i>R</i> ₂ [<i>I</i> > 2σ(<i>I</i>)] (all data)	0.1340
Largest diff. e·Å ⁻³	0.376 and -0.326

Table 7 Bond lengths [Å] for **2**.

C(30)-O(3)	1.442(2)	C(13)-C(18)	1.407(3)
------------	----------	-------------	----------

C(30)-C(29)	1.518(4)	C(14)-C(15)	1.385(3)
C(29)-C(28)	1.506(4)	C(15)-C(16)	1.381(3)
C(28)-C(27)	1.513(3)	C(16)-C(17)	1.383(3)
C(27)-O(3)	1.444(3)	C(17)-C(18)	1.384(3)
C(26)-O(2)	1.446(3)	C(1)-C(4)	1.471(3)
C(26)-C(25A)	1.477(5)	C(1)-C(3)	1.519(3)
C(26)-C(25B)	1.629(6)	C(1)-C(2)	1.526(3)
C(25A)-C(24B)	1.534(8)	C(1)-Li(1)	2.098(4)
C(24B)-C(23)	1.556(5)	C(1)-Li(2)	2.201(4)
C(24A)-C(25B)	1.478(9)	C(3)-C(2)	1.505(3)
C(24A)-C(23)	1.514(6)	C(3)-Li(2)	2.748(4)
C(23)-O(2)	1.436(3)	C(2)-Li(1)	2.368(4)
C(19)-O(1)	1.424(3)	C(4)-C(5)	1.403(3)
C(19)-C(20)	1.429(3)	C(4)-C(9)	1.407(3)
C(20)-C(21)	1.508(3)	C(9)-C(8)	1.387(3)
C(21)-C(22)	1.502(3)	C(8)-C(7)	1.376(3)
C(22)-O(1)	1.429(3)	C(7)-C(6)	1.389(3)
C(10)-C(13)	1.474(3)	C(6)-C(5)	1.382(3)
C(10)-C(12)	1.517(3)	C(31)-C(32)	1.519(3)
C(10)-C(11)	1.524(3)	C(31)-C(31)#1	1.523(4)
C(10)-Li(1)	2.129(4)	C(32)-C(33)	1.524(3)
C(10)-Li(2)	2.263(4)	Li(2)-O(2)	1.952(3)
C(11)-C(12)	1.500(3)	Li(2)-O(3)	1.988(3)
C(11)-Li(2)	2.740(4)	Li(2)-Li(1)	2.448(5)
C(13)-C(14)	1.405(3)	Li(1)-O(1)	1.920(4)

Table 8 Angles [$^{\circ}$] for 2.

O(3)-C(30)-C(29)	105.06(19)	C(10)-C(11)-Li(2)	55.67(12)
C(28)-C(29)-C(30)	101.65(19)	C(11)-C(12)-C(10)	60.70(13)
C(29)-C(28)-C(27)	101.55(19)	C(14)-C(13)-C(18)	115.65(18)
O(3)-C(27)-C(28)	105.82(18)	C(14)-C(13)-C(10)	122.00(17)
O(2)-C(26)-C(25A)	106.2(3)	C(18)-C(13)-C(10)	122.32(18)
O(2)-C(26)-C(25B)	102.2(3)	C(15)-C(14)-C(13)	122.32(19)
C(25A)-C(26)-C(25B)	27.2(2)	C(16)-C(15)-C(14)	120.6(2)
C(26)-C(25A)-C(24B)	98.4(4)	C(15)-C(16)-C(17)	118.6(2)
C(25A)-C(24B)-C(23)	101.2(3)	C(16)-C(17)-C(18)	121.0(2)
C(25B)-C(24A)-C(23)	99.7(4)	C(17)-C(18)-C(13)	121.86(19)
C(24A)-C(25B)-C(26)	100.6(4)	C(4)-C(1)-C(3)	116.30(17)
O(2)-C(23)-C(24A)	106.0(3)	C(4)-C(1)-C(2)	116.11(16)
O(2)-C(23)-C(24B)	102.9(3)	C(3)-C(1)-C(2)	59.23(13)
C(24A)-C(23)-C(24B)	29.8(2)	C(4)-C(1)-Li(1)	129.27(17)
O(1)-C(19)-C(20)	108.6(2)	C(3)-C(1)-Li(1)	113.02(16)
C(19)-C(20)-C(21)	107.0(2)	C(2)-C(1)-Li(1)	79.89(15)
C(22)-C(21)-C(20)	104.56(18)	C(4)-C(1)-Li(2)	117.67(15)
O(1)-C(22)-C(21)	107.50(18)	C(3)-C(1)-Li(2)	93.42(14)
C(13)-C(10)-C(12)	115.95(17)	C(2)-C(1)-Li(2)	126.11(16)

C(13)-C(10)-C(11)	115.80(16)	Li(1)-C(1)-Li(2)	69.37(14)
C(12)-C(10)-C(11)	59.09(13)	C(2)-C(3)-C(1)	60.62(13)
C(13)-C(10)-Li(1)	111.17(16)	C(2)-C(3)-Li(2)	99.16(14)
C(12)-C(10)-Li(1)	100.88(16)	C(1)-C(3)-Li(2)	53.08(12)
C(11)-C(10)-Li(1)	133.02(17)	C(3)-C(2)-C(1)	60.15(13)
C(13)-C(10)-Li(2)	116.14(15)	C(3)-C(2)-Li(1)	100.76(15)
C(12)-C(10)-Li(2)	127.17(16)	C(1)-C(2)-Li(1)	60.71(13)
C(11)-C(10)-Li(2)	90.53(14)	C(5)-C(4)-C(9)	116.21(18)
Li(1)-C(10)-Li(2)	67.66(13)	C(5)-C(4)-C(1)	121.80(17)
C(12)-C(11)-C(10)	60.21(13)	C(9)-C(4)-C(1)	121.93(18)
C(12)-C(11)-Li(2)	102.74(14)	C(8)-C(9)-C(4)	121.7(2)

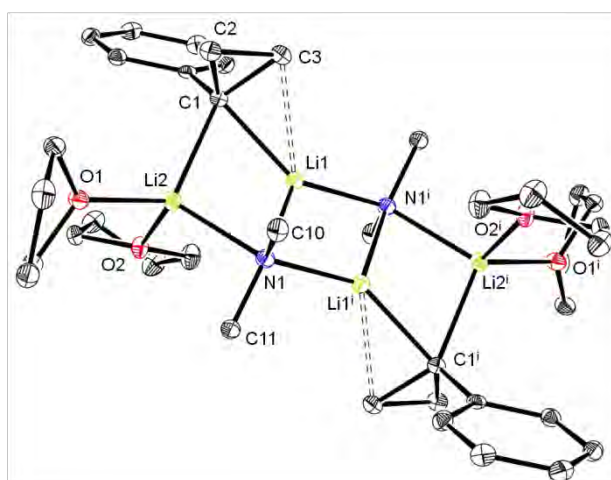


Table 9 Crystal data and structure refinement for **8**.

Formula	$C_{38}H_{62}Li_4N_2O_4$
CCDC	1465290
Mol. wt.	638.66
Crystal system	Triclinic
Space group	$P-1$
a (Å)	8.7871(10)
b (Å)	9.5833(11)
c (Å)	13.1959(13)
α (°)	104.353(4)
β (°)	93.696(4)
γ (°)	116.282(4)
V (Å ³)	945.63(18)
Z	1
Density (g/cm ³)	1.121
Abs. coeff., (mm ⁻¹)	0.069
$F(000)$	348
Crystal size, mm	0.18 x 0.12 x 0.08
θ range, deg	1.63 to 26.37

Limiting indices	-10<=h<=10, -11<=k<=11, -16<=l<=14
$R(\text{int})$	0.0259
Reflections collected	23990
Reflec. Unique [$I > 2\sigma(I)$]	3853
Completeness to θ	99.8%
Data/restraints/param.	3853 / 3 / 227
Goodness-of-fit	1.028
R_1 [$I > 2\sigma(I)$] (all data)	0.0415
wR_2 [$I > 2\sigma(I)$] (all data)	0.1044
Largest diff. $e \cdot \text{\AA}^{-3}$	0.469 and -0.289

Table 10 Bond lengths [\AA] for **8**.

C(1)-C(4)	1.4744(18)	C(13)-C(14)	1.535(2)
C(1)-C(2)	1.5218(18)	C(14)-C(15)	1.523(2)
C(1)-C(3)	1.5257(18)	C(15)-O(1)	1.4391(16)
C(1)-Li(1)	2.131(3)	C(16)-O(2)	1.4449(17)
C(1)-Li(2)	2.216(3)	C(16)-C(17)	1.500(2)
C(2)-C(3)	1.5012(19)	C(17)-C(18)	1.526(2)
C(4)-C(5)	1.4054(19)	C(18)-C(19)	1.515(2)
C(4)-C(9)	1.4074(19)	C(19)-O(2)	1.4441(16)
C(5)-C(6)	1.3910(19)	N(1)-Li(1)	2.014(3)
C(6)-C(7)	1.386(2)	N(1)-Li(1)#1	2.045(3)
C(7)-C(8)	1.389(2)	N(1)-Li(2)	2.133(3)
C(8)-C(9)	1.385(2)	O(1)-Li(2)	1.994(2)
C(10)-N(1)	1.4619(18)	O(2)-Li(2)	1.973(2)
C(11)-N(1)	1.4576(17)	Li(1)-N(1)#1	2.045(3)
C(11)-Li(1)#1	2.757(3)	Li(1)-Li(1)#1	2.371(4)
C(12)-O(1)	1.4396(16)	Li(1)-Li(2)	2.441(3)
C(12)-C(13)	1.520(2)	Li(1)-C(11)#1	2.757(3)

Table 11 Angles [$^\circ$] for **8**.

C(4)-C(1)-C(2)	116.04(11)	C(11)-N(1)-Li(2)	96.80(10)
C(4)-C(1)-C(3)	115.09(11)	C(10)-N(1)-Li(2)	100.69(10)
C(2)-C(1)-C(3)	59.02(9)	Li(1)-N(1)-Li(2)	72.07(9)
C(4)-C(1)-Li(1)	123.12(11)	Li(1)#1-N(1)-Li(2)	137.75(10)
C(2)-C(1)-Li(1)	118.90(11)	C(15)-O(1)-C(12)	104.22(10)
C(3)-C(1)-Li(1)	82.55(10)	C(15)-O(1)-Li(2)	127.42(11)
C(4)-C(1)-Li(2)	112.88(10)	C(12)-O(1)-Li(2)	124.23(10)
C(2)-C(1)-Li(2)	102.49(10)	C(19)-O(2)-C(16)	109.28(10)
C(3)-C(1)-Li(2)	131.88(11)	C(19)-O(2)-Li(2)	124.60(10)
Li(1)-C(1)-Li(2)	68.29(9)	C(16)-O(2)-Li(2)	115.60(11)

C(3)-C(2)-C(1)	60.62(9)	N(1)-Li(1)-N(1)#1	108.54(11)
C(2)-C(3)-C(1)	60.36(9)	N(1)-Li(1)-C(1)	108.37(11)
C(5)-C(4)-C(9)	116.29(12)	N(1)#1-Li(1)-C(1)	142.91(12)
C(5)-C(4)-C(1)	122.21(12)	N(1)-Li(1)-Li(1)#1	54.89(9)
C(9)-C(4)-C(1)	121.42(12)	N(1)#1-Li(1)-Li(1)#1	53.65(9)
C(6)-C(5)-C(4)	121.60(13)	C(1)-Li(1)-Li(1)#1	162.94(17)
C(7)-C(6)-C(5)	120.87(13)	N(1)-Li(1)-Li(2)	56.23(8)
C(6)-C(7)-C(8)	118.62(13)	N(1)#1-Li(1)-Li(2)	155.36(13)
C(9)-C(8)-C(7)	120.64(13)	C(1)-Li(1)-Li(2)	57.52(8)
C(8)-C(9)-C(4)	121.99(13)	Li(1)#1-Li(1)-Li(2)	108.18(14)
N(1)-C(11)-Li(1)#1	46.41(8)	N(1)-Li(1)-C(11)#1	132.94(11)
O(1)-C(12)-C(13)	105.05(11)	N(1)#1-Li(1)-C(11)#1	31.08(5)
C(12)-C(13)-C(14)	104.22(11)	C(1)-Li(1)-C(11)#1	114.00(10)
C(15)-C(14)-C(13)	103.82(12)	Li(1)#1-Li(1)-C(11)#1	80.78(11)
O(1)-C(15)-C(14)	104.97(11)	Li(2)-Li(1)-C(11)#1	170.79(12)
O(2)-C(16)-C(17)	106.34(12)	O(2)-Li(2)-O(1)	99.65(11)
C(16)-C(17)-C(18)	101.94(12)	O(2)-Li(2)-N(1)	106.39(11)
C(19)-C(18)-C(17)	101.90(12)	O(1)-Li(2)-N(1)	122.18(12)
O(2)-C(19)-C(18)	105.52(11)	O(2)-Li(2)-C(1)	109.37(11)
C(11)-N(1)-C(10)	107.20(11)	O(1)-Li(2)-C(1)	117.35(11)
C(11)-N(1)-Li(1)	147.39(12)	N(1)-Li(2)-C(1)	101.22(10)
C(10)-N(1)-Li(1)	104.99(11)	O(2)-Li(2)-Li(1)	100.59(11)
C(11)-N(1)-Li(1)#1	102.51(10)	O(1)-Li(2)-Li(1)	159.74(13)
C(10)-N(1)-Li(1)#1	108.71(11)	N(1)-Li(2)-Li(1)	51.71(8)
Li(1)-N(1)-Li(1)#1	71.46(11)	C(1)-Li(2)-Li(1)	54.20(8)

Symmetry code: #1 -x,-y+2,-z+1

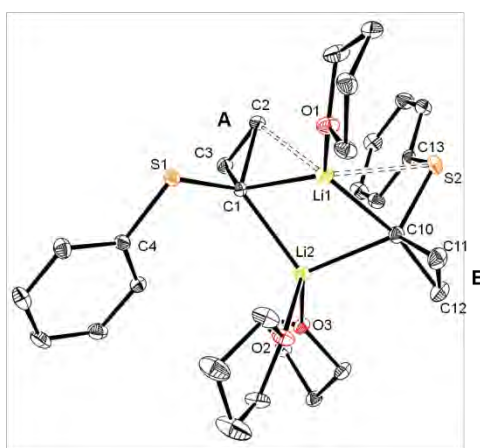


Table 12 Crystal data and structure refinement for **9**.

Formula	C ₃₀ H ₄₂ Li ₂ O ₃ S ₂
Mol. wt.	528.64
Crystal system	Triclinic
Space group	<i>P</i> -1
<i>a</i> (Å)	8.9124(5)

$b(\text{\AA})$	10.1850(5)
$c(\text{\AA})$	18.3639(11)
$\alpha(^{\circ})$	97.801(2)
$\beta(^{\circ})$	92.554(2)
$\gamma(^{\circ})$	115.414(2)
$V(\text{\AA}^3)$	1481.82(14)
Z	2
Density (g/cm^3)	1.185
Abs. coeff., (mm^{-1})	0.207
$F(000)$	568
Crystal size, mm	0.2 x 0.1 x 0.03
θ range, deg	1.13 to 25.68
Limiting indices	$-10 \leq h \leq 10, -12 \leq k \leq 12, -22 \leq l \leq 22$
$R(\text{int})$	0.0317
Reflections collected	55993
Reflec. Unique [$I > 2\sigma(I)$]	5630
Completeness to θ	99.9%
Data/restraints/param.	5630 / 0 / 334
Goodness-of-fit	1.041
R_1 [$I > 2\sigma(I)$] (all data)	0.0457
wR_2 [$I > 2\sigma(I)$] (all data)	0.1011
Largest diff. $e \cdot \text{\AA}^{-3}$	1.153 and -0.544

Table 13 Bond lengths [\AA] for **9**.

C(1)-C(3)	1.524(2)	C(19)-O(1)	1.440(2)
C(1)-C(2)	1.561(2)	C(19)-C(20)	1.514(3)
C(1)-S(1)	1.8210(17)	C(19)-H(19A)	0.9900
C(1)-Li(1)	2.120(4)	C(19)-H(19B)	0.9900
C(1)-Li(2)	2.271(3)	C(20)-C(21)	1.517(3)
C(2)-C(3)	1.490(3)	C(20)-H(20A)	0.9900
C(2)-Li(1)	2.392(4)	C(20)-H(20B)	0.9900
C(2)-H(2A)	0.9900	C(21)-C(22)	1.511(3)
C(2)-H(2B)	0.9900	C(21)-H(21A)	0.9900
C(3)-H(3A)	0.9900	C(21)-H(21B)	0.9900
C(3)-H(3B)	0.9900	C(22)-O(1)	1.447(2)
C(4)-C(9)	1.387(2)	C(22)-H(22A)	0.9900
C(4)-C(5)	1.399(2)	C(22)-H(22B)	0.9900
C(4)-S(1)	1.7587(17)	C(23)-O(2)	1.451(2)
C(5)-C(6)	1.382(3)	C(23)-C(24)	1.504(3)
C(5)-H(5)	0.9500	C(23)-H(23A)	0.9900
C(6)-C(7)	1.385(3)	C(23)-H(23B)	0.9900
C(6)-H(6)	0.9500	C(24)-C(25)	1.471(3)
C(7)-C(8)	1.378(3)	C(24)-H(24A)	0.9900
C(7)-H(7)	0.9500	C(24)-H(24B)	0.9900
C(8)-C(9)	1.392(3)	C(25)-C(26)	1.495(3)

C(8)-H(8)	0.9500	C(25)-H(25A)	0.9900
C(9)-H(9)	0.9500	C(25)-H(25B)	0.9900
C(10)-C(12)	1.528(2)	C(26)-O(2)	1.440(2)
C(10)-C(11)	1.537(2)	C(26)-H(26A)	0.9900
C(10)-S(2)	1.8199(18)	C(26)-H(26B)	0.9900
C(10)-Li(1)	2.094(3)	C(27)-O(5)	1.444(2)
C(10)-Li(2)	2.240(3)	C(27)-C(28)	1.513(2)
C(11)-C(12)	1.493(3)	C(27)-H(27A)	0.9900
C(11)-H(11A)	0.9900	C(27)-H(27B)	0.9900
C(11)-H(11B)	0.9900	C(28)-C(29)	1.519(3)
C(12)-H(12A)	0.9900	C(28)-H(28A)	0.9900
C(12)-H(12B)	0.9900	C(28)-H(28B)	0.9900
C(13)-C(14)	1.394(2)	C(29)-C(30)	1.514(3)
C(13)-C(18)	1.395(3)	C(29)-H(29A)	0.9900
C(13)-S(2)	1.7623(18)	C(29)-H(29B)	0.9900
C(14)-C(15)	1.386(3)	C(30)-O(5)	1.449(2)
C(14)-H(14)	0.9500	C(30)-H(30A)	0.9900
C(15)-C(16)	1.384(3)	C(30)-H(30B)	0.9900
C(15)-H(15)	0.9500	O(1)-Li(1)	1.906(3)
C(16)-C(17)	1.390(3)	O(2)-Li(2)	1.962(3)
C(16)-H(16)	0.9500	O(5)-Li(2)	2.007(3)
C(17)-C(18)	1.381(3)	Li(1)-Li(2)	2.441(4)
C(17)-H(17)	0.9500	Li(1)-S(2)	2.682(3)
C(18)-H(18)	0.9500		

Table 14 Angles [°] for **9**.

C(3)-C(1)-C(2)	57.76(11)	C(22)-C(21)-H(21A)	111.3
C(3)-C(1)-S(1)	109.92(12)	C(20)-C(21)-H(21A)	111.3
C(2)-C(1)-S(1)	104.51(11)	C(22)-C(21)-H(21B)	111.3
C(3)-C(1)-Li(1)	128.04(15)	C(20)-C(21)-H(21B)	111.3
C(2)-C(1)-Li(1)	79.47(13)	H(21A)-C(21)-H(21B)	109.2
S(1)-C(1)-Li(1)	108.19(12)	O(1)-C(22)-C(21)	106.15(15)
C(3)-C(1)-Li(2)	114.62(13)	O(1)-C(22)-H(22A)	110.5
C(2)-C(1)-Li(2)	127.05(13)	C(21)-C(22)-H(22A)	110.5
S(1)-C(1)-Li(2)	124.16(11)	O(1)-C(22)-H(22B)	110.5
Li(1)-C(1)-Li(2)	67.44(12)	C(21)-C(22)-H(22B)	110.5
C(3)-C(2)-C(1)	59.87(11)	H(22A)-C(22)-H(22B)	108.7
C(3)-C(2)-Li(1)	113.60(13)	O(2)-C(23)-C(24)	105.69(16)
C(1)-C(2)-Li(1)	60.61(11)	O(2)-C(23)-H(23A)	110.6
C(3)-C(2)-H(2A)	117.8	C(24)-C(23)-H(23A)	110.6
C(1)-C(2)-H(2A)	117.8	O(2)-C(23)-H(23B)	110.6
Li(1)-C(2)-H(2A)	113.9	C(24)-C(23)-H(23B)	110.6
C(3)-C(2)-H(2B)	117.8	H(23A)-C(23)-H(23B)	108.7
C(1)-C(2)-H(2B)	117.8	C(25)-C(24)-C(23)	103.43(19)

Li(1)-C(2)-H(2B)	69.6	C(25)-C(24)-H(24A)	111.1
H(2A)-C(2)-H(2B)	114.9	C(23)-C(24)-H(24A)	111.1
C(2)-C(3)-C(1)	62.37(12)	C(25)-C(24)-H(24B)	111.1
C(2)-C(3)-H(3A)	117.5	C(23)-C(24)-H(24B)	111.1
C(1)-C(3)-H(3A)	117.5	H(24A)-C(24)-H(24B)	109.0
C(2)-C(3)-H(3B)	117.5	C(24)-C(25)-C(26)	104.25(19)
C(1)-C(3)-H(3B)	117.5	C(24)-C(25)-H(25A)	110.9
H(3A)-C(3)-H(3B)	114.6	C(26)-C(25)-H(25A)	110.9
C(9)-C(4)-C(5)	118.95(16)	C(24)-C(25)-H(25B)	110.9
C(9)-C(4)-S(1)	123.15(13)	C(26)-C(25)-H(25B)	110.9
C(5)-C(4)-S(1)	117.88(14)	H(25A)-C(25)-H(25B)	108.9
C(6)-C(5)-C(4)	120.34(18)	O(2)-C(26)-C(25)	105.77(16)
C(6)-C(5)-H(5)	119.8	O(2)-C(26)-H(26A)	110.6
C(4)-C(5)-H(5)	119.8	C(25)-C(26)-H(26A)	110.6
C(5)-C(6)-C(7)	120.49(18)	O(2)-C(26)-H(26B)	110.6
C(5)-C(6)-H(6)	119.8	C(25)-C(26)-H(26B)	110.6
C(7)-C(6)-H(6)	119.8	H(26A)-C(26)-H(26B)	108.7
C(8)-C(7)-C(6)	119.39(18)	O(5)-C(27)-C(28)	106.31(14)
C(8)-C(7)-H(7)	120.3	O(5)-C(27)-H(27A)	110.5
C(6)-C(7)-H(7)	120.3	C(28)-C(27)-H(27A)	110.5
C(7)-C(8)-C(9)	120.72(18)	O(5)-C(27)-H(27B)	110.5
C(7)-C(8)-H(8)	119.6	C(28)-C(27)-H(27B)	110.5
C(9)-C(8)-H(8)	119.6	H(27A)-C(27)-H(27B)	108.7
C(4)-C(9)-C(8)	120.09(17)	C(27)-C(28)-C(29)	101.83(14)
C(4)-C(9)-H(9)	120.0	C(27)-C(28)-H(28A)	111.4
C(8)-C(9)-H(9)	120.0	C(29)-C(28)-H(28A)	111.4
C(12)-C(10)-C(11)	58.31(12)	C(27)-C(28)-H(28B)	111.4
C(12)-C(10)-S(2)	111.50(13)	C(29)-C(28)-H(28B)	111.4
C(11)-C(10)-S(2)	105.22(12)	H(28A)-C(28)-H(28B)	109.3
C(12)-C(10)-Li(1)	159.66(16)	C(30)-C(29)-C(28)	101.49(14)
C(11)-C(10)-Li(1)	108.56(15)	C(30)-C(29)-H(29A)	111.5
S(2)-C(10)-Li(1)	86.20(11)	C(28)-C(29)-H(29A)	111.5
C(12)-C(10)-Li(2)	103.63(14)	C(30)-C(29)-H(29B)	111.5
C(11)-C(10)-Li(2)	121.04(14)	C(28)-C(29)-H(29B)	111.5
S(2)-C(10)-Li(2)	131.98(12)	H(29A)-C(29)-H(29B)	109.3
Li(1)-C(10)-Li(2)	68.46(12)	O(5)-C(30)-C(29)	105.60(14)
C(12)-C(11)-C(10)	60.54(12)	O(5)-C(30)-H(30A)	110.6
C(12)-C(11)-H(11A)	117.7	C(29)-C(30)-H(30A)	110.6
C(10)-C(11)-H(11A)	117.7	O(5)-C(30)-H(30B)	110.6
C(12)-C(11)-H(11B)	117.7	C(29)-C(30)-H(30B)	110.6
C(10)-C(11)-H(11B)	117.7	H(30A)-C(30)-H(30B)	108.8
H(11A)-C(11)-H(11B)	114.8	C(19)-O(1)-C(22)	109.12(14)
C(11)-C(12)-C(10)	61.15(12)	C(19)-O(1)-Li(1)	127.76(14)
C(11)-C(12)-H(12A)	117.7	C(22)-O(1)-Li(1)	120.04(15)
C(10)-C(12)-H(12A)	117.7	C(26)-O(2)-C(23)	108.97(14)
C(11)-C(12)-H(12B)	117.7	C(26)-O(2)-Li(2)	126.67(14)
C(10)-C(12)-H(12B)	117.7	C(23)-O(2)-Li(2)	119.25(14)
H(12A)-C(12)-H(12B)	114.8	C(27)-O(5)-C(30)	108.75(13)

C(14)-C(13)-C(18)	118.78(17)	C(27)-O(5)-Li(2)	121.68(13)
C(14)-C(13)-S(2)	123.13(14)	C(30)-O(5)-Li(2)	129.33(13)
C(18)-C(13)-S(2)	118.09(14)	O(1)-Li(1)-C(10)	122.67(17)
C(15)-C(14)-C(13)	119.85(17)	O(1)-Li(1)-C(1)	121.53(16)
C(15)-C(14)-H(14)	120.1	C(10)-Li(1)-C(1)	113.56(15)
C(13)-C(14)-H(14)	120.1	O(1)-Li(1)-C(2)	108.79(15)
C(16)-C(15)-C(14)	121.31(18)	C(10)-Li(1)-C(2)	123.64(15)
C(16)-C(15)-H(15)	119.3	C(1)-Li(1)-C(2)	39.91(8)
C(14)-C(15)-H(15)	119.3	O(1)-Li(1)-Li(2)	146.37(18)
C(15)-C(16)-C(17)	118.85(18)	C(10)-Li(1)-Li(2)	58.59(11)
C(15)-C(16)-H(16)	120.6	C(1)-Li(1)-Li(2)	59.24(11)
C(17)-C(16)-H(16)	120.6	C(2)-Li(1)-Li(2)	90.93(13)
C(18)-C(17)-C(16)	120.34(18)	O(1)-Li(1)-S(2)	108.28(14)
C(18)-C(17)-H(17)	119.8	C(10)-Li(1)-S(2)	42.62(8)
C(16)-C(17)-H(17)	119.8	C(1)-Li(1)-S(2)	123.97(14)
C(17)-C(18)-C(13)	120.85(17)	C(2)-Li(1)-S(2)	102.89(12)
C(17)-C(18)-H(18)	119.6	Li(2)-Li(1)-S(2)	92.76(12)
C(13)-C(18)-H(18)	119.6	O(2)-Li(2)-O(5)	99.95(13)
O(1)-C(19)-C(20)	105.85(15)	O(2)-Li(2)-C(10)	105.33(14)
O(1)-C(19)-H(19A)	110.6	O(5)-Li(2)-C(10)	114.52(14)
C(20)-C(19)-H(19A)	110.6	O(2)-Li(2)-C(1)	112.72(14)
O(1)-C(19)-H(19B)	110.6	O(5)-Li(2)-C(1)	120.87(14)
C(20)-C(19)-H(19B)	110.6	C(10)-Li(2)-C(1)	102.79(13)
H(19A)-C(19)-H(19B)	108.7	O(2)-Li(2)-Li(1)	105.53(14)
C(19)-C(20)-C(21)	101.79(15)	O(5)-Li(2)-Li(1)	153.85(17)
C(19)-C(20)-H(20A)	111.4	C(10)-Li(2)-Li(1)	52.95(11)
C(21)-C(20)-H(20A)	111.4	C(1)-Li(2)-Li(1)	53.32(10)
C(19)-C(20)-H(20B)	111.4	C(4)-S(1)-C(1)	104.74(8)
C(21)-C(20)-H(20B)	111.4	C(13)-S(2)-C(10)	105.27(8)
H(20A)-C(20)-H(20B)	109.3	C(13)-S(2)-Li(1)	101.36(9)
C(22)-C(21)-C(20)	102.40(16)	C(10)-S(2)-Li(1)	51.19(9)

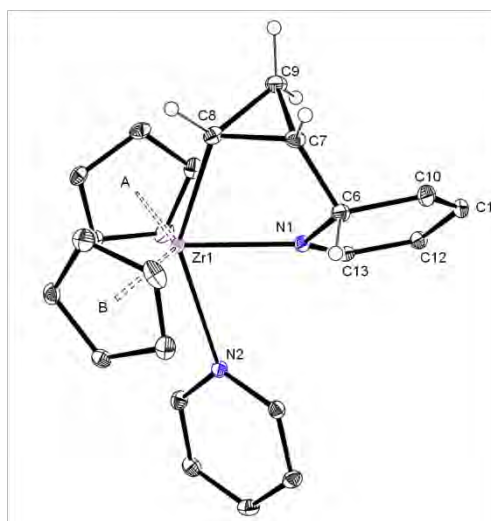


Table 15 Crystal data and structure refinement for **15**.

Formula	$C_{23}H_{24}N_2Zr$
Mol. wt.	419.66
Crystal system	Orthorhombic
Space group	$P b c a$
$a(\text{\AA})$	14.8659(6)
$b(\text{\AA})$	15.2110(7)
$c(\text{\AA})$	16.3176(8)
$\alpha(^{\circ})$	90
$\beta(^{\circ})$	90
$\gamma(^{\circ})$	90
$V(\text{\AA}^3)$	3689.8(3)
Z	8
Density (g/cm^3)	1.511
Abs. coeff., (mm^{-1})	0.605
$F(000)$	1728
Crystal size, mm	0.2 x 0.1 x 0.03
θ range, deg	2.29 to 29.86
Limiting indices	$-20 \leq h \leq 19, -20 \leq k \leq 21, -12 \leq l \leq 12$
$R(\text{int})$	0.0345
Reflections collected	125518
Reflec. Unique [$I > 2\sigma(I)$]	3647
Completeness to θ	68.7%
Data/restraints/param.	3647 / 0 / 235
Goodness-of-fit	1.075
R_1 [$I > 2\sigma(I)$] (all data)	0.0281
wR_2 [$I > 2\sigma(I)$] (all data)	0.0513
Largest diff. $e \cdot \text{\AA}^{-3}$	0.432 and -0.340

Table 16 Bond lengths [\AA] for **15**.

Zr(1)-N(1)	2.2054(14)	C(7)-H(7)	1.0000
Zr(1)-C(8)	2.3062(19)	C(8)-C(9)	1.508(3)
Zr(1)-C(14)	2.5253(16)	C(8)-H(8)	1.0000
Zr(1)-C(4)	2.5318(15)	C(9)-H(9A)	0.9900
Zr(1)-C(15)	2.5343(15)	C(9)-H(9B)	0.9900
Zr(1)-C(18)	2.5498(15)	C(10)-C(11)	1.332(2)
Zr(1)-C(3)	2.5502(15)	C(10)-H(10)	0.9500
Zr(1)-C(2)	2.5544(16)	C(11)-C(12)	1.447(3)
Zr(1)-C(17)	2.5605(16)	C(11)-H(11)	0.9500
Zr(1)-C(1)	2.5633(18)	C(12)-C(13)	1.355(2)
Zr(1)-C(16)	2.5638(16)	C(12)-H(12)	0.9500
Zr(1)-C(5)	2.5756(17)	C(13)-H(13)	0.9500
N(1)-C(13)	1.3652(19)	C(14)-C(18)	1.412(2)
N(1)-C(6)	1.496(2)	C(14)-C(15)	1.413(3)
N(2)-C(19)	1.345(2)	C(14)-H(14)	0.9500
N(2)-C(23)	1.3495(19)	C(15)-C(16)	1.397(3)
C(1)-C(5)	1.403(2)	C(15)-H(15)	0.9500
C(1)-C(2)	1.418(3)	C(16)-C(17)	1.416(2)
C(1)-H(1)	0.9500	C(16)-H(16)	0.9500
C(2)-C(3)	1.390(3)	C(17)-C(18)	1.392(3)
C(2)-H(2)	0.9500	C(17)-H(17)	0.9500
C(3)-C(4)	1.414(3)	C(18)-H(18)	0.9500
C(3)-H(3)	0.9500	C(19)-C(20)	1.381(3)
C(4)-C(5)	1.394(3)	C(19)-H(19)	0.9500
C(4)-H(4)	0.9500	C(20)-C(21)	1.386(2)
C(5)-H(5)	0.9500	C(20)-H(20)	0.9500
C(6)-C(10)	1.503(3)	C(21)-C(22)	1.376(3)
C(6)-C(7)	1.522(2)	C(21)-H(21)	0.9500
C(6)-H(6)	1.0000	C(22)-C(23)	1.386(2)
C(7)-C(9)	1.505(2)	C(22)-H(22)	0.9500
C(7)-C(8)	1.510(2)	C(23)-H(23)	0.9500

Table 17 Angles [$^\circ$] for **15**.

N(1)-Zr(1)-C(8)	72.27(5)	C(3)-C(4)-Zr(1)	74.57(9)
N(1)-Zr(1)-C(14)	131.87(5)	C(5)-C(4)-H(4)	126.0
C(8)-Zr(1)-C(14)	122.10(6)	C(3)-C(4)-H(4)	126.0
N(1)-Zr(1)-C(4)	124.75(6)	Zr(1)-C(4)-H(4)	115.7
C(8)-Zr(1)-C(4)	74.58(7)	C(4)-C(5)-C(1)	108.24(16)
C(14)-Zr(1)-C(4)	103.15(6)	C(4)-C(5)-Zr(1)	72.44(10)
N(1)-Zr(1)-C(15)	137.82(6)	C(1)-C(5)-Zr(1)	73.68(10)
C(8)-Zr(1)-C(15)	91.55(6)	C(4)-C(5)-H(5)	125.9
C(14)-Zr(1)-C(15)	32.42(6)	C(1)-C(5)-H(5)	125.9

C(4)-Zr(1)-C(15)	85.15(6)	Zr(1)-C(5)-H(5)	119.8
N(1)-Zr(1)-C(18)	99.60(5)	N(1)-C(6)-C(10)	114.45(13)
C(8)-Zr(1)-C(18)	117.39(6)	N(1)-C(6)-C(7)	107.40(12)
C(14)-Zr(1)-C(18)	32.31(6)	C(10)-C(6)-C(7)	111.40(16)
C(4)-Zr(1)-C(18)	134.96(6)	N(1)-C(6)-H(6)	107.8
C(15)-Zr(1)-C(18)	53.10(5)	C(10)-C(6)-H(6)	107.8
N(1)-Zr(1)-C(3)	95.05(5)	C(7)-C(6)-H(6)	107.8
C(8)-Zr(1)-C(3)	72.28(6)	C(9)-C(7)-C(8)	60.03(12)
C(14)-Zr(1)-C(3)	132.64(6)	C(9)-C(7)-C(6)	117.14(13)
C(4)-Zr(1)-C(3)	32.30(6)	C(8)-C(7)-C(6)	115.17(15)
C(15)-Zr(1)-C(3)	117.27(6)	C(9)-C(7)-H(7)	117.3
C(18)-Zr(1)-C(3)	164.40(7)	C(8)-C(7)-H(7)	117.3
N(1)-Zr(1)-C(2)	92.45(5)	C(6)-C(7)-H(7)	117.3
C(8)-Zr(1)-C(2)	101.34(6)	C(9)-C(8)-C(7)	59.83(11)
C(14)-Zr(1)-C(2)	123.52(6)	C(9)-C(8)-Zr(1)	121.88(11)
C(4)-Zr(1)-C(2)	52.99(6)	C(7)-C(8)-Zr(1)	113.48(11)
C(15)-Zr(1)-C(2)	129.36(6)	C(9)-C(8)-H(8)	116.3
C(18)-Zr(1)-C(2)	141.26(7)	C(7)-C(8)-H(8)	116.3
C(3)-Zr(1)-C(2)	31.59(6)	Zr(1)-C(8)-H(8)	116.3
N(1)-Zr(1)-C(17)	86.47(5)	C(7)-C(9)-C(8)	60.14(11)
C(8)-Zr(1)-C(17)	86.04(6)	C(7)-C(9)-H(9A)	117.8
C(14)-Zr(1)-C(17)	53.22(7)	C(8)-C(9)-H(9A)	117.8
C(4)-Zr(1)-C(17)	133.50(6)	C(7)-C(9)-H(9B)	117.8
C(15)-Zr(1)-C(17)	53.02(6)	C(8)-C(9)-H(9B)	117.8
C(18)-Zr(1)-C(17)	31.61(6)	H(9A)-C(9)-H(9B)	114.9
C(3)-Zr(1)-C(17)	156.55(7)	C(11)-C(10)-C(6)	123.20(17)
C(2)-Zr(1)-C(17)	171.84(6)	C(11)-C(10)-H(10)	118.4
N(1)-Zr(1)-C(1)	119.75(5)	C(6)-C(10)-H(10)	118.4
C(8)-Zr(1)-C(1)	123.55(6)	C(10)-C(11)-C(12)	119.94(18)
C(14)-Zr(1)-C(1)	91.41(6)	C(10)-C(11)-H(11)	120.0
C(4)-Zr(1)-C(1)	52.81(6)	C(12)-C(11)-H(11)	120.0
C(15)-Zr(1)-C(1)	101.80(6)	C(13)-C(12)-C(11)	118.07(15)
C(18)-Zr(1)-C(1)	114.19(7)	C(13)-C(12)-H(12)	121.0
C(3)-Zr(1)-C(1)	52.73(6)	C(11)-C(12)-H(12)	121.0
C(2)-Zr(1)-C(1)	32.16(6)	C(12)-C(13)-N(1)	126.93(16)
C(17)-Zr(1)-C(1)	144.02(6)	C(12)-C(13)-H(13)	116.5
N(1)-Zr(1)-C(16)	107.06(6)	N(1)-C(13)-H(13)	116.5
C(8)-Zr(1)-C(16)	70.27(6)	C(18)-C(14)-C(15)	107.14(18)
C(14)-Zr(1)-C(16)	53.21(7)	C(18)-C(14)-Zr(1)	74.80(9)
C(4)-Zr(1)-C(16)	101.54(6)	C(15)-C(14)-Zr(1)	74.14(9)
C(15)-Zr(1)-C(16)	31.81(6)	C(18)-C(14)-H(14)	126.4
C(18)-Zr(1)-C(16)	52.72(6)	C(15)-C(14)-H(14)	126.4
C(3)-Zr(1)-C(16)	127.34(6)	Zr(1)-C(14)-H(14)	116.8
C(2)-Zr(1)-C(16)	154.37(5)	C(16)-C(15)-C(14)	108.43(15)
C(17)-Zr(1)-C(16)	32.09(5)	C(16)-C(15)-Zr(1)	75.26(9)
C(1)-Zr(1)-C(16)	133.17(6)	C(14)-C(15)-Zr(1)	73.44(9)
N(1)-Zr(1)-C(5)	144.55(5)	C(16)-C(15)-H(15)	125.8
C(8)-Zr(1)-C(5)	105.26(6)	C(14)-C(15)-H(15)	125.8

C(14)-Zr(1)-C(5)	80.42(6)	Zr(1)-C(15)-H(15)	117.5
C(4)-Zr(1)-C(5)	31.65(6)	C(15)-C(16)-C(17)	107.85(17)
C(15)-Zr(1)-C(5)	76.68(6)	C(15)-C(16)-Zr(1)	72.93(9)
C(18)-Zr(1)-C(5)	111.83(6)	C(17)-C(16)-Zr(1)	73.83(9)
C(3)-Zr(1)-C(5)	52.61(6)	C(15)-C(16)-H(16)	126.1
C(2)-Zr(1)-C(5)	52.69(5)	C(17)-C(16)-H(16)	126.1
C(17)-Zr(1)-C(5)	128.96(5)	Zr(1)-C(16)-H(16)	119.1
C(1)-Zr(1)-C(5)	31.68(5)	C(18)-C(17)-C(16)	107.90(17)
C(16)-Zr(1)-C(5)	104.93(6)	C(18)-C(17)-Zr(1)	73.77(9)
C(13)-N(1)-C(6)	117.34(14)	C(16)-C(17)-Zr(1)	74.09(9)
C(13)-N(1)-Zr(1)	124.98(11)	C(18)-C(17)-H(17)	126.0
C(6)-N(1)-Zr(1)	116.45(9)	C(16)-C(17)-H(17)	126.0
C(19)-N(2)-C(23)	116.36(15)	Zr(1)-C(17)-H(17)	118.1
C(19)-N(2)-Zr(1)	122.06(10)	C(17)-C(18)-C(14)	108.66(16)
C(23)-N(2)-Zr(1)	120.54(12)	C(17)-C(18)-Zr(1)	74.62(9)
C(5)-C(1)-C(2)	107.62(17)	C(14)-C(18)-Zr(1)	72.89(9)
C(5)-C(1)-Zr(1)	74.64(11)	C(17)-C(18)-H(18)	125.7
C(2)-C(1)-Zr(1)	73.57(10)	C(14)-C(18)-H(18)	125.7
C(5)-C(1)-H(1)	126.2	Zr(1)-C(18)-H(18)	118.7
C(2)-C(1)-H(1)	126.2	N(2)-C(19)-C(20)	123.99(15)
Zr(1)-C(1)-H(1)	117.6	N(2)-C(19)-H(19)	118.0
C(3)-C(2)-C(1)	107.98(15)	C(20)-C(19)-H(19)	118.0
C(3)-C(2)-Zr(1)	74.04(9)	C(19)-C(20)-C(21)	118.69(18)
C(1)-C(2)-Zr(1)	74.27(9)	C(19)-C(20)-H(20)	120.7
C(3)-C(2)-H(2)	126.0	C(21)-C(20)-H(20)	120.7
C(1)-C(2)-H(2)	126.0	C(22)-C(21)-C(20)	118.42(17)
Zr(1)-C(2)-H(2)	117.7	C(22)-C(21)-H(21)	120.8
C(2)-C(3)-C(4)	108.07(17)	C(20)-C(21)-H(21)	120.8
C(2)-C(3)-Zr(1)	74.37(9)	C(21)-C(22)-C(23)	119.45(15)
C(4)-C(3)-Zr(1)	73.13(9)	C(21)-C(22)-H(22)	120.3
C(2)-C(3)-H(3)	126.0	C(23)-C(22)-H(22)	120.3
C(4)-C(3)-H(3)	126.0	N(2)-C(23)-C(22)	123.09(17)
Zr(1)-C(3)-H(3)	118.5	N(2)-C(23)-H(23)	118.5
C(5)-C(4)-C(3)	108.01(17)	C(22)-C(23)-H(23)	118.5
C(5)-C(4)-Zr(1)	75.91(9)		

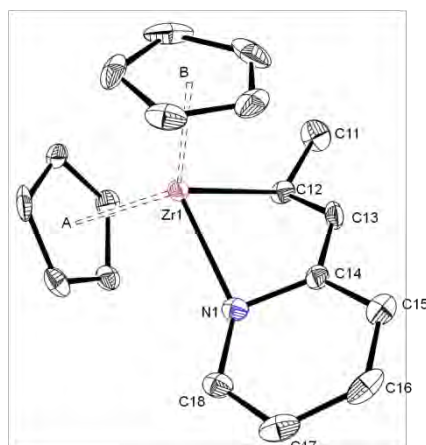


Table 18 Crystal data and structure refinement for **17**.

Formula	C ₁₈ H ₁₉ NZr
Mol. wt.	340.56
Crystal system	Orthorhombic
Space group	<i>P</i> c a 21
<i>a</i> (Å)	24.5559(11)
<i>b</i> (Å)	7.6243(3)
<i>c</i> (Å)	7.9330(3)
α (°)	90
β (°)	90
γ (°)	90
<i>V</i> (Å ³)	1485.23(10)
<i>Z</i>	4
Density (g/cm ³)	1.523
Abs. coeff., (mm ⁻¹)	0.729
<i>F</i> (000)	696
Crystal size, mm	0.1 x 0.04 x 0.04
θ range, deg	3.15 to 25.34
Limiting indices	-29 ≤ <i>h</i> ≤ 29, -9 ≤ <i>k</i> ≤ 9, -9 ≤ <i>l</i> ≤ 9
<i>R</i> (int)	0.0885
Reflections collected	14509
Reflec. Unique [<i>I</i> > 2σ(<i>I</i>)]	2711
Completeness to θ	99.7%
Data/restraints/param.	2711 / 1 / 183
Goodness-of-fit	1.013
<i>R</i> ₁ [<i>I</i> > 2σ(<i>I</i>)] (all data)	0.0631
w <i>R</i> ₂ [<i>I</i> > 2σ(<i>I</i>)] (all data)	0.0619
Largest diff. e·Å ⁻³	0.430 and -0.309

Table 19 Bond lengths [\AA] for **17**.

C(1)-C(5)	1.361(7)	C(9)-Zr(1)	2.538(5)
C(1)-C(2)	1.371(10)	C(9)-H(9)	0.9500
C(1)-Zr(1)	2.558(5)	C(10)-Zr(1)	2.530(4)
C(1)-H(1)	0.9500	C(10)-H(10)	0.9500
C(2)-C(3)	1.400(8)	C(11)-C(12)	1.508(6)
C(2)-Zr(1)	2.524(6)	C(11)-H(11A)	0.9800
C(2)-H(2)	0.9500	C(11)-H(11B)	0.9800
C(3)-C(4)	1.363(8)	C(11)-H(11C)	0.9800
C(3)-Zr(1)	2.491(5)	C(12)-C(13)	1.458(7)
C(3)-H(3)	0.9500	C(12)-Zr(1)	2.269(4)
C(4)-C(5)	1.343(10)	C(12)-H(12)	1.0000
C(4)-Zr(1)	2.492(5)	C(13)-C(14)	1.391(7)
C(4)-H(4)	0.9500	C(13)-Zr(1)	2.573(5)
C(5)-Zr(1)	2.552(4)	C(13)-H(13)	0.9500
C(5)-H(5)	0.9500	C(14)-N(1)	1.383(6)
C(6)-C(10)	1.377(6)	C(14)-C(15)	1.431(6)
C(6)-C(7)	1.421(6)	C(14)-Zr(1)	2.666(5)
C(6)-Zr(1)	2.530(4)	C(15)-C(16)	1.349(7)
C(6)-H(6)	0.9500	C(15)-H(15)	0.9500
C(7)-C(8)	1.385(7)	C(16)-C(17)	1.416(8)
C(7)-Zr(1)	2.527(5)	C(16)-H(16)	0.9500
C(7)-H(7)	0.9500	C(17)-C(18)	1.347(7)
C(8)-C(9)	1.397(7)	C(17)-H(17)	0.9500
C(8)-Zr(1)	2.533(5)	C(18)-N(1)	1.376(6)
C(8)-H(8)	0.9500	C(18)-H(18)	0.9500
C(9)-C(10)	1.393(9)	N(1)-Zr(1)	2.180(4)

Table 20 Angles [$^\circ$] for **17**.

C(5)-C(1)-C(2)	108.1(9)	C(13)-C(14)-Zr(1)	70.9(3)
C(5)-C(1)-Zr(1)	74.3(3)	C(15)-C(14)-Zr(1)	148.6(3)
C(2)-C(1)-Zr(1)	73.0(3)	C(16)-C(15)-C(14)	119.8(5)
C(5)-C(1)-H(1)	125.9	C(16)-C(15)-H(15)	120.1
C(2)-C(1)-H(1)	125.9	C(14)-C(15)-H(15)	120.1
Zr(1)-C(1)-H(1)	118.7	C(15)-C(16)-C(17)	119.7(5)
C(1)-C(2)-C(3)	106.9(6)	C(15)-C(16)-H(16)	120.1
C(1)-C(2)-Zr(1)	75.7(3)	C(17)-C(16)-H(16)	120.1
C(3)-C(2)-Zr(1)	72.5(3)	C(18)-C(17)-C(16)	119.2(5)
C(1)-C(2)-H(2)	126.5	C(18)-C(17)-H(17)	120.4
C(3)-C(2)-H(2)	126.5	C(16)-C(17)-H(17)	120.4
Zr(1)-C(2)-H(2)	117.4	C(17)-C(18)-N(1)	122.4(5)
C(4)-C(3)-C(2)	107.1(5)	C(17)-C(18)-H(18)	118.8
C(4)-C(3)-Zr(1)	74.2(3)	N(1)-C(18)-H(18)	118.8

C(2)-C(3)-Zr(1)	75.1(3)	C(18)-N(1)-C(14)	118.6(4)
C(4)-C(3)-H(3)	126.5	C(18)-N(1)-Zr(1)	141.0(3)
C(2)-C(3)-H(3)	126.5	C(14)-N(1)-Zr(1)	94.2(3)
Zr(1)-C(3)-H(3)	116.5	N(1)-Zr(1)-C(12)	82.21(16)
C(5)-C(4)-C(3)	109.0(6)	N(1)-Zr(1)-C(3)	127.4(2)
C(5)-C(4)-Zr(1)	77.0(3)	C(12)-Zr(1)-C(3)	132.3(2)
C(3)-C(4)-Zr(1)	74.1(3)	N(1)-Zr(1)-C(4)	97.12(19)
C(5)-C(4)-H(4)	125.5	C(12)-Zr(1)-C(4)	128.8(2)
C(3)-C(4)-H(4)	125.5	C(3)-Zr(1)-C(4)	31.75(19)
Zr(1)-C(4)-H(4)	115.4	N(1)-Zr(1)-C(2)	143.40(17)
C(4)-C(5)-C(1)	108.9(9)	C(12)-Zr(1)-C(2)	100.7(2)
C(4)-C(5)-Zr(1)	72.1(3)	C(3)-Zr(1)-C(2)	32.4(2)
C(1)-C(5)-Zr(1)	74.8(3)	C(4)-Zr(1)-C(2)	52.59(18)
C(4)-C(5)-H(5)	125.6	N(1)-Zr(1)-C(7)	134.04(16)
C(1)-C(5)-H(5)	125.6	C(12)-Zr(1)-C(7)	106.96(18)
Zr(1)-C(5)-H(5)	119.3	C(3)-Zr(1)-C(7)	79.7(2)
C(10)-C(6)-C(7)	107.1(6)	C(4)-Zr(1)-C(7)	109.2(2)
C(10)-C(6)-Zr(1)	74.2(2)	C(2)-Zr(1)-C(7)	80.5(2)
C(7)-C(6)-Zr(1)	73.6(3)	N(1)-Zr(1)-C(10)	83.75(19)
C(10)-C(6)-H(6)	126.4	C(12)-Zr(1)-C(10)	87.2(2)
C(7)-C(6)-H(6)	126.4	C(3)-Zr(1)-C(10)	127.4(3)
Zr(1)-C(6)-H(6)	117.8	C(4)-Zr(1)-C(10)	143.9(2)
C(8)-C(7)-C(6)	107.8(5)	C(2)-Zr(1)-C(10)	132.6(2)
C(8)-C(7)-Zr(1)	74.3(3)	C(7)-Zr(1)-C(10)	52.9(2)
C(6)-C(7)-Zr(1)	73.8(3)	N(1)-Zr(1)-C(6)	112.97(16)
C(8)-C(7)-H(7)	126.1	C(12)-Zr(1)-C(6)	80.07(17)
C(6)-C(7)-H(7)	126.1	C(3)-Zr(1)-C(6)	111.47(19)
Zr(1)-C(7)-H(7)	117.8	C(4)-Zr(1)-C(6)	141.8(2)
C(7)-C(8)-C(9)	108.4(5)	C(2)-Zr(1)-C(6)	103.40(18)
C(7)-C(8)-Zr(1)	73.9(3)	C(7)-Zr(1)-C(6)	32.64(15)
C(9)-C(8)-Zr(1)	74.2(3)	C(10)-Zr(1)-C(6)	31.59(14)
C(7)-C(8)-H(8)	125.8	N(1)-Zr(1)-C(8)	111.81(17)
C(9)-C(8)-H(8)	125.8	C(12)-Zr(1)-C(8)	133.24(18)
Zr(1)-C(8)-H(8)	118.0	C(3)-Zr(1)-C(8)	75.17(19)
C(10)-C(9)-C(8)	107.4(5)	C(4)-Zr(1)-C(8)	94.7(2)
C(10)-C(9)-Zr(1)	73.7(3)	C(2)-Zr(1)-C(8)	92.8(2)
C(8)-C(9)-Zr(1)	73.8(3)	C(7)-Zr(1)-C(8)	31.78(16)
C(10)-C(9)-H(9)	126.3	C(10)-Zr(1)-C(8)	52.8(2)
C(8)-C(9)-H(9)	126.3	C(6)-Zr(1)-C(8)	53.22(18)
Zr(1)-C(9)-H(9)	118.2	N(1)-Zr(1)-C(9)	82.68(17)
C(6)-C(10)-C(9)	109.3(7)	C(12)-Zr(1)-C(9)	118.43(18)
C(6)-C(10)-Zr(1)	74.2(3)	C(3)-Zr(1)-C(9)	103.29(19)
C(9)-C(10)-Zr(1)	74.4(3)	C(4)-Zr(1)-C(9)	112.15(19)
C(6)-C(10)-H(10)	125.4	C(2)-Zr(1)-C(9)	124.8(2)
C(9)-C(10)-H(10)	125.4	C(7)-Zr(1)-C(9)	52.91(17)
Zr(1)-C(10)-H(10)	117.9	C(10)-Zr(1)-C(9)	31.9(2)
C(12)-C(11)-H(11A)	109.5	C(6)-Zr(1)-C(9)	52.96(17)
C(12)-C(11)-H(11B)	109.5	C(8)-Zr(1)-C(9)	31.99(15)

H(11A)-C(11)-H(11B)	109.5	N(1)-Zr(1)-C(5)	91.7(2)
C(12)-C(11)-H(11C)	109.5	C(12)-Zr(1)-C(5)	98.0(3)
H(11A)-C(11)-H(11C)	109.5	C(3)-Zr(1)-C(5)	51.8(3)
H(11B)-C(11)-H(11C)	109.5	C(4)-Zr(1)-C(5)	30.9(2)
C(13)-C(12)-C(11)	117.1(4)	C(2)-Zr(1)-C(5)	51.7(2)
C(13)-C(12)-Zr(1)	84.3(3)	C(7)-Zr(1)-C(5)	129.5(2)
C(11)-C(12)-Zr(1)	135.3(3)	C(10)-Zr(1)-C(5)	172.63(19)
C(13)-C(12)-H(12)	105.4	C(6)-Zr(1)-C(5)	154.51(19)
C(11)-C(12)-H(12)	105.4	C(8)-Zr(1)-C(5)	124.5(3)
Zr(1)-C(12)-H(12)	105.4	C(9)-Zr(1)-C(5)	141.8(2)
C(14)-C(13)-C(12)	126.5(5)	N(1)-Zr(1)-C(1)	115.8(2)
C(14)-C(13)-Zr(1)	78.3(3)	C(12)-Zr(1)-C(1)	82.5(3)
C(12)-C(13)-Zr(1)	61.3(2)	C(3)-Zr(1)-C(1)	52.3(3)
C(14)-C(13)-H(13)	116.7	C(4)-Zr(1)-C(1)	51.6(2)
C(12)-C(13)-H(13)	116.7	C(2)-Zr(1)-C(1)	31.3(2)
Zr(1)-C(13)-H(13)	139.2	C(7)-Zr(1)-C(1)	110.1(3)
N(1)-C(14)-C(13)	118.3(4)	C(10)-Zr(1)-C(1)	156.15(18)
N(1)-C(14)-C(15)	118.6(5)	C(6)-Zr(1)-C(1)	124.8(2)
C(13)-C(14)-C(15)	123.0(5)	C(8)-Zr(1)-C(1)	123.5(3)
N(1)-C(14)-Zr(1)	54.6(2)	C(9)-Zr(1)-C(1)	154.9(3)
		C(5)-Zr(1)-C(1)	30.90(16)

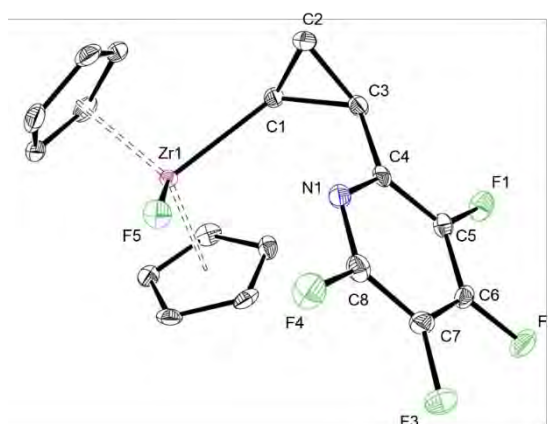


Table 21 Crystal data and structure refinement for **20**.

Formula	$C_{18}H_{14}F_5NZr$
Mol. wt.	430.52
Crystal system	Monoclinic
Space group	$P 21/n$
$a(\text{\AA})$	8.0437(4)
$b(\text{\AA})$	20.0860(8)
$c(\text{\AA})$	10.1234(5)
$\alpha(^{\circ})$	90
$\beta(^{\circ})$	99.426(2)

$\gamma(^{\circ})$	90
$V(\text{\AA}^3)$	1613.51(13)
Z	4
Density (g/cm^3)	1.772
Abs. coeff., (mm^{-1})	0.735
$F(000)$	856
Crystal size, mm	0.08 x 0.06 x 0.02
θ range, deg	2.76 to 25.35
Limiting indices	$-9 \leq h \leq 9, -24 \leq k \leq 24, -12 \leq l \leq 12$
$R(\text{int})$	0.0433
Reflections collected	22426
Reflec. Unique [$I > 2\sigma(I)$]	2956
Completeness to θ	99.9%
Data/restraints/param.	2956 / 0 / 226
Goodness-of-fit	1.068
R_1 [$I > 2\sigma(I)$] (all data)	0.0319
wR_2 [$I > 2\sigma(I)$] (all data)	0.0552
Largest diff. $e \cdot \text{\AA}^{-3}$	0.298 and -0.296

Table 22 Bond lengths [\AA] for 20.

C(1)-C(2)	1.503(3)	C(10)-H(10)	1.0000
C(1)-C(3)	1.544(3)	C(11)-C(12)	1.408(4)
C(1)-Zr(1)	2.301(2)	C(11)-Zr(1)	2.502(2)
C(1)-H(1)	1.0000	C(11)-H(11)	1.0000
C(2)-C(3)	1.508(3)	C(12)-C(13)	1.397(4)
C(2)-H(2A)	0.9900	C(12)-Zr(1)	2.490(2)
C(2)-H(2B)	0.9900	C(12)-H(12)	1.0000
C(3)-C(4)	1.474(3)	C(13)-Zr(1)	2.533(2)
C(3)-H(3)	1.0000	C(13)-H(13)	1.0000
C(4)-N(1)	1.348(3)	C(14)-C(15)	1.395(3)
C(4)-C(5)	1.383(3)	C(14)-C(18)	1.405(3)
C(5)-F(1)	1.351(3)	C(14)-Zr(1)	2.518(2)
C(5)-C(6)	1.373(3)	C(14)-H(14)	1.0000
C(6)-F(2)	1.338(2)	C(15)-C(16)	1.400(3)
C(6)-C(7)	1.372(3)	C(15)-Zr(1)	2.533(2)
C(7)-F(3)	1.353(3)	C(15)-H(15)	1.0000
C(7)-C(8)	1.370(3)	C(16)-C(17)	1.406(3)
C(8)-N(1)	1.303(3)	C(16)-Zr(1)	2.515(2)
C(8)-F(4)	1.344(3)	C(16)-H(16)	1.0000
C(9)-C(13)	1.389(4)	C(17)-C(18)	1.404(3)
C(9)-C(10)	1.398(4)	C(17)-Zr(1)	2.511(2)
C(9)-Zr(1)	2.542(2)	C(17)-H(17)	1.0000
C(9)-H(9)	1.0000	C(18)-Zr(1)	2.502(2)

C(10)-C(11)	1.401(4)	C(18)-H(18)	1.0000
C(10)-Zr(1)	2.530(2)	F(5)-Zr(1)	1.9498(13)

Table 23 Angles [°] for **20**.

C(2)-C(1)-C(3)	59.33(15)	Zr(1)-C(16)-H(16)	125.5
C(2)-C(1)-Zr(1)	125.35(16)	C(18)-C(17)-C(16)	107.4(2)
C(3)-C(1)-Zr(1)	130.00(14)	C(18)-C(17)-Zr(1)	73.40(13)
C(2)-C(1)-H(1)	110.9	C(16)-C(17)-Zr(1)	73.92(13)
C(3)-C(1)-H(1)	110.9	C(18)-C(17)-H(17)	125.9
Zr(1)-C(1)-H(1)	110.9	C(16)-C(17)-H(17)	125.9
C(1)-C(2)-C(3)	61.68(15)	Zr(1)-C(17)-H(17)	125.9
C(1)-C(2)-H(2A)	117.6	C(17)-C(18)-C(14)	108.1(2)
C(3)-C(2)-H(2A)	117.6	C(17)-C(18)-Zr(1)	74.08(13)
C(1)-C(2)-H(2B)	117.6	C(14)-C(18)-Zr(1)	74.39(13)
C(3)-C(2)-H(2B)	117.6	C(17)-C(18)-H(18)	125.6
H(2A)-C(2)-H(2B)	114.7	C(14)-C(18)-H(18)	125.6
C(4)-C(3)-C(2)	121.0(2)	Zr(1)-C(18)-H(18)	125.6
C(4)-C(3)-C(1)	119.83(18)	C(8)-N(1)-C(4)	119.1(2)
C(2)-C(3)-C(1)	58.99(15)	F(5)-Zr(1)-C(1)	105.42(7)
C(4)-C(3)-H(3)	115.2	F(5)-Zr(1)-C(12)	103.68(8)
C(2)-C(3)-H(3)	115.2	C(1)-Zr(1)-C(12)	128.31(8)
C(1)-C(3)-H(3)	115.2	F(5)-Zr(1)-C(11)	132.61(7)
N(1)-C(4)-C(5)	119.0(2)	C(1)-Zr(1)-C(11)	99.41(8)
N(1)-C(4)-C(3)	119.18(19)	C(12)-Zr(1)-C(11)	32.78(8)
C(5)-C(4)-C(3)	121.8(2)	F(5)-Zr(1)-C(18)	85.06(7)
F(1)-C(5)-C(6)	118.6(2)	C(1)-Zr(1)-C(18)	126.30(8)
F(1)-C(5)-C(4)	120.6(2)	C(12)-Zr(1)-C(18)	97.80(8)
C(6)-C(5)-C(4)	120.9(2)	C(11)-Zr(1)-C(18)	111.38(8)
F(2)-C(6)-C(7)	120.2(2)	F(5)-Zr(1)-C(17)	115.14(7)
F(2)-C(6)-C(5)	120.7(2)	C(1)-Zr(1)-C(17)	123.11(8)
C(7)-C(6)-C(5)	119.1(2)	C(12)-Zr(1)-C(17)	79.02(8)
F(3)-C(7)-C(8)	122.6(2)	C(11)-Zr(1)-C(17)	81.40(8)
F(3)-C(7)-C(6)	120.8(2)	C(18)-Zr(1)-C(17)	32.52(8)
C(8)-C(7)-C(6)	116.6(2)	F(5)-Zr(1)-C(16)	136.21(7)
N(1)-C(8)-F(4)	116.5(2)	C(1)-Zr(1)-C(16)	90.83(8)
N(1)-C(8)-C(7)	125.2(2)	C(12)-Zr(1)-C(16)	96.61(9)
F(4)-C(8)-C(7)	118.2(2)	C(11)-Zr(1)-C(16)	81.87(8)
C(13)-C(9)-C(10)	107.9(2)	C(18)-Zr(1)-C(16)	53.67(8)
C(13)-C(9)-Zr(1)	73.75(13)	C(17)-Zr(1)-C(16)	32.49(8)
C(10)-C(9)-Zr(1)	73.52(13)	F(5)-Zr(1)-C(14)	84.37(7)
C(13)-C(9)-H(9)	125.7	C(1)-Zr(1)-C(14)	95.06(8)
C(10)-C(9)-H(9)	125.7	C(12)-Zr(1)-C(14)	129.64(8)
Zr(1)-C(9)-H(9)	125.7	C(11)-Zr(1)-C(14)	133.07(8)
C(9)-C(10)-C(11)	108.4(2)	C(18)-Zr(1)-C(14)	32.49(8)
C(9)-C(10)-Zr(1)	74.48(13)	C(17)-Zr(1)-C(14)	53.75(8)

C(11)-C(10)-Zr(1)	72.74(13)	C(16)-Zr(1)-C(14)	53.39(8)
C(9)-C(10)-H(10)	125.5	F(5)-Zr(1)-C(10)	120.48(8)
C(11)-C(10)-H(10)	125.5	C(1)-Zr(1)-C(10)	74.85(8)
Zr(1)-C(10)-H(10)	125.5	C(12)-Zr(1)-C(10)	53.60(8)
C(10)-C(11)-C(12)	107.4(2)	C(11)-Zr(1)-C(10)	32.32(8)
C(10)-C(11)-Zr(1)	74.94(14)	C(18)-Zr(1)-C(10)	143.58(9)
C(12)-C(11)-Zr(1)	73.13(14)	C(17)-Zr(1)-C(10)	112.30(9)
C(10)-C(11)-H(11)	125.9	C(16)-Zr(1)-C(10)	102.85(9)
C(12)-C(11)-H(11)	125.9	C(14)-Zr(1)-C(10)	154.71(9)
Zr(1)-C(11)-H(11)	125.9	F(5)-Zr(1)-C(15)	113.41(7)
C(13)-C(12)-C(11)	107.8(2)	C(1)-Zr(1)-C(15)	74.79(8)
C(13)-C(12)-Zr(1)	75.56(14)	C(12)-Zr(1)-C(15)	128.45(9)
C(11)-C(12)-Zr(1)	74.09(13)	C(11)-Zr(1)-C(15)	111.75(8)
C(13)-C(12)-H(12)	125.6	C(18)-Zr(1)-C(15)	53.52(8)
C(11)-C(12)-H(12)	125.6	C(17)-Zr(1)-C(15)	53.61(8)
Zr(1)-C(12)-H(12)	125.6	C(16)-Zr(1)-C(15)	32.19(8)
C(9)-C(13)-C(12)	108.5(2)	C(14)-Zr(1)-C(15)	32.07(8)
C(9)-C(13)-Zr(1)	74.47(14)	C(10)-Zr(1)-C(15)	123.12(9)
C(12)-C(13)-Zr(1)	72.15(14)	F(5)-Zr(1)-C(13)	79.18(7)
C(9)-C(13)-H(13)	125.5	C(1)-Zr(1)-C(13)	117.32(8)
C(12)-C(13)-H(13)	125.5	C(12)-Zr(1)-C(13)	32.29(9)
Zr(1)-C(13)-H(13)	125.5	C(11)-Zr(1)-C(13)	53.52(9)
C(15)-C(14)-C(18)	108.1(2)	C(18)-Zr(1)-C(13)	116.37(8)
C(15)-C(14)-Zr(1)	74.53(13)	C(17)-Zr(1)-C(13)	108.35(8)
C(18)-C(14)-Zr(1)	73.12(12)	C(16)-Zr(1)-C(13)	128.86(9)
C(15)-C(14)-H(14)	125.6	C(14)-Zr(1)-C(13)	146.50(8)
C(18)-C(14)-H(14)	125.6	C(10)-Zr(1)-C(13)	52.87(8)
Zr(1)-C(14)-H(14)	125.6	C(15)-Zr(1)-C(13)	160.67(9)
C(14)-C(15)-C(16)	108.0(2)	F(5)-Zr(1)-C(9)	88.68(8)
C(14)-C(15)-Zr(1)	73.41(13)	C(1)-Zr(1)-C(9)	85.59(8)
C(16)-C(15)-Zr(1)	73.22(13)	C(12)-Zr(1)-C(9)	53.42(8)
C(14)-C(15)-H(15)	125.7	C(11)-Zr(1)-C(9)	53.48(9)
C(16)-C(15)-H(15)	125.7	C(18)-Zr(1)-C(9)	148.01(8)
Zr(1)-C(15)-H(15)	125.7	C(17)-Zr(1)-C(9)	131.25(8)
C(15)-C(16)-C(17)	108.3(2)	C(16)-Zr(1)-C(9)	133.66(9)
C(15)-C(16)-Zr(1)	74.59(13)	C(14)-Zr(1)-C(9)	172.94(9)
C(17)-C(16)-Zr(1)	73.59(13)	C(10)-Zr(1)-C(9)	32.00(9)
C(15)-C(16)-H(16)	125.5	C(15)-Zr(1)-C(9)	153.47(9)
C(17)-C(16)-H(16)	125.5	C(13)-Zr(1)-C(9)	31.78(8)

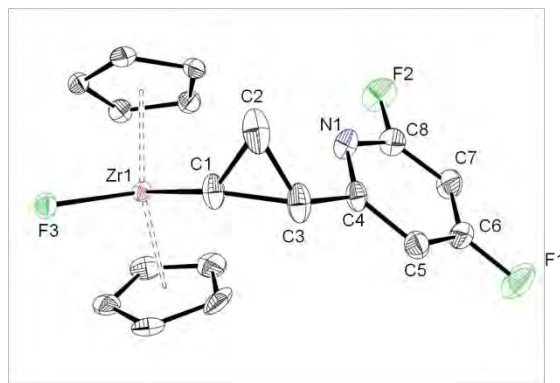


Table 24 Crystal data and structure refinement for **21**.

Formula	$C_{18}H_{16}F_3NZr$
Mol. wt.	394.54
Crystal system	Orthorhombic
Space group	Pcn
$a(\text{\AA})$	26.6459(5)
$b(\text{\AA})$	13.7759(2)
$c(\text{\AA})$	8.6639(2)
$\alpha(^{\circ})$	90
$\beta(^{\circ})$	90
$\gamma(^{\circ})$	90
$V(\text{\AA}^3)$	3180.27(11)
Z	8
Density (g/cm^3)	1.648
Abs. coeff., (mm^{-1})	0.720
$F(000)$	1584
Crystal size, mm	0.18 x 0.10 x 0.03
θ range, deg	2.88 to 26.37
Limiting indices	$33 \leq h \leq 33, -17 \leq k \leq 17, -10 \leq l \leq 10$
$R(\text{int})$	0.0467
Reflections collected	61084
Reflec. Unique [$I > 2\sigma(I)$]	3251
Completeness to θ	99.8%
Data/restraints/param.	3251 / 0 / 208
Goodness-of-fit	1.297
R_1 [$I > 2\sigma(I)$] (all data)	0.0500
wR_2 [$I > 2\sigma(I)$] (all data)	0.0866
Largest diff. $e \cdot \text{\AA}^{-3}$	0.804 and -1.445

Table 25 Bond lengths [\AA] for **21**.

C(1)-C(2)	1.475(7)	C(10)-Zr(1)	2.528(4)
C(1)-C(3)	1.520(6)	C(11)-C(12)	1.393(6)
C(1)-Zr(1)	2.260(4)	C(11)-Zr(1)	2.521(4)
C(2)-C(3)	1.483(7)	C(12)-C(13)	1.401(6)
C(3)-C(4)	1.483(6)	C(12)-Zr(1)	2.522(4)
C(4)-N(1)	1.344(5)	C(13)-Zr(1)	2.496(4)
C(4)-C(5)	1.379(6)	C(14)-C(15)	1.369(7)
C(5)-C(6)	1.367(6)	C(14)-C(18)	1.373(7)
C(6)-F(1)	1.348(5)	C(14)-Zr(1)	2.494(4)
C(6)-C(7)	1.362(7)	C(15)-C(16)	1.417(8)
C(7)-C(8)	1.375(6)	C(15)-Zr(1)	2.507(4)
C(8)-N(1)	1.306(5)	C(16)-C(17)	1.420(7)
C(8)-F(2)	1.351(5)	C(16)-Zr(1)	2.515(4)
C(9)-C(10)	1.395(6)	C(17)-C(18)	1.379(6)
C(9)-C(13)	1.412(6)	C(17)-Zr(1)	2.510(4)
C(9)-Zr(1)	2.501(4)	C(18)-Zr(1)	2.504(4)
C(10)-C(11)	1.414(6)	F(3)-Zr(1)	1.967(2)

Table 26 Angles [°] for **21**.

C(2)-C(1)-C(3)	59.3(3)	C(13)-Zr(1)-C(9)	32.83(14)
C(2)-C(1)-Zr(1)	136.7(4)	F(3)-Zr(1)-C(18)	81.21(13)
C(3)-C(1)-Zr(1)	139.6(3)	C(1)-Zr(1)-C(18)	119.53(17)
C(1)-C(2)-C(3)	61.8(3)	C(14)-Zr(1)-C(18)	31.90(15)
C(4)-C(3)-C(2)	120.5(5)	C(13)-Zr(1)-C(18)	102.13(15)
C(4)-C(3)-C(1)	122.1(4)	C(9)-Zr(1)-C(18)	118.16(15)
C(2)-C(3)-C(1)	58.9(3)	F(3)-Zr(1)-C(15)	133.53(14)
N(1)-C(4)-C(5)	121.8(4)	C(1)-Zr(1)-C(15)	102.25(18)
N(1)-C(4)-C(3)	118.1(4)	C(14)-Zr(1)-C(15)	31.78(17)
C(5)-C(4)-C(3)	120.1(4)	C(13)-Zr(1)-C(15)	90.98(17)
C(6)-C(5)-C(4)	117.8(4)	C(9)-Zr(1)-C(15)	81.09(16)
F(1)-C(6)-C(7)	118.8(4)	C(18)-Zr(1)-C(15)	52.79(16)
F(1)-C(6)-C(5)	118.6(4)	F(3)-Zr(1)-C(17)	84.41(14)
C(7)-C(6)-C(5)	122.6(4)	C(1)-Zr(1)-C(17)	87.64(17)
C(6)-C(7)-C(8)	113.8(4)	C(14)-Zr(1)-C(17)	53.39(16)
N(1)-C(8)-F(2)	115.0(4)	C(13)-Zr(1)-C(17)	131.94(15)
N(1)-C(8)-C(7)	127.4(4)	C(9)-Zr(1)-C(17)	134.77(15)
F(2)-C(8)-C(7)	117.6(4)	C(18)-Zr(1)-C(17)	31.94(15)
C(10)-C(9)-C(13)	108.3(4)	C(15)-Zr(1)-C(17)	53.83(17)
C(10)-C(9)-Zr(1)	75.0(2)	F(3)-Zr(1)-C(16)	115.86(17)
C(13)-C(9)-Zr(1)	73.4(2)	C(1)-Zr(1)-C(16)	76.78(17)
C(9)-C(10)-C(11)	107.5(4)	C(14)-Zr(1)-C(16)	53.63(17)
C(9)-C(10)-Zr(1)	72.8(2)	C(13)-Zr(1)-C(16)	123.73(19)
C(11)-C(10)-Zr(1)	73.5(2)	C(9)-Zr(1)-C(16)	108.21(19)
C(12)-C(11)-C(10)	108.4(4)	C(18)-Zr(1)-C(16)	53.38(16)
C(12)-C(11)-Zr(1)	74.0(2)	C(15)-Zr(1)-C(16)	32.79(18)

C(10)-C(11)-Zr(1)	74.0(2)	C(17)-Zr(1)-C(16)	32.84(17)
C(11)-C(12)-C(13)	108.2(4)	F(3)-Zr(1)-C(11)	87.75(12)
C(11)-C(12)-Zr(1)	73.9(2)	C(1)-Zr(1)-C(11)	89.93(16)
C(13)-C(12)-Zr(1)	72.7(2)	C(14)-Zr(1)-C(11)	132.83(15)
C(12)-C(13)-C(9)	107.7(4)	C(13)-Zr(1)-C(11)	53.61(14)
C(12)-C(13)-Zr(1)	74.8(2)	C(9)-Zr(1)-C(11)	53.61(14)
C(9)-C(13)-Zr(1)	73.8(2)	C(18)-Zr(1)-C(11)	149.07(15)
C(15)-C(14)-C(18)	108.6(5)	C(15)-Zr(1)-C(11)	134.59(16)
C(15)-C(14)-Zr(1)	74.6(3)	C(17)-Zr(1)-C(11)	171.58(15)
C(18)-C(14)-Zr(1)	74.4(2)	C(16)-Zr(1)-C(11)	153.38(17)
C(14)-C(15)-C(16)	108.3(5)	F(3)-Zr(1)-C(12)	80.43(12)
C(14)-C(15)-Zr(1)	73.6(3)	C(1)-Zr(1)-C(12)	121.44(16)
C(16)-C(15)-Zr(1)	73.9(3)	C(14)-Zr(1)-C(12)	105.71(15)
C(15)-C(16)-C(17)	106.3(4)	C(13)-Zr(1)-C(12)	32.41(14)
C(15)-C(16)-Zr(1)	73.3(3)	C(9)-Zr(1)-C(12)	53.77(14)
C(17)-C(16)-Zr(1)	73.4(2)	C(18)-Zr(1)-C(12)	117.13(14)
C(18)-C(17)-C(16)	107.2(5)	C(15)-Zr(1)-C(12)	123.21(17)
C(18)-C(17)-Zr(1)	73.8(2)	C(17)-Zr(1)-C(12)	147.94(15)
C(16)-C(17)-Zr(1)	73.8(3)	C(16)-Zr(1)-C(12)	155.99(19)
C(14)-C(18)-C(17)	109.5(5)	C(11)-Zr(1)-C(12)	32.06(13)
C(14)-C(18)-Zr(1)	73.7(2)	F(3)-Zr(1)-C(10)	119.67(12)
C(17)-C(18)-Zr(1)	74.3(2)	C(1)-Zr(1)-C(10)	81.98(16)
C(8)-N(1)-C(4)	116.6(4)	C(14)-Zr(1)-C(10)	118.83(16)
F(3)-Zr(1)-C(1)	94.42(12)	C(13)-Zr(1)-C(10)	53.84(14)
F(3)-Zr(1)-C(14)	108.85(14)	C(9)-Zr(1)-C(10)	32.20(14)
C(1)-Zr(1)-C(14)	130.29(17)	C(18)-Zr(1)-C(10)	150.33(15)
F(3)-Zr(1)-C(13)	106.50(12)	C(15)-Zr(1)-C(10)	105.55(16)
C(1)-Zr(1)-C(13)	135.82(16)	C(17)-Zr(1)-C(10)	154.30(15)
C(14)-Zr(1)-C(13)	79.23(15)	C(16)-Zr(1)-C(10)	121.48(17)
F(3)-Zr(1)-C(9)	134.19(12)	C(11)-Zr(1)-C(10)	32.52(13)
C(1)-Zr(1)-C(9)	107.51(16)	C(12)-Zr(1)-C(10)	53.56(13)
C(14)-Zr(1)-C(9)	87.09(16)		

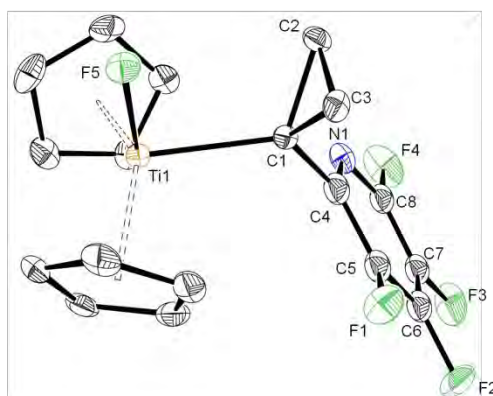


Table 27 Crystal data and structure refinement for **24**.

Formula	C ₁₈ H ₁₄ F ₅ NTi
Mol. wt.	387.20
Crystal system	Orthorhombic
Space group	<i>P</i> n a 21
<i>a</i> (Å)	15.5533(5)
<i>b</i> (Å)	7.9028(2)
<i>c</i> (Å)	12.8442(3)
α (°)	90
β (°)	90
γ (°)	90
V(Å ³)	1578.74(7)
<i>Z</i>	4
Density (g/cm ³)	1.629
Abs. coeff., (mm ⁻¹)	0.596
<i>F</i> (000)	784
Crystal size, mm	0.18 x 0.1 x 0.03
θ range, deg	3.03 to 25.34
Limiting indices	-18<= <i>h</i> <=16, -9<= <i>k</i> <=9, -15<= <i>l</i> <=15
<i>R</i> (int)	0.0342
Reflections collected	22481
Reflec. Unique [<i>I</i> >2 σ (<i>I</i>)]	2889
Completeness to θ	99.8%
Data/restraints/param.	2889 / 1 / 202
Goodness-of-fit	1.058
<i>R</i> ₁ [<i>I</i> >2 σ (<i>I</i>)] (all data)	0.0585
w <i>R</i> ₂ [<i>I</i> >2 σ (<i>I</i>)] (all data)	0.1583
Largest diff. e·Å ⁻³	1.197 and -0.442

Table 28 Bond lengths [\AA] for 24.

C(1)-C(4)	1.465(6)	C(10)-C(11)	1.390(8)
C(1)-C(3)	1.526(6)	C(10)-Ti(1)	2.385(5)
C(1)-C(2)	1.538(6)	C(11)-C(12)	1.413(9)
C(1)-Ti(1)	2.226(4)	C(11)-Ti(1)	2.411(4)
C(2)-C(3)	1.516(7)	C(12)-C(13)	1.393(8)
C(4)-N(1)	1.374(6)	C(12)-Ti(1)	2.414(6)
C(4)-C(5)	1.386(7)	C(13)-Ti(1)	2.408(5)
C(5)-F(1)	1.285(6)	C(14)-C(15)	1.402(8)
C(5)-C(6)	1.400(9)	C(14)-C(18)	1.437(9)
C(6)-F(2)	1.332(7)	C(14)-Ti(1)	2.399(5)
C(6)-C(7)	1.363(10)	C(15)-C(16)	1.374(8)
C(7)-C(8)	1.319(9)	C(15)-Ti(1)	2.421(5)
C(7)-F(3)	1.368(7)	C(16)-C(17)	1.387(8)
C(8)-N(1)	1.295(7)	C(16)-Ti(1)	2.393(5)

C(8)-F(4)	1.352(7)	C(17)-C(18)	1.402(9)
C(9)-C(10)	1.399(8)	C(17)-Ti(1)	2.369(6)
C(9)-C(13)	1.413(8)	C(18)-Ti(1)	2.393(6)
C(9)-Ti(1)	2.350(5)	F(5)-Ti(1)	1.853(3)

Table 29 Angles [°] for **24**.

C(4)-C(1)-C(3)	115.5(3)	C(1)-Ti(1)-C(10)	106.72(18)
C(4)-C(1)-C(2)	115.0(4)	C(9)-Ti(1)-C(10)	34.4(2)
C(3)-C(1)-C(2)	59.3(3)	C(17)-Ti(1)-C(10)	139.5(2)
C(4)-C(1)-Ti(1)	122.0(3)	F(5)-Ti(1)-C(16)	107.56(17)
C(3)-C(1)-Ti(1)	115.2(3)	C(1)-Ti(1)-C(16)	75.88(17)
C(2)-C(1)-Ti(1)	114.0(3)	C(9)-Ti(1)-C(16)	140.22(19)
C(3)-C(2)-C(1)	59.9(3)	C(17)-Ti(1)-C(16)	33.85(19)
C(2)-C(3)-C(1)	60.7(3)	C(10)-Ti(1)-C(16)	173.3(2)
N(1)-C(4)-C(5)	118.4(4)	F(5)-Ti(1)-C(18)	120.23(18)
N(1)-C(4)-C(1)	118.6(4)	C(1)-Ti(1)-C(18)	127.42(19)
C(5)-C(4)-C(1)	122.9(4)	C(9)-Ti(1)-C(18)	84.6(2)
F(1)-C(5)-C(4)	123.7(5)	C(17)-Ti(1)-C(18)	34.2(2)
F(1)-C(5)-C(6)	117.2(5)	C(10)-Ti(1)-C(18)	118.9(2)
C(4)-C(5)-C(6)	119.0(5)	C(16)-Ti(1)-C(18)	56.09(19)
F(2)-C(6)-C(7)	121.1(7)	F(5)-Ti(1)-C(14)	86.14(19)
F(2)-C(6)-C(5)	119.6(7)	C(1)-Ti(1)-C(14)	128.45(16)
C(7)-C(6)-C(5)	119.3(5)	C(9)-Ti(1)-C(14)	96.02(18)
C(8)-C(7)-C(6)	118.1(5)	C(17)-Ti(1)-C(14)	57.4(2)
C(8)-C(7)-F(3)	122.1(6)	C(10)-Ti(1)-C(14)	123.1(2)
C(6)-C(7)-F(3)	119.8(6)	C(16)-Ti(1)-C(14)	56.17(19)
N(1)-C(8)-C(7)	125.7(6)	C(18)-Ti(1)-C(14)	34.9(2)
N(1)-C(8)-F(4)	115.5(6)	F(5)-Ti(1)-C(13)	130.99(18)
C(7)-C(8)-F(4)	118.8(5)	C(1)-Ti(1)-C(13)	117.42(18)
C(10)-C(9)-C(13)	107.3(5)	C(9)-Ti(1)-C(13)	34.5(2)
C(10)-C(9)-Ti(1)	74.2(3)	C(17)-Ti(1)-C(13)	83.2(2)
C(13)-C(9)-Ti(1)	75.0(3)	C(10)-Ti(1)-C(13)	56.4(2)
C(11)-C(10)-C(9)	109.0(5)	C(16)-Ti(1)-C(13)	116.9(2)
C(11)-C(10)-Ti(1)	74.2(3)	C(18)-Ti(1)-C(13)	73.5(2)
C(9)-C(10)-Ti(1)	71.5(3)	C(14)-Ti(1)-C(13)	101.5(2)
C(10)-C(11)-C(12)	107.5(5)	F(5)-Ti(1)-C(11)	97.5(2)
C(10)-C(11)-Ti(1)	72.1(3)	C(1)-Ti(1)-C(11)	78.42(15)
C(12)-C(11)-Ti(1)	73.1(3)	C(9)-Ti(1)-C(11)	56.92(18)
C(13)-C(12)-C(11)	108.2(5)	C(17)-Ti(1)-C(11)	125.9(2)
C(13)-C(12)-Ti(1)	73.0(3)	C(10)-Ti(1)-C(11)	33.7(2)
C(11)-C(12)-Ti(1)	72.9(3)	C(16)-Ti(1)-C(11)	144.4(2)
C(12)-C(13)-C(9)	108.0(5)	C(18)-Ti(1)-C(11)	129.6(2)
C(12)-C(13)-Ti(1)	73.4(3)	C(14)-Ti(1)-C(11)	152.92(17)
C(9)-C(13)-Ti(1)	70.5(3)	C(13)-Ti(1)-C(11)	56.3(2)
C(15)-C(14)-C(18)	106.4(5)	F(5)-Ti(1)-C(12)	131.09(17)

C(15)-C(14)-Ti(1)	73.9(3)	C(1)-Ti(1)-C(12)	84.74(17)
C(18)-C(14)-Ti(1)	72.3(3)	C(9)-Ti(1)-C(12)	56.9(2)
C(16)-C(15)-C(14)	108.7(5)	C(17)-Ti(1)-C(12)	92.44(19)
C(16)-C(15)-Ti(1)	72.3(3)	C(10)-Ti(1)-C(12)	56.2(2)
C(14)-C(15)-Ti(1)	72.3(3)	C(16)-Ti(1)-C(12)	118.6(2)
C(15)-C(16)-C(17)	109.7(5)	C(18)-Ti(1)-C(12)	99.30(19)
C(15)-C(16)-Ti(1)	74.5(3)	C(14)-Ti(1)-C(12)	132.4(2)
C(17)-C(16)-Ti(1)	72.2(3)	C(13)-Ti(1)-C(12)	33.58(19)
C(16)-C(17)-C(18)	107.6(5)	C(11)-Ti(1)-C(12)	34.1(2)
C(16)-C(17)-Ti(1)	74.0(3)	F(5)-Ti(1)-C(15)	80.29(17)
C(18)-C(17)-Ti(1)	73.8(3)	C(1)-Ti(1)-C(15)	95.10(17)
C(17)-C(18)-C(14)	107.6(5)	C(9)-Ti(1)-C(15)	129.67(19)
C(17)-C(18)-Ti(1)	72.0(3)	C(17)-Ti(1)-C(15)	56.21(19)
C(14)-C(18)-Ti(1)	72.8(3)	C(10)-Ti(1)-C(15)	150.0(2)
F(5)-Ti(1)-C(1)	91.83(16)	C(16)-Ti(1)-C(15)	33.16(19)
F(5)-Ti(1)-C(9)	96.93(17)	C(18)-Ti(1)-C(15)	56.36(19)
C(1)-Ti(1)-C(9)	135.20(17)	C(14)-Ti(1)-C(15)	33.81(18)
F(5)-Ti(1)-C(17)	136.46(17)	C(13)-Ti(1)-C(15)	129.88(19)
C(1)-Ti(1)-C(17)	93.56(18)	C(11)-Ti(1)-C(15)	173.12(19)
C(9)-Ti(1)-C(17)	108.9(2)	C(12)-Ti(1)-C(15)	148.6(2)
F(5)-Ti(1)-C(10)	78.72(18)	C(8)-N(1)-C(4)	119.4(5)

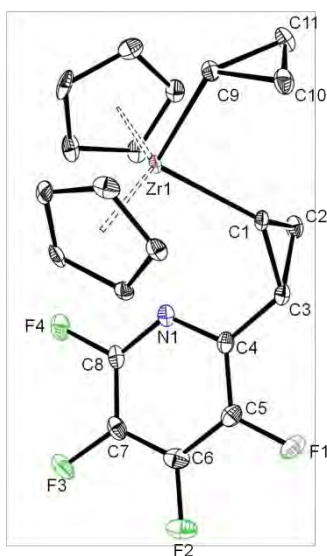


Table 30 Crystal data and structure refinement for **28**.

Formula	$C_{21}H_{19}F_4NZr$
Mol. wt.	452.59
Crystal system	Triclinic
Space group	<i>P</i> -1
<i>a</i> (Å)	8.0369(5)
<i>b</i> (Å)	8.0887(5)

$c(\text{\AA})$	15.9905(10)
$\alpha(^{\circ})$	94.671(2)
$\beta(^{\circ})$	92.716(2)
$\gamma(^{\circ})$	119.381(2)
$V(\text{\AA}^3)$	1578.74(7)
Z	2
Density (g/cm^3)	1.673
Abs. coeff., (mm^{-1})	0.657
$F(000)$	456
Crystal size, mm	0.1 x 0.08 x 0.02
θ range, deg	2.57 to 26.37
Limiting indices	$-9 \leq h \leq 10, -10 \leq k \leq 9, -19 \leq l \leq 19$
$R(\text{int})$	0.0517
Reflections collected	18230
Reflec. Unique [$I > 2\sigma(I)$]	3612
Completeness to θ	98.6%
Data/restraints/param.	3612 / 0 / 244
Goodness-of-fit	1.042
R_1 [$I > 2\sigma(I)$] (all data)	0.0469
wR_2 [$I > 2\sigma(I)$] (all data)	0.0996
Largest diff. $e \cdot \text{\AA}^{-3}$	1.200 and -0.997

Table 31 Bond lengths [\AA] for 28.

C(1)-C(2)	1.502(4)	C(12)-C(16)	1.405(5)
C(1)-C(3)	1.548(4)	C(12)-Zr(1)	2.506(3)
C(1)-Zr(1)	2.288(3)	C(12)-H(12)	1.0000
C(1)-H(1)	1.0000	C(13)-C(14)	1.418(5)
C(2)-C(3)	1.506(5)	C(13)-Zr(1)	2.520(3)
C(2)-H(2A)	0.9900	C(13)-H(13)	1.0000
C(2)-H(2B)	0.9900	C(14)-C(15)	1.402(5)
C(3)-C(4)	1.470(4)	C(14)-Zr(1)	2.517(3)
C(3)-H(3)	1.0000	C(14)-H(14)	1.0000
C(4)-N(1)	1.348(4)	C(15)-C(16)	1.404(5)
C(4)-C(5)	1.388(4)	C(15)-Zr(1)	2.527(3)
C(5)-F(1)	1.352(4)	C(15)-H(15)	1.0000
C(5)-C(6)	1.375(5)	C(16)-Zr(1)	2.509(3)
C(6)-F(2)	1.330(4)	C(16)-H(16)	1.0000
C(6)-C(7)	1.377(5)	C(17)-C(21)	1.396(4)
C(7)-F(3)	1.351(4)	C(17)-C(18)	1.412(5)
C(7)-C(8)	1.377(5)	C(17)-Zr(1)	2.492(3)
C(8)-N(1)	1.306(4)	C(17)-H(17)	1.0000
C(8)-F(4)	1.344(4)	C(18)-C(19)	1.400(5)
C(9)-C(11)	1.508(4)	C(18)-Zr(1)	2.493(3)

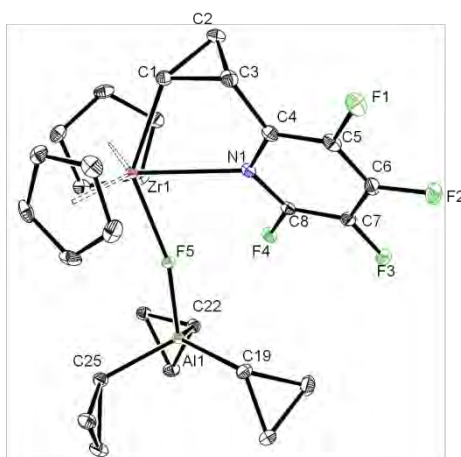
C(9)-C(10)	1.516(4)	C(18)-H(18)	1.0000
C(9)-Zr(1)	2.266(3)	C(19)-C(20)	1.399(5)
C(9)-H(9)	1.0000	C(19)-Zr(1)	2.531(3)
C(10)-C(11)	1.492(5)	C(19)-H(19)	1.0000
C(10)-H(10A)	0.9900	C(20)-C(21)	1.408(4)
C(10)-H(10B)	0.9900	C(20)-Zr(1)	2.548(3)
C(11)-H(11A)	0.9900	C(20)-H(20)	1.0000
C(11)-H(11B)	0.9900	C(21)-Zr(1)	2.538(3)
C(12)-C(13)	1.397(5)	C(21)-H(21)	1.0000

Table 32 Angles [°] for **28**.

C(2)-C(1)-C(3)	59.2(2)	C(17)-C(18)-Zr(1)	73.51(18)
C(2)-C(1)-Zr(1)	131.7(2)	C(19)-C(18)-H(18)	125.6
C(3)-C(1)-Zr(1)	136.1(2)	C(17)-C(18)-H(18)	125.6
C(2)-C(1)-H(1)	107.2	Zr(1)-C(18)-H(18)	125.6
C(3)-C(1)-H(1)	107.2	C(20)-C(19)-C(18)	108.1(3)
Zr(1)-C(1)-H(1)	107.2	C(20)-C(19)-Zr(1)	74.68(18)
C(1)-C(2)-C(3)	62.0(2)	C(18)-C(19)-Zr(1)	72.33(18)
C(1)-C(2)-H(2A)	117.6	C(20)-C(19)-H(19)	125.7
C(3)-C(2)-H(2A)	117.6	C(18)-C(19)-H(19)	125.7
C(1)-C(2)-H(2B)	117.6	Zr(1)-C(19)-H(19)	125.7
C(3)-C(2)-H(2B)	117.6	C(19)-C(20)-C(21)	108.2(3)
H(2A)-C(2)-H(2B)	114.7	C(19)-C(20)-Zr(1)	73.36(18)
C(4)-C(3)-C(2)	120.4(3)	C(21)-C(20)-Zr(1)	73.54(17)
C(4)-C(3)-C(1)	119.1(3)	C(19)-C(20)-H(20)	125.6
C(2)-C(3)-C(1)	58.9(2)	C(21)-C(20)-H(20)	125.6
C(4)-C(3)-H(3)	115.5	Zr(1)-C(20)-H(20)	125.6
C(2)-C(3)-H(3)	115.5	C(17)-C(21)-C(20)	107.8(3)
C(1)-C(3)-H(3)	115.5	C(17)-C(21)-Zr(1)	72.08(17)
N(1)-C(4)-C(5)	118.5(3)	C(20)-C(21)-Zr(1)	74.31(17)
N(1)-C(4)-C(3)	119.3(3)	C(17)-C(21)-H(21)	125.8
C(5)-C(4)-C(3)	122.2(3)	C(20)-C(21)-H(21)	125.8
F(1)-C(5)-C(6)	118.0(3)	Zr(1)-C(21)-H(21)	125.8
F(1)-C(5)-C(4)	120.6(3)	C(9)-Zr(1)-C(1)	95.47(11)
C(6)-C(5)-C(4)	121.5(3)	C(9)-Zr(1)-C(17)	128.60(11)
F(2)-C(6)-C(5)	120.8(3)	C(1)-Zr(1)-C(17)	112.01(11)
F(2)-C(6)-C(7)	120.3(3)	C(9)-Zr(1)-C(18)	98.46(12)
C(5)-C(6)-C(7)	118.9(3)	C(1)-Zr(1)-C(18)	136.42(11)
F(3)-C(7)-C(8)	122.0(3)	C(17)-Zr(1)-C(18)	32.90(11)
F(3)-C(7)-C(6)	121.7(3)	C(9)-Zr(1)-C(12)	126.54(12)
C(8)-C(7)-C(6)	116.4(3)	C(1)-Zr(1)-C(12)	114.80(11)
N(1)-C(8)-F(4)	116.5(3)	C(17)-Zr(1)-C(12)	80.70(11)
N(1)-C(8)-C(7)	125.3(3)	C(18)-Zr(1)-C(12)	88.84(12)
F(4)-C(8)-C(7)	118.2(3)	C(9)-Zr(1)-C(16)	95.90(12)
C(11)-C(9)-C(10)	59.1(2)	C(1)-Zr(1)-C(16)	137.09(11)

C(11)-C(9)-Zr(1)	120.5(2)	C(17)-Zr(1)-C(16)	92.15(11)
C(10)-C(9)-Zr(1)	123.5(2)	C(18)-Zr(1)-C(16)	82.10(11)
C(11)-C(9)-H(9)	114.3	C(12)-Zr(1)-C(16)	32.55(12)
C(10)-C(9)-H(9)	114.3	C(9)-Zr(1)-C(14)	88.66(11)
Zr(1)-C(9)-H(9)	114.3	C(1)-Zr(1)-C(14)	85.44(11)
C(11)-C(10)-C(9)	60.2(2)	C(17)-Zr(1)-C(14)	134.15(11)
C(11)-C(10)-H(10A)	117.8	C(18)-Zr(1)-C(14)	135.74(11)
C(9)-C(10)-H(10A)	117.8	C(12)-Zr(1)-C(14)	53.85(11)
C(11)-C(10)-H(10B)	117.8	C(16)-Zr(1)-C(14)	53.68(11)
C(9)-C(10)-H(10B)	117.8	C(9)-Zr(1)-C(13)	121.27(11)
H(10A)-C(10)-H(10B)	114.9	C(1)-Zr(1)-C(13)	85.39(11)
C(10)-C(11)-C(9)	60.7(2)	C(17)-Zr(1)-C(13)	104.10(11)
C(10)-C(11)-H(11A)	117.7	C(18)-Zr(1)-C(13)	120.37(12)
C(9)-C(11)-H(11A)	117.7	C(12)-Zr(1)-C(13)	32.27(11)
C(10)-C(11)-H(11B)	117.7	C(16)-Zr(1)-C(13)	53.65(11)
C(9)-C(11)-H(11B)	117.7	C(14)-Zr(1)-C(13)	32.70(11)
H(11A)-C(11)-H(11B)	114.8	C(9)-Zr(1)-C(15)	74.01(11)
C(13)-C(12)-C(16)	108.2(3)	C(1)-Zr(1)-C(15)	115.00(11)
C(13)-C(12)-Zr(1)	74.45(18)	C(17)-Zr(1)-C(15)	124.44(11)
C(16)-C(12)-Zr(1)	73.87(18)	C(18)-Zr(1)-C(15)	108.52(11)
C(13)-C(12)-H(12)	125.5	C(12)-Zr(1)-C(15)	53.75(12)
C(16)-C(12)-H(12)	125.5	C(16)-Zr(1)-C(15)	32.37(12)
Zr(1)-C(12)-H(12)	125.5	C(14)-Zr(1)-C(15)	32.27(11)
C(12)-C(13)-C(14)	107.8(3)	C(13)-Zr(1)-C(15)	53.69(11)
C(12)-C(13)-Zr(1)	73.29(18)	C(9)-Zr(1)-C(19)	75.38(11)
C(14)-C(13)-Zr(1)	73.53(18)	C(1)-Zr(1)-C(19)	116.26(11)
C(12)-C(13)-H(13)	125.8	C(17)-Zr(1)-C(19)	53.77(11)
C(14)-C(13)-H(13)	125.8	C(18)-Zr(1)-C(19)	32.35(12)
Zr(1)-C(13)-H(13)	125.8	C(12)-Zr(1)-C(19)	120.79(12)
C(15)-C(14)-C(13)	107.9(3)	C(16)-Zr(1)-C(19)	106.65(11)
C(15)-C(14)-Zr(1)	74.25(18)	C(14)-Zr(1)-C(19)	153.77(11)
C(13)-C(14)-Zr(1)	73.77(17)	C(13)-Zr(1)-C(19)	152.70(12)
C(15)-C(14)-H(14)	125.7	C(15)-Zr(1)-C(19)	121.72(11)
C(13)-C(14)-H(14)	125.7	C(9)-Zr(1)-C(21)	120.25(10)
Zr(1)-C(14)-H(14)	125.7	C(1)-Zr(1)-C(21)	83.71(10)
C(14)-C(15)-C(16)	108.0(3)	C(17)-Zr(1)-C(21)	32.22(10)
C(14)-C(15)-Zr(1)	73.48(18)	C(18)-Zr(1)-C(21)	53.70(10)
C(16)-C(15)-Zr(1)	73.11(19)	C(12)-Zr(1)-C(21)	106.61(11)
C(14)-C(15)-H(15)	125.8	C(16)-Zr(1)-C(21)	124.17(11)
C(16)-C(15)-H(15)	125.8	C(14)-Zr(1)-C(21)	149.90(11)
Zr(1)-C(15)-H(15)	125.8	C(13)-Zr(1)-C(21)	118.21(11)
C(15)-C(16)-C(12)	108.2(3)	C(15)-Zr(1)-C(21)	156.54(11)
C(15)-C(16)-Zr(1)	74.51(18)	C(19)-Zr(1)-C(21)	53.29(10)
C(12)-C(16)-Zr(1)	73.58(18)	C(9)-Zr(1)-C(20)	88.10(11)
C(15)-C(16)-H(16)	125.6	C(1)-Zr(1)-C(20)	86.24(11)
C(12)-C(16)-H(16)	125.6	C(17)-Zr(1)-C(20)	53.43(10)
Zr(1)-C(16)-H(16)	125.6	C(18)-Zr(1)-C(20)	53.40(11)
C(21)-C(17)-C(18)	108.1(3)	C(12)-Zr(1)-C(20)	134.13(11)

C(21)-C(17)-Zr(1)	75.70(17)	C(16)-Zr(1)-C(20)	135.35(11)
C(18)-C(17)-Zr(1)	73.59(17)	C(14)-Zr(1)-C(20)	170.74(10)
C(21)-C(17)-H(17)	125.5	C(13)-Zr(1)-C(20)	150.08(11)
C(18)-C(17)-H(17)	125.5	C(15)-Zr(1)-C(20)	152.97(11)
Zr(1)-C(17)-H(17)	125.5	C(19)-Zr(1)-C(20)	31.96(11)
C(19)-C(18)-C(17)	107.8(3)	C(21)-Zr(1)-C(20)	32.15(10)
C(19)-C(18)-Zr(1)	75.32(18)	C(8)-N(1)-C(4)	119.5(3)


Table 33 Crystal data and structure refinement for **29**.

Formula	$C_{27}H_{29}AlF_5NZr$
Mol. wt.	580.71
Crystal system	Triclinic
Space group	<i>P</i> -1
$a(\text{\AA})$	8.0046(3)
$b(\text{\AA})$	10.9827(5)
$c(\text{\AA})$	14.3561(7)
$\alpha(^{\circ})$	89.916(2)
$\beta(^{\circ})$	78.973(2)
$\gamma(^{\circ})$	84.569(2)
$V(\text{\AA}^3)$	1233.03(9)
<i>Z</i>	2
Density (g/cm^3)	1.564
Abs. coeff., (mm^{-1})	0.536
$F(000)$	592
Crystal size, mm	0.15 x 0.11 x 0.02
θ range, deg	1.45 to 26.37
Limiting indices	$-10 \leq h \leq 9, -13 \leq k \leq 13, -17 \leq l \leq 17$
$R(\text{int})$	0.0235
Reflections collected	28356
Reflec. Unique [$I > 2\sigma(I)$]	5025

Completeness to θ	99.9%
Data/restraints/param.	5025 / 0 / 316
Goodness-of-fit	1.075
R_1 [$I > 2\sigma(I)$] (all data)	0.0216
wR_2 [$I > 2\sigma(I)$] (all data)	0.0517
Largest diff. $e \cdot \text{\AA}^{-3}$	0.427 and -0.274

Table 34 Bond lengths [\AA] for **29**.

C(1)-C(2)	1.502(2)	C(14)-C(18)	1.400(2)
C(1)-C(3)	1.524(2)	C(14)-C(15)	1.404(2)
C(1)-Zr(1)	2.3140(15)	C(14)-Zr(1)	2.5285(15)
C(2)-C(3)	1.531(2)	C(15)-C(16)	1.419(2)
C(3)-C(4)	1.465(2)	C(15)-Zr(1)	2.5353(15)
C(4)-N(1)	1.3671(19)	C(16)-C(17)	1.401(2)
C(4)-C(5)	1.379(2)	C(16)-Zr(1)	2.5158(15)
C(5)-F(1)	1.3482(18)	C(17)-C(18)	1.415(2)
C(5)-C(6)	1.375(2)	C(17)-Zr(1)	2.4815(15)
C(6)-F(2)	1.3250(18)	C(18)-Zr(1)	2.4752(15)
C(6)-C(7)	1.380(2)	C(19)-C(21)	1.513(2)
C(7)-F(3)	1.3342(18)	C(19)-C(20)	1.516(2)
C(7)-C(8)	1.378(2)	C(19)-Al(1)	1.9660(15)
C(8)-N(1)	1.3243(19)	C(20)-C(21)	1.477(2)
C(8)-F(4)	1.3292(17)	C(22)-C(23)	1.529(2)
C(9)-C(13)	1.396(3)	C(22)-C(24)	1.530(2)
C(9)-C(10)	1.410(3)	C(22)-Al(1)	1.9702(15)
C(9)-Zr(1)	2.5240(16)	C(23)-C(24)	1.494(2)
C(10)-C(11)	1.400(3)	C(25)-C(26)	1.531(2)
C(10)-Zr(1)	2.5313(16)	C(25)-C(27)	1.534(2)
C(11)-C(12)	1.405(2)	C(25)-Al(1)	1.9648(16)
C(11)-Zr(1)	2.5285(16)	C(26)-C(27)	1.491(2)
C(12)-C(13)	1.397(2)	N(1)-Zr(1)	2.5270(12)
C(12)-Zr(1)	2.5104(15)	Zr(1)-F(5)	2.1654(8)
C(13)-Zr(1)	2.5332(15)	F(5)-Al(1)	1.8089(9)

Table 35 Angles [$^\circ$] for **28**.

C(2)-C(1)-C(3)	60.78(11)	C(1)-Zr(1)-C(18)	127.40(5)
C(2)-C(1)-Zr(1)	129.12(11)	F(5)-Zr(1)-C(17)	115.47(4)
C(3)-C(1)-Zr(1)	115.49(10)	C(1)-Zr(1)-C(17)	99.13(5)
C(1)-C(2)-C(3)	60.32(10)	C(18)-Zr(1)-C(17)	33.17(5)
C(4)-C(3)-C(1)	115.34(13)	F(5)-Zr(1)-C(12)	123.49(4)
C(4)-C(3)-C(2)	112.40(13)	C(1)-Zr(1)-C(12)	80.63(6)
C(1)-C(3)-C(2)	58.91(10)	C(18)-Zr(1)-C(12)	102.90(5)

N(1)-C(4)-C(5)	119.71(14)	C(17)-Zr(1)-C(12)	81.67(5)
N(1)-C(4)-C(3)	116.93(13)	F(5)-Zr(1)-C(16)	127.89(4)
C(5)-C(4)-C(3)	122.96(14)	C(1)-Zr(1)-C(16)	72.95(5)
F(1)-C(5)-C(6)	118.85(14)	C(18)-Zr(1)-C(16)	54.45(5)
F(1)-C(5)-C(4)	119.59(14)	C(17)-Zr(1)-C(16)	32.56(6)
C(6)-C(5)-C(4)	121.49(14)	C(12)-Zr(1)-C(16)	96.18(5)
F(2)-C(6)-C(5)	121.01(15)	F(5)-Zr(1)-C(9)	79.30(5)
F(2)-C(6)-C(7)	120.54(15)	C(1)-Zr(1)-C(9)	95.55(6)
C(5)-C(6)-C(7)	118.38(14)	C(18)-Zr(1)-C(9)	129.13(6)
F(3)-C(7)-C(8)	121.32(14)	C(17)-Zr(1)-C(9)	129.50(6)
F(3)-C(7)-C(6)	121.14(14)	C(12)-Zr(1)-C(9)	53.55(5)
C(8)-C(7)-C(6)	117.52(14)	C(16)-Zr(1)-C(9)	149.46(6)
N(1)-C(8)-F(4)	117.60(13)	F(5)-Zr(1)-N(1)	71.00(4)
N(1)-C(8)-C(7)	124.84(14)	C(1)-Zr(1)-N(1)	68.99(5)
F(4)-C(8)-C(7)	117.51(13)	C(18)-Zr(1)-N(1)	123.78(5)
C(13)-C(9)-C(10)	107.50(15)	C(17)-Zr(1)-N(1)	136.37(5)
C(13)-C(9)-Zr(1)	74.34(9)	C(12)-Zr(1)-N(1)	133.19(5)
C(10)-C(9)-Zr(1)	74.08(9)	C(16)-Zr(1)-N(1)	107.28(5)
C(11)-C(10)-C(9)	108.15(15)	C(9)-Zr(1)-N(1)	93.97(5)
C(11)-C(10)-Zr(1)	73.83(9)	F(5)-Zr(1)-C(11)	96.44(5)
C(9)-C(10)-Zr(1)	73.52(9)	C(1)-Zr(1)-C(11)	112.99(6)
C(10)-C(11)-C(12)	107.76(16)	C(18)-Zr(1)-C(11)	82.32(6)
C(10)-C(11)-Zr(1)	74.04(9)	C(17)-Zr(1)-C(11)	76.31(6)
C(12)-C(11)-Zr(1)	73.10(9)	C(12)-Zr(1)-C(11)	32.37(6)
C(13)-C(12)-C(11)	107.97(15)	C(16)-Zr(1)-C(11)	104.15(6)
C(13)-C(12)-Zr(1)	74.82(9)	C(9)-Zr(1)-C(11)	53.54(6)
C(11)-C(12)-Zr(1)	74.53(9)	N(1)-Zr(1)-C(11)	147.32(5)
C(9)-C(13)-C(12)	108.57(16)	F(5)-Zr(1)-C(14)	74.08(4)
C(9)-C(13)-Zr(1)	73.61(9)	C(1)-Zr(1)-C(14)	114.69(5)
C(12)-C(13)-Zr(1)	73.02(9)	C(18)-Zr(1)-C(14)	32.48(5)
C(18)-C(14)-C(15)	108.41(14)	C(17)-Zr(1)-C(14)	53.96(5)
C(18)-C(14)-Zr(1)	71.66(8)	C(12)-Zr(1)-C(14)	133.98(5)
C(15)-C(14)-Zr(1)	74.17(9)	C(16)-Zr(1)-C(14)	53.81(5)
C(14)-C(15)-C(16)	107.93(15)	C(9)-Zr(1)-C(14)	149.22(6)
C(14)-C(15)-Zr(1)	73.64(9)	N(1)-Zr(1)-C(14)	91.76(5)
C(16)-C(15)-Zr(1)	72.93(9)	C(11)-Zr(1)-C(14)	114.26(5)
C(17)-C(16)-C(15)	107.55(14)	F(5)-Zr(1)-C(10)	70.09(4)
C(17)-C(16)-Zr(1)	72.37(9)	C(1)-Zr(1)-C(10)	123.35(6)
C(15)-C(16)-Zr(1)	74.44(9)	C(18)-Zr(1)-C(10)	96.74(6)
C(16)-C(17)-C(18)	108.38(14)	C(17)-Zr(1)-C(10)	104.08(6)
C(16)-C(17)-Zr(1)	75.07(9)	C(12)-Zr(1)-C(10)	53.41(5)
C(18)-C(17)-Zr(1)	73.17(9)	C(16)-Zr(1)-C(10)	135.06(6)
C(14)-C(18)-C(17)	107.71(14)	C(9)-Zr(1)-C(10)	32.40(7)
C(14)-C(18)-Zr(1)	75.85(9)	N(1)-Zr(1)-C(10)	117.65(6)
C(17)-C(18)-Zr(1)	73.66(9)	C(11)-Zr(1)-C(10)	32.13(6)
C(21)-C(19)-C(20)	58.36(11)	C(14)-Zr(1)-C(10)	120.86(6)
C(21)-C(19)-Al(1)	124.48(12)	F(5)-Zr(1)-C(13)	111.29(5)
C(20)-C(19)-Al(1)	124.07(11)	C(1)-Zr(1)-C(13)	70.30(6)

C(21)-C(20)-C(19)	60.70(11)	C(18)-Zr(1)-C(13)	133.80(6)
C(20)-C(21)-C(19)	60.94(11)	C(17)-Zr(1)-C(13)	113.17(6)
C(23)-C(22)-C(24)	58.49(9)	C(12)-Zr(1)-C(13)	32.16(6)
C(23)-C(22)-Al(1)	118.66(11)	C(16)-Zr(1)-C(13)	119.46(6)
C(24)-C(22)-Al(1)	118.63(10)	C(9)-Zr(1)-C(13)	32.05(6)
C(24)-C(23)-C(22)	60.78(10)	N(1)-Zr(1)-C(13)	102.19(5)
C(23)-C(24)-C(22)	60.72(10)	C(11)-Zr(1)-C(13)	53.20(6)
C(26)-C(25)-C(27)	58.21(10)	C(14)-Zr(1)-C(13)	166.00(6)
C(26)-C(25)-Al(1)	119.89(11)	C(10)-Zr(1)-C(13)	53.09(6)
C(27)-C(25)-Al(1)	119.07(11)	Al(1)-F(5)-Zr(1)	164.93(5)
C(27)-C(26)-C(25)	60.97(10)	F(5)-Al(1)-C(25)	105.91(5)
C(26)-C(27)-C(25)	60.83(10)	F(5)-Al(1)-C(19)	101.31(5)
C(8)-N(1)-C(4)	117.73(13)	C(25)-Al(1)-C(19)	112.64(7)
C(8)-N(1)-Zr(1)	128.17(10)	F(5)-Al(1)-C(22)	105.85(5)
C(4)-N(1)-Zr(1)	111.91(9)	C(25)-Al(1)-C(22)	110.31(6)
F(5)-Zr(1)-C(1)	139.17(4)	C(19)-Al(1)-C(22)	119.30(7)
F(5)-Zr(1)-C(18)	82.47(4)		

Résumé en français

A. Chapitre 1

Dans ce chapitre nous présentons la synthèse de complexes de cyclopropyllithium. Notre étude s'est particulièrement focalisée sur les interactions C–C agostiques.

I.1.Introduction

Les organolithiens sont des composés utilisés dans tous les laboratoires de synthèse, et sont impliqués dans des réactions de déprotonation, de transmetallation ou encore de substitution nucléophile. Contrairement à ce que pourrait suggérer la façon simpliste de les écrire, RLi, les organolithiens sont rarement monomériques et forment des agrégats. Par exemple, les structures à l'état solide du MeLi et du *n*-BuLi sont présentées en Schéma 1, et forment respectivement un tétramère et un hexamère.

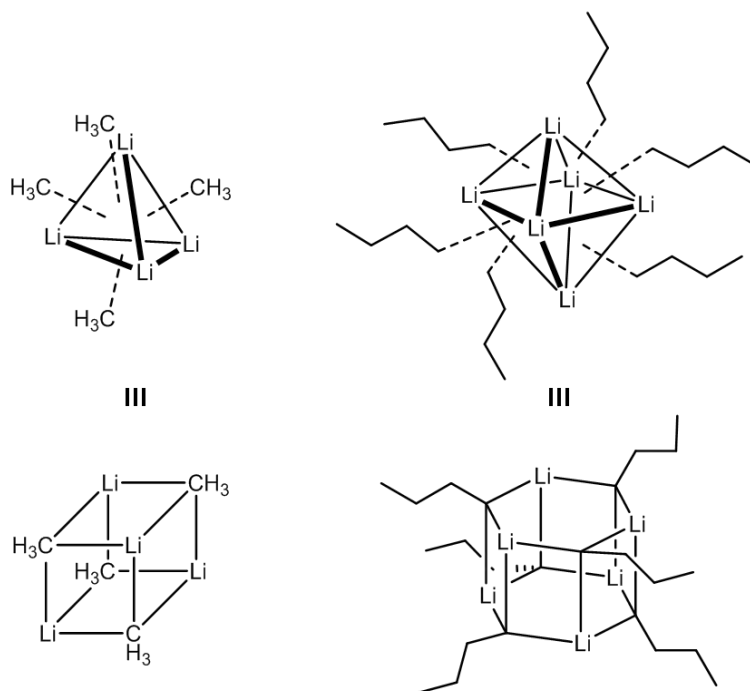


Schéma 1 Structures à l'état solide de $[\mu_3\text{-MeLi}]_4$ (gauche) et $[\mu_3\text{-}n\text{-BuLi}]_6$ (droite).

Le contrôle de la réactivité des organolithiens implique le contrôle de leur agrégation, à l'état solide ou en solution. Plusieurs facteurs régissent la taille des agrégats :

- la taille du carbanion, plus celui-ci est encombré stériquement, et plus les agrégats tendent à être petits.

- l'utilisation de bases de Lewis dans le milieu telles que des éthers (Et₂O, thf, dme...) ou des polyamines (tmeda, pmdta...). Ces bases vont se coordiner au centre Li⁺, vont le stabiliser, et peuvent ainsi casser les interactions secondaires responsables de l'agrégation (voir ci-dessous). L'ajout de bases permet un contrôle précis de l'agrégation, celle-ci diminuant avec le caractère donneur de la base et/ou l'augmentation de sa denticité.

- la concentration et la température. Cependant, si la taille des agrégats suit le principe de Le Chatelier en ce qui concerne la concentration (la taille des agrégats augmente lorsque la concentration augmente), l'influence de la température peut varier dans un sens ou l'autre selon les espèces.

Un dernier facteur influence la taille des agrégats, il s'agit des interactions secondaires. Ces interactions sont de nature électrostatique et sont observées lorsque qu'un groupe riche en densité électronique se trouve à proximité du centre Li⁺ électropositifs. Trois types d'interactions peuvent être observés dans les organolithiens ne contenant que du carbone et de l'hydrogène : les interactions entre le système π d'un cycle aromatique et le cation Li⁺, les interactions C–H agostiques et les interactions C–C agostiques. Des exemples de structures présentant les deux premiers types d'interactions sont présentés en Schéma 2.

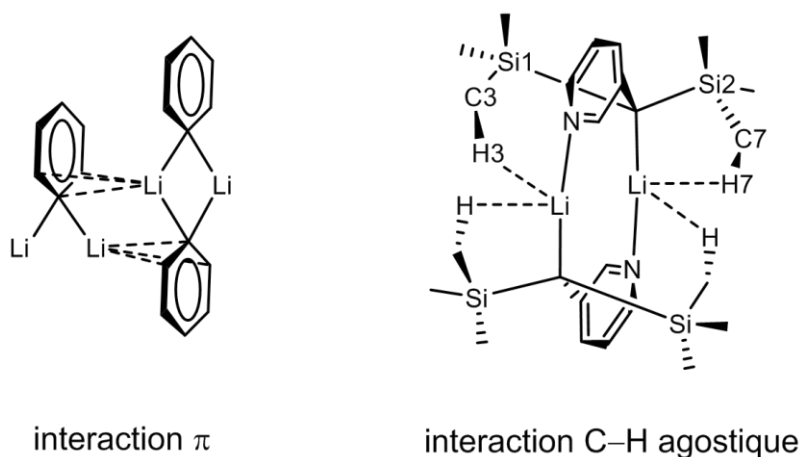


Schéma 2 Exemples de complexes présentant des interactions secondaires. Un fragment du complexe $\{[\mu\text{-PhLi}]_2\}_\infty$ (à gauche) et le complexe $[2\text{-(Me}_3\text{Si)}_2\text{CLiC}_5\text{H}_4\text{N}]_2$ (à droite).

Les interactions C–C agostiques sont beaucoup plus rares, et n’ont jamais été complètement caractérisées pour les organolithiens. C’est pourquoi nous nous sommes penchés sur la synthèse de dérivés du cyclopropyllithium, afin d’étudier ces interactions, le groupement cyclopropyle ayant la particularité de préférer interagir avec ses liaisons C–C plutôt qu’avec ses liaisons C–H.

De plus, dans la famille des cycloalkyllithiens, seuls le *c*-PenLi et le *c*-HexLi ont été isolés et totalement caractérisés (Schéma 3).

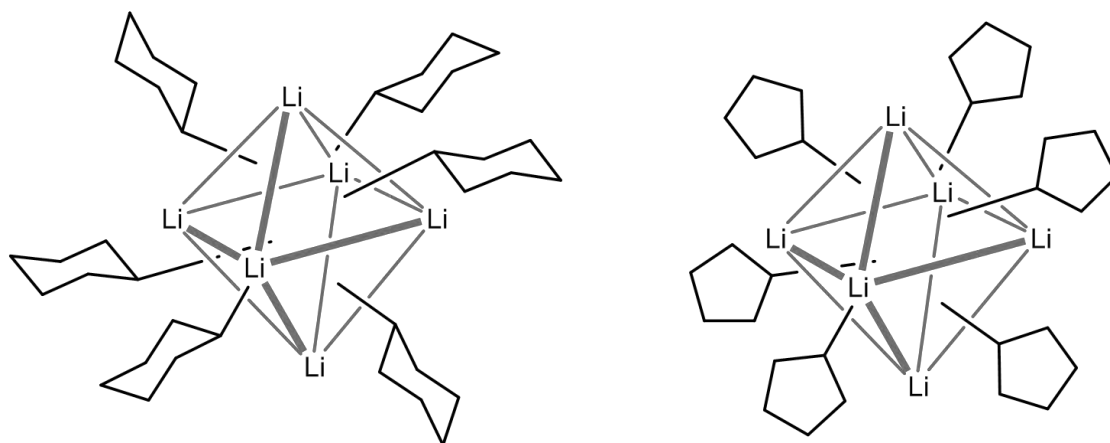


Schéma 3 Structures à l'état solide du *c*-HexLi (à gauche) et du *c*-PenLi (à droite).

Toutefois, de nombreux essais infructueux d'analyse par DRX de cristaux de *c*-PrLi nous ont poussé à nous intéresser à des dérivés stabilisés, et plus simples à isoler.

I.2. Résultats et discussion

Différents cyclopropyles substitués en α ont été synthétisés. Afin de permettre la délocalisation de la charge négative du carbanion, nous avons utilisé les groupes trimethylsilyle, phenyl, et phenylsulfure. Bien que des complexes de lithium des trois cyclopropyles correspondant aient été obtenus, nous nous focalisons dans ce résumé sur les résultats les plus aboutis obtenus à partir du phenylcyclopropyllithium.

a. Synthèse du phenylcyclopropyllithium

Le phenylcyclopropane étant un produit commercial, la première stratégie utilisée pour obtenir le phenylcyclopropyllithium a été la déprotonation de l'hydrocarbure par du *n*-BuLi dans l'hexane en présence de tmeda (Schéma 4, voie A).

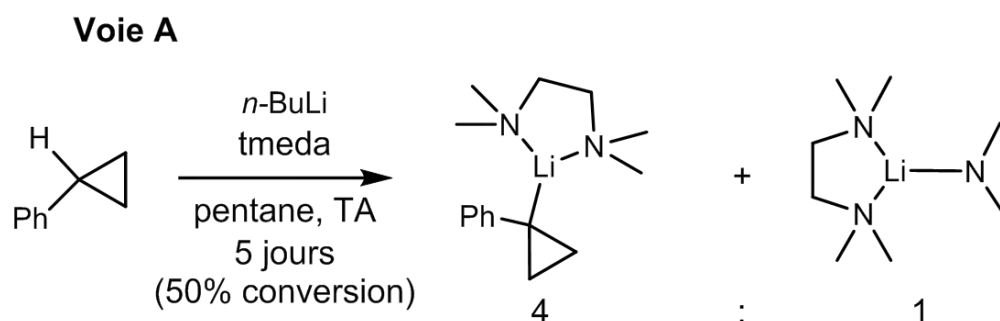
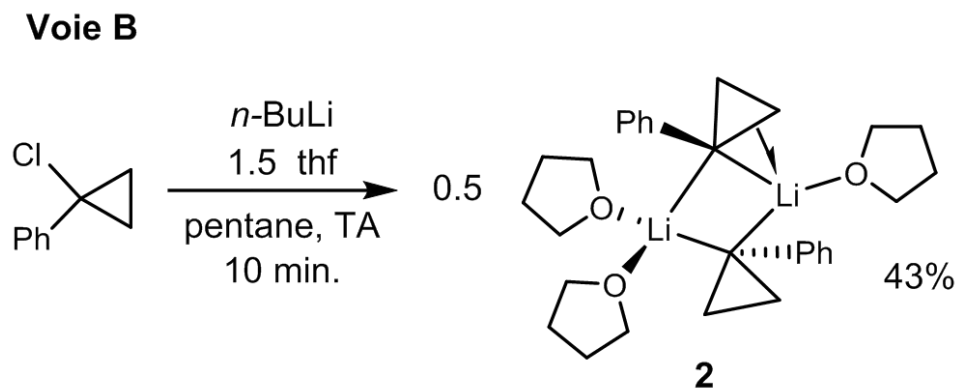


Schéma 4 Réaction de déprotonation du phenylcyclopropane.

Bien que le produit attendu ait été obtenu, une cassure de la tmeda a également été observée, et est accompagnée par la formation de diméthylamidure de lithium (LiNMe_2). Nous avons rencontré des difficultés lors de la séparation de ce composé, et nous avons donc modifié notre stratégie de synthèse. Nous avons donc considéré la réaction d'échange halogène/métal entre le 1-chloro-1-phenylcyclopropane et le *n*-BuLi (Schéma 5, voie B). Cette réaction est très rapide (10 min) et nous avons pu isoler un nouveau complexe $[\text{Li}(\text{thf})_2(\mu\text{-}c\text{-CPhC}_2\text{H}_4)_2\text{Li}(\text{thf})]$ (**2**) avec un rendement de 43 %. L'espèce **2** possédant 3 thf a toujours été obtenue durant la réaction ou lors d'une étape de recristallisation, et cela, quelque soit la quantité de thf dans le milieu. **2** a été complètement caractérisé par DRX, spectroscopie RMN et analyse élémentaire.

Schéma 5 Synthèse de **2**.

b. Structure à l'état solide

A l'état solide (Figure 17), **2** est un dimère avec deux groupements 1-phenylcyclopropyle pontant deux Li^+ par les carbones C1 (groupe A) et C10 (groupe B). De façon surprenante, chacun des ions Li^+ est coordonné par un nombre différent de molécules de thf. Alors que Li2 est lié à deux molécules de thf (dont l'une est désordonnée) selon une géométrie pseudo-tétraogonale, Li1 est trigonal plan (somme de ses angles = 360°) avec seulement un thf coordonné. Bien que les longueurs des liaisons $\text{Li}-\mu\text{-C}\alpha$ impliquant Li2 [$\text{Li2}-\text{C1}$ 2.201(4), $\text{Li2}-\text{C10}$ 2.263(4) Å] soient dans l'intervalle attendu pour ce type de composé, les longueurs équivalentes impliquant le tricoordonné Li1 [$\text{Li1}-\text{C1}$ 2.098(4), $\text{Li1}-\text{C10}$ 2.129(4) Å] sont significativement plus courtes.

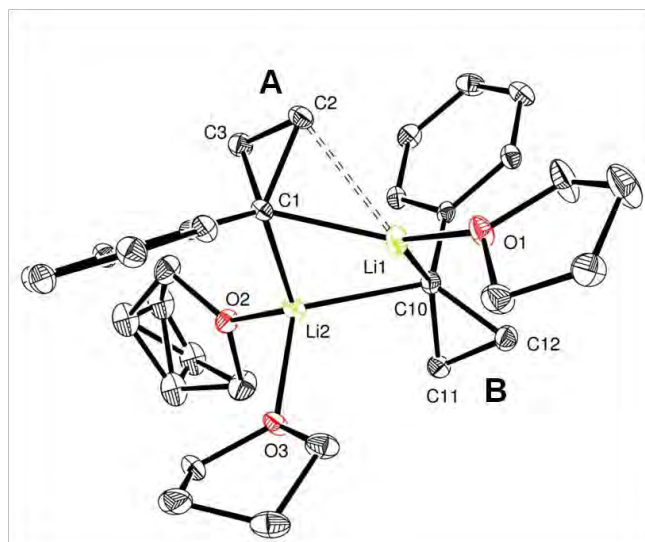


Figure 17 Représentation ORTEP de $[Li(thf)_2(\mu\text{-}c\text{-}CPhC_2H_4)_2Li(thf)]$ (**2**). Les ellipsoïdes sont représentés avec un niveau de probabilité de 30%, les hydrogènes ont été omis pour des raisons de clarté. L'interaction secondaire $Li\cdots C-C$ est représentée par une liaison double pointillée. Longueurs de liaisons (Å) et angles ($^\circ$) marquants: $Li1-C1$ 2.098(4), $Li1-C10$ 2.129(4), $Li2-C1$ 2.201(4), $Li2-C10$ 2.263(4), $Li1\cdots C2$ 2.368(4), $C1-C2$ 1.526(3), $C1-C3$ 1.519(3), $C2-C3$ 1.505(3), $C10-C11$ 1.524(3), $C10-C12$ 1.517(3), $C11-C12$ 1.500(3); $Li1-C1-C2$ 79.89(15), $Li1-C1-C3$ 113.02(16), $Li1-C10-C12$ 100.88(16), $Li1-C10-C11$ 133.02(17), $Li2-C1-C2$ 126.11(16), $Li2-C1-C3$ 93.42(14), $Li2-C10-C11$ 90.53(14), $Li2-C10-C12$ 127.17(16).

Cette structure non-symétrique s'accompagne d'une courte distance entre $Li1$ et l'un des carbones β ($C2$) du ligand cyclopropyle **A** [$Li1\cdots C2$ 2.368(4) Å]. L'angle associé $Li-C\alpha-C\beta$ [$Li1-C1-C2$ 79.89(15) $^\circ$] est également plus aigu. Ces différences ne sont pas observées pour le groupement cyclopropyle **B** qui apparaît comme non distordu. Les autres distances $Li\cdots C\beta$ sont bien plus longues, ce qui exclut toute autre interaction [$Li1\cdots C12$ 2.838(4), $Li2\cdots C3$ 2.748(4), $Li2\cdots C11$ 2.740(4) Å]. Cette distorsion ne semble pas être le résultat d'un encombrement stérique, puisque des calculs théoriques montrent que $Li1$ pourrait s'accommoder d'un second ligand thf (voir paragraphe ci-dessous). Nous proposons donc que cette situation s'explique par l'existence d'une distorsion C-C agostique.

c. Calculs DFT

Des calculs DFT ont été réalisés dans le but de valider la structure électronique de **2**. L'optimisation (PBE0, def2TZVP) de **2** a résulté en une structure non symétrique similaire à celle obtenue par DRX (Figure 18). Elle comprend la même distorsion du cycle **A** vers le lithium tricoordiné, avec une distance $Li\cdots C\beta$ de 2.33 Å et un angle $Li-C\alpha-C\beta$ de 80 $^\circ$. La

distance la plus courte entre Li1 et un H sur C β est 2.12 Å, et ne peut pas être considérée comme très courte pour ce type de complexe. Ainsi, cela exclut qu'une interaction C–H agostique soit à l'origine de la distorsion observée. En revanche, une preuve de l'existence d'une interaction agostique C–C provient de la valeur calculée de la constante de couplage J_{CC} . Si l'on considère $J_{C_2C_3}$ comme une référence de cette valeur dans le cyclopropane libre (12.4 Hz), on constate qu'un abaissement significatif du $J_{C\alpha C\beta}$ ($J_{C_1C_2} = -3.4$ Hz) a été calculé par rapport aux trois autres valeurs de $J_{C\alpha C\beta}$ du complexe (Figure 18). Le J_{CH} mentionné au-dessus a une valeur normale de 139 Hz. Une analyse de la population naturelle ou une NBO indiquent la présence d'une charge négative plus forte sur C2 par rapport à C3 appartenant au cycle A, mais aussi par rapport aux deux C β s du cycle B, confirmant la nature électrostatique de l'interaction Li1...C2.

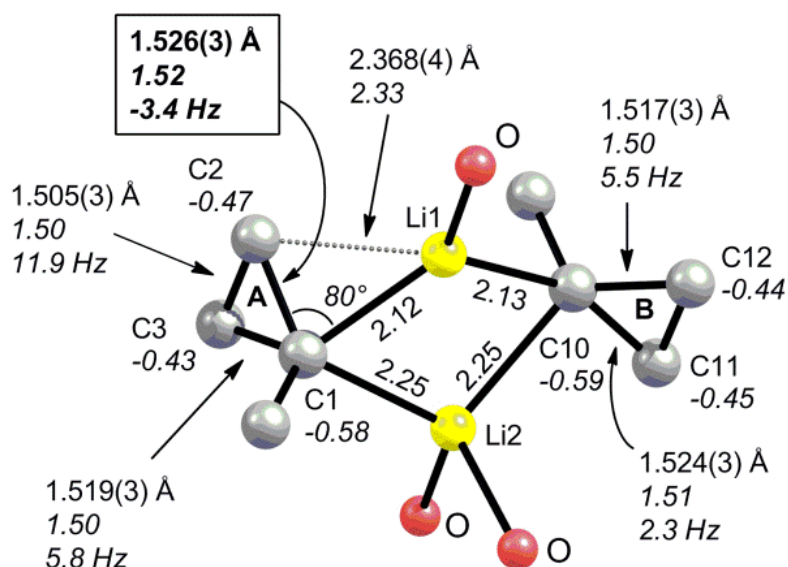


Figure 18 Cœur de la structure de **2** optimisée par DFT. Légende: longueur de liaison expérimentale (en haut), longueur de liaison et J_{CC} calculés (en italique). La numérotation des atomes reprend celle de la structure cristalline, et est accompagnée des charges naturelles calculées (au). Dans le cas des groupements phényles et des ligands thf, seuls les carbones ipso et les atomes d'oxygène sont respectivement représentés pour des raisons de clarté. De même les hydrogènes n'ont pas été représentés.

Nous avons également pu optimiser le complexe **2-thf**, produit fictif de l'addition d'un thf supplémentaire sur Li1 dans **2**. Comme on peut le voir en Figure 19, dans ce cas toutes les liaisons entre les C α et les ions lithium tétracoordinés sont très similaires. Les distances les plus courtes entre des C β et des ions Li $^+$ valent 2.57 et 2.64 Å, ce qui exclut toute interaction significative. Les conformations prises par les deux groupes phenylcyclopropyles ainsi que

par les cycles phenyles minimisent la gêne stérique avec les quatre ligands thf. La différence d'énergie entre **2-thf** et **2** plus une molécule de thf est négligeable (2 kJ/mol). Ainsi, nous pouvons conclure que la gêne stérique pourrait être supportée dans 2-thf, et donc la présence d'une interaction agostique C–C dans **2** au lieu d'une molécule de thf donne une idée qualitative de la force de cette interaction.

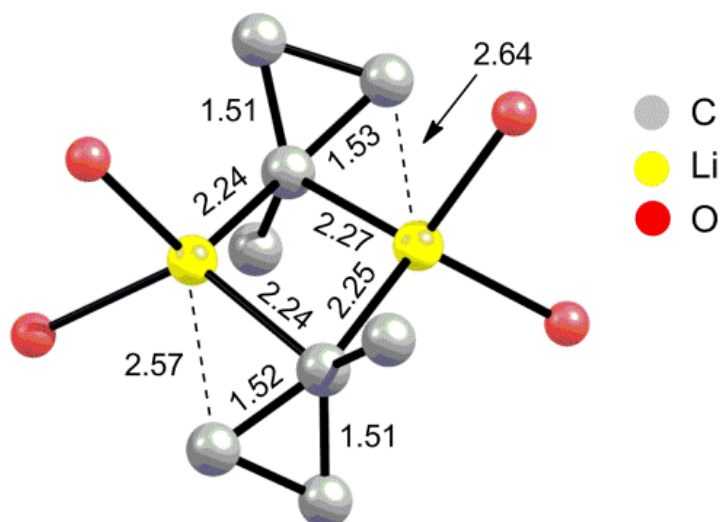


Figure 19 Cœur de la structure de **2-thf** optimisée par DFT avec les distances pertinentes en Å. Dans le cas des groupements phenyles et des ligands thf, seuls les carbones ipso et les atomes d'oxygène sont respectivement représentés pour des raisons de clarté. De même les hydrogènes n'ont pas été représentés.

Cette approche jointe entre l'analyse par DRX et les calculs DFT a permis la caractérisation de la première interaction C–C agostique dans un complexe organolithien.

B. Chapitre 2

Dans ce chapitre nous étudions la synthèse de complexes cyclopropylcalcium.

I.1.Introduction

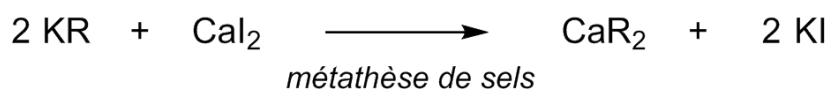
Le calcium est le 20^{ème} élément de la classification périodique. Il appartient à la famille des alcalino-terreux. C'est un élément très électropositif ($\chi(\text{Ca}) = 1.04$), oxophile et qui forme des liaisons à caractère ionique avec les autres éléments. Le calcium est très abondant, non toxique et peu cher. Pourtant, sa chimie organométallique, contrairement à celle de son analogue le magnésium, est encore peu développée. Deux raisons peuvent expliquer cela :

-le calcium métallique est très peu réactif et des protocoles spécifiques sont nécessaires pour l'utiliser en synthèse.

-les complexes organométalliques du calcium sont très sensibles à la présence d'eau et d'air, et sont sujets à différents types de réactions de redistribution, dont la plus connue est l'équilibre de Schlenk.

Les deux voies de synthèse des composés organocalcium les plus utilisées sont présentées en Schéma 6. Il s'agit (i) de la métathèse de sels entre l'iodure de calcium (CaI_2) et un organopotassium, et (ii) de l'activation du calcium par dissolution dans l'ammoniac liquide puis évaporation de ce dernier, suivie par l'addition oxydante d'un halogénoalcane RX (réaction de type Grignard).

(i)



(ii)

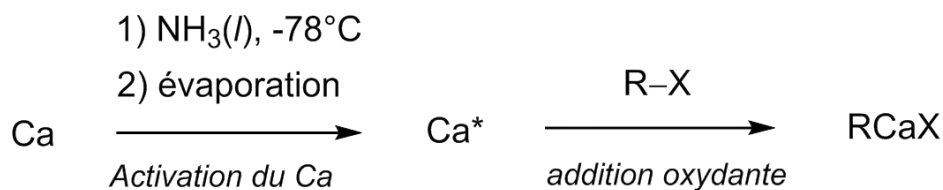


Schéma 6 Voies de synthèse communes pour la formation d'organocalcium.

En utilisant l'une ou l'autre de ces méthodes, des complexes variés ont été obtenus et caractérisés, notamment benzyl-, allyl-, aryl-, vinyl- et alkylcalcium. Par exemple, la structure d'un alkylcalcium $[(\text{SiMe}_3)\text{CH}_2\text{Ca}(\text{thp})_4\text{I}]$ synthétisé par la voie (ii) et reporté récemment est présentée ci-dessous (Schéma 7)

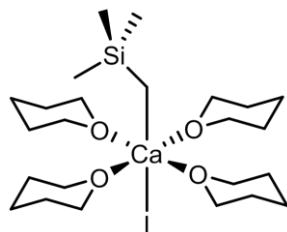


Schéma 7 Structure à l'état solide de $[(\text{SiMe}_3)\text{CH}_2\text{Ca}(\text{thp})_4\text{I}]$.

Toutefois, aucun complexe cyclopropylcalcium n'a été reporté jusqu'à maintenant. Nous pensons que ce motif pourrait interagir avec le calcium, qui est déficient en électron, au moyen d'une rare interaction C–C agostique. Afin de vérifier cette hypothèse, nous avons synthétisé des complexes de dérivés cyclopropylcalcium.

1.2. Résultats et discussion

a. Métathèse de sels

Afin de procéder à une métathèse de sels, nous avons commencé par synthétiser un précurseur organopotassien. Le cyclopropylpotassium n'ayant jamais été reporté, nous avons synthétisé un dérivé connu. Nous avons choisi le 1-phenylcyclopropylpotassium (**10**) dont la synthèse est présentée en Schéma 8. Cette espèce doit être synthétisée et manipulée en dessous de -40°C , sinon une réaction auto-catalysée de dégradation d'éther survient (Schéma 8).

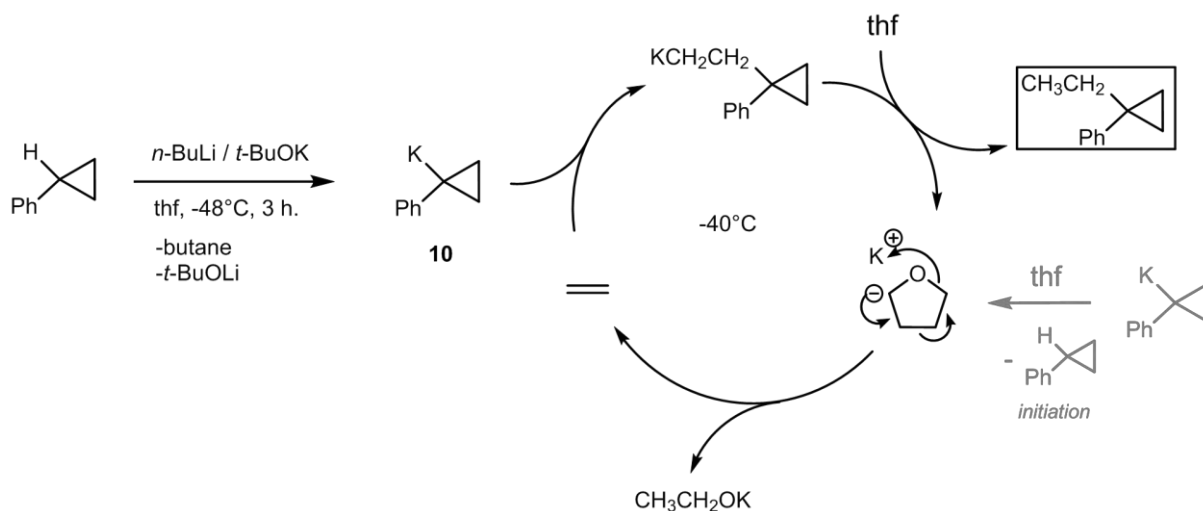


Schéma 8 Synthèse de **10** et du 1-éthyl-1-phényl-cyclopropane.

Nous avons obtenu une poudre rouge avec un rendement d'environ 55%, mais bien que celle-ci contenait majoritairement **10**, une proportion non négligeable de tert-butoxide de potassium et de $[(\text{Ph}-c\text{-C}_3\text{H}_4)\text{CH}_2\text{CH}_2\text{K}]$ a été observée. Nous avons néanmoins fait réagir ce solide avec du CaI_2 (Schéma 9).

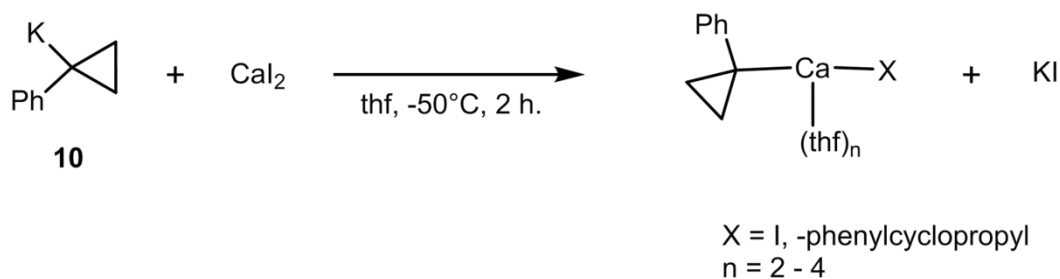


Schéma 9 Réaction entre **10** et CaI_2 .

Une analyse RMN a montré la formation d'au moins trois nouvelles espèces phénylcyclopropyles métallées avec des signaux caractéristiques : *Hortho+meta* (zone: δ 6.79-6.62), *Hpara* (zone: δ 6.35-6.08) and $\text{H}\beta$ (deux zones: δ 0.64-0.60 et 0.36-0.33). Ces signaux sont très semblables à ceux observés pour le complexe 2. Ces espèces sont beaucoup plus stables vis-à-vis des éthers que le précurseur organopotassien. De plus, toutes reforment bien le phénylcyclopropane par hydrolyse. Il semble donc que nous ayons bien formé des

complexes phenylcyclopropylcalcium, cependant, du fait de leur grande solubilité, elles n'ont pu être séparées et/ou cristallisées pour l'instant.

b. Addition oxydante sur le Ca*

Le groupement cyclopropyle ressemblant aux groupements aryle et vinyle, nous avons utilisé la méthode d'addition oxydante de l'iodocyclopropane sur du Ca activé (Ca*). Lorsque la réaction se fait dans le thp, une conversion de 70% a été mesurée pour l'iodocyclopropane en complexes cyclopropylcalcium heteroleptic [*c*-PrCa(thp)_xI] (**11**) et homoleptic [(*c*-Pr)₂Ca(thp)_x] (**12**) (Schéma 10).

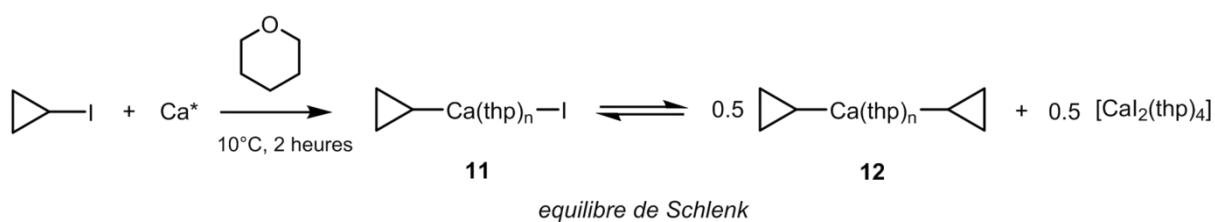


Schéma 10 Synthèse des complexes **11** et **12**.

11 et **12** ont été complètement convertis en cyclopropane par hydrolyse. Ces complexes ont été caractérisés par RMN du ¹H (Figure 20) et du ¹³C.

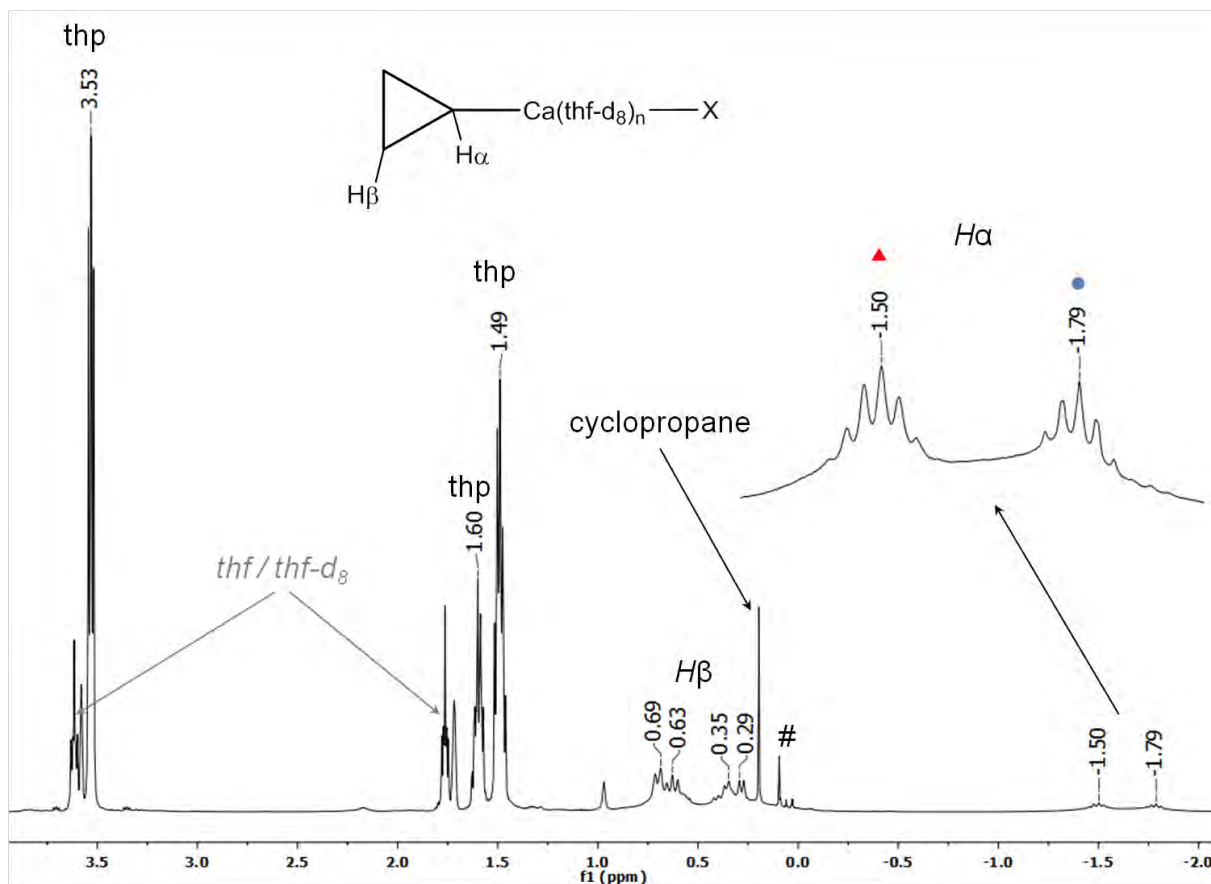


Figure 20 Spectre RMN ^1H d'un mélange de **11** et/ou **12** dans le thf-d_8 . # = graisse. Les signaux des deux composés sont représentés par des triangles rouges et par des cercles bleus. $X = \text{I}, \text{C}_3\text{H}_5$.

Les signaux caractéristiques de cyclopropyles métallés en α sont observés : deux ensembles de signaux larges pour H_β et H_β' d'une part et un signal large pour H_α d'autre part qui résonnent respectivement à δ 0.75-0.50, δ 0.40-0.20 et δ -1.50 - -1.80 dans le spectre du ^1H ; deux signaux larges à δ 7.9 (C_α) et δ 7.0 (C_β) dans le spectre du ^{13}C . Nous essayons à présent d'isoler l'un de ces complexes par cristallisation, dans le but de compléter ces analyses par une structure par DRX.

11 et **12** sont les premiers complexes cyclopropyl de calcium reportés, mais constituent aussi les premiers exemples de synthèse d'alkylcalciums non stabilisés.

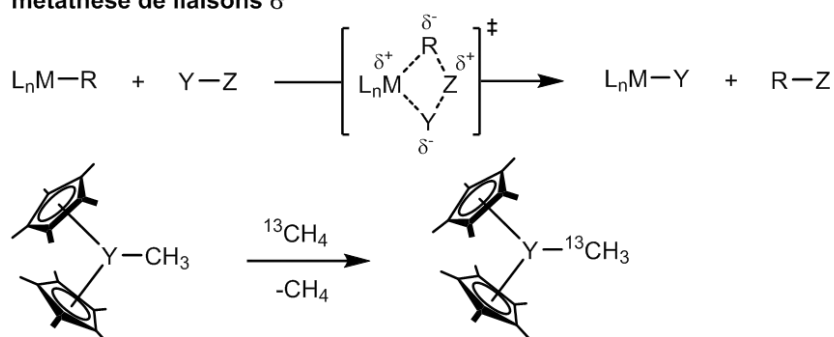
C. Chapitre 3

Dans ce chapitre nous étudions l'activation de liaisons C–H de la pyridine et C–F de la pentafluoropyridine par le dicyclopropylzirronocène.

I.1.Introduction

L'activation de liaisons par les complexes des métaux de la gauche peut se faire principalement selon deux mécanismes. Soit le complexe est très réactif, et le mécanisme est la métathèse de liaisons σ , soit une réaction intramoléculaire d'abstraction d'un H en alpha génère une espèce insaturée transitoire qui va ensuite activer la liaison cible (Schéma 11).

metathèse de liaisons σ



abstraction d'un H- α / addition-1,2

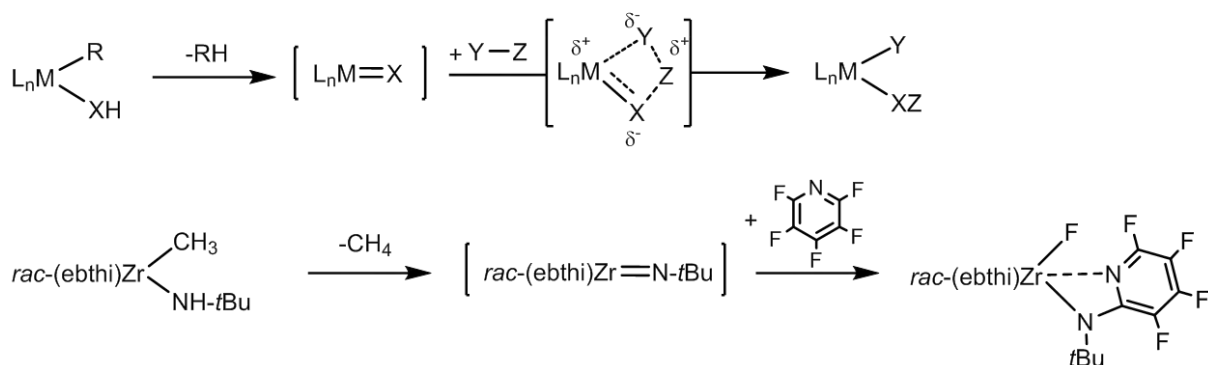


Schéma 11 Le mécanisme de la métathèse de liaison σ , avec l'exemple de l'activation du méthane par $[Cp^*_2Y(CH_3)]$ (en haut), et le mécanisme de l'abstraction d'un H- α suivie par une addition 1,2, avec l'exemple de l'activation de la pentafluoropyridine par $[rac-(ebthi)ZrMe(NHt-Bu)]$ (en bas). Ebthi : ethylenebis(tetrahydro)indenyl.

Pour générer des complexes très réactifs, un autre mécanisme plus rare peut être rencontré, il s'agit de l'abstraction d'un H β . Ce mécanisme est présenté dans le cas du complexe étudié, le $[Cp_2Zr(c-C_3H_5)_2]$ (Schéma 12). L'abstraction d'un H β génère le complexe

transitoire $[\text{Cp}_2\text{Zr}(\eta^2\text{-}c\text{-C}_3\text{H}_4)]$ qui peut être piégé par la triméthylphosphine (Schéma 12). Cet intermédiaire peut également réagir avec des substrats insaturés par insertion dans la liaison Zr–C, ou faire de l'activation de liaisons C–H du benzène, du furane ou du thiophène.

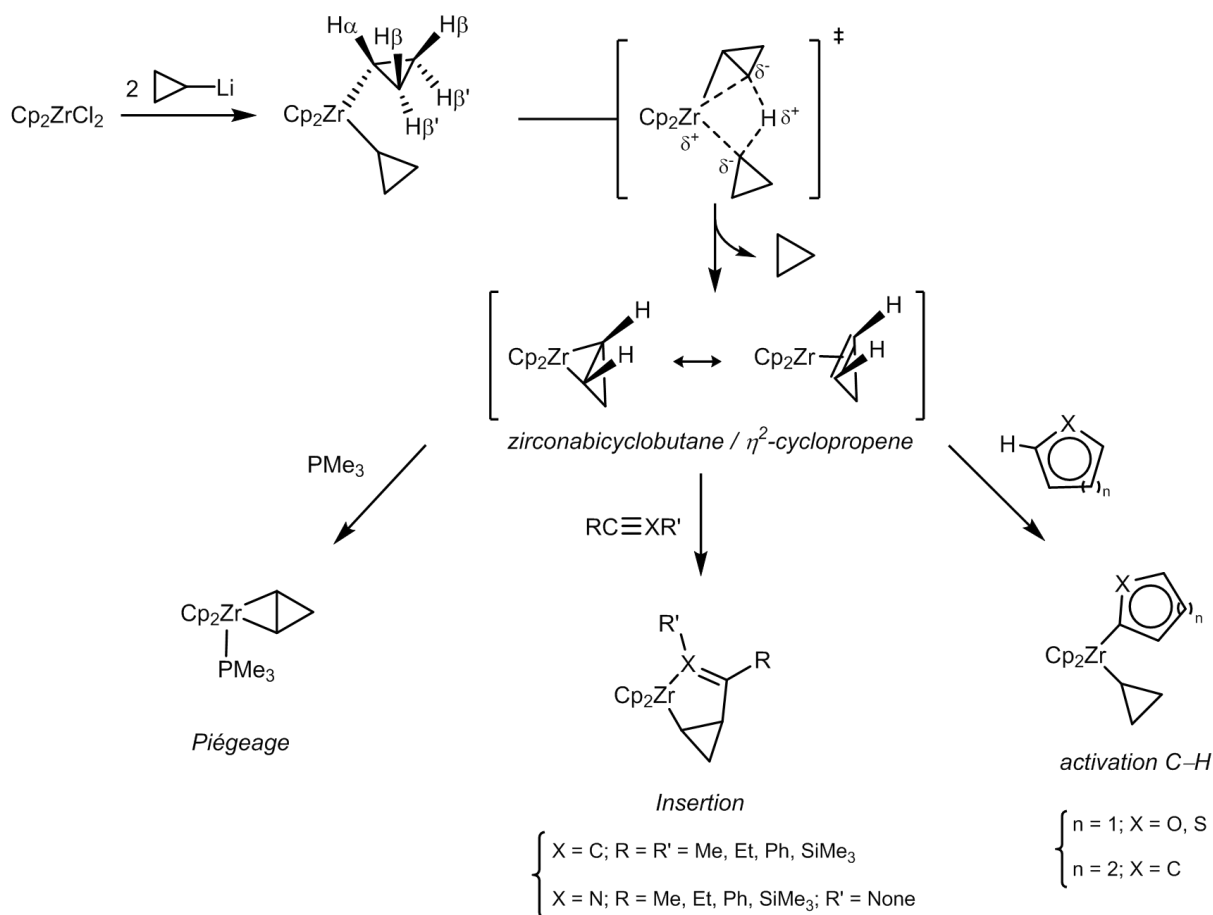


Schéma 12 Synthèse et réactivité du dicyclopropylzirconocène $[\text{Cp}_2\text{Zr}(c\text{-C}_3\text{H}_5)_2]$.

Nous présentons ici la réaction entre $[\text{Cp}_2\text{Zr}(c\text{-C}_3\text{H}_5)_2]$ et la pyridine qui n'avait jamais été étudiée jusqu'alors. De plus, les complexes du zirconium peuvent se révéler efficaces pour l'activation de la liaison C–F forte et inerte (BDE = 536 ± 21 kJ/mol). Nous étudierons donc l'activation stœchiométrique de la liaison C–F de la pentafluoropyridine, puis en s'inspirant de systèmes existants, nous tenterons de rendre cette transformation catalytique.

I.2. Résultats et discussion

a. Activation de la pyridine

Le $[\text{Cp}_2\text{Zr}(c\text{-C}_3\text{H}_5)_2]$ (**13**) a été dissous dans de la pyridine et chauffé à 45°C pendant 3 jours. Nous avons observé la formation de cyclopropane, prouvant que le complexe transitoire $[\text{Cp}_2\text{Zr}(\eta^2\text{-}c\text{-C}_3\text{H}_4)]$ (**14**) a été formé. Ce dernier a réagi avec la pyridine pour donner $[\text{Cp}_2\text{Zr}(\text{py})\{\kappa^2\text{-N,C}^8\text{-}(2\text{-}c\text{-C}_3\text{H}_4)\text{-C}_5\text{H}_5\text{N}\}]$ (**15**) présenté dans le Schéma 13. Cette réaction est régiosélective en position-2 de la pyridine et stéréospécifique avec le Zr et la pyridine déaromatisée étant en *syn* du cyclopropyle. Lorsque **15** a été dissous dans le pentane et recristallisé à -40°C , le complexe violet $[\text{Cp}_2\text{Zr}\{\kappa^2\text{-N,C}^8\text{-}(2\text{-}c\text{-C}_3\text{H}_4)\text{-C}_5\text{H}_5\text{N}\}]$ (**16**) s'est formé spontanément et a été obtenu avec un rendement de 89%. Ces complexes ont été caractérisés par spectroscopie RMN, DRX et analyse élémentaire.

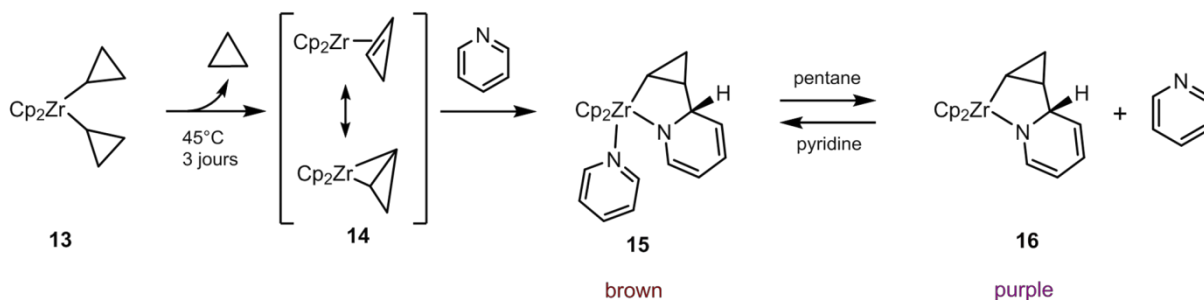


Schéma 13 Réaction entre **13** et la pyridine pour donner **15** et **16**.

Une étude mécanistique à l'aide de pyridine deutériée a démontré qu'il n'y avait pas d'activation C–H durant la réaction, mais que le mécanisme était un couplage oxydant C–C entre la pyridine et **14**.

Lorsque la réaction entre **13** et la pyridine se fait en présence d'une quantité catalytique d'une base forte (ici NaH), un nouveau produit $[\text{Cp}_2\text{Zr}\{\kappa^2\text{-N,C}^8\text{-}(2\text{-C}_3\text{H}_5)\text{-C}_5\text{H}_4\text{N}\}]$ (**17**) est observé après 4 jours de réaction à 45°C (Schéma 14). **17**, obtenu avec un rendement de 95%, a été complètement caractérisé par spectroscopie RMN, DRX et analyse élémentaire. Le mécanisme de la formation de **17** a été élucidé (Schéma 14) : Un pré-équilibre acido/basique provenant de la déprotonation de **15** évolue vers l'ouverture du cycle cyclopropyle, instantanément suivie par la protonation du nouveau complexe **17**. La formation

de **17** à partir de **15** est l'étape cinétiquement déterminante de la transformation totale *via* une activation de la liaison C–H.

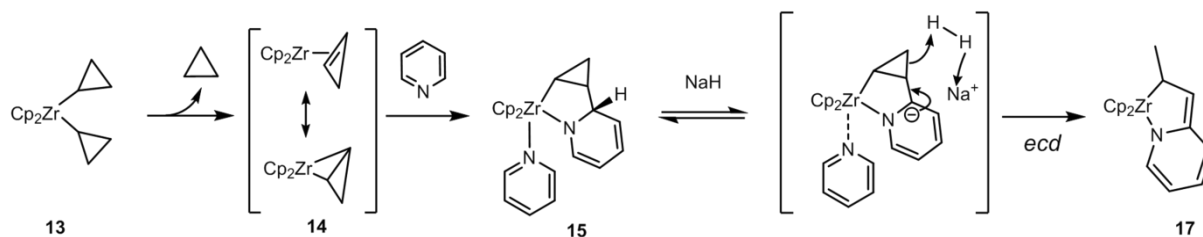


Schéma 14 Mécanisme de la formation de **17**.

b. Activation de la pentafluoropyridine

13 a été dissous dans du cyclohexane avec 10 éq. de pentafluoropyridine et chauffé à 45°C pendant 3 jours. L'évaporation de la solution et le lavage au pentane du solide beige résultant nous a permis d'obtenir le produit d'activation C–F [$\text{Cp}_2\text{ZrF}\{(2\text{-C}_5\text{F}_4\text{N})\text{-}c\text{-C}_3\text{H}_4\}$] (**20**) avec un rendement de 85% (Schéma 15). Comme dans le cas de la réaction avec la pyridine, cette transformation est régiosélective en position-2 et stéréospécifique. **20** a été caractérisé par spectroscopie RMN, DRX et analyse élémentaire.

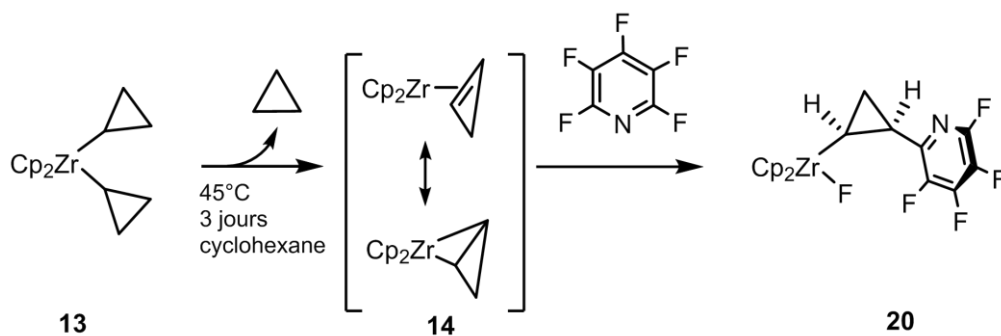


Schéma 15 Réaction entre **13** et la pentafluoropyridine pour donner **20**.

Pour comprendre le mécanisme de la formation de **20**, des calculs DFT ont été réalisés et leur résultat est présenté en Figure 21 ci-dessous. Ce profil énergétique montre bien que l'abstraction d'un H β est l'étape cinétiquement déterminante de la réaction, avec un état de transition situé 108 kJ/mol au-dessus de **13**. Par comparaison, l'écart d'énergie entre **14**/ $\text{C}_5\text{F}_5\text{N}$ et le deuxième état de transition n'est que de 37 kJ/mol. **20** est beaucoup plus stable que

n'importe laquelle des autres espèces impliquées dans la transformation. En effet, **20** est stabilisé de 268 kJ/mol par rapport à **13**, une conséquence de la formation d'une liaison Zr–F très forte, qui est la force motrice de la réaction. Ces calculs ne montrent pas de pré-coordination de la pyridine fluorée qui aurait pu expliquer la sélectivité pour la position-2.

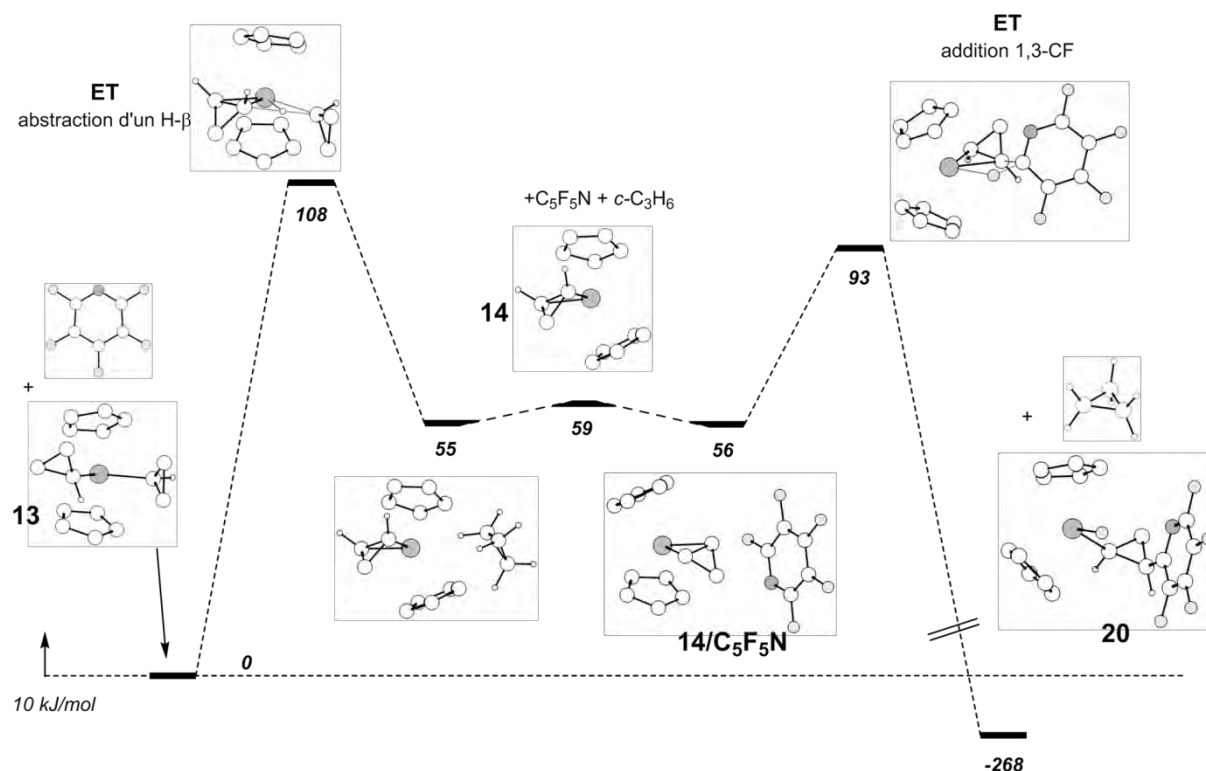


Figure 21 Surface d'énergie potentielle (ΔE) pour la réaction entre la pentafluoropyridine et **13** (kJ/mol). Code couleur : blanc = C,H; gris clair = F; gris foncé = Zr, N.

L'activation de la liaison C–F ayant été réalisée de manière stœchiométrique, nous nous sommes ensuite penchés sur le passage à une transformation catalytique. La difficulté de mettre en place un cycle catalytique d'activation C–F avec les métaux de la gauche tient à la formation de liaisons M–F très fortes. Une technique consiste à introduire dans le milieu des centres métalliques qui vont former à leur tour des liaisons encore plus fortes avec le fluor et vont donc agir comme des puits à fluor. Dans le Tableau 1 ci-dessous, sont présentés les BDE de différents métaux de la gauche ainsi que celles de potentiels candidats en tant que puits à fluor.

Tableau 1 BDE pour des espèces diatomiques en phase gazeuse.

Liaison	C-F	Ti-F	Zr-F	Ta-F	Li-F	Mg-F	Si-F	Al-F
ΔH (kJ/mol)	536 \pm 21	569 \pm 34	623 \pm 63	573 \pm 13	577 \pm 21	462 \pm 21	540 \pm 13	664 \pm 6

La BDE la plus grande étant celle de la liaison Al-F, nous avons choisi un complexe d'aluminium pour extraire le fluor du composé **20**. Le cycle catalytique présenté en Figure 22 a donc été étudié.

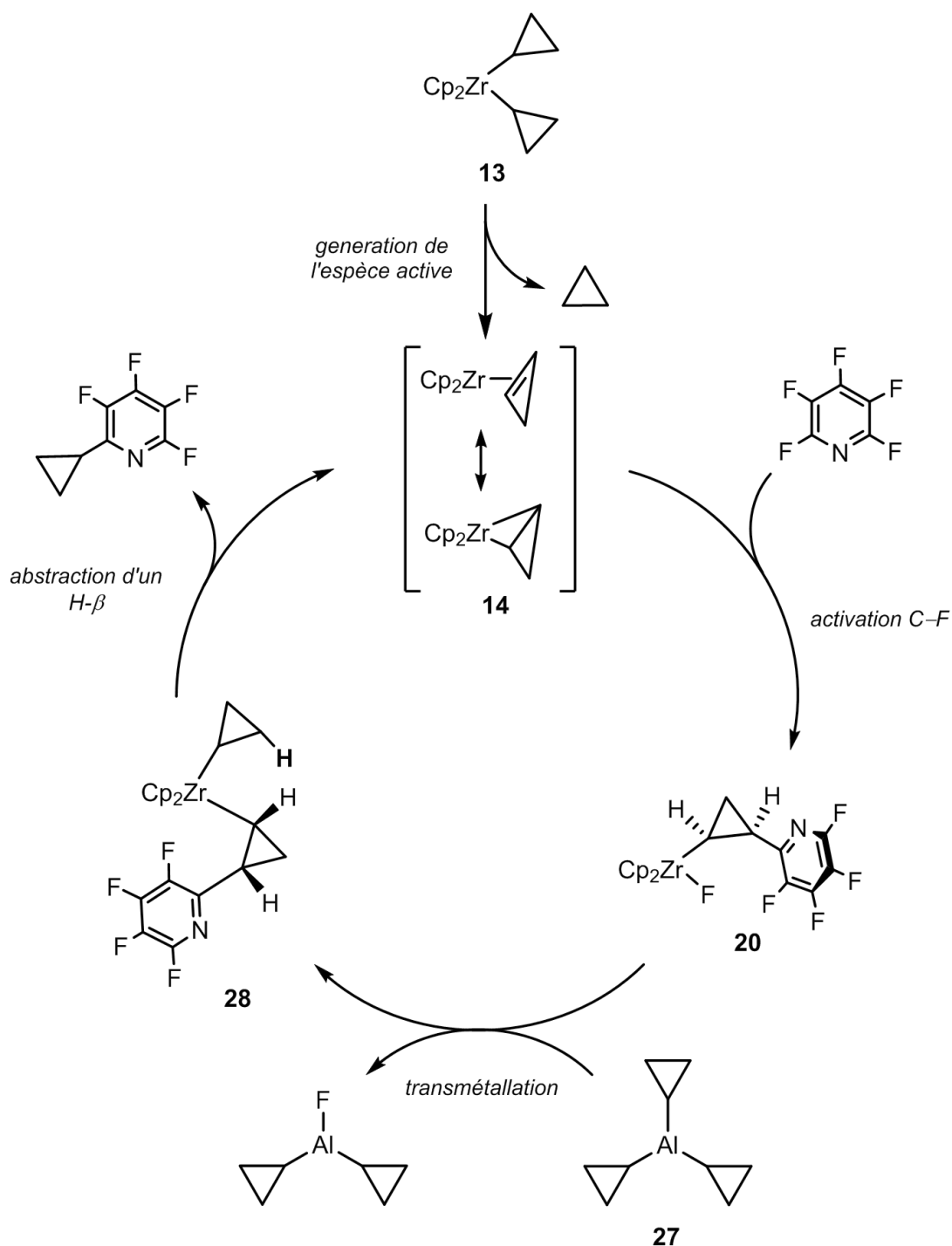


Figure 22 Cycle catalytique proposé pour la formation de 2-cyclopropyltetrafluoropyridine.

Afin de valider ce cycle catalytique, chaque étape a été étudiée séparément. Nous avons vu précédemment la formation du composé **20**. Lorsque **20** et le tricyclopropyle aluminium (**27**) sont mélangés dans du cyclohexane à température ambiante, le produit de transmétallation $[\text{Cp}_2\text{Zr}(c\text{-C}_3\text{H}_5)\{(2\text{-C}_5\text{F}_4\text{N})\text{-}c\text{-C}_3\text{H}_4\}]$ (**28**) a été obtenu en quelques heures

(Schéma 16). De plus, des cristaux formés dans le milieu réactionnel, et analysés par DRX ont révélé un intermédiaire réactionnel zwitterionique $[\text{Cp}_2\text{Zr}(2\text{-C}_5\text{F}_4\text{N})\text{-}c\text{-C}_3\text{H}_4]^+[(\mu\text{-F})\text{-}(c\text{-C}_3\text{H}_5)_3\text{Al}]^-$ (**29**). **28** et **29** ont été caractérisés par DRX et spectroscopie RMN.

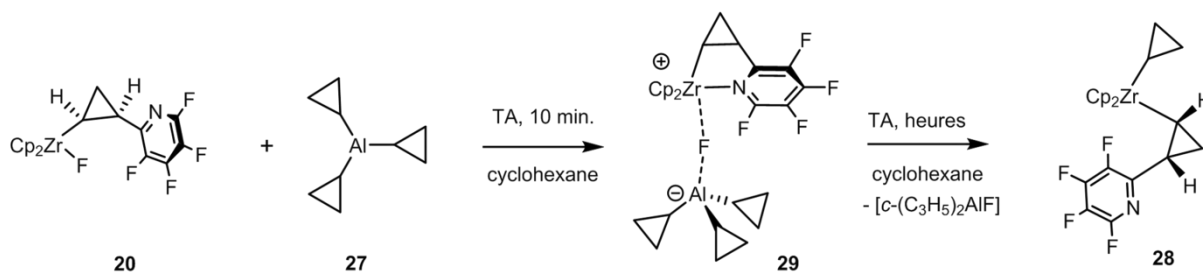


Schéma 16 Synthèse des complexes **28** and **29**.

Cette étape du cycle ayant été validée, nous avons chauffé **28** à 45°C en présence de pentafluoropyridine dans le cyclohexane pendant 21 jours. L'abstraction d'un H β du groupement cyclopropyltetrafluoropyridine a été observée et le complexe **14** a été généré, puis a réagi avec la pentafluoropyridine pour donner **20** (Schéma 17). Cette dernière réaction stœchiométrique a validé la faisabilité du cycle catalytique. Des tests catalytiques sont désormais en cours.

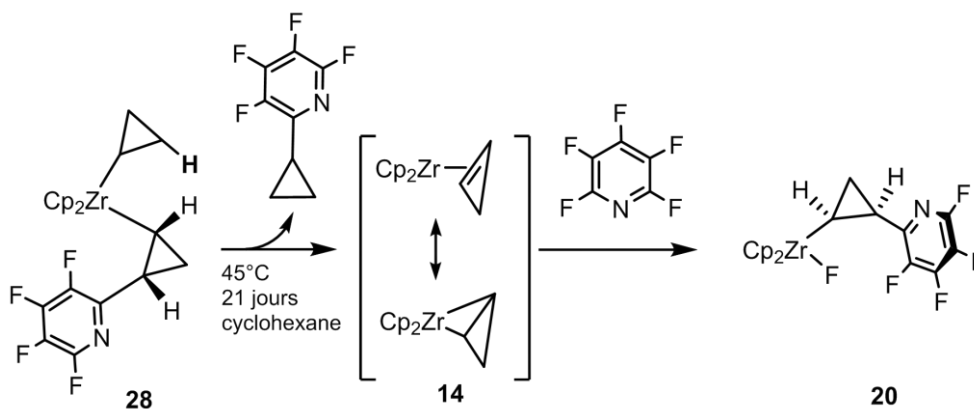


Schéma 17 Formation du complexe **20** par cassure de la liaison C-F de la pentafluoropyridine par le complexe **28**.

Thèse soutenue par : Quentin DUFROIS – Directeurs de thèse : Michel ETIENNE et Chiara DINOI – Date de soutenance : Vendredi 25 novembre 2016 – Lieu de soutenance : Laboratoire de Chimie de Coordination du CNRS (Toulouse, France) – Discipline : Chimie organométallique de coordination.

Résumé

La thèse présente la chimie de complexes de métaux électropositifs portant le groupe cyclopropyle.

La première partie du manuscrit décrit la synthèse et la caractérisation de dérivés du cyclopropyllithium ayant pour formule $[1-R-c-C_3H_4Li]$ ($R = SiMe_3, Ph, SPh$). Des agrégats originaux, organisés autour de centres Li^+ stabilisés par la peu commune interaction CC agostique, sont présentés. Cette interaction a une influence marquée sur l'agrégation des composés à l'état solide et parfois en solution. Sa coordination compétitive, sur un Li^+ , avec des atomes donneurs (O, N et S) permet une évaluation qualitative de sa force.

La deuxième partie du manuscrit présente la synthèse du nouveau complexe cyclopropylcalcium. Ce composé est caractérisé par une étude RMN complète. C'est le premier alkylcalcium non-stabilisé.

La troisième partie du manuscrit contient une étude de la réactivité du dicyclopropylzirconocène $[Cp_2Zr(c-C_3H_5)_2]$ vis-à-vis de la pyridine et de pyridines fluorées. La formation d'un intermédiaire η^2 -cyclopropène mène à la déaromatisation et à l'activation C–H de la pyridine, mais aussi à l'activation C–F de la pentafluoropyridine. Une étude préliminaire de l'activation catalytique de la liaison C–F de la pentafluoropyridine par $[Cp_2Zr(c-C_3H_5)_2]$ en présence de tricyclopropylaluminium est aussi présentée.

Summary

The manuscript presents the chemistry of electropositive metal complexes bearing the cyclopropyl group.

This first part of the manuscript describes the synthesis and characterisation of cyclopropyllithium derivatives of the formula $[1-R-c-C_3H_4Li]$ ($R = SiMe_3, Ph, SPh$). Original aggregates displaying low valent Li^+ centres stabilised by the rare CC agostic interaction are presented. This interaction influences the aggregation of the compounds in the solid state and sometimes in solution. A qualitative evaluation of its strength is provided by competitive coordination on Li^+ vs donor atoms such as O, N and S.

The second part of the manuscript presents the synthesis of the new cyclopropylcalcium complex. This compound is characterised by a full NMR study. It is the first non-stabilised alkylcalcium compound.

The third part of the manuscript contains a reactivity study of dicyclopropylzirconocene $[Cp_2Zr(c-C_3H_5)_2]$ towards pyridine and fluorinated pyridines. Dearomatisation and C–H bond activation of pyridine, together with C–F bond activation of pentafluoropyridine result from the initial formation of a η^2 -cyclopropene intermediate. A preliminary study of the catalytic C–F bond cleavage of pentafluoropyridine by $[Cp_2Zr(c-C_3H_5)_2]$ in the presence of tricyclopropylaluminium is also presented.

Mots clés : *Chimie organométallique – Chimie de coordination – Ligand cyclopropyle – Synthèse – Métaux de la gauche – Activation de liaisons – Interaction CC agostique – Catalyse.*